UNIVERSITY OF SOUTHAMPTON

FACULTY OF NATURAL AND ENVIRONMENTS SCIENCES

Ocean and Earth Sciences

Quantification and characterisation of particle export into the mesopelagic

By

Jennifer Siân Riley

Thesis for the degree of Doctor of Philosophy

May 2012

UNIVERSITY OF SOUTHAMPTON
FACULTY OF NATURAL AND ENVIRONMENTS SCIENCES
OCEAN AND EARTH SCIENCES

Abstract

Doctor of Philosophy

Quantification and characterisation of particle export into the mesopelagic

By
Jennifer Siân Riley

Export in the ocean is the process whereby particles sink out of the surface ocean and into the mid water column (mesopelagic). It is an integral part of the biological carbon pump (BCP) and is in part responsible for transferring particulate organic carbon (POC) into the deeper ocean where it can be removed from contact with the atmosphere for climatically significant timescales. The majority of this POC is thought to be exported from the surface ocean in two pools characterised by their sinking speeds; fast (> 100 m d^{-1}) and slow (< 10 m d^{-1}). Both particle size, affected by the phytoplankton community structure, and density, determined by the proportion of biominerals (calcite and opal) and organic material (carbon) present, affect the sinking speed of particles. Biomineral facilitated sinking, enhancing particle density is known as ballasting. Current uncertainties associated with the particle export include; (1) how particle size and density influence particle sinking speeds; (2) the size and magnitude of the fast and slow sinking pools of POC and; (3) the depth to which the fast and slow flux penetrates into the interior of the ocean. Two research cruises were undertaken to the northeast Atlantic (Porcupine Abyssal Plain (PAP) site) and Arctic to collect individual sinking particles and measure bulk fluxes using the Marine Snow Catcher (MSC).

During both cruises large discrete particles were collected, and their sinking rate and size measured. Two types of particle were identified; marine snow aggregates (MSA) and aggregate protist complexes (APC). Only particle size positively correlated with sinking speed, suggesting particle size plays a more significant role in regulating sinking speed than density. Theoretical calculations indicate the relative importance of density increases with depth, as particles get smaller due to remineralisation. Thus the importance of ballasting is likely to increase with depth in the ocean.

Measurement of total export at the PAP site using the MSC revealed a fast and slow sinking flux of 54 mg C m^{-2} day^{-1} (40 %) and 92 mg C m^{-2} day^{-1} (60 %) respectively. It is concluded that the fast sinking flux supplies the deep (> 3000 m) sediment flux and is potentially ballasted, due to the observed presence of APC particles, consisting of a MSA particle centred on a foraminifera test. In contrast the slow sinking flux is likely entirely remineralised in the top 500 m and unballasted.

Taxonomic examination of exported MSA particles at 50 m and bulk deeper fluxes (175 – 600 m) at the PAP site indicated that some component of the slow sinking flux was diatom related and reaches at least 600 m. Comparison with the seasonal succession of diatom species suggests that deepest fluxes may be the remnants of seasonally earlier surface blooms. Furthermore it was observed that calcite is preferentially exported in MSA, enhancing their sinking speed, via a ballasting effect and is important for diatom POC export to the sediments.

Measurement of the fast and slow sinking fluxes in the Arctic ice covered and open water environments, using the MSC showed no attenuation between 50 and 100 m or differences between environments. Thus the average Arctic fast and slow sinking fluxes were 159 mg C m^{-2} d^{-1} (68 %) and 76 mg C m^{-2} d^{-1} (32 %) respectively. It was also observed that faecal pellets were responsible for most (> 90 %) of the fast flux and that export fluxes were likely sustained by the productivity generated by both the sea ice and water column phytoplankton communities.

Traditionally the majority of carbon export is thought to occur via rapid pulses of material. The distributions of fast and slow sinking particles were different between the two locations presented in this thesis. The fast:slow ratio was 40:60 % at the PAP site and 68:32 % in the Arctic. Comparison with other studies in the literature suggests that at a global scale an average of 60 % of the flux is slow sinking between 50 and 300 m. This suggests that new ways of conceptualising carbon export in the oceans need to be considered.

Contents

List of figures

List of tables

List of accompanying materials

Figures

Tables

Declaration of authorship

I, Jennifer Siân Riley declare that the thesis entitled **'Quantification and characterization of particle export into the mesopelagic'** and the work presented in the thesis are both my own, and have been generated by me as the result of my own original research. I confirm that:

- this work was done wholly or mainly while in candidature for a research degree at this University;
- where any part of this thesis has previously been submitted for a degree or any other qualification at this University or any other institution, this has been clearly stated;
- where I have consulted the published work of others, this is always clearly attributed;
- where I have quoted from the work of others, the source is always given. With the exception of such quotations, this thesis is entirely my own work;
- I have acknowledged all main sources of help;
- where the thesis is based on work done by myself jointly with others, I have made clear exactly what was done by others and what I have contributed myself;
- parts of this work have been published as:

  Riley, J. S., Sanders, R., Marsay, C., Le Moigne, F. A. C., Achterberg, E. P., and Poulton, A. J. (2012), The relative contribution of fast and slow sinking particles to ocean carbon export, *Global Biogeochemical Cycles*, *26*(1), GB1026, 10.1029/2011gb004085.

Signed: ……..

Date:…….

Acknowledgements

The first person who must be thanked is Richard Sanders, without his constant enthusiasm and drive this project would never have come to life. With increasing demands on his time Richard has always made sure that I have had the help and support needed, and for this I am eternally grateful. Ray Leakey has also always been available at the other end of the phone, providing thoughtful and useful advice which has helped me complete this thesis. As principal scientist Ray also enabled my participation in the Arctic cruise which was an unforgettable experience. My thanks also go to Eric Achterberg for providing the funding for this project through the NERC SOFI Doctoral Training Grant Award (NE/F012462/1) and for the comments provided on the chapters of this thesis. Alex Poulton, although not a supervisor has always made time for me, whether it was to offer help in the lab, scientific advice or just let me talk at him, and his help will not be forgotten. I would also like to thank Richard Lampitt for giving me access to the Marine Snow Catcher and for originally showing me how to deploy it.

I would like to acknowledge all the people involved with the two research cruises undertaken as part of this PhD. My thanks go to the crew of the RRS *Discovery* during the PAP site cruise and RRS *James Clark Ross* during the Arctic cruise. Thanks also go to Kevin Saw and Sam Ward for coordinating the PELAGRA deployments during the PAP site cruise. Thank you to Chris Marsay (NOC, Southampton) who donated some PELAGRA flux samples, before geochemically destroying them and Frederic Le Moigne (NOC, Southampton) and Maria Villa (Universidad de Sevilla) who provided thorium flux measurements during the PAP site cruise. Further thanks go to those who provided complementary data from the Arctic cruise and include, Eithne Tynan for providing the primary productivity measurements, Estelle Dumont for analysis of the physics data, Tim Brand and Sharon McNeill for providing the nutrient data, Ronnie Glud for his estimates of the sea ice community primary productivity and Ray Leakey, Elaine Mitchell, Sian Lordsmith (SAMS) for the sea ice algae biomass. I am also grateful to David Johns at SAHFOS for access to the CPR data base and Stephanie Henson for plotting the CPR tracks.

To my friends, both in Southampton and further afield, I cannot tell you how much help and support you have given me over the last 4 years. Sian Henley who is never on the other end of the phone when you call, but always phones back, is a constant source of inspiration and amusement. Charlotte Marcinko and Anastasia Charalampopoulou have been there through the good and bad moments encouraging me to continue when I am having a ‘duck day’. Rob Howlin, Gary Watmough and Mark Stinchcombe, you make me laugh, which is one of the most important things to do when undertaking a PhD. Also to Mark, thank you for having James, without whom I would have never been able to go on the PAP site cruise and get 3 chapters worth of data!

The final recognition should go to my family, especially my parents Gill and Martin, but also my sister Dorcas. Without their unconditional patience and love, I would never have had the encouragement to get to where I am today. Thank you does not describe how much your support means to me.

Abbreviations

AE	Assimilation efficiency
ANOSIM	Analysis of similarity
APC	Aggregate protist complex
b	Flux attenuation coefficient
BSi	Biogenic silica
C_D	Drag Coefficient
CF	Conversion factor
CN	Cellulose Nitrate
Conc.	Concentration
CPR	Continuous Plankton Recorder
CTD	Conductivity Temperature Density
D_C	Density (number) of cells per MSA particle
DF	Deeper water flux samples
DOC	Dissolved organic carbon
DIC	Dissolved inorganic carbon
E	Egestion
EGC	East Greenland Current
ESD	Equivalent spherical diameter
e-ratio	Export ratio
FP	Faecal Pellet
FPs	Faecal Pellets
GM	Greenwich Meridian
H’	Shannon Wiener Diversity Index
I	Ingestion
IC	Ice covered
IPCC	Intergovernmental Panel on Climate Change
IRSC	Indented rotating sphere carousel
IS	Ice Station
J’	Pielou’s Evenness
KF	Kongsfjorden
MLC	Mixed layer community
MLD	Mixed Layer Depth
MSA	Marine Snow Aggregate
MSC	Marine Snow Catcher
NMDS	Non Metric Dimensional Scaling
OW	Open Water
p	Porosity

PAP	Porcupine Abyssal Plain
PELAGRA	Particle Export measurements using a Lagrangian trap
POC	Particulate organic carbon
PIC	Particulate inorganic carbon
ppm	parts per million
Re	Reynolds number
Rs	Spearman's Rank
SAMS	Scottish Association for Marine Science
SAHFOS	Sir Alastair Hardy Foundation for Marine Science
SEM	Scanning Electron Microscope
S.D.	Standard deviation
SI	Sea Ice
SIMPER	Similarity percentage
SIZ	Seasonal Ice Zone
Temp	Temperature
TEP	Transparent exopolymer particle
U	Sinking speed
V	Volume
WSC	West Spitsbergen Current
XSD	Excess density

Chapter 1: Introduction

1.1 The biological carbon pump and global climate

The quantity and type (dissolved, particulate, organic and inorganic) of carbon in the open ocean is controlled predominantly by two mechanisms; the solubility pump and the biological carbon pump [*Volk and Hoffert*, 1985]. Carbon dioxide (CO_2) entering the ocean from the atmosphere via the solubility pump is dependent on the atmospheric CO_2 concentration and hydrographic properties of the water, such as temperatures, mixing and the degree to which the waters are already saturated with CO_2. The biological carbon pump involves the production of organic carbon from CO_2 and nutrients, and is controlled by the euphotic zone plankton community [*Falkowski et al.*, 1998; *Sabine et al.,* 2004].

Both the biological carbon pump and the solubility pump transfer carbon from the surface to the deep ocean. This, alongside the observations of the coupling between atmospheric CO_2 and global temperature over glacial / interglacial timescales [*Berner et al.*, 1978] led to the hypothesis that much of the excess CO_2 was stored in the deep ocean [*Broecker*, 1982]. More recently it has been suggested that atmospheric CO_2 concentrations are in fact highly sensitive to the depth at which organic carbon is remineralised back into inorganic forms [*Kwon et al.*, 2009], which in itself is related to particle sinking speeds and the nature of the material exported.

The biological carbon pump is driven by photosynthetic phytoplankton. Photosynthesis is the process whereby inorganic carbon (CO_2) is reduced to organic carbon and is fuelled by light and nutrients with the aid of the pigment chlorophyll-a to catalyse the reaction [*Falkowski et al.*, 2003]. In the surface ocean essential macronutrients such as nitrate and phosphate occur in relatively low concentrations but increase with depth [*Redfield*, 1934]. Surface macronutrients are supplied by the upwelling of deep nutrient rich waters, driven by ocean circulation and mixing [*Sarmiento et al.*, 2006].

Generally it is thought that nitrate is the limiting nutrient in the ocean [*Tyrrell*, 1999]. However, recent work in the North Atlantic has indicated that production can be co-

limited by both nitrate and phosphate [*Moore et al.*, 2008]. Traditionally it has been thought that for optimal photosynthesis phytoplankton require nitrate and phosphate in a ratio of 16 : 1, the Redfield ratio [*Redfield*, 1934]. However, more recent studies have indicated that this ratio is an average and individual species can have widely differing elemental stoichiometry [*Klausmeier et al.*, 2004; *Arrigo*, 2005]. Micronutrients such as iron are also vital in determining the rate of primary production as they are important for cellular functions and growth [*Zehr and Kudela*, 2009].

The atmosphere is an important source of micronutrient supply to the open ocean particularly in coastal regions of the North Atlantic and Pacific [*Duce et al.*, 1991]. Sufficient concentrations of macronutrients, such as nitrate, phosphate and silicate, in the surface ocean coupled with limiting micronutrients, such as iron, can result in high nutrient low chlorophyll regions where production does not exhaust the supply of new nutrients [*Boyd et al.*, 2007]. Thus, the limitation of primary production by nutrients in the ocean is a complex function of the macro and micronutrient concentration and availability, and the ratio in which different phytoplankton species require nutrients.

Primary production that is sustained by the supply of nitrate from below the winter mixed layer, and by nitrogen (N) inputs from the atmosphere is referred to as new production. Production fuelled by N supplied from the remineralisation of organic matter is termed regenerated production [*Dugdale and Goering*, 1967]. The relative ratio of new production to total (new + regenerated) production is known as the f-ratio [*Eppley and Peterson*, 1979]. In the North Atlantic, the early onset of the diatom spring bloom is fuelled mainly by new nutrients, as deep winter mixing brings nutrient rich waters to the surface. In contrast late summer production has a greater dependency upon regenerated nutrients as the upwelled nitrate is gradually utilised [*Sanders et al.*, 2005]. Thus the f-ratio can be seen to vary seasonally within an ocean region. The large seasonality of the high latitude regions results in significantly higher f-ratios than in sub tropical environments which are less seasonal [*Laws et al.*, 2000].

With the onset of the seasonal primary production, phytoplankton biomass builds up in the surface ocean [*Sieracki et al.*, 1993]. Higher trophic level organisms such as zooplankton graze down the phytoplankton community, respiring some of the organic carbon into dissolved inorganic carbon (DIC). However, not all of the phytoplankton biomass is respired, a fraction escapes and sinks out of the euphotic zone, this carbon is exported [*Boyd and Trull*, 2007].

The majority of carbon that sinks out the surface ocean is typically aggregated particles or faecal pellets [*Turner*, 2002]. As these particles sink they undergo continued remineralisation, driven by both bacteria and zooplankton grazing, recycling

the organic carbon back into DIC [*Steinberg et al.*, 2008b]. When remineralisation occurs above the winter mixed layer depth it is likely that the remineralised carbon will be transported back into the surface ocean, and potentially the atmosphere. If the particle sinks below the winter mixed layer, it is likely that the carbon will remain in the deep ocean for climatically significant timescales, this carbon is said to be sequestered [*Buesseler et al.*, 2007b]. However, sequestered carbon is only ~ 1 % of surface production [*Poulton et al.*, 2006]. Ultimately any carbon which reaches the deep ocean waters will be returned to the surface ocean via ocean overturning on timescales between 1 and 1000 years [*Sarmiento et al.*, 2006].

Knowledge of the strength and efficiency of the biological carbon pump is aids the understanding of how it functions. One method of comparing the strength of the biological carbon pump between ocean regions is to examine the amount of carbon exported from the surface ocean. The fraction of primary productivity that is exported is the e-ratio. Depending on the location and season anywhere between 10 and 70 % of primary productivity can be exported from the euphotic zone, although more typical values range between 10 and 30 % [*Lignell et al.*, 1993; *Wassmann*, 1998; *Wassmann et al.*, 2004; *Thomalla et al.*, 2008; *Buesseler and Boyd*, 2009] and the magnitude of export is dependent upon the mismatch in the peak blooms of phytoplankton and zooplankton communities (the latter remineralise organic matter produced by the phytoplankton community) [*Wassmann*, 1998]. The efficiency by which carbon is transferred through the mesopelagic or twilight zone (~ 100 – 1000 m) depends on the rate of heterotrophic remineralisation and ranges between 20 and > 90 % [*Martin et al.*, 1987; *Buesseler et al.*, 2007b; *Buesseler and Boyd*, 2009].

Estimates of global carbon export driven by the biological carbon pump vary between 5 and 11 Gt C yr^{-1} [*Laws et al.*, 2000; *Henson et al.*, 2011]. Anthropogenic CO_2 emissions were estimated to be 9 Gt C yr^{-1} in 2010 [*Peters et al.*, 2012] which is within the same order of magnitude as export driven by the biological carbon pump [*Laws et al.*, 2000; *Henson et al.*, 2011]. Without the biological carbon pump it is predicted that atmospheric CO_2 concentrations would be ~ 200 parts per million (ppm) greater than they are today [*Parekh et al.*, 2006].

A recent IPCC (Intergovernmental Panel on Climate Change) document reported an increase in atmospheric CO_2 concentrations from pre-industrial values of 280 ppm (parts per million) [*Neftel et al.*, 1985; *Friedli et al.*, 1986] to 393 ppm in 2012 [*IPCC*, 2007; *Tans and Keeling*, 2012]. Increases in atmospheric CO_2 concentrations raise the partial pressure of CO_2 in the atmosphere, thus enabling more CO_2 to diffuse into the oceans. It is currently unclear exactly what the full effects of continued rises in atmospheric and oceanic CO_2 will be on the functioning of the biological carbon pump

and carbon export [*Doney et al.*, 2011]. Only by understanding the current functioning of the biological carbon pump can future changes to the system be measured and fully comprehended. However, the complexity and interconnectivity of the biological carbon pump as it is currently understood makes measurements of its current functioning difficult.

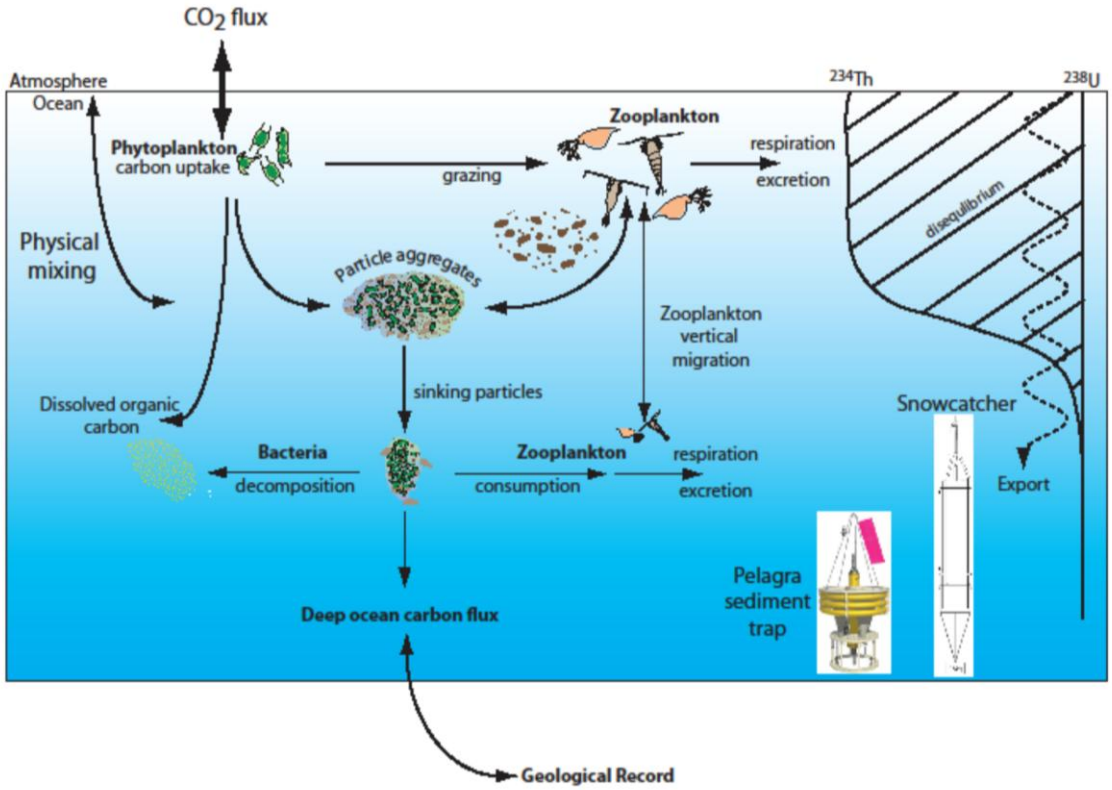

Figure 1.1 (Left) Schematic representation of the interconnectivity of the individual components constituting the biological carbon pump, highlighting biological transformations between dissolved and particulate phases and their export to depth. Also identified is the schematic representation of the oceanic uptake of CO_2 by the solubility pump. (Right) Schematic representations of flux measurement methods including Uranium/Thorium disequilibria, PELAGRA sediment traps and Marine Snow Catchers. Adapted from US JGOFS [*Painter*, 2012].

With this in mind, this thesis focuses on the quantification and characterisation of particle export into the mesopelagic ocean, with particular emphasis on particulate organic carbon (POC) fluxes. Particular attention will be paid to processes influencing particle transfer from the surface to the deep ocean and how these observations differ between different ocean regions. The following provides a general review of the major processes contributing to the biological carbon pump, including factors affecting particle export and methods of measuring and predicting particle export.

1.2 Factors affecting particle export

Four major factors influence the amount of exported POC; 1) the total amount of POC produced in the surface ocean via primary production (discussed in section 1.1); 2) the rate of marine snow aggregate and faecal pellet formation; 3) the rate of particle destruction and; 4) the rate of particle export [*De La Rocha and Passow*, 2007].

1.2.1 Particle Formation

Somewhat frustratingly the terms particle and aggregate are used interchangeably in the literature and there is not necessarily one clear definition of each. A particle may refer to a single phytoplankton cell, a faecal pellet (FP) or a marine snow aggregate (MSA). For clarity, in this thesis the term particle is used in conjunction with both the terms MSA and FP. Faecal pellets (FPs) are those particles egested by zooplankton and surrounded by a peritrophic membrane [*Turner*, 2002], whilst MSA refers to a grouping of individual particles forming a new larger cohesive particle [*Gordon*, 1970]. Aggregate production occurs through physical aggregation of smaller particles whilst faecal pellet formation occurs via biological production [*Alldredge and Silver*, 1988; *Burd and Jackson*, 2009].

The particle size spectra in the ocean ranges from viruses and bacteria to whales [*Sheldon et al.*, 1972]. Aggregation processes connect the two ends of this spectrum together. With regards to particle export, aggregation enables tiny suspended particles and dissolved material to form larger particles that can then sink. Thus the rate of particle aggregation affects the speed at which material is removed from an area of the ocean [*Burd and Jackson*, 2009]. Marine snow aggregates > 500 µm [*Alldredge and Silver*, 1988] are formed by such aggregation processes when primary inorganic and organic particles, phytoplankton and detritus collide due to Brownian motion, differential settling and fluid shear. Simplistically, the rate at which individual particles aggregate is a function of the concentration of the primary particles, their encounter rate and the probability that upon collision they will stick together [*Kiorboe*, 2001]. As a result marine snow can have a wide range of morphologies and characteristics, from loose associations of small particles to more cohesive assemblages [*Alldredge and Silver*, 1988].

The formation of MSA by aggregation processes has implications for their structure. The arrangement of the primary particles making up the entire marine snow aggregate results in a fractal geometry [*Vicsek*, 1989]. In simplistic terms the fractal nature of the MSA is how much the volume of the primary particles fill the total available volume of

the entire aggregate. Objects can have a maximum of 3 fractal dimensions. Most MSA have a fractal dimension significantly less than 3, meaning the primary particles do not totally fill the available space as defined by the MSA boundary [*Burd and Jackson*, 2009]. The ultimate fractal geometry of a MSA is dependent upon the how the primary particles collided and their stickiness [*Jiang and Logan*, 1991].

Particle stickiness is governed by the particle type, the property of the particle surface and the cellular production of sticky molecules [*Passow and Alldredge*, 1995]. Laboratory studies have indicated that some diatom species are more sticky than others [*Kiørboe et al.*, 1990] and can mediate the compounds that are able to stick to their surfaces [*Waite et al.*, 1995]. Transparent exopolymer particles (TEP) are sticky acidic polysaccharide molecules, which are produced by a diverse group of phytoplankton, in particular diatoms and by bacteria [*Passow*, 2002; *Gardes et al.*, 2011]. Particles of TEP are thought to play a key role in marine snow aggregation processes for example increased TEP concentrations have been noted towards the end of diatom blooms during mass export events [*Passow et al.*, 1994].

The second type of particle responsible for much of the POC export in the ocean are FPs. Early work on sinking particles focussed on FPs, formed as zooplankton repackage sinking carbon into larger particles. Excreted FPs are denser than aggregates and thus sink faster, exporting carbon more efficiently [*Turner*, 2002]. The contribution of FPs to global carbon export is variable [*Dam et al.*, 1995; *Roman et al.*, 2000; *Ducklow et al.*, 2001] ranging between 99 % [*Bishop et al.*, 1977] and 1 % [*Pilskaln and Honjo*, 1987]. The phytoplankton upon which zooplankton feed is important for the formation of FP and their subsequent rate of export [*Turner*, 2002]. When phytoplankton concentrations are higher than the minimum needed to sustain zooplankton energy requirements, zooplankton are thought to undertake 'superfluous feeding' whereby more food is ingested than is physically required and proportionately less is digested. This results in FPs with increased carbon contents [*Conover*, 1966]. However, this phenomenon of superfluous feeding may not occur in all zooplankton species [*Clarke et al.*, 1988]. The volume of the FPs produced linearly increases with the availability of food up to a maximum size which is dependent upon the zooplankton species [*Ayukai and Nishizawa*, 1986; *Butler and Dam*, 1994; *Uye and Kaname*, 1994; *Huskin et al.*, 2000].

1.2.2 Particle degradation

The amount of carbon exported is a balance between particle formation and the destruction or remineralisation processes. Marine snow aggregates are sites of net heterotrophic activity as both bacteria and zooplankton solubilise POC into DOC

[*Kiorboe*, 2000]. They are also sites of elevated bacterial activity in comparison to the surrounding sea water [*Silver et al.*, 1978]. Bacteria within MSA utilise hydrolytic enzymes to solubilise the POC [*Smith et al.*, 1992]. The DOC produced from bacterial solubilisation of MSA can be released to the surrounding waters where it is respired (or remineralised) by free living microbes [*Cho and Azam*, 1988]. The number of bacteria colonising the MSA, which scales with its size [*Kiorboe*, 2000], determines the time taken to remineralise the carbon, ranging between days and months [*Ducklow et al.*, 1982; *Alldredge and Youngbluth*, 1985; *Ploug et al.*, 1999].

Marine snow aggregates are a food source for zooplankton species [*Lampitt*, 1992]. Different zooplankton species show varying affinities for grazing upon MSA [*Kiorboe*, 2000], thus the degree of remineralisation by zooplankton species will be dependent upon the community present. Such grazing processes remineralise POC, utilising it for metabolic processes such as respiration and releasing it as DOC and FPs [*Turner*, 2002; *Steinberg et al.*, 2008b]. Zooplankton remineralisation results in MSA carbon turnover within a few days. Similarly to bacteria, the number of grazers per MSA scales with aggregate size [*Kiorboe*, 2000]. A secondary mechanism whereby zooplankton degrade MSA is via physical fragmentation processes due to pleopod and/or tail movements [*Goldthwait et al.*, 2004]. Furthermore processes such as coprophagy, which includes zooplankton removal of the peritrophic membrane (coprochaly) and/or physical fragment the FPs (coprorhexy) [*Iversen and Poulsen*, 2007], are important mechanisms for FP degradation [*Turner*, 2002].

Both bacterial and zooplankton carbon demands have been shown to be spatially variable. Depending on location, zooplankton carbon demands are either equal to or greater than bacterial carbon demands [*Kiorboe*, 2000; *Steinberg et al.*, 2008b]. Furthermore, the cumulative metabolic carbon demand of bacteria and zooplankton at depths between 150 and 1000 m is thought to be greater than the change in POC flux over the same depth range, suggestive of significant amounts of zooplankton grazing in the surface waters at night [*Steinberg et al.*, 2008b]. Thus much of the particle degradation must occur above 100 m [*Wassmann et al.*, 2004].

1.2.3 Particle sinking speeds

Size, shape and density determine the overall sinking speed of a particle. Individual cells sink at rates between 1 and 30 m d^{-1} [*Smayda*, 1971] whilst MSA and FP sink at speeds between 5 – 2700 m d^{-1} [*Turner*, 2002]. The speed at which MSA and FP sinks in part determines how much remineralisation a particle undergoes, with faster sinking particles undergoing less remineralisation so that more carbon will reach the deep ocean [*Armstrong et al.*, 2009]. Measuring particle sinking speed is difficult. Either

individual MSA and FP need to be collected and their sinking rates measured or interpretations between peak bulk fluxes in sediment trap profiles must be made, to enable the average particle sinking speed to be calculated. The collection and handling of particles may result in damage to their structure which will affect their measured sinking speed [*Alldredge and Gotschalk*, 1988], whilst sinking speeds derived from inferences between peak sediment trap fluxes are dependent on the analytical method of choice [*Xue and Armstrong*, 2009]. The most recent work on particle sinking speeds, using the Indented Rotating Sphere Carousel (IRSC) sediment trap [*Peterson et al.*, 2005], has indicated that globally particle flux can be simplified into a fast (> 326 m d^{-1}) and a slow (0.7 – 11 m d^{-1}) pool of sinking particles [*Alonso-González et al.*, 2010].

Physical parameters including particle size, density and shape characterise individual particle sinking speeds in the ocean. *Alldredge and Gotschalk* [1988] presented a force balance equation (1.1) which states that for any object sinking at a terminal velocity the force of gravity, pulling it down, is balanced by retarding drag forces caused by fluid flow around the object.

$$V(\Delta\rho)g = 0.5C_D A\rho_f U^2 \qquad \text{(Eq. 1.1)}$$

Where V is the volume, $\Delta\rho$ the particle excess density, g is the acceleration due to gravity, C_D the drag coefficient, A the projected area in the direction of sinking and U the sinking speed. Excess density is the effective weight of an object in a fluid. In the ocean, the excess density of a sinking particle is the difference between the particle (ρ_s) and sea water density (ρ_f; equation 2). If the density of an object is greater than the surrounding fluid it is said to be negatively buoyant and will sink [*Denny*, 1993]. Consequently, objects of higher density will sink faster than those of lower density. Eventually however a particle will reach terminal sinking velocity.

$$p_s - p_f \qquad \text{(Eq. 1.2)}$$

The density of sea water is a function of water temperature, salinity and pressure [*Millero and Huang*, 2010] with an estimated global surface range of 1.025 – 1.028 g cm^{-3} [Brown et al., 2001]. Particle density depends upon the constituent parts from which the particle is formed. Typically particles are formed from combinations of particulate organic carbon (POC; density of 1.06 g cm^{-3}), calcium carbonate or particulate inorganic carbon (PIC; density of 2.71 g cm^{-3}), biogenic silica (BSi; density of 2.1 g cm^{-3}) and lithogenic materials (e.g. quartz has a density of 2.65 g cm^{-3}) [*Klaas and Archer*, 2002]. Absolute measurements of MSA density are near impossible to

make since quantification of individual component particles is difficult and complete MSA themselves are too small for individual accurate weight measurements. Therefore, it has been assumed that the density of the organic matter in a MSA is similar to zooplankton FP wet density (which consists of many of the types of particles found in marine snow) and ranges between 1.23 and 1.25 g cm^{-3} [*Alldredge and Gotschalk*, 1988; *De La Rocha and Passow*, 2007].

The drag coefficient (C_D) describes the effect of an objects shape on sinking speed. Objects with smaller C_D are generally more streamlined than those with larger C_D and therefore will sink faster [*Takahashi and Be*, 1984]. Typically C_D is calculated using the particle sinking speed, size and the ratio of the fluid density to viscosity [*Denny*, 1993]. For any object moving through a fluid two drag forces arise to oppose the downward motion; pressure and viscous drag. The movement of water molecules away from the leading edge of the sinking particle and their subsequent movement back behind the particle after it has passed forms pressure drag. Thus it is affected by the particles projected area in the direction of sinking [*Vogel*, 1994]. Viscous drag is dependent on the particles surface area and arises because molecules of water stick to an objects surface and so have no relative motion (the no slip condition). As distance from the particle surface increases the relative velocity of the adjacent water molecules increases due to shear stresses [*Mann and Lazier*, 1996; *Berdalet and Estrada*, 1997]. For small objects such as sinking particles, it is mainly viscous forces that govern their sinking velocity [*Mann and Lazier*, 1996].

The surface area of marine particles is determined by their fractal geometry and porosities. *Johnson et al.* [1996] showed fractal aggregates have increased sinking speeds compared to non fractal aggregates. This is due to the heterogeneous distribution of primary particles within the aggregate, increasing the porosity of the particle and reducing the viscous drag in relation to the cross sectional surface area. Fractal aggregates increase their porosity as a function of increasing size [*Meakin*, 1987; *Gregory*, 1997]. The permeability (connectivity of the aggregate pores) of a fractal aggregate is related to the distribution of primary particles constituting the entire aggregate. By definition the component particles of a fractal aggregate must themselves be composed of smaller fractal particle clusters, which have relatively smaller permeability than the whole aggregate [*Li and Logan*, 1997; *Li and Logan*, 2001].

The fractal nature, thus porosity of aggregates is also important for determining the overall particle density. In effect the porosity of a particle is a measure of the fraction not occupied by solid matter and is estimated to be ~ 99 % of the total particle volume [*Alldredge and Gotschalk*, 1988]. Thus the greater the porosity the less dense a particle

will be, assuming the pores are not clogged with other molecules. Particles such as TEP can fill the pore spaces of aggregates and, due to their density which is significantly lower than sea water (0.7 – 0.84 g cm^{-3}), may result in neutrally buoyant or even ascending particles [*Azetsu-Scott and Passow*, 2004].

1.3 Measuring and predicting particle export

Both direct and indirect methods for measuring particle export are available. Traditionally the amount of nitrate brought to the surface ocean by winter mixing (new production) was thought to be balanced by the export flux of organic material [*Eppley and Peterson*, 1979; *Christian et al.*, 1997]. However, measuring export through nutrient flux to the surface has not been widely applied across the ocean due to disagreement between the absolute magnitudes of new and total production measurements based on upward fluxes of ^{3}He and direct measurements of net primary production using O_2 [*Jenkins*, 1982; *Jenkins and Goldman*, 1985; *Hayward*, 1991]. Another indirect method for measuring particle export is based on the assumption that the amount of primary production fuelled by nitrate uptake should be proportional to the amount of carbon export occurring in a particular area of the ocean. The methodology, developed by *Eppley and Peterson* [1979], requires at-sea incubation experiments using the stable isotope ^{15}N to label molecules of nitrate ($^{15}NO_3^{2-}$). These $^{15}NO_3^{2-}$ labelled molecules are then assimilated into the actively growing cells via photosynthesis. Thus the rate of uptake of the $^{15}NO_3^{2-}$ enables calculations of production.

The final, perhaps more commonly used, indirect method to measure particle, export is via the use of radioactive tracers such as Thorium-234 (^{234}Th) and Polonium-210 (^{210}Po). Both ^{234}Th and ^{210}Po are particle reactive and stick to the surface of particulate matter. Any particles sinking through the water column will remove the ^{234}Th and ^{210}Po stuck to their surface creating a measurable deficit compared to the predicted concentration of ^{234}Th and ^{210}Po based on the radioactive decay of their parent molecules (uranium / lead respectively; Figure 6.1). If measurements of the of POC: ^{234}Th / ^{210}Po ratio are made, the flux of that particulate phase can be calculated from the observable deficit of radionuclide in the ocean [*Buesseler et al.*, 1993; *Sarin et al.*, 1999; *Stewart et al.*, 2005; *Van der Loeff et al.*, 2006; *Verdeny et al.*, 2008; *Verdeny et al.*, 2009].^{234}Th has a short half life (24.1 days) and is used to measure monthly export fluxes whilst ^{210}Po has a longer half life (138.4 days) and can be used to measure seasonal fluxes [*Verdeny et al.*, 2008; *Verdeny et al.*, 2009].

The drawback to using indirect methods is that no information about the particle properties such as sinking speeds, porosity, mass and density can be obtained. To measure these properties the export flux must be quantitatively collected and measured. Tethered sediment traps are the traditional tool used to collect sinking particulate material. However, comparison between tethered sediment trap and radionuclide fluxes have indicated a mismatch in flux estimates made within the top 1000 m. Such mismatches have been attributed to factors such as water flow across the mouth of the sediment trap, preventing particles from entering the collecting funnel, and remineralisation of trapped material within the collection pot due to the presence of actively swimming species [*Scholten et al.*, 2001]. Hence, tethered sediment traps are now generally restricted to measuring deep (> 1000 m) ocean fluxes, where remineralisation is lower [*Honjo and Manganini*, 1993; *Antia et al.*, 2001]. Neutrally buoyant sediment traps such as PELAGRA (Figure 6.1; [*Lampitt et al.*, 2008]) have now been developed, which are able to drift with the prevailing currents and water masses, thus significantly reducing hydrodynamic losses of sinking particles from the top of the sediment trap funnel [*Buesseler et al.*, 2007a].

Although tethered and neutrally buoyant sediment traps are good tools for measuring bulk fluxes and particle mass they cannot easily measure individual particle properties such as sinking speed or size. Recent developments in sediment trap technology have enabled the bulk flux to be separated into smaller fractions for which the settling speeds can be measured, but this approach does not still allow individual particle measurements to be made [*Peterson et al.*, 1993; *Peterson et al.*, 2005]. To measure individual particles, equipment such as polyacrilyamide gels must be deployed which trap and preserve individual sinking particles into a viscous medium for later image analysis [*Ebersbach and Trull*, 2008]. Similarly, the Marine Snow Catcher (MSC) can be deployed to collect individual sinking particles from large volumes of water for image analysis [*Lampitt et al.*, 1993]. In coastal waters divers have been deployed at shallow depths to manually collect large sinking marine snow aggregates [*Alldredge and Gotschalk*, 1988]. This latter option is impractical in open water regions of the ocean and at depths greater than a few meters. The overall problem with the current techniques to collect individual sinking particles is that they do not provide any information about bulk fluxes or geochemical properties

1.3.1 Predicting flux attenuation

The most widely used quantitative expression predicting the rate of carbon attenuation with depth is the *Martin et al.* [1987] parameterisation (Equation 1.3).

$$F(z) = F(z_0) \cdot \left(\frac{z_0}{z} \right)^b \quad \text{(Eq. 1.3)}$$

Where *F(z)* is the predicted flux at some depth (*z*), $F(z_0)$ is the measured flux at a reference depth (z_0) and *b* is the exponential parameter predicting the rate of attenuation. Simplistically this relationship is a power law expression predicting the unmeasured flux at some depth within the water column, from a measured flux at a reference depth. The original formulation based on tethered sediment trap measurements estimated *b* at 0.858. Recent advances in flux measurement technology, utilising neutrally buoyant sediment traps and satellite observational data (based on chlorophyll, sea surface temperature and incident light levels at the surface) have shown *b* to be spatially variable, ranging between 0.3 to 1.33 [*Lampitt et al.*, 2008; *Buesseler and Boyd*, 2009; *Henson et al.*, 2012]. These recent observations of variability in *b* and alternative mathematical expressions [*Armstrong et al.*, 2002; *Francois et al.*, 2002; *Howard et al.*, 2006] have led to the applicability of the Martin curve as a parameterisation for flux attenuation to be questioned.

1.3.2 The ballast hypothesis

Armstrong et al. [2002] first noted that POC fluxes are empirically linked in a quantitative relationship to biomineral fluxes. They suggested some fraction of the POC flux may be protected from remineralisation by the biomineral flux (Figure 1.2). Protection may occur either internally due to the formation of biomineral tests [*Lowenstam and Weiner*, 1989] or externally due to organic matter adsorption into the physical structure of inorganic material [*Lawrence*, 1994]. This led to the development of a mechanistic based model whereby POC fluxes are determined by biomineral fluxes. *Francois et al.* [2002] also developed an alternative model to the Martin *et al.* [1987] flux parameterisation. Their algorithm predicts > 80 % of the global variability in carbon flux transfer efficiency (i.e. how efficiently carbon is exported between two depths) based on the carbonate flux to the deep ocean. A similar relationship with biogenic opal was not found which led to the conclusion that regions of the ocean that are opal dominated, have lower transfer efficiencies than regions of the ocean which are calcium carbonate dominated. Thus the phytoplankton community present may have important implications for carbon export.

Following on from the studies by *Armstrong et al.* [2002] and *Francois et al.* [2002] came the formulation of the 'ballast hypothesis'. It was observed that fluxes of organic carbon are tightly correlated with fluxes of dense biominerals ($CaCO_3$ and opal produced by coccolithophores and foraminifera, and diatoms respectively) and

lithogenic particles [*Klaas and Archer*, 2002] in deep (> 1000 m) global sediment trap data sets (Figure 1.3). This relationship has also been extended to the surface ocean [*Sanders et al.*, 2010].

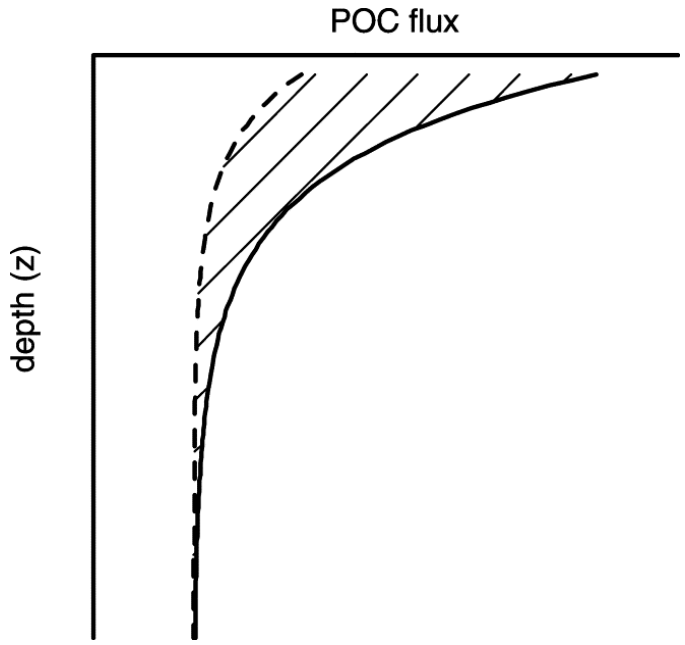

Figure 1.2 Schematic representation of the attenuation of the total POC flux (solid black line) and the biomineral protected POC flux (dashed line). The hatched area represents the POC excess within the water column that can be measured directly. Figure taken from *Armstrong et al.* [2002]

However, observed correlations do not confirm a causal relationship between sinking speed and biomineral content. It is still unknown whether POC fluxes are driven by mineral ballasting or whether POC may 'stick' together biominerals that are too small to sink on their own into larger more rapidly sinking particles [*De La Rocha and Passow*, 2007]. Laboratory studies using roller tanks to produce artificial MSA have indicated that increasing biomineral content resulted in smaller total MSA size and a decreasing POC: biomineral ratio to a constant 5 % (weight per weight [*Hamm*, 2002; *Passow and De La Rocha*, 2006]. This may reflect the carrying capacity of POC in the ocean suggesting that POC 'sweeps' up biomineral phases gluing them together until a sufficient density is reached to be able to sink [*Passow*, 2004].

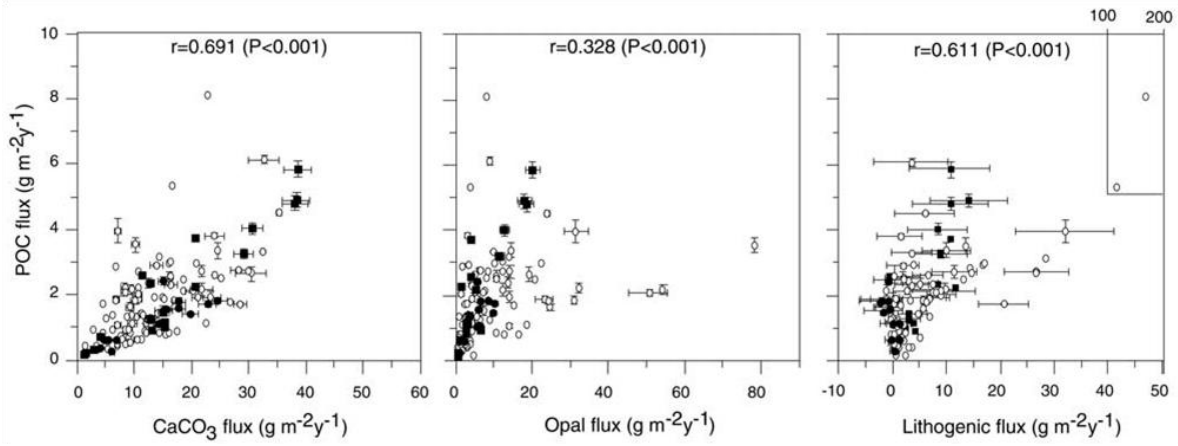

Figure 1.3 Correlative relationships between POC and $CaCO_3$, opal and lithogenic fluxes in deep ocean sediment traps taken from *Klaas and Archer* [2002]. Error bars represent 1 standard deviation. Black circles indicate data where samples have been corrected for the remineralised / dissolved phases. Open circles indicate data where this correction has not been applied.

1.4 Motivation and aims of the thesis

There were three motives for this study. Firstly, was the need to better understand the processes influencing individual particle sinking speeds. Much of the recent research has focussed solely on density driven carbon export in the light of the seminal papers by *Armstrong et al. [2002], Francois et al. [2002],* and *Klaas and Archer* [2002]. However, it is well known that particle size also plays a key role in determining particle sinking speeds [*Johnson et al.*, 1996]. Therefore, there is clearly a need for a more holistic approach examining both the influence of particle size and density on particle sinking speeds, thus carbon export.

Many measurements of particle flux examined bulked particles collected in either sediment traps or in large volume filtration systems [*Buesseler et al.*, 1993; *Peterson et al.*, 1993; *Buesseler et al.*, 2000; *Peterson et al.*, 2005; *Lampitt et al.*, 2008]. Although these are beneficial for analyses of bulk flux properties such as POC, PIC, BSi and sinking speeds (if using the Indented Rotating Sphere Carousel IRSC sediment trap) they are not informative for individual particle properties such as size, sinking speeds or taxonomic composition. The MSC (the equipment of choice in this study) has previously been used to collect individual sinking MSA and FP to examine individual particle properties [*Lampitt et al.*, 1993]. However, the methodology has not been developed to calculate bulk fluxes from each deployment. The second motivation for this study focused on the need to be able to examine both individual MSA and FP exported out of the euphotic zone, thereby simultaneously quantifying bulk fluxes.

The third motivation for this study was to examine the relative contribution of fast and slow sinking particles and the processes influencing their export to depth. Biominerals produced by both coccolithophores and diatoms are potentially important for facilitating the transfer of organic carbon to depth in the ocean, protecting the organic matter and influencing the transfer efficiency of carbon to depth [*Armstrong et al.*, 2002; *Francois et al.*, 2002; *Klaas and Archer*, 2002]. However, how these processes relate to the fast and slow sinking pools of particles is unclear.

Two research cruises were undertaken to investigate these three motivations. The first in 2009 to the Porcupine Abyssal Plain (PAP) site focussed on carbon export from the upper ocean (50 m) into the mesopelagic. The second cruise occurred in 2010 to the Arctic Ocean (Svalbard), with the aim of improving the understanding of how changes in sea ice conditions may influence Arctic ecosystems and carbon export. On both cruises the MSC was deployed multiple times to collect individual sinking particles in order to measure their characteristics (including sinking speed, size and the coccolithophore and diatom community composition) and estimate bulk POC fluxes.

The individual aims of this thesis were to:

1) Investigate the sensitivity of individual particle sinking speeds to changes in particle excess density and diameter.
2) Develop and test a methodology to measure bulk export fluxes using the MSC.
3) Investigate the magnitudes of POC fluxes in various marine settings using the marine snow catcher.
4) Investigate the depth to which the fast and slow flux penetrates into the interior of the ocean.

1.5 Thesis outline

Chapter 2 describes the relative influence of particle size and density on sinking rates. Particles were collected from both the Porcupine Abyssal Plain (PAP) site and the Arctic in summer 2009 and 2010 respectively. The sensitivity of particle sinking speed to changes in particle size and density are explored with the use of a manipulated Stokes Law equation, parameterising particle size, density, shape and roundness. The results are discussed in the context of carbon export and future climate change.

Chapter 3 describes the observations of total particulate organic carbon (POC), particulate inorganic carbon (PIC) and biogenic silica (BSi) fluxes measured at the PAP site using the Marine Snow Catcher during summer 2009. Fluxes are defined in terms of a fast and slow sinking pool. The novel calculations presented in the chapter are

fully validated via comparison with concurrent, independent estimates of POC flux. The results are discussed in the context of particle formation, POC supply to the abyss and biomineral ballasting. This chapter has been published as:

Riley, J. S., Sanders, R., Marsay, C., Le Moigne, F., Achterberg, E. P., and Poulton, A. (2012), The relative contribution of fast and slow sinking particles to ocean carbon export, *Global Biogeochemical Cycles*, 10.1029/2011GB004085.

Chapter 4 examines the contribution of coccolithophores and diatoms to fast and slow sinking POC fluxes at the PAP site. Flux samples were collected using the MSC and neutrally buoyant sediment traps and were taxonomically examined. The results are discussed in the context of the penetration of the slow flux into the mesopelagic and the role of coccolithophores and diatoms in fluxes to the deep ocean.

Chapter 5 presents flux data collected in the Arctic Ocean (near Svalbard), in both open water and ice covered environments. Fluxes are broken into their constituent fast and slow sinking pools, following the equations derived in chapter 3. The results are discussed in the context of the magnitudes of the fast and slow fluxes in the Arctic Ocean and the role of primary productivity in sustaining these fluxes.

Chapter 6 aims to provide an overarching summary of the previous four chapters including comparisons of the fast and slow fluxes between the PAP site and Arctic regions and explore the potential controls on the magnitude of the fast and slow sinking fluxes as a guide for future areas of research.

Chapter 2: The influence of particle size and density on carbon export

2.1 Abstract

Marine snow aggregates sink through the water column and transfer particulate organic carbon (POC) from the surface to the deep ocean, thereby regulating atmospheric CO_2 concentrations. Both particle size and density influence sinking speeds. However, it is unclear whether the observed variability in sinking rates is more strongly influenced by natural variability in particle size or density. In order to investigate the effects of size and density on particle sinking speed two types of particle were collected between 50 – 400 m in the North Atlantic and Arctic Oceans which included: Marine Snow Aggregates (MSA; n = 106, sinking speed (U) = 124 (± 101) m day^{-1}, equivalent spherical diameter (ESD) = 683 (± 347) µm, excess density (XSD) = 0.009 (± 0.0009) g cm^{-3}) and Aggregate Protist Complexes (APC; n = 6, U = 280 (± 150) m day^{-1}, ESD = 836 (± 257) µm, XSD = 0.04 (± 0.02) g cm^{-3}) which resembled MSA with a distinct biomineral centre (numbers are averages with standard deviations). Only particle size was positively correlated with sinking speed (Spearman's Rank correlation coefficient 0.2, $p < 0.01$), suggesting particle size played a more significant role in regulating sinking speed than density. Theoretical calculations suggest that APC sinking speeds are more sensitive to observed changes in excess density than size, suggestive of a ballasting effect. However, MSA sinking speeds are more sensitive to observed changes in particle size than density. Thus density controls over sinking rate are more important for particles of higher density. Extrapolation of the particle size spectrum into the range typical of the deep ocean indicates the relative importance of density increases with depth as particles get smaller. It is suggested that the importance of the ballast effect increases with depth in the ocean as particles become smaller due to remineralisation processes. In the surface ocean the ballast effect is of secondary importance to particle size in determining particle sinking speeds. This work highlights key areas on which future research should focus to elucidate the influence of particle size and density on sinking speeds.

2.2 Introduction

The biological carbon pump transports carbon from the surface to the abyssal ocean [*Boyd and Trull*, 2007]. The estimated magnitude of particulate organic carbon (POC) export is between 5 and 11 Gt C y^{-1} [*Laws et al.*, 2000; *Henson et al.*, 2011]. However, mesopelagic remineralisation results in only ~ 1% of the exported POC reaching the deep (depths below 1 km) ocean [*Poulton et al.*, 2006]. Once in the deep ocean, the carbon is sequestered away from the atmosphere for hundreds to thousands of years [*Buesseler et al.*, 2007b]. Particle sinking speeds control the transit time through the mesopelagic, thus influencing the degree to which POC is remineralised [*Armstrong et al.*, 2009].

Fast sinking particles which contain carbon, such as marine snow aggregates (MSA), are thought to be the main vector for carbon transfer to the deep ocean [*Alonso-González et al.*, 2010; *Riley et al.*, 2012]. Marine snow aggregates are ubiquitous throughout the ocean and contribute significantly to POC fluxes. MSA may be composed of individual organisms and / or aggregated highly degraded detritus [*Alldredge and Gotschalk*, 1988]. The speed at which MSA sink is reported to range from 16 to 386 m day^{-1}, depending on their composition, size and density [*Turner*, 2002]. However, it is unclear how particle size and density influence the variability in MSA sinking speeds.

Particle size, density and porosity are key factors influencing particle sinking speed [*De La Rocha and Passow*, 2007]. In order to sink a particle must be large enough to overcome the viscous drag imparted by the surrounding seawater. This is mathematically described by the Reynolds number (Re) of a particle. Re is the ratio of inertial forces to viscous forces acting upon a particle, and for most marine snow aggregates Re varies between 1 and 20 [*Alldredge and Gotschalk*, 1988]. The smaller a particle the greater the viscous force it will experience and the slower its sinking speed (for a full discussion of viscous forces on particles refer to *Mann and Lazier* [1996] and the references therein). Observations of the size spectra of particles in the ocean suggest that sizes can range between 1 µm and 1 m, and that small particles (150 – 500 µm) become relatively more abundant with depth [*Sheldon et al.*, 1972; *Stemmann et al.*, 2002].

In addition to being of sufficient size to sink a particle must have a density in excess of seawater [*Mann and Lazier*, 1996]. Marine snow aggregates have a fractal geometry [*Vicsek*, 1989] formed by coagulation of smaller particles [*Jackson and Burd*, 1998]. Fractal dimensions describe, by an exponential function, the relationship between the

mass and radius of the particle as a whole and the mass and radius of all the individual component particles in the particle. Thus the density of an MSA is in part determined by its fractal dimension (which usually ranges between 1.3 and 2.3) and the constituent particles from which it forms [*Burd and Jackson*, 2009]. These fractal dimensions relate to the porosity of the particle which is thought to be > 95 % in the surface ocean. Thus, the density of a particle is a function of the fraction of the particle not occupied by solid matter and the density of the constituent particles themselves [*Alldredge*, 1998].

The density or specific gravity of the most common organic constituents of POC, such as proteins and amino acids, are very close to that of seawater [*Francois et al.*, 2002], so enhancement of particle density ('ballasting') via incorporation of biomineral or lithogenic materials is needed to enhance sinking rates [*Klaas and Archer*, 2002; *Sanders et al.*, 2010]. The POC:biomineral flux ratio decreases from ~ 4 in the euphotic zone to < 1 below 500 m [*Koeve*, 2002], thereby increasing the relative abundance of biominerals with depth, which by inference would increase the particles density assuming the porosity and fractal nature of the particle remained constant with depth.

Stokes' Law (Eq. 2.1) is the traditional expression used to describe particle sinking speed as a function of its size and density. Stokes' Law is only valid for situations where viscous forces dominate, and Reynolds numbers (Re) are < 0.5 [*Alldredge and Gotschalk*, 1988]. Therefore Stokes' law, which is based on observations of spherical particles, does not describe the sinking speeds of fractal aggregates very well [*Johnson et al.*, 1996; *De La Rocha and Passow*, 2007].

$$U = (1 - P)\frac{2}{9}\frac{gr^2(\Delta\rho)}{\mu} \qquad \text{(Eq. 2.1)}$$

Where U is the particle sinking speed, P is the porosity, g is the acceleration due to gravity, r is the particle radius, $\Delta\rho$ is the particle density in excess of sea water and μ is the dynamic viscosity of seawater. Prediction of aggregate sinking velocities using Stokes Law is complicated by the fractal nature of the particles and the fact that most particles are not spherical [*Logan and Wilkinson*, 1990; *Jiang and Logan*, 1991].

Alternative mathematical expressions of particle sinking speed describe a balance between the gravitational forces, causing the particle to sink (including density) and viscous forces (which account for the particle shape via the parameter drag coefficient (C_D)), slowing the descent of the particle [*Alldredge and Gotschalk*, 1988]. However the C_D of an MSA is difficult to measure and is therefore empirically derived from the

particle sinking speed. This leads to an impasse in which sinking speed is calculated from a term derived from sinking speed. Therefore application of the *Alldredge and Gotschalk* [1988] equation to predict sinking speeds is inappropriate.

Dietrich [1982] developed an empirical equation, accounting for the effects of size, density, shape and roundness, on the settling velocity of particles without invoking the C_D (Equation 2.2).

$$U = 1.71E^{-4} \times \sqrt[3]{\left[\frac{\Delta\rho^2 \times g^2 \times ESD^6}{\rho_f{}^2 \times k\upsilon^2}\right] \times \left[\frac{\Delta\rho \times g \times k\upsilon}{\rho_f}\right]} \qquad \text{(Eq. 2.2)}$$

ESD is the particle equivalent spherical diameter (in mm), Δp is the fluid density and $k\upsilon$ is the kinematic viscosity of seawater. This equation may be preferential to the Stokes' Law equation in situations where the Reynolds number is > 0.5. For most MSA, where Re ranges between 1 and 20 [*Alldredge and Gotschalk*, 1988], Stokes' Law cannot be applied to predict sinking speeds. Therefore, application of Dietrich's [1982] (Equation 2.2) to describe particle sinking speeds as a function of size and density is preferable to the Stokes' Law or *Alldredge and Gotschalk* [1988] equation.

Insights into the processes determining particle sinking speeds is important for the understanding of organic carbon export and carbon sequestration. Predicted changes in phytoplankton community structure, towards smaller species [*Bopp et al.*, 2005] and potential changes in rates of biomineral formation [*Riebesell and Tortell*, 2011] may impact particle size and density, thus sinking speeds and associated carbon export between the surface and deep ocean. Consequently, the aim of this chapter is to examine whether variations in particle size or density play a more significant role in determining particle sinking speed. In order to achieve this aim a sensitivity analysis will be undertaken to understand how different particle properties, with an emphasis on particle size and density, will affect MSA sinking speeds using Dietrich's [1982] equation. These results will be discussed in the context of oceanic carbon export.

2.3 Methods

2.3.1 Particle collection

Particles were collected during two cruises, D341 on RRS *Discovery* at the Porcupine Abyssal Plain (PAP) site (49°N 16.5°W; July – August 2009) and JR219 on RRS *James*

Clark Ross in the region between Svalbard and Greenland (~80°N; June – July 2010). All particles were collected using a Marine Snow Catcher (MSC) [*Lampitt et al.*, 1993]. At the PAP site particles were collected from 50 m depth and divided into Marine Snow Aggregates (MSA) and Aggregate Protist Complexes (APC, consisting of a MSA with a distinct protist centre; Figure 2.1) using microscopy. Arctic particles were collected from depths between 50 – 400 m and were only MSA. The Arctic and PAP site MSA particles were grouped together for statistical analysis.

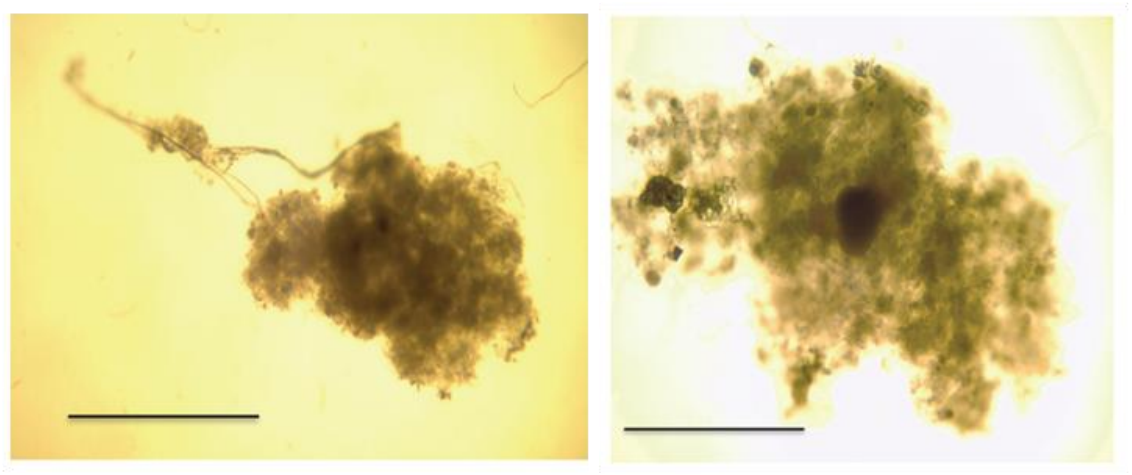

Figure 2.1 Examples of marine snow particles. (Left) Marine Snow Aggregate (MSA); (Right) Aggregate Protist Complex (APC). The scale bar in each figure is 1 mm.

2.3.2 Water density and kinematic viscosity

In order to utilise Dietrich's equation to predict particle sinking speeds the values for the density and kinematic viscosity of the fluid in which the particles were settling needed to be defined. Both the density and kinematic viscosity of water are sensitive to changes in temperature, with lower temperature waters such as those in the Arctic (~ 0°C) having higher densities than those at the PAP site (~ 15°C). Denser waters will result in slower particle sinking speeds. This study assumed a water density of 1.0267 g cm^{-3}, an average of PAP (1.0264 g cm^{-3}) and Arctic (1.027 g cm^{-3}) values and a kinematic viscosity of 0.014 cm^{-2} s^{-1} taken as an average of PAP (0.012 cm^{-2} sec^{-1}) and the Arctic (0.016 cm^{-2} sec^{-1}) kinematic viscosities [*Kaye and Laby*, 1995]. It must be noted that using these average values to estimate particle sinking speeds as a function of size or density may result in an over or under estimation of particle sinking speeds. A sensitivity analysis of particle sinking speed to variability in water density and kinematic viscosity was undertaken to assess the impact of using average values.

2.3.3 Particle sinking speeds and equivalent spherical diameters

The sinking rates and equivalent spherical diameters (ESD) of 62 MSA and 6 APC from the PAP site and 44 MSA from the Arctic were measured. Sinking speeds (m day^{-1}) were recorded in a 2 L glass measuring cylinder, filled with surface sea water kept at a constant temperature close to the ambient surface water temperature (15°C for PAP, 5°C for Arctic) [*Martin et al.*, 2010]. Particles at the PAP site were photographed using a Meiji Techno Japan MX microscope and Infinity 1 camera. In the Arctic, particles were imaged using a Brunel SP-95-I inverted microscope (x4 magnification) with an Olympus digital camera. The ESD was determined from the projected two dimensional particle areas measured in the digital images using Image J software [*Abramoff et al.*, 2004]. (See Chapter 3, section 3.3.3 for more details on particle collection methods).

2.3.4 Particle porosity and density

The density of MSA was calculated as a weighted function of the particle porosity (assuming that the pores were filled with ambient sea water) and the density of solid organic matter (assumed to be 1.24 g cm^{-3}, an average of 1.23 g cm^{-3} and 1.25 g cm^{-3} as quoted in the literature [*Alldredge and Gotschalk*, 1988; *De La Rocha and Passow*, 2007]). In the literature the porosity of particles is assumed to be 99 % in the surface ocean [*Alldredge*, 1998]. Assuming 1 % organic matter (ranging between 1.23 g cm^{-3} and 1.25 g cm^{-3}) and 99 % porosity, the calculated density and excess density of the particle is 1.029 (± 0.0001) and 0.002 (± 0.0001) g cm^{-3}, assuming a sea water density of 1.0265 g cm^{-3} (an average of the PAP and Arctic water densities, Table 2.1).

% Porosity	% OM	Minimum Weighted Density (g cm^{-3})	Maximum Weighted Density (g cm^{-3})	Average Weighted Density (g cm^{-3})	SD	Average Excess Density (g cm^{-3})	SD
99	1	1.029	1.029	1.029	0.0001	0.002	0.0001
98	2	1.031	1.031	1.030	0.0003	0.004	0.0003
97	3	1.032	1.033	1.033	0.0004	0.006	0.0004
96	4	1.035	1.035	1.035	0.0006	0.009	0.001
95	5	1.037	1.038	1.037	0.0007	0.011	0.001

Table 2.1 Maximum, minimum and average standard deviation values of MSA given the range of potential percentage porosity and organic matter contents. The minimum density calculation assumes an organic matter density of 1.23 g cm^{-3} [*Alldredge and Gotschalk*, 1988] and the maximum density calculation assumed an organic matter density of 1.25 g cm^{-3} [*De La Rocha and Passow*, 2007]. The units are in g cm^{-3}. The underlined data indicates the density values which best reproduce the particle sinking speeds when applied to the Dietrich [1982] equation.

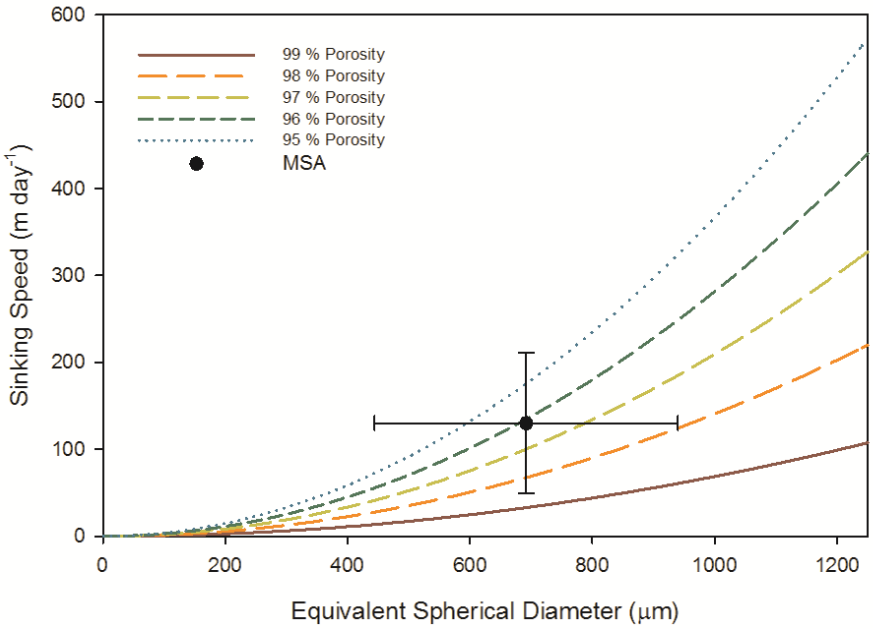

Figure 2.2 The coloured lines indicate particle sinking speed, calculated following equation 2.2, as a function of ESD for the given range of excess densities and therefore porosities (table 2.1). Superimposed are the average ESD and sinking speed measurements (with standard deviations) of MSA taken from both Arctic and PAP site MSA particles.

In order to verify if this assumed 99 % porosity is accurate *Dietrich's* [1982] equation (Equation 2.2) was utilised to predict the particle sinking speed as a function of ESD (Figure 2.2), assuming a constant excess density of 0.002 g cm^{-3} (Table 2.1). Superimposing the mean observed ESD and sinking speeds for the MSA onto this plot estimation of whether modelled sinking speeds accurately reproduced the observed sinking speeds can be undertaken, and by extension validating the estimated porosity. It was found that an assumed 99 % porosity underestimated the sinking speeds. This suggests that for the sampled particles, based on the assumption that the pores are filled with ambient sea water, the porosity must be somewhat lower than 99 %, resulting in a higher density and faster sinking speed. Alternatively the equation may not be suitable for estimating particle porosity. However, since predicted particle sinking speeds are similar to those observed, this latter possibility is rejected.

To determine a more accurate porosity (and thus density), multiple ESD were plotted versus sinking speed curves (Figure 2.2), using a range of densities based on porosities varying between 99 – 95 % and the maximum (1.25 g cm^{-3} [*De La Rocha and Passow*, 2007]) and minimum (1.23 g cm^{-3} [*Alldredge and Gotschalk*, 1988]) possible densities for organic matter (Table 2.1). Comparing the predicted sinking speeds to those observed it was found that a porosity of ~ 96 % reproduced the observed sinking speeds most accurately. This value of 96 % porosity, gave an organic matter density of

1.035 (± 0.0006) g cm^{-3} and an excess density of 0.009 (± 0.001) g cm^{-3} for the marine snow aggregate particles in this study (Table 2.1 underlined).

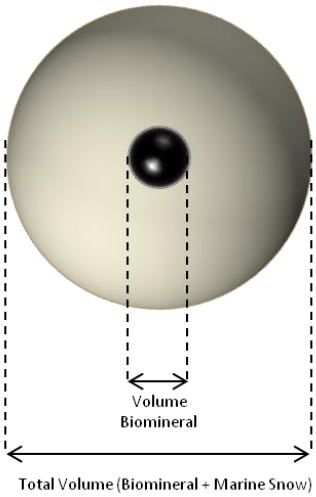

Figure 2.3 Schematic representation of APC particle. Black centre is the biomineral and surrounding grey is the enveloping marine snow.

Aggregate protist complex densities were calculated as a weighted function of the density of the central biomineral test (assumed to be an empty foraminifera test with a density of 2.71 g cm^{-3} [*Smayda*, 1971]) and surrounding marine snow (Figure 2.3). The density of the marine snow was assumed to be 1.035 g cm^{-3}, with 96 % porosity (Table 2.2). The total density of the APC was calculated as a weighted function of the fraction biomineral volume and fraction marine snow volume. The volumes were estimated from the 2D areas measured using the Image J software [*Abramoff et al.*, 2004]. The area measurements were then converted into equivalent spherical volumes (ESV).

ESV Biomineral (mm^{-3})	ESV Marine Snow (mm^{-3})	Total ESV (mm^{-3})	Fraction Marine Snow	Fraction Biomineral Centre	Density of biomineral	Marine Snow Density (g cm^{-3})	Weighted Density (g cm^{-3})	Excess Density (g cm^{-3})
0.03	1.54	1.6	0.98	0.02	2.71	1.035	1.07	0.04
0.04	2.21	2.2	0.98	0.02	2.71	1.035	1.06	0.04
0.01	1.66	1.7	0.99	0.01	2.71	1.035	1.05	0.02
0.01	1.92	1.9	0.99	0.01	2.71	1.035	1.05	0.02
0.01	0.98	1.0	0.99	0.01	2.71	1.035	1.06	0.03
0.01	0.18	0.2	0.97	0.03	2.71	1.035	1.09	0.06
Average							1.06	0.04
Standard Deviation							0.02	0.02

Table 2.2 Individual measurements of APC biomineral centre and surrounding marine snow to calculate the weighted density and excess density (assuming a water density of 1.026 g cm^{-3}).

2.4 Results

2.4.1 Sinking speed and ESD

	PAP MSA	Arctic MSA	APC
Sinking Speed (m d^{-1})	162 (± 74)	86 (± 69)	280 (± 150)
ESD (µm)	736 (± 236)	631 (± 255)	836 (± 257)
Density (g cm^{-3})	1.035 (± 0.0006)	1.035 (± 0.0006)	1.06 (± 0.02)
Excess density (g cm^{-3})	0.009 (± 0.0006)	0.009 (± 0.0006)	0.04 (± 0.02)

Table 2.3 MSA and APC measured and estimated particle properties.

The mean sinking speed (with propagated standard deviation) of all MSA from both locations and APC from the PAP site were 124 (± 101) m day^{-1} and 280 (± 150) m day^{-1} respectively. MSA and APC sinking speeds were significantly different (log transformation, Student t-test, $p < 0.36$). The mean ESD for PAP and Arctic MSA was 683 (± 347) µm and for APC 836 (± 257) µm, and were not significantly different (Table 2.3; see appendix A.1, tables A.1 and A.2 for full data tables of ESD).

2.4.2 Particle density and excess density

In total 6 APC particles were imaged and the fraction biomineral and surrounding organic matter was measured, enabling the calculation of an average density and excess density of 1.06 (± 0.02) and 0.04 (± 0.02) g cm^{-3} respectively (Table 2.3). Calculated density and excess density values for MSA were 1.035 (± 0.0006) and 0.009 (± 0.0006) g cm^{-3} respectively, assuming a 96 % porosity (Table 2.1; see appendix A.1, tables A.1 and A.2 for full data tables of sinking speeds).

2.4.3 Calculated particle sinking speeds

The calculated sinking speeds based on *Dietrich* [1982] (Equation 2.2, Figure 2.2 and 2.5) show that sinking speed increased as a function of increasing excess density or ESD, when all other variables are held constant. Hence small particles sink slower than larger particles with the same density, whilst less dense particles sink slower than denser particles of the same size. Comparison of the calculated sinking speeds with the observed sinking speeds indicates equation 2.2 successfully predicted the particle observed sinking speeds.

2.5 Discussion

2.5.1 Limitations and assumptions

Before discussing the results in the context of how particle size and density control sinking speeds with depth in the ocean the potential limitations and assumptions applied to the methods applied in this study need to be identified. Firstly, MSA were grouped from two different environments into a single class of particles. This assumed that there were no significant differences between the constituent particles forming the MSA in the two environments. This was chosen for two reasons, firstly the MSA in the Arctic appeared morphologically similar to those at the PAP site and secondly grouping the samples from two sites together enabled examination of a larger and more statistically robust data set.

As a result of this grouping average fluid density values had to be used in equation 2.2. In order to assess how sensitive predicted sinking speeds may be to these average values utilised *Dietrich's* [1982] settling velocity equation. Two simulations were run assuming particle excess density is 0.009 g cm^{-3} and ESD is 683 μm, i.e. the mean values presented for MSA from the PAP site and Arctic. The first simulation applied a water density of 1.0264 g cm^{-3} (PAP site), resulting in a sinking speed of 141.1 m day^{-1}. Comparatively the second simulation using a water density of 1.027 g cm^{-3} (Arctic) resulted in a sinking speed of 141.02 m day^{-1}. Thus within the constraints of the equation 2.2, using an average water density value of 1.0267 g cm^{-3} does not greatly affect the calculated sinking speed values, and the choice of averaging two water density values is robust.

A similar sensitivity analysis was undertaken to determine how sensitive sinking speeds were to changes in the kinematic viscosity of sea water. Again two simulations were run with an assumed particle excess density is 0.009 g cm^{-3} and ESD is 692 μm, i.e. the mean values presented for MSA from the PAP site and Arctic. The first simulation applied a kinematic viscosity of 0.012 cm^{-2} s^{-1} (PAP site), resulting in a sinking speed of 164.5 m d^{-1}. Comparatively, the second simulation using a kinematic viscosity of 0.016 cm^{-2} s^{-1} (Arctic) resulted in a sinking speed of 123.4 m day^{-1}. Thus within the constraints of the equation 2.2, using an average kinematic viscosity of 0.014 cm^{-2} s^{-1} results in a difference in sinking speed of ± ~ 20 m d^{-1}. This is smaller than the range and standard deviations of the observed sinking speeds but larger than the range of sinking speeds driven by changes in water density.

A final sensitivity analysis was undertaken to determine how sensitive sinking speeds were to changes in the particle excess density as a result of variations in fluid density.

Two simulations were undertaken with an assumed particle ESD of 683 μm and $k\upsilon$ of 0.014 cm^{-2} s^{-1}, i.e. the mean values presented for the PAP site and Arctic particles and waters. The first simulation applied the minimum achievable excess density value of 0.0086 g cm^{-3} (based on a MSA density of 1.035 g cm^{-3} and a fluid density of 1.0264 g cm^{-3}). This yielded a sinking speed of 127.6 m d^{-1}. Comparatively the second simulation using a maximum excess density of 0.08 g cm^{-3} (based on a MSA density of 1.035 g cm^{-3} and a fluid density of 1.027 g cm^{-3}) yielded a sinking speed of 139.8 m d^{-1}. Thus within the constraints of the equation 2.2, using an average excess density value of 0.002 g cm^{-3}, (based on a fluid density of 1.0265 g cm^{-3} and a solid density of 1.24 g cm^{-3}) results in a difference in sinking speed of 12 m d^{-1}. Once again this error is well within the range of observed sinking speeds.

Handling of the particles may have affected the observed sinking rates. *Alldredge and Gotschalk* [1988] documented a 4 fold increase in aggregate sinking speeds after the particles were handled compared to in situ measurements made whilst scuba diving. It cannot be ruled out that the handling of the particles may have altered the fractal nature and thus porosity of the particles, thus altering their sinking speeds. However, the sinking speeds of handled MSA collected in the coastal region of California, by *Alldredge and Gotschalk* [1988] and *Asper* [1987] were significantly lower (74 ± 39 and 36 m d^{-1} respectively) than the observed sinking speeds in this study. In comparison the sinking speeds in this study are far more comparable with measurements of particle sinking speeds from the Porcupine Seabight in the North East Atlantic (100 – 150 m day^{-1} [*Lampitt*, 1985]). Furthermore, a collation of multiple studies measuring marine snow aggregate sinking speeds in Turner [2002] indicates sinking speeds can range between 16 and 368 m d^{-1}. Thus, although the particle sinking speeds in this study may have been altered by handling, it is believed that this effect was minimal.

Particle porosity is not necessarily constant between particles, as assumed, but varies as a function of particle size [*Kajihara*, 1971; *Logan and Hunt*, 1987; *Alldredge and Gotschalk*, 1988]. The variability in particle sizes documented by *Alldredge and Gotschalk* [1988] (1 – 100 mm diameter) and *Asper* [1987] (1 – 5 mm) are far greater than the particle ESD range (0.069 – 0.083 mm) observed in this study. The ESD range presented in this study is 0.2 % of *Alldredge and Gotschalk* [1988] and 5 % of *Asper* [1982]. Assuming the relationship between particle size and porosity stands it is proposed that the variability in porosity in these particles will be much smaller than that documented by *Alldredge and Gotschalk* [1988]. Thus the underestimation of particle variability driven by changes in porosity is likely to be minimal.

Furthermore, *Alldredge and Gotschalk* [1988] showed a wide range of particle excess densities. A constant MSA excess density was applied in this chapter. The density of

the primary particles making up MSA is not accurately known but estimated to be the same as wet FP densities [*Alldredge and Gotschalk*, 1988]. Furthermore the overall density of MSA is heavily dependent upon the particle porosity, the variability of which is assumed to be small. Thus it is inferred that the range of MSA excess densities is also likely to be small.

2.5.2 The application of Dietrich's equation to model particle sinking speeds.

Equation 2.2 was applied to the observed ESD and calculated density values from the MSA and APC particles to predict particle sinking speeds. Observed MSA sinking speeds ranged between 12 and 416 m d^{-1} whilst those for APC ranged between 66 and 475 m d^{-1} (see appendix A.1 for full data tables). In comparison, over the absolute range of measured ESD (195 – 1257 μm), sinking speeds calculated from equation 2.2 ranged between 10 – 200 m d^{-1} whilst for the range of excess densities (0.00816 – 0.06 g cm^{-3}) sinking speeds calculated from equation 2.2 ranged between and 200 – 800 m d^{-1}. If the sinking speed calculated using equation 2.2 is compared to those calculated using the Stokes Law formulation (Equation 2.1) a range of 0.0004 – 0.016 m d^{-1} is found for the observed range of ESD, and a range of 0.093 – 0.068 m d^{-1} for the observed range of excess densities. Clearly the sinking speeds estimated using Stokes Law significantly underestimate the observed sinking speeds, likely a result of not accounting for the shape and fractal nature of the MSA. In contrast the sinking speeds calculated using Dietrich's equation (2.2) do a much better job of replicating the observed sinking speeds. This is proposed because of the parameterisation of factors such as the drag coefficient and other shape factors, which Stokes Law does not account for.

2.5.3 The role of size and density in determining particle sinking speed

The second aim of this study was to examine whether variations in particle size or density play a more significant role in determining particle sinking speed in both the surface and deep ocean. Initial examination of all particle sinking speeds, ESDs and densities in the surface ocean shows a weak positive correlation between particle ESD and sinking speed (Figure 2.4a; Spearman's Rank correlation coefficient of 0.2, $p < 0.01$, $n = 113$). However, no statistical correlation is observed between particle density and sinking speed (Figure 2.4b). This suggests that, the larger particles sink faster than smaller particles. The role of density in regulating sinking speed is less clear since the sinking speeds and densities of MSA and APC were significantly different from one another, despite the lack of correlative relationship.

Perhaps the largest uncertainty in this approach to determine the roles of size and density on particle sinking speed is the use of estimated rather than observed density values, assuming a constant density for each particle regardless of individual composition. This issue was addressed by using a numerical simulation, employing equation 2.2, to investigate the sensitivity of sinking speed to changes in particle size and density throughout the water column. Clearly the data set is restricted to the top 400 m of the water column. However, based on the particle size spectra data from *Stemmann et al.* [2002] it is assumed that a simplified binary model of particle sizes being between 500 and 1000 µm in the top 500 m, and between 0 – 500 µm below 500 m. This approach should enable some conclusions to be drawn regarding both the surface and deep ocean.

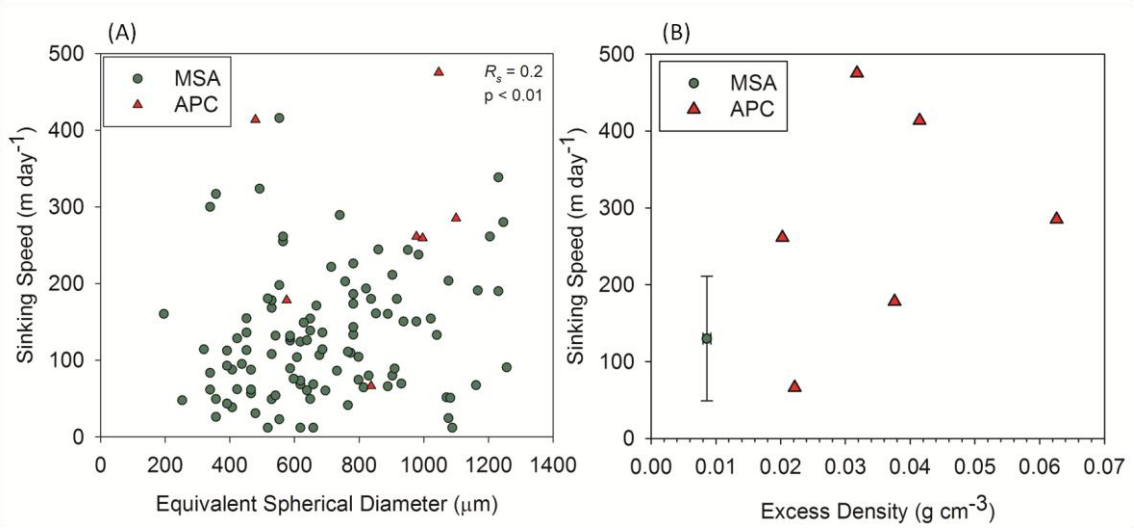

Figure 2.4 Scatter plots showing (A) the weak positive correlation between particle ESD and sinking speed (B) no correlation between excess density and sinking speeds. For the MSA the excess density is the calculated mean value, based on the range of literature values, with standard deviations assuming 96% porosity plotted against the mean and standard deviation of the sinking speeds measured.

The decreasing POC: biomineral ratio with depth [*Koeve*, 2002] almost certainly drives an increase in excess density. However, no other study estimates the magnitude by which excess density increases with depth. The range of excess densities for the surface ocean varies between 0.0084 – 0.06 g cm^{-3}. Therefore it is assumed that the range and variability of the density values observed for the surface ocean in this study remain constant with depth.

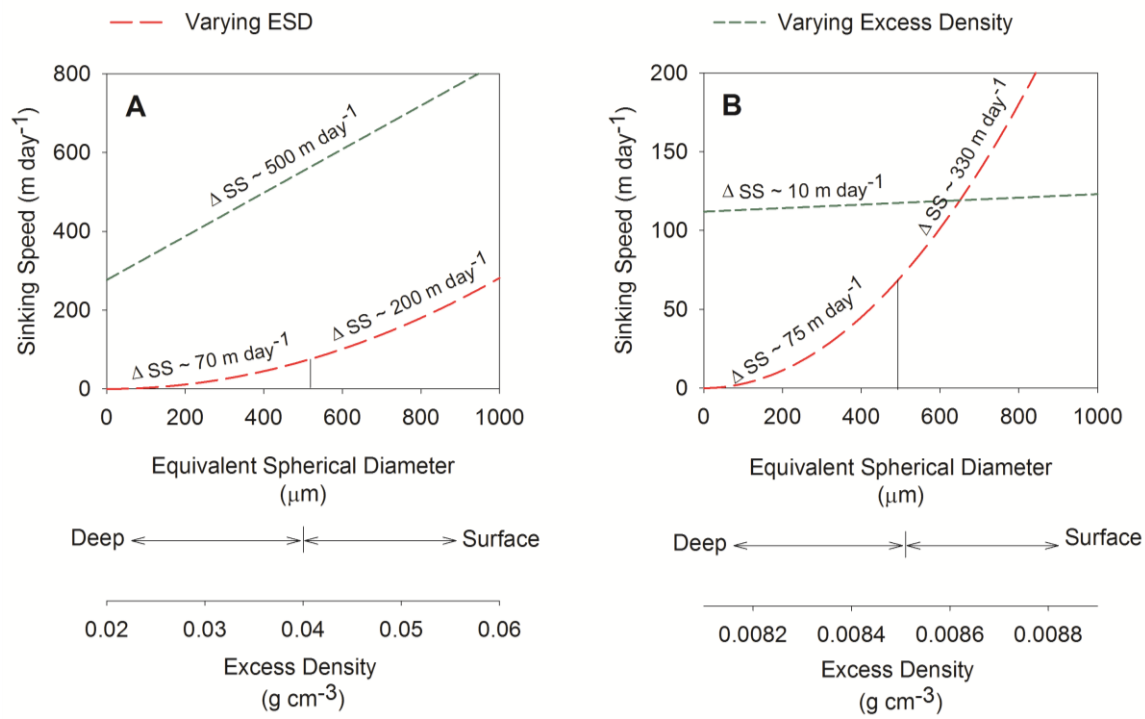

Figure 2.5 Changes in sinking speed as a function of particle ESD and excess density as modelled following Equation 1.1. The notation surface and deep is assuming a two box model simplifying the spectrum of particle sizes into a 500 – 1000 μm range at the surface and a 0 – 500 μm range at depth, outlined in the text. The green short dashed line shows sinking speed in response to variations in excess density when ESD is held constant. The red long dashed line shows sinking speed response to variations in ESD whilst excess density is held constant. (A) Shows the approximate excess density range for the APC particles collected at PAP. (B) Shows the approximate excess density range for the MSA particles collected at PAP and the Arctic

There are clear differences in morphology and sinking speeds between MSA and APC. Therefore, comparison of the sensitivity of predicted particle sinking speeds for both MSA and APC to observed variability in both size and density was undertaken. Firstly, when examining APC (Figure 2.5 a) it is seen that changes in ESD result in sinking speed variations of ~ 200 m day^{-1} in the surface ocean (particle size range of 500 – 1000 μm) and ~ 70 m day^{-1} in the deep ocean (particle size range of 0 – 500 μm). Concurrently, the range of excess densities calculated causes a variation in sinking speed of ~ 500 m day^{-1} in both the surface and deep ocean (Figure 2.5 a). Hence for APC it is possible to conclude that observed changes in particle excess density drive greater variations sinking speeds in both the surface and deep ocean compared to particle ESD.

Secondly, when examining MSA (Figure 2.5 b) it is seen that changes in ESD result in sinking speed variations of ~ 330 m day^{-1} in the surface ocean (particle size range of 500 – 1000 μm) and ~ 75 m day^{-1} in the deep ocean (particle size range of 0 – 500 μm). Concurrently, the range of excess densities calculated causes a variation in sinking speed of ~ 10 m day^{-1} in both the surface and deep ocean. Thus, for MSA it is

concluded that observed changes in size drive greater variability in sinking speeds than observed changes in excess density in both the surface and deep ocean. Thus the sinking rate of particles of relatively higher density, such as APC, are more susceptible to changes in particle density than the sinking speeds of relatively less dense particles, such as MSA.

MSA constituted ~ 90 % of the particles collected at the PAP site and 100% of the aggregated particles in the Arctic. Hence MSA particles are numerically more important than APC, and will export more POC from the surface ocean. On this basis, it is suggested that in the top 500 m variability in particle size is more important in controlling POC export than variability in excess density. This indicates that ecosystem structure, which regulates aggregate formation processes (grazing, transparent exopolymer particle formation), is probably more important for upper ocean POC export than biomineral ballasting. However, as these particles are exported into the deep ocean, where particle size is likely to decrease, the relative importance of excess density increases, as indicated by figure 2.5 and the reported POC: biomineral flux ratios [*Koeve*, 2002].

The conclusions drawn thus far are based on the likely false assumption that the range and variability of density does not change with depth in the ocean. This assumption can be tested using sinking speed and size spectra profiles from the literature. If the range and variability of density does not change with depth, then below 500 m as smaller particles become relatively more abundant [*Stemmann et al.*, 2002], sinking speeds would also be expected to decrease if size is the dominant control. However, estimates of particle sinking speeds from sediment trap data, suggest that they remain rather constant with depth [*Xue and Armstrong*, 2009]. This implies that particle density must increase with depth, counterbalancing the predicted decrease in sinking speed due to smaller particle sizes.

Assuming a constant sinking speed of ~ 200 m day^{-1} and a decrease in ESD from 750 µm to 250 µm with depth it is predicted, utilising equation 2.2 [*Dietrich*, 1982], that density must increase by at least 0.09 g cm^{-3} between the surface (0 – 500 m) and deep (500 – 1000 m) ocean. For MSA particles, an increase in density of this magnitude would result in a density comparable to an APC particle, where the sinking speed is most sensitive to changes in density. Thus the proposed concept of size driven sinking speeds in the surface ocean, and an increasing importance of density influenced sinking speeds in the deep ocean, is likely.

Biominerals are thought to ballast POC, facilitating its sinking in both the surface and deep ocean [*Klaas and Archer*, 2002; *Sanders et al.*, 2010]. It is clear that a relatively

small increase in excess density (i.e. from 0.009 g cm^{-3} (MSA) to 0.04 g cm^{-3} (APC)) can have a large impact on sinking speed. The sinking speeds of lower density particles such as MSA have a low sensitivity to variations in excess density. In comparison the sinking speed of higher density particles such as APC have a higher sensitivity to variations in excess density. Thus it is suggested that the susceptibility for particle sinking to be driven by density increases at higher particle densities.

2.6 Conclusions

In conclusion it is proposed that for the majority of carbon export from the euphotic zone size is the predominant control over particle sinking speeds. However, a shift in the POC: biomineral ratio occurs in the mesopelagic zone, where the relative importance of biominerals becomes sufficient to increase particle density, thereby controlling particle sinking speed [*Klaas and Archer*, 2002; *Thomalla et al.*, 2008]. The depth of such a change will be spatially variable and dependent upon the characteristics of the surface ocean ecosystem from which the particles originate; i.e. the ratio of POC and biomineral production to export, the size structure of the community and sinking particles, and the transformative processes particles are subjected to during their transition from the euphotic to the mesopelagic. It is proposed that this shift occurs in the upper mesopelagic (< 500 m), where POC remineralisation which controls the shift in POC:biomineral ratio is greatest. Potential changes in the phytoplankton community structure and biomineral formation [*Bopp et al.*, 2005; *Riebesell and Tortell*, 2011] may therefore impact the depth at which this transition occurs, thus the controls on particle sinking speed and thereby the amount of carbon exported.

The work presented in this study builds on previously well studied areas of science. However, the novelty of this work derives from the application of a mathematical expression to more accurately predict particle sinking speeds, without compromising Stokes' Law or using equations which utilise the drag coefficient term (which was not directly measured). With this ability to accurately predict particle sinking speeds, the sensitivity of sinking speeds has been examined and compared to realistic variations in particle size and density. Traditionally carbon export mechanisms have been accounted to either density or size driven processes. The conclusions drawn have the potential to offer a new way of conceptualising ocean carbon export with size and density driven export occurring at different points in the water column. Two hypotheses result from the novel concepts drawn in this chapter, which state that for the majority of carbon export in the ocean;

- Size controls sinking speeds in the top 500 m
- Density has an increasingly significant role below 500 m.

These hypotheses are based on theoretical calculations and a relatively small data set thereby highlighting key gaps in existing observational data. Important areas which need to be addressed include, refining observations of particle size spectra with depth, determining the absolute variability of individual aggregate densities and measuring the absolute changes in particle density with depth in the water column. With such observations more accurate analysis, building on that carried out in this chapter, could then be undertaken to further elucidate the relative importance of particle size and density on carbon export.

Chapter 3: The relative contribution of fast and slow sinking particles to ocean carbon export

3.1 Abstract

Particulate organic carbon (POC) generated by primary production and exported to depth, is an important pathway for carbon transfer to the abyss, where it is stored over climatically significant timescales. These processes constitute the biological carbon pump. A spectrum of particulate sinking velocities exists throughout the water column, however numerical models often simplify this spectrum into suspended, fast and slow sinking particles. Observational studies suggest the spectrum of sinking speeds in the ocean is strongly bimodal with > 85 % POC flux contained within two pools with sinking speeds of <10 m day^{-1} and > 350 m day^{-1}. The Marine Snow Catcher (MSC) was deployed to estimate the magnitudes of the suspended, fast and slow sinking pools and their fluxes at the Porcupine Abyssal Plain site (48°N, 16.5°W) in summer 2009. The POC concentrations and fluxes determined were 0.2 µg C L^{-1} and 54 mg C m^{-2} day^{-1} for fast sinking particles, 5 µg C L^{-1} and 92 mg C m^{-2} day^{-1} for slow sinking particles and 97 µg C L^{-1} for suspended particles. The flux estimates were comparable with radiochemical tracer methods and neutrally buoyant sediment traps. The observations imply: 1) biomineralising protists, on occasion, act as nucleation points for aggregate formation and accelerate particle sinking; 2) fast sinking particles alone were sufficient to explain the abyssal POC flux; and 3) there is no evidence for ballasting of the slow sinking flux and the slow sinking particles were probably entirely remineralised in the twilight zone.

3.2 Introduction

The transfer of particulate organic carbon (POC) from the surface ocean to depth is termed the biological carbon pump [*Boyd and Trull*, 2007] and has the capacity to modify atmospheric carbon dioxide concentrations over climatically significant timescales [*Sigman and Boyle*, 2000]. As POC sinks through the twilight zone (ranging from the base of the euphotic zone to ~1000 m depth [*Buesseler and Boyd*, 2009]) up to 90 % may be remineralised [*Martin et al.*, 1987] into inorganic forms by heterotrophic activity and returned to the surface ocean through vertical mixing [*Robinson et al.*, 2010]. Sequestration only occurs when POC sinks below the maximum depth of the winter mixed layer (~1000 m) and into the deep ocean [*Buesseler et al.*, 2007b]. However, the efficiency of oceanic POC sequestration (elaborated upon by *Boyd and Trull* [2007]) is low with only ~ 1 % of total primary production reaching abyssal depths of 3000 m [*Poulton et al.*, 2006].

Two types of sinking particle are considered to be the main vectors of POC export; faecal pellets (FP) and marine snow aggregates (MSA). Faecal pellets, formed by zooplankton, have high densities and enhanced sinking speeds [*Wilson et al.*, 2008] which range between 5 – 2700 m day^{-1} depending on the species of origin [*Turner*, 2002]. Marine snow is broadly defined as aggregates > 500 µm [*Alldredge and Silver*, 1988] with sinking rates between 10 and 386 m day^{-1} [*Alldredge and Gotschalk*, 1988; *Nowald et al.*, 2009]. The density and composition of individual aggregates is dependent upon the local plankton community structure [*Alldredge and Gotschalk*, 1990].

Ballasting of POC with biominerals is thought to facilitate its transfer to the deep ocean. However, the mechanism driving the relationship between POC and biominerals is uncertain [*De La Rocha and Passow*, 2007]. Biomineral or lithogenic ballasting of sinking POC potentially protects the sinking POC from mesopelagic remineralisation [*Armstrong et al.*, 2002; *Francois et al.*, 2002]. Furthermore, the entrainment of extra density into sinking POC via the incorporation of biominerals and lithogenic material facilitates POC transfer between the euphotic zone and the deep (>1000 m) ocean [*Klaas and Archer*, 2002; *Sanders et al.*, 2010]. Alternatively, POC may act as a glue, sticking biominerals together which would otherwise have been too small to sink [*Passow*, 2004; *Passow and De La Rocha*, 2006]. Within the scope of this chapter the term ballast will be used to discuss the addition of density into sinking POC via heavy biomineral fractions.

Direct observations of bulk POC fluxes can be made using a range of instrumentation. The deployment of tethered sediment traps is restricted to the deep (> 3000 m) ocean due to under-trapping effects in the upper ocean [*Buesseler et al.*, 2007a]. Tethered Indented Rotating Sphere Carousels (IRSC) sediment traps, which collect data in both a traditional sediment trap and more novel settling velocity modes [*Peterson et al.* 1993; 2005] and free drifting sediment traps, including PELAGRA (Particle Export measurement using a LAGRAngian trap [*Lampitt et al.*, 2008]) and NBSTs (Neutrally Buoyant Sediment Traps [*Buesseler et al.*, 2000]) minimise POC under-trapping effects and are deployed in the upper ocean. Radiochemical tracer techniques such as thorium-234 (^{234}Th) can also be used to estimate POC fluxes throughout the water column [*Buesseler et al.*, 1993; *Van der Loeff et al.*, 2006]. Individual particles can be collected throughout the water column using technologies such as Marine Snow Catchers [*Lampitt et al.*, 1993] and polyacrylamide gels [*Lundsgaard*, 1995; *Ebersbach and Trull*, 2008].

When considering carbon export from a biogeochemical perspective POC is often grouped (by sinking speed) into three pools, consisting of a small proportion of fast sinking particles, a second class of slower sinking particles and a remaining suspended particle field, despite this being an oversimplification of a complex spectra of particle sinking speeds [*Fasham et al.*, 1990; *Kriest and Evans*, 1999; *Boyd and Stevens*, 2002]. Direct observations of the spectra of particle sinking speeds, compiled from a global data set using an IRSC sediment trap suggest that slow sinking particles (sinking speeds ranging between 0.7 – 11 m day^{-1}) account for ~ 60 % of the total POC flux whilst sinking speeds > 326 m day^{-1} contribute ~ 25 % to the total POC flux in the top 300 m of the water column. Overall > 85 % of the global carbon flux can be explained by a strongly bimodal distribution of sinking speeds although some geographical variability is apparent [*Alonso-González et al.*, 2010].

In this study observational POC standing stocks and flux data are presented, collected using a Marine Snow Catcher (MSC). The MSC is a large volume (100L) water bottle (Figure 3.1) consisting of two detachable sections. Upon deployment in the water column the MSC is closed at depth using a messenger operated closure release. Water enters the bottle during descent through the water column via two large terminal openings, designed to minimise turbulent flow of water into the bottle. Post deployment the MSC is placed on deck for 2 hours whilst any particles present settle onto the base of the bottom 7 L chamber. After settling, the top 93 L of water is drained off gently to avoid mixing of water in the top and base sections. During this draining process no physical separation of the top and base water samples occurs. The upper section of the MSC is then detached, leaving any particles on the bottom of the 7 L base section.

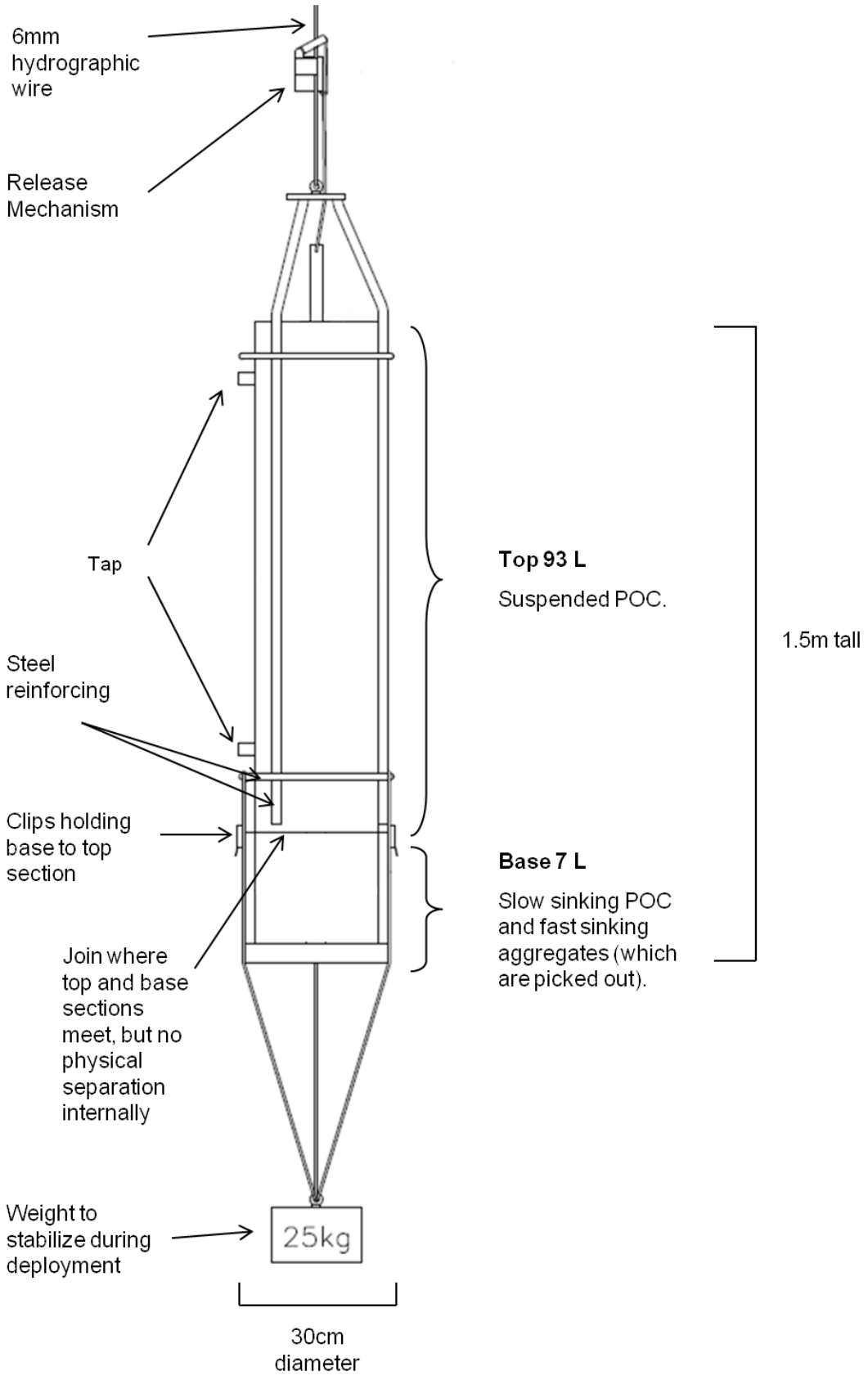

Figure 3.1 General arrangement of the Marine Snow Catcher.

This study presents upper ocean POC, calcite and opal standing stock and flux data for three pools, suspended, fast sinking and slow sinking which have been operationally defined by the 2 hour settling period. The suspended pool consists of those particles which remain in the upper section of the MSC following settling and have no flux. Fast sinking material is defined as aggregated particles picked off the bottom of the base chamber, whilst the slow sinking pool is determined from the difference in particle concentrations between the top and base sections of the MSC. The calculations are validated with contemporaneous measurements of POC fluxes. The results presented are utilised to discuss the potential formation mechanisms of fast sinking particles and the transfer and ballasting of POC fluxes into the deep ocean.

3.3 Methods

3.3.1 Site Description

Sinking particles were collected at the Porcupine Abyssal Plain (PAP) site (48°N, 16.5°W) using the MSC during RRS *Discovery* cruise D341 (8th July to 13th August, 2009). The depth of the winter mixed layer at this site is typically ~350 m [*Steinhoff et al.*, 2010] and the annually integrated primary productivity ~200 g C m^{-2} y^{-1} [*Lampitt et al.*, 2010].

3.3.2 Particle Collection

The MSC (Figure 3.1) was deployed nine times (see appendix B.1 for precise locations) at 50 m depth, which corresponded to the approximate depth of the mixed layer at the time of sampling. In total 459 individual aggregates, which had settled onto the bottom of the base chamber during each settling period, were picked using a Pasteur pipette and classified under an optical microscope. Two categories of particles containing organic matter were observed (Figure 3.2); Marine Snow Aggregates (MSA, 429 particles) and particles consisting of a distinct solid biomineralising protist centre enveloped in marine snow, termed Aggregate Protist Complexes (APC, 30 particles). Post-settling (2 hours) water samples for POC, calcite and opal analysis were collected from the top 93 L and the bottom 7 L chamber of the MSC. Samples of POC, calcite and opal from the top and base sections of the MSC were only available for the last 5 stations. Thus the sinking speed, aggregate area, aggregate POC content, stocks and fluxes presented in this manuscript only corresponds to the last 5 stations. However, when discussing the relative abundance of MSA and APC particles, data from all 9 stations will be used.

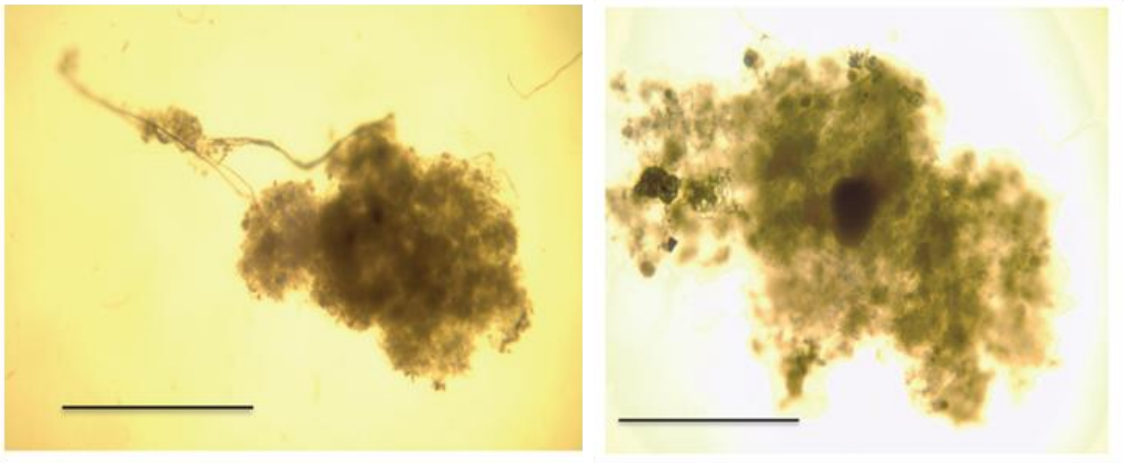

Figure 3.2 Examples of marine snow particles. (Left) Marine Snow Aggregate (MSA); (Right) Aggregate Protist Complex (APC). The scale bar in each figure is 1 mm.

3.3.3 Particle settling experiments

The sinking rates of 110 picked particles were determined by placing them in a glass 2 L measuring cylinder, filled with surface sea water from the ship's underway supply and kept at ambient water temperature (~15°C). Individual particles were placed into the measuring cylinder using a Pasteur pipette, a few centimetres below the water surface so any motion was due to natural sinking [*Martin et al.*, 2010]. Two sinking times were recorded as individual particles passed two discrete points within the measuring cylinder. The two sinking rate observations of individual particles from each experiment were highly reproducible, with average standard errors of ± 4% for MSA and ± 19% for APC.

Particles were retrieved after each experiment using a Pasteur pipette and initial photography of each particle was undertaken on the ship to aid further classification. Particles were then preserved in 5 % buffered formalin. High quality images (x4 magnification) of the preserved particles were taken after the cruise, using a camera microscope (Meiji Techno Japan MX microscope with an Infinity 1 camera). Comparison of photographs for 11 particles taken at sea and post-cruise constrained changes in particle area due to storage and preservation at ± 17 %.

3.3.4 POC, calcite and opal determination

Concentrations of POC in the top and the base of the MSC were determined by filtration of 1.5 - 2 L of water onto pre-combusted (450°C, 12 hours) glass fibre filters (25 mm diameter GF/F, Whatman). Filters were stored in petri dishes at -20°C, acid fumed and analyzed using an elemental analyser (Thermo Finnegan Flash EA1112). The

concentration of POC contained within the total aggregates collected from each deployment was calculated using the empirical relationship proposed by Alldredge [1998]. Calcite measurements were made on 1 – 1.5 L water samples from the top and base of the MSC, filtered onto 0.8 µm polycarbonate membrane filters (Whatman). Samples were rinsed with a slightly alkaline (pH 9) de-ionised water rinse solution to remove any remaining sea water and frozen at -20°C prior to analysis. In the laboratory samples were extracted in 2 % nitric acid and analysed using Inductively Coupled Plasma Optical Emission Spectrometry (Perkin Elmer Optima 4300 DV ICP-OES). For opal determination 1 – 1.5 L of sea water was filtered onto 0.8 µm polycarbonate filters (Whatman), digested using 0.2 M sodium hydroxide (80°C, 4 hours) and then neutralised with 0.1 M hydrochloric acid. Silicate concentrations were subsequently determined using an autoanalyser (Skalar Sanplus) [*Poulton et al.*, 2006].

3.3.5 Calculation of slow and fast sinking particle concentrations

Assuming the base concentration is greater than the top concentration after the 2 hour settling period the slow sinking particle concentrations were determined. The difference in concentration in the top and base of the MSC enables the excess of carbon in the base (7 L) of the MSC to be calculated. This difference must then be scaled to the ratio of the base: total volume of the MSC (Equation 3.1).

$$\underset{Concentration}{Slow\ Sinking}\ (\mu g\ L^{-1}) = (Conc._{Base} - Conc._{Top}) \times R_{B:T} \qquad \text{(Eq. 3.1)}$$

Where $Conc._{Base}$ and $Conc._{Top}$ are the concentrations in the base and top sections of the MSC respectively and $R_{B:T}$ is the ratio of the base volume (7 L) to the total volume (100 L) i.e. $\frac{7}{100}$ or 0.07

Fast sinking POC concentrations were determined by calculating the total mass of POC carried in the fast sinking aggregates as a fraction of the total volume of the MSC Equation 3.2).

$$Fast\ Sinking\ POC\ (\mu g\ L^{-1}) = {POC_{Agg} \times N} \Big/ {V_{Total}} \qquad \text{(Eq. 3.2)}$$

Where POC_{Agg} is the average mass of POC per aggregate calculated following Alldredge [1998], N is the total number of aggregates collected during each deployment and V_{Total} is the total volume of the MSC (100L; Figure 1). This equation cannot be applied to

calculate the fast sinking opal or calcite concentrations since no literature conversion factor is available. Thus estimates for calcite and opal were not calculated.

3.3.6 Calculation of fluxes

Fluxes were calculated following standard calculations dividing mass by area and time. However, given the base volume of 7 L, a top volume of 93 L and an assumption of a homogenous distribution of particles throughout the entire MSC at the start of the settling period, 7 % of the sinking material must have originated in the base section. Therefore the final flux value was scaled to 93 % to account for this. (Equation 3.3);

$$Flux(\mu g\, m^{-2} day^{-1}) = \left({}^{Mass}/_{MSC\ Area} \Big/ {}_{Sinking\ Time} \right) \times F_{Top} \qquad \text{(Eq. 3.3)}$$

Where the term *Mass* applies to the mass of slow or fast sinking particles indentified in the MSC, the *MSC Area* is the horizontal footprint of the base chamber (0.06 m^2; Figure 1), the *Sinking Time* is the time taken for either the fast or slow particles to sink (see section 3.3.3) and F_{Top} is the fraction of POC not in the base section at the start of the settling period (i.e. 93 L out of 100 L or 0.93). The total flux was calculated from the sum of the slow and fast fluxes.

3.4 Results

3.4.1 POC, calcite and opal concentrations in the top and base chambers of the MSC

The average concentration of POC (± 1 standard deviation [S.D.]) in the water from the top section of the MSC across all stations sampled after the 2 hours settling was 97 (± 17) µg C L^{-1} whilst the average concentration of POC in the water from the bottom chamber was 170 (± 24) µg C L^{-1}. The average concentrations in the top and base of the MSC were normally distributed and the differences between the top and base were significantly different from one another (Student t-test, $p < 0.001$), consistent with a slow sinking flux of POC occurring within the MSC during the settling period.

The average concentrations of calcite in the top and base water samples from the MSC were 4 (± 3) µg L^{-1} and 8 (± 3) µg L^{-1}, respectively. Statistical analysis showed a normal distribution of concentrations however a Student t-test indicates that the mean top and base values were not significantly different ($p < 0.1$). Further analysis using

Pearson's correlation coefficient also showed no significant relationship ($p < 0.37$) between the top and base concentrations. This suggests either that there was little or no slow sinking flux of calcite within the MSC during the settling period or that the distribution of calcite was patchy across the sampling site and more extensive sampling was needed to identify any relationship.

The average concentrations of opal within the top and base of the MSC were 3 (± 1) μg L^{-1} and 8 (± 2) μg L^{-1} respectively. The range of concentrations was not normally distributed and results of a Mann Whitney-U test indicated a significant difference ($p < 0.03$) between the top and bottom chambers. This implies that there was a flux of opal into the base of the MSC during the settling period (see appendix B.2 for POC, calcite and opal concentrations measured at each station Tables B.2, B.3 and B.4).

3.4.2 POC and opal concentration of suspended, slow and fast sinking pools

Suspended concentrations were assumed to be the material remaining in the top section of the MSC after the 2 hour settling period, slow sinking concentrations were calculated following equation 3.1 (see appendix B.3, Table B.5 and B.6) and fast sinking concentrations were calculated following equation 3.2 (Tables 3.1 and 3.2). There is confidence in the measurements of the total pool of POC present within the MSC since all of the fast sinking particles were picked and the total concentration of the slow sinking particles was measured by homogenising the remaining 7 L in the base chamber (after removal of the fast sinking aggregates) prior to filtering a 2 L sub sample.

Station #	Fast Sinking POC conc. (μg L^{-1})	Slow Sinking POC conc. (μg L^{-1})	Suspended POC conc. (μg L^{-1})	Total POC conc. (μg L^{-1})	Suspended Opal conc. (μg L^{-1})	Slow Sinking Opal conc. (μg L^{-1})
16589	0.2	5	109	115	5	0.1
16593	0.1	6	119	125	3	0.5
16605	0.1	4	78	82	No Data	No Data
16620	0.2	5	89	94	4	0.4
16660	0.3	5	92	97	2	0.3
Average	0.2	5	97	103	3	0.3
SD	0.1	1	17	10	1	0.2
Av %	0.2	5	95	100	-	-
RSD %	47	12	17	9	-	-

Table 3.1 Suspended, fast sinking and slow sinking POC and opal concentrations, calculated after 2 hour settling period. Av % is the average % of the total concentration for each of the fast and slowand suspended componenets. RSD is the relative standard deviation, i.e. the standard deviation expressed as a percentage of the total fast, slow or suspended concentration.

Station Number	N [a]	Average ESV (mm^{-3}) [b]	Average POC ($\mu g\ agg^{-1}$) [c]	Total Mass (μg C) [d]	Total Concentration ($\mu g\ C\ L^{-1}$) [e]
16589	30	0.4 (± 0.3)	0.6 (± 0.1)	19 (± 3)	0.2 (± 0.03)
16593	17	0.2 (± 0.2)	0.5 (± 0.1)	8 (± 1)	0.1 (± 0.01)
16605	19	0.2 (± 0.3)	0.5 (± 0.1)	9 (± 1)	0.1 (± 0.01)
16620	30	0.5 (± 0.6)	0.7 (± 0.1)	21 (± 3)	0.2 (± 0.03)
16660	53	0.3 (± 0.2)	0.5(± 0.1)	26 (± 4)	0.3 (± 0.04)
Average		0.3	0.6	17	0.2
SD		0.1	0.1	8	0.1

Table 3.2 Data for calculation of, aggregate POC content, total mass of fast sinking POC and fast sinking concentration for each MSC deployment.

[a] The total number of MSA and APC picked from the base of the MSC in 100 L.

[b] Particle areas were measured using the image analysis software Image-J [*Abramoff et al*, 2004], calibrated using a stage graticule under magnification identical to the particle. From this average particle ESV was calculated per station with associated standard deviation (shown in brackets).

[c] Calculated using the average ESV and the empirical relationship proposed by Alldredge [1998]; POC ($\mu g\ agg^{-1}$) = 0.99 × ESV (mm^{-3})$^{0.52}$. The values in the brackets represent the maximum and minimum range of possible concentrations for the particle carbon content, given the quoted standard errors in Alldredge [1998].

[d] The total mass of fast sinking POC is calculated by multiplying the average POC content per aggregate at each station by the number of aggregates collected at each station (Equation 2).

[e] The total concentration of fast sinking POC is then calculated by dividing the total mass by the volume of the MSC (100L; Equation 2).

Concentrations of POC averaged across all stations (± 1 S.D.) within the fast sinking, slow sinking and suspended fractions were 0.2 (± 0.1), 5 (± 1) and 97 (± 17) $\mu g\ C\ L^{-1}$ respectively (Table 3.1). Fast sinking POC contributed (with relative standard deviations) 0.2 (± 47) % whilst the slow sinking fraction and suspended material contributed ~5 (± 12) % and ~95 (± 17) % in terms of total POC (Figure 3.3). The mean suspended concentration of opal within the MSC was 3 (± 1) $\mu g\ L^{-1}$ whilst the mean slow sinking pool was 0.3 (± 0.2) $\mu g\ L^{-1}$ (Table 3.1; appendix B.3 for full data tables documenting the calculation of the slow sinking pools of POC and opal). No data for opal content of the fast sinking aggregated particles were available. Furthermore, no concentrations of calcite were calculated for the three pools since there was no significant difference between the average top and base sections concentrations of the MSC (section 3.1). Unfortunately the lack of opal and calcite data for the fast sinking pool prevents us from investigating how the fast and slow sinking biomineral pools scale relatively to each other.

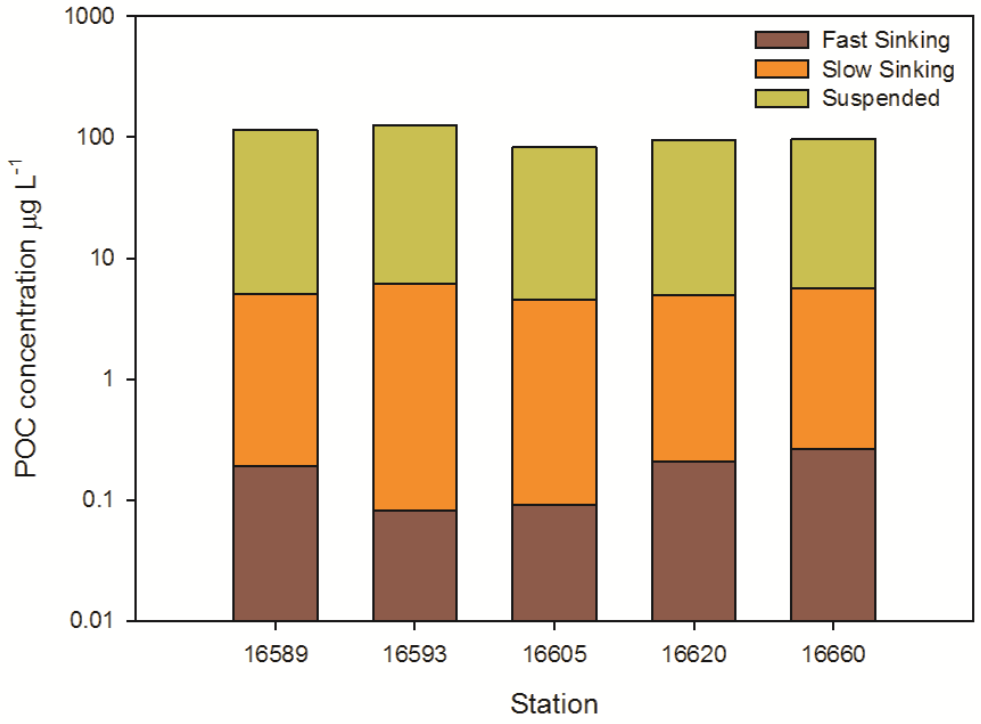

Figure 3.3 POC concentrations of the suspended, slow and fast sinking pools. (n.b. note the logarithmic scale on the y axis).

3.4.3 Sinking speeds of slow and fast pools

The sinking speed of the slow settling fraction was estimated assuming; firstly that all of the fast sinking MSA particles had been picked from the base chamber, ensuring the fast and slow particle pools are separated from one another; and secondly that the slow sinking particles were homogenously distributed within the MSC prior to settling. The sinking speed of particles can be calculated following equation 3.4. The sinking time was constant at 2 hours (0.083 days), thus the only variable is the distance the particles sank, assuming that all of the slow sinking particles had reached the base section. Assuming a homogenous distribution of particles at the start of the 2 hour settling period, particles are estimated to sink at an average of 9 m day^{-1} settling from the midpoint of the MSC (0.75 m) but may range between ~ 0 m day^{-1} and 18 m day^{-1} depending on the starting location of a slow sinking particle in the MSC.

$$Sinking\ Speed\ (m\,day^{-1}) = Distance / Time \qquad \text{(Eq. 3.4)}$$

The sinking speed of the fast pool was determined as a weighted average (± 1 S.D.) of the MSA (average of 180 (± 22) m day^{-1}) and the APC (average of 232 (± 58) m day^{-1}) settling speeds determined in the sinking experiments. Overall, the weighted average

sinking speed of the fast sinking pool was 181 (± 8) m day^{-1}, with a sinking time of ~ 0.005 days.

Station #	Mass of fast sinking POC (µg)	Mass of slow sinking POC (µg)	Flux of fast sinking POC (mg $m^{-2} d^{-1}$)	Flux of slow sinking POC (mg $m^{-2} d^{-1}$)	Mass of slow sinking Opal (µg)	Flux of slow sinking Opal (mg $m^{-2} d^{-1}$)
16589	19	488	61	88	13	2
16593	8	602	26	109	51	9
16605	9	444	30	80	No Data	No Data
16620	21	470	67	85	41	8
16660	26	535	85	97	32	6
Average	17	508	54	92	34	6
SD	8	62	25	11	16	3
Av %	-	-	37	63	-	-
RSD %	-	-	47	12	-	-

Table 3.3 Calculated masses (see appendix B.3, tables B.5 and B.6, for further details about the calculation of mass) and fluxes (following equation 3) of POC and opal after the 2 hour settling period.

3.4.4 Export fluxes of POC and opal

The average (± 1 S.D.) fast sinking POC flux across all stations was calculated to be 54 (± 25) mg C m^{-2} day^{-1} (~37 (± 47) % of the total flux) whilst the average slow sinking POC flux, was 92 (± 11) mg C m^{-2} day^{-1} (~63 (± 12) % of the total flux; Table 3.3). Overall a total flux of POC at the base of the mixed layer (both fast and slow sinking pools) of 146 (± 26) mg C m^{-2} day^{-1} was determined. An opal export flux of 6 (± 3) mg C m^{-2} day^{-1} (Table 3.3) was calculated for the slow sinking fraction, no calculation could be made for the fast or total fluxes since no data were available for the fast sinking particle opal content.

3.5 Discussion

3.5.1 Comparison of MSC POC fluxes with other upper ocean flux estimates

The averaged total POC fluxes at the PAP site for the period 2003 – 2005, obtained from PELAGRA deployments, were 72 mg C m^{-2} day^{-1} in the upper 175 m of the water column (Figure 3.4, [*Lampitt et al.*, 2008]). A PELAGRA deployment (4th – 6th August, cruise D341), concurrent with the MSC deployments presented in this chapter, determined a POC flux of 84 (± 8) mg C m^{-2} day^{-1} at 51 m, which was close to the total

POC flux determined using the MSC (146 (± 26) mg C m^{-2} day^{-1}, Figure 4). The broad similarity of flux measurements between PELAGRA and MSC suggests the MSC is capable of producing comparable estimates of upper ocean POC fluxes.

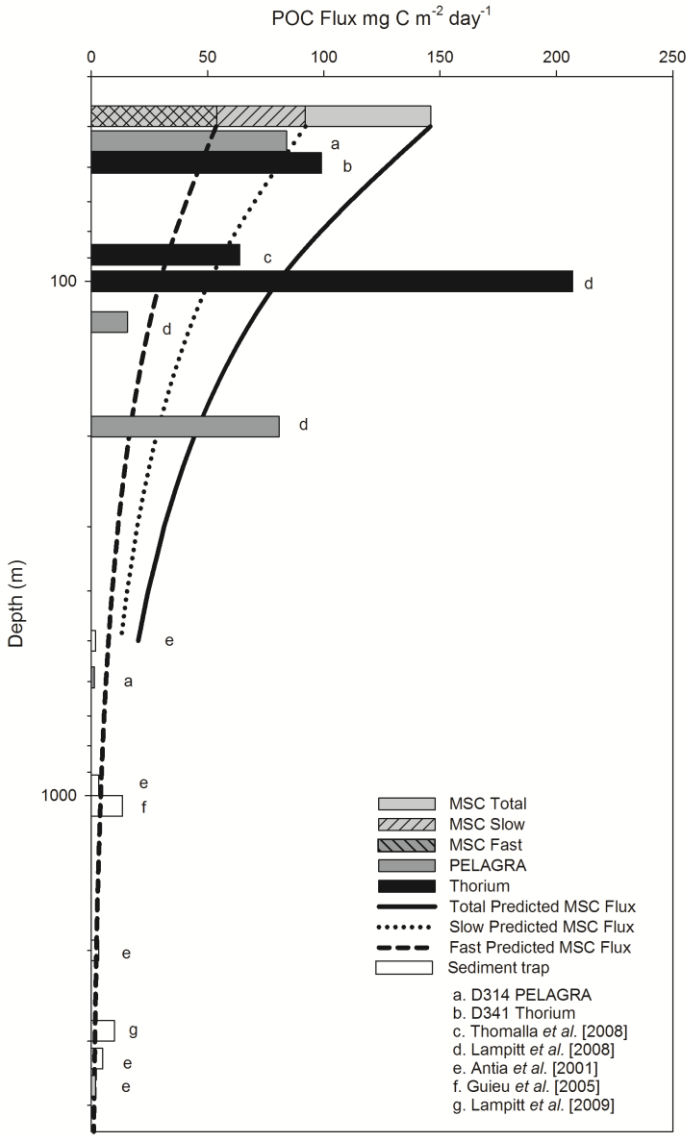

Figure 3.4 Comparison of C flux estimates using different sampling techniques with MSC data. Superimposed on top of this is the predicted POC flux values from the MSC based on the Martin et al. [1987] equation.

An alternative approach used to estimate POC export uses the particle reactive tracer ^{234}Th [*Buesseler et al.*, 1993; *Van der Loeff et al.*, 2006]. Export measurements in the vicinity of the PAP site have been made on a number of occasions since 1993 using the ^{234}Th technique (Figure 3.4). Thomalla *et al.* [2008] determined a POC flux of 64 mg C m^{-2} day^{-1} at 100 m and Lampitt *et al.* [2008] estimated a flux of 207 mg C m^{-2} day^{-1} at 100 m. Measurements of ^{234}Th made at the PAP site during cruise D341 yielded a

station average flux of 99 (±41) mg C m^{-2} day^{-1} at 56 m (Figure 3.4). It is clear that there is variability in the estimates of C flux made using the ^{234}Th technique, however the contemporaneous data is comparable with the flux estimates made using the MSC (146 mg C m^{-2} day^{-1}).

3.5.2 Assessment of the validity of the calculations

The calculation of the suspended and slow sinking pools of both POC and opal rely upon the assumption that all particles within the MSC were homogenously distributed at the beginning of the two hour settling period. Therefore, on average, a slow sinking particle will sink half the height of the MSC (0.75 m) in two hours and have an average settling velocity of 9 m day^{-1}. However, some particles will clearly settle faster or slower than this, resulting in an under or over estimation of the sinking speed. An increase in the sinking velocity of the slow sinking fraction, greater than 9 m day^{-1}, as assumed in section 3.3, would result in an even larger flux than that estimated from the ^{234}Th or PELAGRA, hence this scenario is considered unlikely given the MSC flux is higher than either the PELAGRA or the ^{234}Th derived flux.

Conversely, some particles will originate above the midpoint of the MSC and not penetrate the base section during the 2 hour settling period, leading to a potential underestimation of the slow sinking pool and an overestimation of the suspended pool. The potential impact of such a scenario is estimated by deriving two simultaneous equations, to calculate the suspended and slow sinking POC, assuming 50 % of the slow sinking flux had not penetrated the base section. Under this revised estimate the general distribution of material in the various classes is similar to that found under the initial assumptions, with POC concentrations in the suspended, slow and fast sinking pools being 89 %, 10 % and < 1% respectively (see appendix B.4, table B7 and the following text).

Using this new slow sinking pool size to estimate the associated flux (assuming a sinking speed of 9 m day^{-1} and that particles sank from the midpoint of the MSC in 2 hours), gives a slow sinking flux of 191 mg C m^{-2} day^{-1}. When added to the fast POC flux a total flux estimate of 245 mg C m^{-2} day^{-1} was calculated. This total MSC POC flux is approximately 40 % greater than the initial estimate (146 mg C m^{-2} day^{-1}) and approximately 60 % greater than independent estimates made using PELAGRA (84 mg C m^{-2} day^{-1}) and ^{234}Th (99 mg C m^{-2} day^{-1}). It therefore seems likely that the initial estimate of the size of the slow sinking pool was relatively robust and that the range of sinking speeds between ~ 0 and 18 m day^{-1} with an average of ~ 9 m day^{-1} is also reasonably close to reality.

3.5.3 Formation of fast sinking particles

Lee *et al*. [2009] suggest a 'catalyst' initiates the aggregation process which forms fast sinking particles. An increase in bulked POC flux observed at the PAP site during 2001 correlated with observed increases in radiolarian populations [*Lampitt et al*., 2009], which may have acted as a nucleation point promoting fast sinking particle aggregation. Of the fast sinking particles identified across all 9 deployments 30 consisted of organic matter aggregated around a biomineralised protist (APC, Figure 2). This suggests that the presence of planktonic organisms can indeed act as nucleation points for individual particle aggregation and accelerate their sinking rate. However since APC contributed such a small proportion of total sinking material collected, other 'catalysts' must also be important. These may include the production of sticky transparent exopolymer particles (TEP) [*Alldredge and Gotschalk*, 1990; *Passow et al*., 2001] by diatoms.

3.5.4 Fluxes of POC to the deep ocean

Large (>53 µm) rapidly sinking particles are thought to be relatively rare within the water column [*McCave*, 1975], with estimates of fast sinking particle concentrations in the Indian Ocean and Panama Basin contributing 3 – 15 % to total POC [*Mullin*, 1965; *Bishop et al*., 1980]. Alonso-González *et al.* [2010] suggest fast sinking particles alone supply the abyssal POC flux due to their rapid transit time through the water column. The fast sinking particles collected in this study, with an equivalent spherical diameter of 195 – 1639 µm, contributed 0.2 (± 47) % to the total POC concentration (Figure 3.3). However, given the small contribution of fast sinking particles and the remineralisation processes which occur within the twilight zone it is unclear whether these particles would truly sustain the observed POC fluxes to the abyss.

Applying the flux attenuation parameterization of *Martin et al.* [1987] (Chapter 1) to the fast sinking flux estimates (54 (± 25) mg C m^{-2} day^{-1}; section 3.4.4) a deep flux of 2 mg C m^{-2} day^{-1} (at 3000 m, Figure 3.4) is predicted, close to the deep sediment trap flux estimates of 1.8 – 10 mg C m^{-2} day^{-1} at 3000 – 3500 m [*Antia et al*., 2001; *Lampitt et al*., 2009]. Applying the same *Martin et al.* [1987] parameterization to the 50 m total flux value (146 mg C m^{-2} day^{-1}; the sum of the fast and slow flux values) yields a deep flux estimate of 4 mg C m^{-2} day^{-1}, also within the range of the deep sediment trap fluxes. Thus based on the predicted attenuated flux values it is not possible to determine whether fast sinking particles alone or a combination of fast and slow fluxes supply POC to the deep ocean.

Deep sediment trap data indicate a seasonal flux of POC to the sea floor, with peak fluxes lagging the maxima in surface productivity by ~ 40 days [*Lampitt et al.*, 2010]. The determined sinking speeds of 181 m day^{-1} and 9 m day^{-1} (see section 3.3) for the fast and slow sinking particles results in a transit time between 50 and 4500 m of ~ 30 and 500 days respectively. The 40 day lag time between primary maxima in primary productivity and deep POC fluxes, and the estimated transit time of the fast sinking flux are comparable, implying fast sinking particles are the major contributor to the deep sediment trap fluxes [*Alonso-González et al.*, 2010] undergoing reduced remineralisation [*Wakeham et al.*, 2009]. The long transit time of the slow sinking POC suggests complete remineralisation in the upper water column. Furthermore, if the slow sinking particles were to reach the abyss, the long transit time to the deep ocean would likely mask any seasonal signal observed in the deep sediment traps. Thus it is surmised that the slower sinking particles are at this site equally important in terms of total flux out of the euphotic zone but contribute negligibly to abyssal carbon transfer.

3.5.5 Does a biomineral ballasting effect occur?

Quantitative analysis of the relationship between biomineral and POC concentrations of the fast sinking particles is not possible due to a lack of data on the calcite and opal contents. Despite this, the APC sank approximately 50 % faster (~232 (± 58) m day^{-1}) than MSA (~180 (± 22) m day^{-1}; section 3.4.3). This implies that some component of the fast flux is actively ballasted. This is consistent with the observed pulses of POC to the abyss associated with increases in biomineralising organisms at the PAP site [*Lampitt et al.*, 2009]. Whether the remaining MSA flux is ballasted or simply sinks quickly because the aggregates are large enough to overcome the viscous effects of sea water [*Alldredge and Gotschalk*, 1988] is not clear. However in light of the results of Chapter 2 it may be that it is the size of the MSA particles which is more important in determining the particle sinking speed in the upper ocean, where the particles were collected.

The average slow sinking POC flux showed no corresponding flux of slow sinking calcite in the MSC during settling (section 3.4.1), suggesting no ballasting relationship with calcite. However, if the distribution of calcite is patchy across the PAP site, a ballasting relationship may still exist in discrete areas. In comparison, a slow sinking flux of opal was calculated (section 3.4.1) but correlation analysis of the slow sinking opal and POC fluxes revealed no significant relationship (Spearman's Rank Correlation Coefficient, $p < 0.75$, 0.05 confidence level), implying the average flux of POC was not ballasted by opal. From the ^{234}Th derived POC and biomineral fluxes presented by *Sanders et al.* [2010], it was concluded that an upper ocean ballasting relationship was likely. Critical re-examination of their findings identifies a small flux of POC occurring

with no associated biomineral flux. It is hypothesised this small flux of POC represents the slow sinking flux, which may be unballasted by either calcite or opal.

3.6 Conclusion

This work contributes to the growing body of evidence that POC in the surface ocean can be best conceptualised using a three pool model; consisting of suspended, slow sinking and fast sinking fractions, despite being an oversimplification of the global variability in particle sinking speeds. The key findings of this study suggest:

1. The MSC provides a comparable alternative to other technologies as a method of measuring POC stocks and fluxes in the upper ocean, enabling both the occurrence and magnitudes of the fast and slow sinking POC fluxes to be examined.
2. Nucleation around a biomineralising organism may aid particle formation. This supports the argument by Lampitt et al. [2009] that biomineralising protist mediated export may be important at the PAP site.
3. Fast sinking POC, produced in the euphotic zone contributes negligibly to total POC stocks, but is sufficient to supply POC to the abyss. Further to this it is suggested that the fast flux is, at least in part, ballasted by biominerals and is most important in terms of carbon sequestration.
4. Slow sinking POC is likely to be remineralised in the twilight zone due to its slow transit time though the water column. Furthermore the slow sinking flux may not be ballasted. Thus the slow sinking particles are an unlikely source of POC to the abyss.

The geographical extent over which this three pool model is valid is uncertain. However, the synthesis of studies from the Mediterranean and subarctic and subtropical Pacific, presented by Alonso-González *et al.* [2010] strongly support the conclusions drawn here. Therefore it seems likely to have a wider significance than simply the North East Atlantic Ocean. A key question for future research is to define the processes which regulate the relative sizes of the fast and slow sinking pools and the magnitudes of their respective fluxes. For example, it may be the case that a constant background flux of slow sinking material occurs with a fast sinking pool superimposed on it by episodic events such as upwelling, storms, eddies or the spring diatom bloom. Potential shifts in the relative magnitudes of the fast and slow sinking pools, favouring the formation of slow sinking POC may result in a change in the partitioning of CO_2 between the atmosphere and ocean. Thus greater quantities of POC would be respired in the upper ocean, with consequences for global climate [*Kwon et al.*, 2009].

Chapter 4: Coccolithophores, diatoms and the fast and slow export fluxes

4.1 Abstract

Phytoplankton are a key driver of the biological carbon pump, photosynthesising and producing organic carbon which is exported to depth. Slow sinking fluxes of particulate organic carbon (POC) and biogenic silica (BSi), but not particulate inorganic carbon (PIC), have been observed at the Porcupine Abyssal Plain (PAP) site at 50 m and have been predicted to reach ~ 500 m depth. Additionally sediments at the PAP site are dominated by coccolithophore PIC whilst diatom POC is thought to be more abundant than coccolithophore POC in the deep (3000 m) sediment traps, based on geochemical observations. It is hypothesised that the slow sinking flux is associated with diatoms, the fast sinking flux is associated with coccolithophores and that diatom POC is transferred to the deep ocean in MSA potentially due to PIC ballasting. Fast sinking marine snow aggregates (MSA) were collected in the marine snow catcher (MSC, 50 m). Neutrally buoyant PELAGRA traps collected bulk fluxes between 175 and 630 m depth. Microscopic identification and enumeration of the coccolithophores and diatoms was undertaken in all samples. Coccolithophore cell bound POC fluxes ranged between 0.03 (± 0.16) and 282 (± 119) μg C m^{-2} d^{-1} whilst diatom cell bound POC fluxes ranged between 361 (± 5) and 6586 (± 4709) μg C m^{-2} d^{-1}. The diatom species present in the flux samples were observed to change with depth, which when compared to the seasonal diatom succession revealed a temporal succession of diatom species with increasing depth and a deep penetration of the slow sinking pool of particles as predicted in chapter 3. Within the MSA, coccosphere PIC fluxes were ~ 50 % of total cell bound biomineral flux whilst diatom cell bound POC contributed ~ 99 % to the total cell bound POC export in MSA. Observations imply that, (1) some component of the slow sinking flux is associated with diatoms and traces the surface seasonal succession of diatom species with depth; (2) the slow sinking flux is observed to reach at least 600 m; (3) coccolithophores dominate the fast sinking biomineral flux in MSA and; (4) the diatom POC flux to the sediments may be associated with coccolithophore PIC in the MSA.

4.2 Introduction

Photosynthetic phytoplankton are an integral part of the biological carbon pump, taking up CO_2 and creating particulate organic carbon (POC) [*Boyd and Trull*, 2007]. This POC can aggregate, forming rapidly sinking particles which export carbon to the abyss. These particles are known as marine snow aggregates (MSA) [*Alldredge and Jackson*, 1995]. Annually 5 – 11 Gt of POC are exported from the euphotic zone [*Laws et al.*, 2000; *Henson et al.*, 2011]. However as particles sink remineralisation processes attenuate this POC flux [*Martin et al.*, 1987] resulting in only ~ 1 % of exported POC sinking below 1000 m [*Poulton et al.*, 2006].

The peak in the seasonal cycle of phytoplankton in temperate waters (the spring bloom) is recorded in deep sediment trap fluxes [*Lampitt et al.*, 2010], thus the seasonal cycle of phytoplankton production relates to the magnitude of POC export [*Henson et al.*, 2009]. During winter, enhanced mixing brings nutrient rich waters to the surface ocean. These elevated nutrients, coupled with water column stratification initiates rapid diatom growth and the onset of the spring bloom [*Sieracki et al.*, 1993; *Pommier et al.*, 2009]. Following the initial diatom bloom, as irradiance levels continue to increase into the summer and nutrient level decrease, coccolithophores succeed diatoms [*Eppley et al.*, 1969; *Leblanc et al.*, 2009]. Coccolithophore blooms are particularly extensive in the temperate and subarctic regions of the north Atlantic and consist of highly diverse species [*Brown and Yoder*, 1994; *Broerse et al.*, 2000; *Ziveri et al.*, 2000].

Both diatoms and coccolithophores produce biominerals. Coccolithophores, through the process of calcification produce calcite (particulate inorganic carbon, PIC) containing coccoliths which form a coccosphere around the cellular protoplasm [*Young*, 1994]. Diatoms, through silicification, produce opaline (biogenic silica, BSi) frustules [*Poulton et al.*, 2006]. The presence of biominerals is thought to determine the magnitude of the POC fluxes [*Armstrong et al.*, 2002] with correlations between POC and biomineral fluxes, especially PIC, in both the surface and deep being inferred as evidence for biomineral ballasting [*Francois et al.*, 2002; *Klaas and Archer*, 2002; *Sanders et al.*, 2010]. However correlation does not necessarily imply a causal relationship and the exact mechanism driving this ballasting relationship, be it enhancement of particle density [*Klaas and Archer*, 2002], biomineral protection of POC [*Armstrong et al.*, 2002] or POC gluing biominerals together [*Passow*, 2004], remains unclear [*De La Rocha and Passow*, 2007].

Individual diatom cells sink between 1 and 30 m day^{-1} [*Smayda*, 1971] whilst individual coccolithophores sink between 1 and 10 m day^{-1} [*Young*, 1994]. Significant export events often marked as seasonal pulses of rapidly sinking aggregates are often diatom associated, with the onset of the spring bloom [*Michaels and Silver*, 1988; *Honjo and Manganini*, 1993; *Buesseler*, 1998]. Aggregates and faecal pellets sink between 5 and 2700 m day^{-1} [*Turner*, 2002]. Thus the incorporation of phytoplankton into rapidly sinking MSA and FP facilitates their transfer, and that of the associated POC, to the deep ocean [*Boyd and Trull*, 2007]. Sinking POC can be subdivided into a slow (7 – 11 m d^{-1}) and fast (> 300 m d^{-1}) sinking pool [*Alonso-González et al.*, 2010], which constitutes ~ 60 and 40 % respectively of the flux out of the euphotic zone at the PAP site (Chapter 3 [*Riley et al.*, 2012]).

Previous studies which examined the role of phytoplankton in particle flux in the north east Atlantic have observed diatom dominated export fluxes in the subtropical gyre in the top 300 m of the water column [*Passow and Peinert*, 1993]. However, coccolithophore oozes, dominated by species such as *Emiliana huxleyi, Gephyrocapsa mullerae, Calcidiscus leptoporus* and *Coccolithus pelagicus* govern the mass flux to the deep sediments in the north east Atlantic [*Ziveri et al.*, 2000]. Geochemical analysis of deep sediment trap material indicates that diatom derived POC is more important than coccolithophore POC for fluxes in the north east Atlantic Porcupine Abyssal Plain (PAP) site [*Salter et al.*, 2010]. Thus it is hypothesised that diatom POC is transferred to the deep ocean by coccolithophore PIC ballast rather than by its own BSi ballast in aggregated particles such as marine snow.

Chapter 3 observed a slow sinking flux of biogenic silica but not of calcite at the PAP site, implying that diatoms are the main contributors to the slow flux. Furthermore it was hypothesised, based on both the sinking speed and the Martin [1987] attenuation curves, that the slow sinking flux would reach ~ 500 m depth. It is envisaged that either; (1) a decrease in the diversity of exported diatom species will be observed with depth, due to preferential remineralisation / dissolution of species sinking at different speeds, or (2) given the slow sinking speed and transit time of ~ 60 days to 600 m, a chronology of spring bloom species will be observed with depth.

Furthermore, the absence of calcite in the slow flux (Chapter 3) but dominance of coccolithophore oozes in the sediments [*Ziveri et al.*, 2000] suggest that the majority of the calcite flux is found in the fast sinking MSA. In order to investigate these theories, taxonomic identification of the diatom and coccolithophore species in sinking material exported between 50 and 600 m was undertaken and compared to the species composition of the surface ocean community sampled at the time and to the seasonal succession of species sampled using the continuous plankton recorder (CPR).

4.3 Methods

4.3.1 Sampling

Sampling was conducted during cruise D341 (RRS Discovery 8th July to 13th August 2009). Water samples for mixed layer phytoplankton community structure were taken from CTD casts. Individual marine snow aggregates (MSA, ~ 500 µm diameter) were collected from 5 deployments of the Marine Snow Catcher (MSC) at 50 m [Lampitt et al., 1993]. Individual particle sinking speeds and areas were measured (as detailed in chapter 3) and the phytoplankton incorporated into the MSA were counted (as outlined below). Samples of sinking organic matter were collected from 175 m, 280 m, 300 m, 450 m and 600 m depth using neutrally buoyant PELAGRA traps [Lampitt et al., 2008] for determination of the phytoplankton community exported through the mesopelagic.

Two water column profiles were sampled during the cruise (Table 4.1) consisting of the mixed layer community (MLC), MSA and deeper water flux (DF from the PELAGRA samples between 175 and 630 m). Samples were all collected from approximately the same location. The first profile (14th July) collected water samples from the MLC and deeper water fluxes at 280 m and 630 m. The second profile (3rd August) collected samples from the MLC, MSA from 50 m and deeper water fluxes at 175 m, 300 m and 450 m.

Sample	Lat. Start	Lat. End	Long. Start	Long. End	Distance travelled (km)	Direction Travelled (°)
Profile 1 (14/07/09)						
Mixed Layer Community	49.03	n/a	16.48	n/a	n/a	n/a
DF (280 m)	49.04	49.02	16.50	16.76	19.09	263
DF (630 m)	49.04	49.02	16.50	16.67	12.59	259
Profile 2 (3/08/09)						
Mixed Layer Community	54.65	n/a	16.43	n/a	n/a	n/a
Marine Snow Aggregates (50 m)	48.97	n/a	16.42	n/a	n/a	n/a
DF (175 m)	48.92	48.80	16.39	16.96	43.78	252
DF (300 m)	48.92	48.78	16.39	17.02	48.65	251
DF (450 m)	48.91	48.79	16.39	17.03	48.69	253

Table 4.1 Profiles from the PAP site sampled on 14/07/09 NBS 03/08/09. Mixed layer community corresponds to phytoplankton samples taken from 5, 25 and 50 m water depth. Marine snow aggregates refers to individual particles collected using the marine snow catcher. DF refers to the deeper water flux samples collected using the PELAGRA traps. PELAGRA traps were deployed for a minimum of 48 hours, thus a start and end latitude and longitude are shown.

4.3.2 Mixed layer community

Coccolithophore MLC was determined from CTD water samples at 5, 25 and 50 m depth. 500 mL of each sample was filtered onto a 25 mm diameter, 0.8 µm nominal

pore size cellulose nitrate (CN; Whatmann) filter under low (< 400 bar) pressure. A GFF (Fisherbrand) filter was used as a backing filter to achieve an even distribution of the cells. Each CN filter was rinsed with a slightly alkaline (pH 9) de-ionised water solution to remove any salt and dried for ~ 8 hours in a warm (~ 30 °C) oven. Half of the filter, was prepared for scanning electron microscopy (SEM) image analysis at x 5000 magnification using a Scanning Electron Microscope (Leo 1450VP, Carl Zeiss, Germany) [*Charalampopoulou et al.*, 2011]. For each sample, either 225 fields of view (FOV) or 300 coccospheres (whichever first) were enumerated and identified to species level following Young et al. [2003].

Diatom species were enumerated in 100 mL water samples from 5, 25 and 50 m, preserved with 2 mL of Lugols iodide solution and stored in brown bottles in a dark, cool environment. 50 mL sub samples were placed in a Hydrobios plankton counting chamber (Duncan and Associates Ltd.) and settled for a minimum of 12 hours. Post settling, the main genera of diatoms were identified using an inverted microscope (Brunel SP95I). All diatom species within the settled chamber were counted.

The number of cells per mL for each coccolithophore and diatom species was calculated following [*Bollmann et al.*, 2002] (Equation 4.1);

$$D_C = \frac{F \times C}{A \times V} \qquad \text{(Eq. 4.1)}$$

Where D_C is the density of cells per unit volume, F is the filtered area or area counted, C is the number of cells actually counted and V is the volume filtered or settled. For both diatoms and coccolithophores counts were integrated between 5 and 50 m depth to give an estimate of the total mixed layer community (MLC).

4.3.3 Marine Snow Aggregate community

In total 30 particles were collected using the MSC and picked out of the base chamber of the MSC. Their sinking speeds were measured and each particle imaged (see chapter 3 for details on collection methods) prior to preservation on 0.8 µm nominal pore size CN (Whatmann) filters. The filters were trimmed and mounted onto a glass slide with a protective cover slip using Norland Optical Adhesive (No. 74 Technoptics). Slides were left to cure in UV light for a few hours. Coccolithophore species were identified under polarising light, using an oil immersion objective at x 1000 magnification and diatom species were counted under plain light at x 400 magnification using a polarising light microscope (Brunel SP200). For each sample the total coccospheres and diatoms were enumerated and identified to species level following *Frada et al.* [2010] and *Carmelo* [1997].

4.3.4 Deep flux diatom and coccolithophore community

During the cruise 5 PELAGRA deployments were undertaken to sample the DF. The PELAGRA trap pots were filled with brine solution denser than seawater and spiked with chloroform (0.5 % volume / volume) to preserve any sinking material. Upon recovery the material collected was further preserved using 5 % (volume / volume) buffered formalin and stored in dark bottles in a cool environment until further analysis. Due to the concentrated nature of the material approximately 1 mL of preserved DF material was pipetted into a centrifuge tube and diluted with 9 mL of slightly alkaline (pH 9) de-ionised water. This 10 mL dilution was then gently shaken to homogenise the sample. 5 mL was then filtered onto a pre weighed, 25 mm diameter, cellulose nitrate (0.8 µm nominal pore size) filter, under a low (< 400 bar) vacuum. Weighing was undertaken using a Sartorius ME-5 microbalance (precision ± 1 µg). Filters were rinsed with 2 mL of slightly alkaline (pH 9) de-ionised water, dried overnight in a warm (30°C) oven. Once dry filters were re-weighed to determine the mass of material filtered. Two replicates of each dilution were filtered. Filters were split in half, with one portion prepared for SEM microscopy and coccolithophore enumeration, the other portion was mounted on a glass slide for diatom enumeration using light microscopy, as outlined above.

4.3.5 Species specific POC, PIC and BSi conversions

Conversion factors were applied to the coccolithophore and diatom raw cell counts (which in all cases only included intact cells) to calculate species specific masses of POC (particulate organic carbon), PIC (particulate inorganic carbon) and BSi (biogenic silica) for all diatoms and coccolithophores (Table 4.2). Coccolithophore POC estimates were made utilising the conversion factors of *Poulton et al.* [2010] and *Young et al.* [2003]. Coccolith PIC estimates were determined from coccolith dimensions following *Young and Ziveri* [2000]. Coccosphere PIC was estimated by multiplying individual coccolith PIC by the estimated numbers of coccoliths per coccosphere [*Boeckel and Baumann*, 2008; *Poulton et al.*, 2010]. Diatom POC was calculated by measuring the individual cell dimensions (n = 10) and applying the conversion factors of [*Kovala and Larrance*, 1966] as applied by *Poulton et al.* [2007]. BSi was calculated assuming a silica: carbon ratio of 0.13 [*Brzezinski*, 1985].

Species	Cell POC [pg]	Reference	Coccolith calcite [pg]	SD	Reference	Av. # coccoliths per cell	SD	Reference	Av. Cell Calcite [pg]	Cell BSi [pg]	Reference
Coccolithophores											
Emiliana huxleyi and Gephyrocapsa mullerae	7.2	[Poulton et al., 2010]	5.15	4.03	[Young and Ziveri, 2000]	17	2.83	[Poulton et al., 2010]	88	–	–
Syracosphaera pulchra	51.6	[Young et al., 2003]	13.50		[Young and Ziveri, 2000]	45		[Boeckel and Baumann, 2008]	610	–	–
Calcidiscus leptoporus	54	[Poulton and Young unpub.]	75.00		[Young and Ziveri, 2000]	14		[Poulton and Young unpub.]	1050	–	–
Coccolithus pelagicus	46.8	[Young et al., 2003]	356.00		[Young and Ziveri, 2000]	8		[Poulton and Young unpub.]	2850	–	–
Diatoms											
Bacteriastrum spp.	240	[Kovala and Larrance, 1966]	–		–	–	–		–	156	[Brzezinski, 1985]
Thalassiosira spp.	744	[Kovala and Larrance, 1966]	–		–	–	–		–	486	[Brzezinski, 1985]
Rhizosolenia spp.	4956	[Kovala and Larrance, 1966]	–		–	–	–		–	3222	[Brzezinski, 1985]
Cylindrotheca spp.	1164	[Kovala and Larrance, 1966]	–		–	–	–		–	756	[Brzezinski, 1985]
Navicula spp.	660	[Kovala and Larrance, 1966]	–		–	–	–		–	432	[Brzezinski, 1985]
Pseudonitzchia spp.	3384	[*Kovala and Larrance*, 1966]	–		–	–	–		–	2202	[Brzezinski, 1985]

Table 4.2 Species specific conversions for cell bound POC, PIC and BSi. The SD values for the *E. huxleyi and G. mullerae* result from an average coccolith calcite and number of coccoliths per coccosphere being calculated. *E. huxleyi and G. mullerae* had to be classified together because it was not always possible to distinguish clearly between the two species. Poulton and Young observations of coccoliths per coccosphere are from samples collected in the Mauritanian upwelling system.

4.3.6 Flux calculations

Fluxes of coccolithophore and diatom POC and biominerals associated with each individual MSA particle were calculated following equation 4.2. The total counts for each species (coccolithophore or diatoms; Appendix C.1) per MSA were divided by MSC area and the time it took each particle to sink (appendix C.2). This cell flux per aggregate (appendix C.3, table C.3) was then multiplied by the respective conversion factor for POC, PIC or BSi to calculate the organic carbon and biomineral fluxes for each species of coccolithophore and diatom (appendix C.4, tables C.4 and C.5). The sinking time was calculated as a ratio of half the height of the MSC:measured sinking speed of each MSA. Half the height of the MSC was used assuming a homogenous distribution of MSA throughout the 100 L sample at the start of the settling period (as discussed in chapter 3).

$$Flux = \left(D_C / Area / R_{H:SS}\right) \cdot CF \qquad \text{(Eq. 4.2)}$$

Where D_C is the species specific cell density per MSA, *Area* is the vertical footprint of the MSC (0.06 m^2) and $R_{H:SS}$ is the ratio of half the MSC height (0.75 m) to sinking speed (average of 173 (± 40) m d^{-1}, n = 9) and CF is the conversion factor for each species (Table 4.2). The sinking speeds of the MSA were measured on board the ship using a measuring cylinder filled with ambient sea water and a stop watch, immediately after collection. The total MSA flux for each species was then calculated by taking an average coccolithophore and diatom species POC and biomineral flux per MSA (Appendix C5 tables C6) and multiplying by the total number of aggregates collected during the deployment (n = 30; appendix C5, table C6).

For the DF samples individual coccolithophore and diatom POC, PIC and BSi fluxes were calculated for each sample. The number of cells filtered was calculated by multiplying the filtered area by the raw cell counts and dividing by the analysed area and the total mass filtered (Appendix C Tables C7-11) [*Bollmann et al.*, 2002]. This was then scaled to the total number of cells per PELAGRA collection pot by multiplying by the total mass of the material collected in the pot (*Marsay* unpublished; Appendix C, Tables C.7 and C.12). The flux of cells in each of the DF samples was then calculated by dividing the number of cells per pot by the PELAGRA sampling cone area and the sampling time (Appendix C, table C.13). This cell flux per DF sample was then multiplied by the respective conversion factor for POC, PIC or BSi (Table 4.2) to calculate the organic carbon and biomineral fluxes for each species of coccolithophore and diatom. (Equation 4.2; Appendix C; tables C.14-15).

$$Flux = \left(R_{(D_C \times m_P)} / A_{Cone} / Time\right) \cdot CF \quad \text{(Eq. 4.2)}$$

Where $R_{(D_C \times M_P)}$ is the multiplication of the phytoplankton cell density per mass filtered: DF mass per pot, A_{Cone} is the area of the PELAGRA sampling cone and *Time* is the sampling time. Average fluxes (and standard deviations) were calculated from the replicate measurements at each depth and the errors were propagated through to provide a final estimate of the error in the total coccolithophore and diatom fluxes at each depth (Appendix C, Tables C.16–17).

4.3.7 Community diversity and multivariate data analysis

The diversity of the phytoplankton community was estimated for the species specific POC fluxes using the Shannon–Weiner Diversity index (H') and Pielou's evenness (J'). H' is a measure of both species diversity and richness and ranges from low (< 0.1 – 0.5) to high values (> 1.5 – 2). J' gives an indication of how even POC is distributed between species without accounting for species richness and ranges from low (< 0.1 – 0.4) to high (> 0.7 – 1) [*Poulton et al.*, 2007].

Multivariate statistical analyses using E–PRIMER (v. 6.0) [*Clarke and Gorley*, 2006] were utilised to examine any changes in species specific coccolithophore and diatom POC and biomineral contribution to standing stocks and fluxes between samples. Data was standardised to each sample total (either flux or mass of coccolithophores or diatoms) to give relative species abundances and fourth–root transformed to reduce data skewing. Analysis was carried out using Bray–Curtis similarity to determine changes in species POC contribution with depth. Samples were clustered into groups that were mutually similar using hierarchical agglomerative clustering (CLUSTER) and non metric multidimensional scaling (NMDS) analysis. Differences were confirmed by performing an analysis of similarities (ANOSIM) on the *a priori* identified clusters. Characteristic and discriminating species were identified using the similarity percentage (SIMPER) routine. Characteristic species are those responsible for the clustering of samples whilst discriminating species are those responsible for differences between groups. Characteristic species were those contributing > 90% to the Bray–Curtis similarity within each group. Discriminating species were defined as those which cumulatively contributed > 50 % to the Bray–Curtis dissimilarity between groups.

4.3.8 Continuous plankton recorder data

Continuous plankton recorded (CPR) data denoting the seasonal evolution of diatom species in the upper ocean [*Richardson et al.*, 2006] were compared with the species

present in the DF samples to determine if changes in the phytoplankton species occurring with depth relate to the changes in the upper ocean community structure over time. Data were obtained via SAHFOS (Sir Alastair Hardy Foundation for Ocean Science) for the E5 region, for the period February to August 2009 (Appendix C.5 Figure C3.1). Monthly data were averaged across the region. Smaller phytoplankton species may be under-sampled by the large (270 µm) mesh size of the collecting silk resulting in significant underestimation of absolute phytoplankton numbers. Nevertheless, the CPR data has been proven to represent a consistent proportion of the larger phytoplankton species, reflecting the major patterns in the sampled phytoplankton distributions and abundances [*Batten et al.*, 2003]. Consequently, when utilising the CPR data, interpretations were made in a semi quantitative way, examining the relative abundance of diatom species prior to and during the cruise.

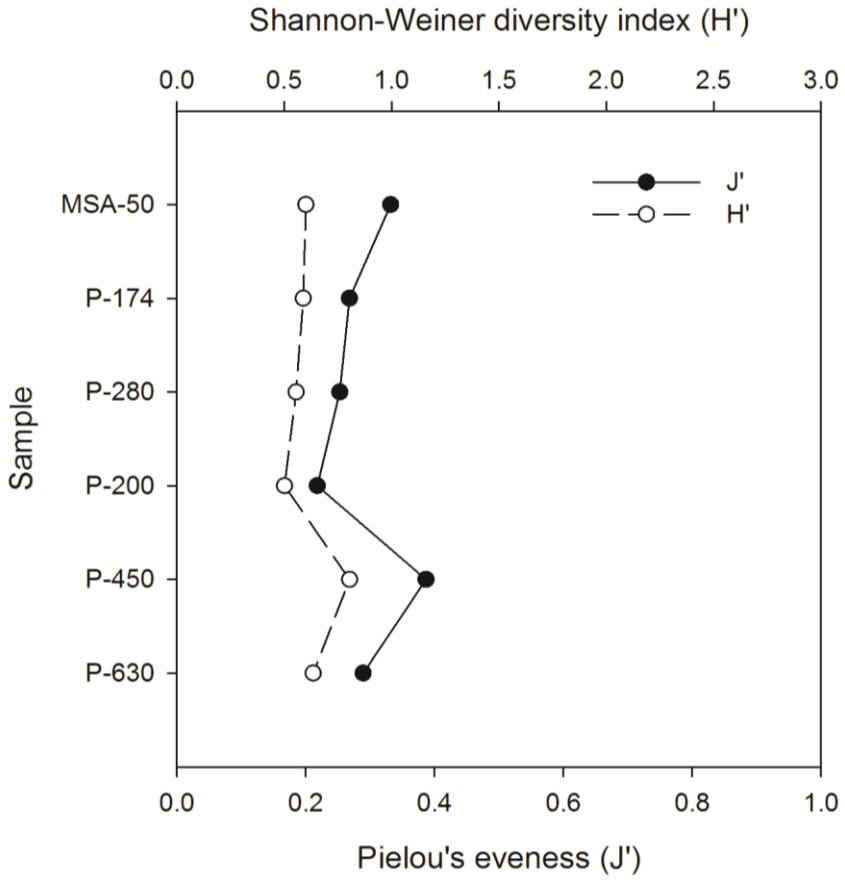

Figure 4.1 Diversity indices for total coccolithophore and diatom species POC across each sample type (y-axis). The y-axis also corresponds to increasing depth.

4.4 Results

4.4.1 Community composition

Sample	Profile 1			Profile 2				
	MLC	P-280	P-630	MLC	MSA-50	P-175	P-300	P-450
Number of species	10	9	9	16	8	8	9	9
E .huxleyi and *G. Muellerae*	*	*	*	*	*	*	*	*
Syracosphaera pulchra	*	*	*	*	*	*	*	*
Calcidiscus leptoporus	*	*	*	*	*	*	*	*
Coccolithus pelagicus	*			*	*			
Bacteriastrum spp.		*	*	*			*	*
Thalassiosira spp.	*	*	*	*	*	*	*	*
Guinardia spp.					*			
Leptocylindrus spp.				*				
Planktoniella spp.				*				
Rhizosolenia spp.		*	*			*	*	*
Proboscia spp.	*			*				
Tropidoneis spp.	*			*				
Cylindrotheca spp.	*	*	*	*		*	*	*
Navicula spp.	*	*	*	*	*	*	*	*
Thalassionema spp.	*							
Pseudonitzschia spp.		*	*	*	*	*	*	*
Gyrosigma spp.				*				
Pleurosigma spp.				*				
Thalassiothrix spp.				*				

Table 4.3 Coccospheres, coccoliths and diatom species identified across the two profiles (detailed in table 4.1). Stars represent the presence of a species. Blank is the absence of that species in the sample. MLC stands for the integrated mixed layer community, between 0 and 50 m, P-280 etc. represents the PELAGRA deployment and corresponding depth to measure the deep flux (DF) and (MSA-50) are the marine snow aggregates (MSA) collected from 50 m depth. The MSA sample an average of 9 individual particles which were collected and microscopically counted for coccolithophore and diatom cells. Mixed layer samples are integrated to 50 m, based on 3 depths counted (5, 25 and 50m).

In total 15 diatom species and 5 coccolithophore species were identified across the two profiles (Table 4.3). Coccolithophore species occurred ubiquitously across most depths. In comparison diatoms show a much patchier distribution across all the samples with only 4 species, *Thalassiosira spp., Cylindrotheca spp. Navicula spp.* and *Pseudonitzschia spp.,* being identified in > 75% of samples. Generally no decrease in the number of coccolithophore or diatom species was apparent with depth across the two profiles, with an average of 10 species identified per sample. Species which individually accounted for less than 5 % of the total diatom and coccolithophore

community, including *Guinardia spp., Leptocylindricus spp., Planktoniella spp., Tropidoneis spp., Gyrosigma spp., Pleurosigma spp.* and *Thalassiothrix spp.,* were not included in the carbon and biomineral conversions due to their low abundances. Overall, community diversity estimated using the Shannon-Weiner diversity index was relatively constant with depth (0.6). Similarly the distribution of phytoplankton species was fairly even with depth (Pielou's evenness 0.3; Figure 4.1).

4.4.2 Phytoplankton POC and biomineral standing stocks

Phytoplankton species were integrated across all depths sampled within the mixed layer to estimate the integrated MLC concentrations of POC, PIC and BSi (Table 4.4). In both MLC samples (14/07/09 and 03/08/09) diatom POC concentrations (4.34 and 7.81 μg m^{-2} respectively) were greater than coccolithophore POC concentrations (0.03 and 0.06 μg m^{-2} respectively). *Cylindrotheca spp.* contributed > 65 % of the total diatom POC standing stock whilst *Syracosphaera pulchra* contributed ~ 79 % of the total coccolithophore POC standing stock (Appendix C, tables C20 and C21). Coccosphere calcite was 0.762 and 0.863 μg m^{-2} in both samples respectively. Both *Syracosphaera pulchra* and *Calcidiscus leptoporus* cumulatively contributed > 90 % to the total coccosphere standing stock. The standing stock of BSi in both samples was 2.8 and 5.8 μg m^{-2} respectively with *Cylindrotheca sp.* contributing > 80 %.

	Integrated MLC (14/07/09) μg m^{-2}	Integrated MLC (03/08/09) μg m^{-2}	Average μg m^{-2}
Coccolithophore POC	0.027	0.053	0.04 (± 0.013)
Diatom POC	4.339	7.805	4.572 (± 3.233)
Coccosphere Calcite	0.762	0.863	0.813 (± 0.051)
Diatom biogenic silica	2.802	5.069	3.935 (± 1.13)

Table 4.4 Phytoplankton POC, PIC and BSi standing stocks integrated across the mixed layer.

4.4.3 Species specific POC and biomineral phytoplankton fluxes

Overall it is clear that diatoms are more significant for POC export out of the surface ocean, in general contributing > 90 % of both the total flux and the fast MSA flux. The same trend holds for the biomineral flux with diatom BSi constituting > 90 % and coccolithophore PIC < 10 % of the total flux. However in MSA this trend changes with coccolithophore PIC and diatom BSi each exporting ~ 50 % of the total biomineral flux (Figure 4.3).

	Profile 1			Profile 2		
	P-280	P-630	MSA	P-175	P-300	P-450
	μg m^{-2} d^{-1}	μg m^{-2} d^{-1}	μg m^{-2} d^{-1}	μg m^{-2} d^{-1}	μg m^{-2} d^{-1}	μg m^{-2} d^{-1}
POC						
Coccolithophores	0.19 (± 0.21)	0.13 (± 0.18)	282 (± 119)	0.13 (± 0.25)	0.16 (± 0.26)	0.03 (± 0.16)
Diatoms	1712 (± 0.27)	1516 (± 8)	6586 (± 4709)	780 (± 0.17)	1311 (± 8)	361 (± 5)
Biominerals						
Coccosphere PIC	0.22 (± 0.04)	0.36 (± 0.13)	4266 (± 1959)	0.65 (± 0.4)	0.22 (± 0.07)	0.1 (± 0.04)
Diatom BSi	60 (± 17)	59 (± 2.8)	4291 (± 3065)	24 (± 6)	43 (± 2)	14 (± 0.8)

Table 4.5 Cell bound and detrital POC, PIC and BSi fluxes measured across the two profiles at the PAP site.

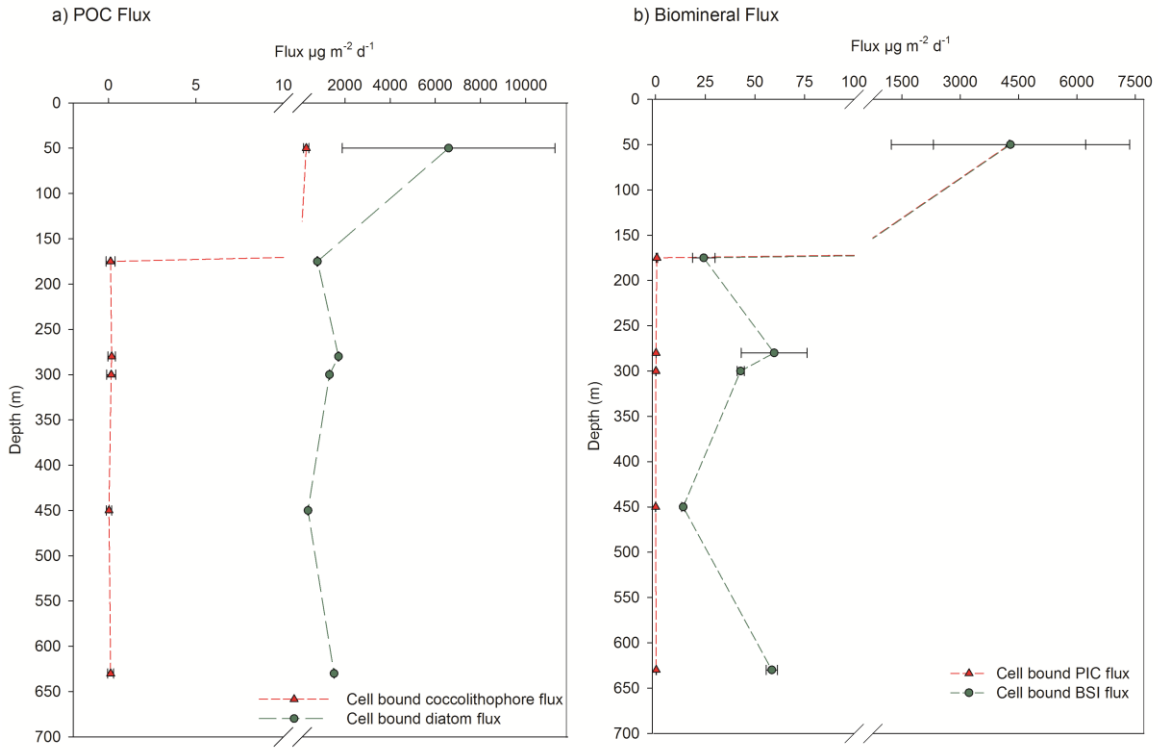

Figure 4.2 DF and MSA flux profiles for (a) POC and (b) biominerals. Coccolithophore and diatom fluxes refer to the cell bound flux calculations. The MSA detrital POC flux was calculated using the total POC flux measurement presented in chapter 2. Note break in x-axis in both plots.

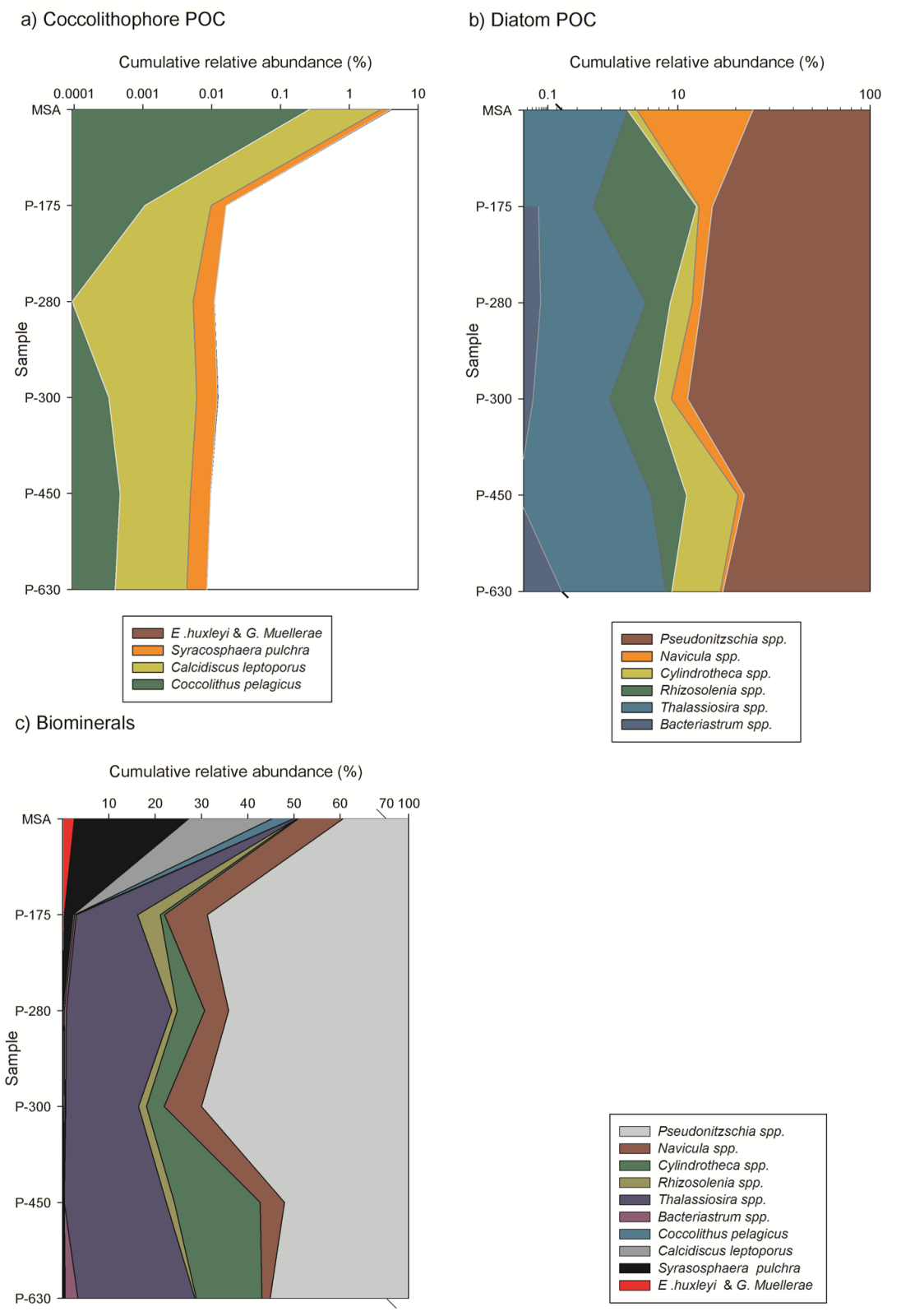

Figure 4.3 Cumulative relative abundances of (a) coccolithophore POC flux, (b) diatom POC flux and (c) coccolithophore and diatom biomineral fluxes. Note the break in the x-axis in plots b and c. Note the x-axis log scale in a and b.

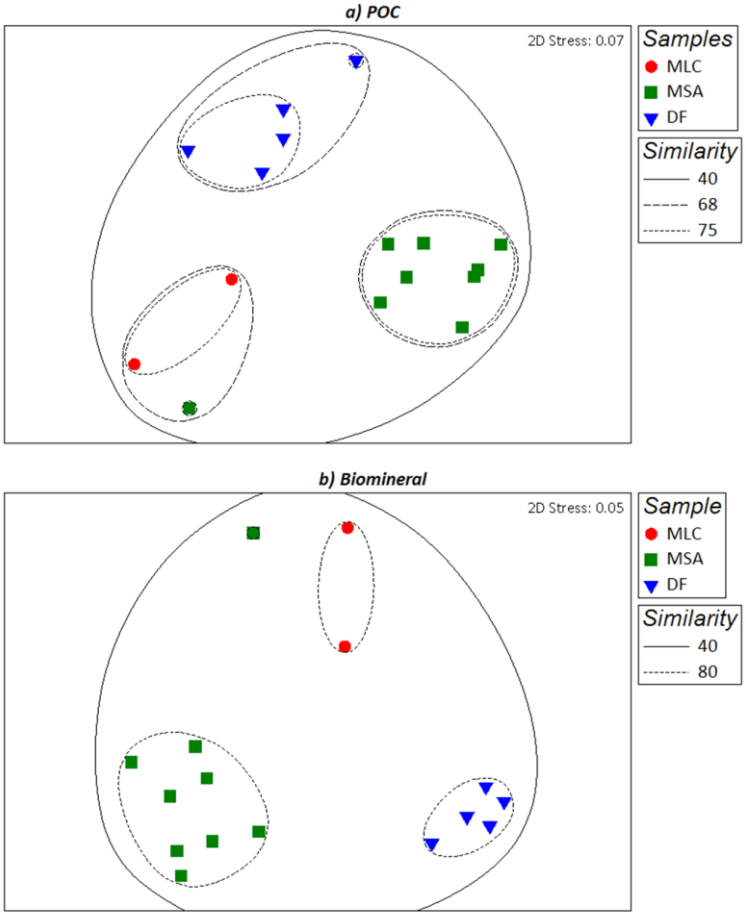

Figure 4.4 Multivariate cluster analysis of (a) POC and (b) Biominerals in the mixed layer community (untransformed data in concentration units) and exported flux measured in the PELAGRA and MSA samples (untransformed data in flux units). The analysis compares the relative abundance of coccolithophore and diatom cell bound POC and biominerals. MLC is the mixed layer community samples, MSA is the Marine Snow Aggregate samples, and DF is the Deep Flux samples.

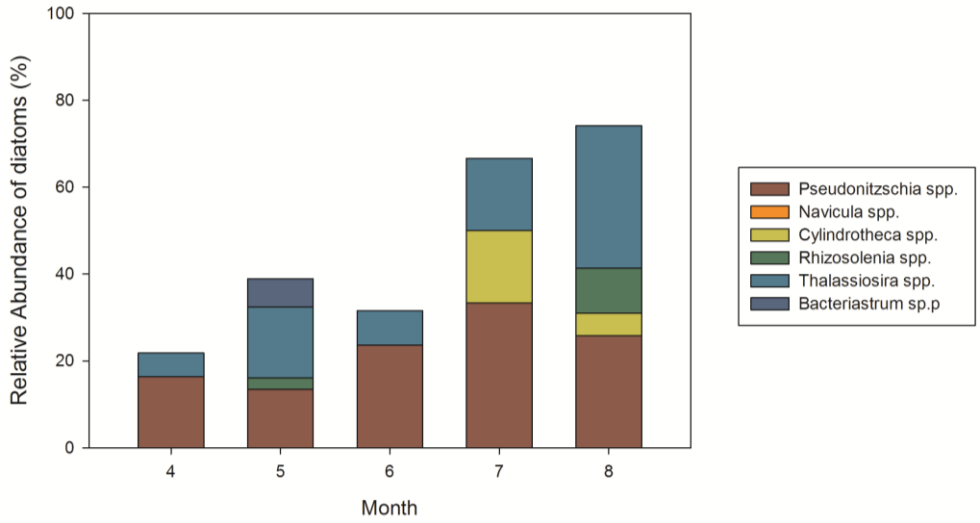

Figure 4.5 Monthly averages for CPR diatom seasonal succession for the E5 region (which includes the PAP site) in 2009. *Navicula spp.* was included in the legend for this plot as it was observed in the sinking material but was not recorded by the CPR.

Coccolithophore POC fluxes were low in all DF (~ 1 µg m^{-2} d^{-1}) and showed little variability with depth. The MSA coccolithophore POC fluxes (282 (± 119) µg m^{-2} d^{-1}) were relatively larger than in the DF samples (Table 4.5, Figures 4.2 and 4.3). *Syracosphaera pulchra* and *Calcidiscus leptoporus* cumulatively contributed > 60 % of the total coccolithophore flux (Figure 4.3 and appendix C for individual coccolithophore species fluxes). Overall diatom POC fluxes were considerably higher than coccolithophore POC fluxes, contributing between 361 (± 5) and 6586 (± 4709) µg m^{-2} d^{-1} (Table 4.5). In all samples *Pseudonitzschia spp.* contributed > 75 % of the total POC flux (Figure 4.3, appendix C).

Coccosphere PIC fluxes were generally low and constant in the DF samples (< 0.65 (± 0.4) µg m^{-2} d^{-1} (Figure 4.2, Table 4.5)). The exception to this was the MSA sample which had a coccosphere PIC flux of 4266 (±1959) µg m^{-2} d^{-1}, driven by *Syracosphaera pulchra* (> 90 %, Figure 4.3). Cell bound biogenic silica fluxes were generally higher than cell bound PIC fluxes. The DF of BSi ranged between 14 (± 0.8) and 60 (± 17) µg m^{-2} d^{-1} whilst the MSA BSi flux was relatively higher again (4291 (± 3065) µg m^{-2} d^{-1}). *Pseudonitzschia spp.* contributed > 84 % of the total cell bound BSi flux.

POC (75 % similarity)			Biomineral (80 % similarity)		
MLC	MSA	DF	MLC	MSA	DF
Cylindrotheca spp. (41 %)	*Pseudonitzschia spp.* (37 %)	*Pseudonitzschia spp.* (30 %)	*Cylindrotheca spp.* (50 %)	*Syracosphaera pulchra* (23 %)	*Pseudonitzschia spp.* (26 %)
Navicula spp. (20 %)	*Navicula spp.* (31 %)	*Thalassiosira spp.* (20 %)	*S. pulchra* (15 %)	*Pseudonitzschia spp.* (22 %)	*Thalassiosira spp.* (19 %)
Thalassiosira spp. (15 %)	*S. pulchra.* (12 %)	*Cylindrotheca spp.* (16 %)	*C. pelagicus* (13 %)	*Navicula spp.* (19 %)	*Navicula spp.* (19 %)
S. pulchra (11 %)	*E. huxleyi / G. mullaerae* (7 %)	*Rhizosolenia spp.* (12 %)	*Navicula spp.* (12 %)	*C. leptoporus* (15 %)	*Cylindrotheca spp.* (12 %)
C. Pelagicus (7 %)	*Calcidiscus leptoporus* (7 %)	*Navicula spp.* (9 %)	*Thalassiosira spp.* (6 %)	*E. huxleyi / G. mullaerae* (13 %)	*Rhizosolenia spp.* (9 %)
		S. pulchra (4 %)	*C. leptoporus* (6 %)		*C. leptoporus* (6 %)
					E. huxleyi / G. mullaerae (5 %)

Table 4.6 Characteristic species of the POC and biomineral clusters identified in figure 4.4. Percentages indicate the % contribution to the cluster similarity.

4.4.4 Multivariate analysis of community structure

NMDS analysis of all POC standing stock and flux samples revealed 3 clusters (MLC, MSA and DF samples) at 75 % similarity (plus one MSA and DF outlier), $p < 0.05$, NMDS stress level of < 0.07 (Figure 4.4). The results of the ANOSIM test ($p < 0.001$, $R > 0.7$) further confirmed the differences between the first three clusters. Characteristic and discriminating species of the clusters are indicated in Table 4.6 and 4.7. Cluster and NMDS analysis of the biomineral standing stock and flux samples showed 3 significantly clusters (MLC, MSA, and DF) at 80 % similarity (plus one MSA outlier), $p < 0.05$, NMDS stress level of < 0.1 (Figure 4.4). Characteristic and discriminating species of the clusters are indicated in Table 4.6 and 4.7.

POC (75 % similarity level)	MLC	MSA
MSA	*Cylindrotheca spp.* (39 %) *Pseudonitzschia spp. (26 %)*	
DF	*Pseudonitzschia spp.* (22 %) *Rhizosolenia spp. (19 %)* *Cylindrotheca spp. (18 %)*	*Rhizosolenia spp.* (20 %) *Cylindrotheca spp. (19 %)* *Thalassiosira spp. (15 %)*
Biomineral (80 % similarity level)	MLC	MSA
MSA	*Cylindrotheca spp.* (31 %) *Pseudonitzschia spp.* (18 %) *C. leptoporus (13 %)*	
DF	*Pseudonitzschia spp.* (21 %) *C. pelagicus* (19 %) *Cylindrotheca spp. (14 %)*	*Thalassiosira spp.* (15 %) *Cylindrotheca spp. (15 %)* *S. pulchra (14 %)* *Rhizosolenia spp. (11 %)*

Table 4.7 Discriminating species of the POC and biomineral clusters identified in figure 4.4. Percentages indicate the % contribution to the differences between clusters.

4.4.5 Continuous plankton recorder data

Figure 4.5 shows a subset of the total CPR community data recorded between April and August 2009. Only those species which co-occurred in both the CPR and flux data sets have been shown for simplicity of interpretation (the full species lists for the CPR data can be found in appendix C.5, tables C18 and C19). The relative (rather than absolute) abundances of diatom species in the CPR data have been plotted due to the methodological sampling issues associated with the CPR (discussed in section 4.3.8). Overall it is clear that the earliest seasonal surface community data for 2009 represents the smallest proportion of the exported species observed (~ 20 %). However, as the season continues and the CPR data set co-occurs with the timing of the research cruise when the flux samples were collected, an increasing proportion of the exported species observed are represented in the CPR data (~ 75 % in August).

The general trend of the CPR data shows that *Pseudonitzschia spp.* was consistently abundant between April and August, however *Cylindrotheca spp.* and *Rhizosolenia spp.* significantly increased in abundance in July and August. *Bacteriastrum spp.* was only observed in May. The species which were not seen in the exported material but were in the CPR data in April were *Chaetoceros spp.* (49 %) and *Thalassionema nitzschioides* (29 %). In August the species not in the exported material but in the CPR data were *Chaetoceros spp.* (10 %), *Thalassionema nitzschioides* (5 %), *Thalassiothrix longissima* (5 %) and *Dactyliosolen mediterraneus* (5 %). (See appeddix C.15 for full CPR species list).

4.5 Discussion

Phytoplankton spatial and temporal heterogeneity may result in differences in the species identified at depth in the two profiles (sampled at a 3 week interval). Given the spatial and temporal differences between the profiles sampled it may be anticipated that samples from each profile would cluster separately from one another. However, the multivariate analysis showed that all samples from both profiles clustered into distinct MLC, MSA and PELAGRA groupings despite differences in both time and space. It is therefore concluded that there is little spatial and temporal variability in the phytoplankton community during the sampling period. The data will be discussed as one cohesive profile from this point onwards.

The representability of the CPR data can be assessed by comparing the species present in the surface lugols samples taken during the cruise and the CPR record. *Navicula spp.* occurred at all depths in the export flux data (Figure 4.3) but not the CPR data (Figure 4.5). Clearly there must have been *Navicula spp.* in the surface community at some point in time to have been exported to depth. However, *Navicula spp.* is a small (5 – 100 µm) diatom [*Carmelo*, 1997], thus the large mesh size (270 µm) of the CPR, combined with the spatial heterogeneity of phytoplankton communities and the spatial variability in the CPR sampling tracks mean this species is likely to be under sampled. However, the predominance of *Pseudonitzschia spp.* in both the MSA fluxes and DF samples (Figure 4.3) and the CPR data (Figure 4.5), as well as the abundance of *Cylindrotheca spp.* in July, mirrored in the MLC sampled at the time of the cruise (appendix C) strengthen the confidence in the CPR representation of the temporal evolution of the bloom at the PAP site.

4.5.1 Diatoms and the slow flux

The first aim of this chapter was to investigate the association between diatoms and the slow sinking flux based on the results of chapter 3, where a slow BSi flux but no slow PIC flux was observed. The first scenario proposed suggested that as particles sink they undergo remineralisation and dissolution processes, thus slow sinking diatoms would show a decrease in abundance with depth compared to faster sinking species, which undergo relatively less remineralisation. Thus it would be expected that the diversity of species will decrease with depth as slow sinking species are remineralised leaving only the faster sinking species in the deepest samples. However, analysis of the community diversity data indicates that species diversity remains constant with depth, indicative of no loss of species. Thus the first hypothesis that the slow sinking diatom community will decrease in diversity with depth and reflect attenuation of the present surface community is likely not correct.

The alternative hypothesis proposed that a seasonal succession of diatoms would be observed in the exported material, with deeper depths relating to species found earlier in the season in the surface community. Comparison of the exported diatom species with the CPR seasonal succession data shows *Bacteriastrum spp.* only occurred in May in the CPR record. The presence of the same species in the DF samples down to 630 m may indicate that part of the flux profile represents the temporal evolution of the diatom bloom and the slow flux does penetrate to at least 600 m depth. Assuming the *Bacteriastrum spp.* occurred ~ 60 days prior to sampling, the sinking speed of the *Bacteriastrum spp.* POC flux must be ~ 3 – 11 m d^{-1}, in line with the slow sinking flux (sinking speed calculated in chapter 3).

The rate at which particles sink is important in governing the distribution of CO_2 between the atmosphere and ocean [*Kwon et al.*, 2009]. The slower a particle sinks the longer it will take to penetrate into the ocean and the more carbon will be remineralised above the winter mixed layer thus able to return to the atmosphere. The average winter mixed later depth at the PAP site between 2003 and 2007 ranged between 150 and 225 m [*Steinhoff et al.*, 2010]. Thus it is suggested that at least some of the slow sinking flux is able to sink below the winter mixed layer at the PAP site. It is not possible to say if all of the slow sinking flux reaches 600 m as the data presented here is qualitative rather than quantitative.

The multivariate analysis of the relative abundance of species specific POC shows that 50 % of the differences between the surface community (identified in the lugols samples) and the exported community were accounted for by *Pseudonitzschia spp.* and *Cylindrotheca spp.*. The CPR record shows that *Cylindrotheca spp.* only occurred in the

surface waters in July, thus to have reached 600 m within ~ 14 days they would have to sink at ~ 50 m d^{-1}. This indicates that diatoms may also be associated with faster sinking particles.

Previous studies have shown that nutrients may play an important role in the diatom cell physiology and regulation of its buoyancy. In particular silica limitation results in much faster cell sinking speeds than under nutrient replete conditions [*Bienfang et al.*, 1982; *Nelson and Brzezinski*, 1990] because buoyancy regulation is thought to be an energy intensive process, requiring ATP, formed from photosynthesis [*Bienfang*, 1981]. Silicate is thought to become limiting for diatoms at ca. 2 µM [*Egge and Aksnes*, 1992]. The ambient surface (5 m) water silicate concentrations measured during the cruise were 0.6 – 0.7 µmol L^{-1}. Thus silicic acid concentrations are likely to be limiting, resulting in faster sinking speeds of the diatom cells occurring in July / August contributing to the POC flux. Thus it is proposed that nutrient availability may control the relative magnitudes of the fast and slow diatom fluxes. Furthermore as the growing season proceeds and nutrients become increasingly depleted, the community structure may shift and/or the sinking speed of the species exported from the surface community may increase.

Some species were found in the CPR record but not in the exported flux. In April (Figure 4.5) this discrepancy is largest with ~ 80 % of the community recorded by the CPR not documented in the exported material in July. Of the missing species in April, 49 % of were *Chatocerous spp.,* a chain forming diatom with individual cell sinking speeds of 16 – 30 m d^{-1} [*Passow*, 1991], which is relatively more susceptible to biomineral dissolution [*Schroder-Ritzrau et al.*, 2001]. It may be that the *Chatocerous spp.* present in April have either sunk out of the top 600 m too quickly to still be observed at depth in July / August, or that they have undergone dissolution processes, thus have not been preserved in the exported material later in the season. It is not possible to determine which process (rapid sinking or dissolution) occurred given the data presented in this chapter.

A further explanation may lie in the fact that *Chatocerous spp.* form resting spores at the end of their life cycle or when growing conditions are poor [*Kuwata and Takahashi*, 1999]. Since spores were not counted their presence would not be accounted for in the data presented in this chapter. Overall it seems likely that the large under representation of diatoms in the exported material compared to those species present earlier in the season (recorded in the CPR record) can be explained by a combination of dissolution processes, rapid sinking or spore formation.

4.5.2 Coccolithophores, diatoms and the flux to the sediments

Based on the results of chapter 3 and the observation of coccolithophore oozes in the sediments of the PAP site [*Ziveri et al.*, 2000] it was proposed that PIC is preferentially exported in the fast flux. The export of coccolithophore species cannot be compared with the seasonal surface community succession in the same way as the diatom community. This is because coccolithophores are under sampled by the CPR due to a mesh size (270 µm) larger than the diameter of many coccolithophore species (coccosphere size range of ~ 4 – 20 µm [*Young*, 1994]).

Examination of the species specific coccolithophore flux at depth shows, unlike the diatoms, no change in the occurrence of species between the surface and deepest samples. Assuming that the concept of the change in species with depth in the DF samples represents the evolution of the spring bloom, as previously discussed, this suggests that either there was no seasonal succession of coccolithophores apparent in the flux profile and/or that there is no slow sinking flux of coccolithophores (as observed n chapter 3). The lack of slow sinking PIC flux may be attributed to individual coccolithophores being generally too small to sink as efficiently as diatoms, which are much larger (10 – 150 µm) and for some species, are chains forming, which can increasing their effective size [*Carmelo*, 1997].

In order to be transferred to the sediments coccolithophores must be exported in the fast sinking particles. The major coccolithophore species contributing to MSA export fluxes of both PIC and POC were *Emiliana huxleyi, Gephyrocapsa mullerae, Syracosphaera pulchra* and *Calcidiscus leptoporus* which match the species previously observed in the sediments at the PAP site [*Ziveri et al.*, 2000]. The cumulative relative abundance of coccolithophores exported across all samples (Figure 4.3) shows that the MSA had the highest coccolithophore POC (~ 5 %) and biomineral (~ 50 %, PIC) abundance. In comparison the PELAGRA samples contained < 1 % of the total abundance of coccolithophore POC and PIC. This implies that the vast majority of the coccolithophore POC and PIC were exported in the rapidly sinking MSA, thus supporting the initial hypothesis that PIC export is associated with MSA.

Statistical analysis of MSA sinking speed and associated coccolithophore PIC flux indicates a positive linear relationship (r^2 = 0.6, $p < 0.009$; Spearman's Rank Correlation Coefficient 0.7, $p < 0.03$, $n = 9$). In comparison no statistical relationship (Spearman's Rank Correlation Coefficient 0.6, $p < 0.09$) is observed between diatom BSi and MSA sinking speeds (Figure 4.6). This suggests that it is the greater density of the PIC that is increasing the particle sinking speeds and facilitating the transfer of material to depth, rather than the lower density diatom BSi, despite its greater relative

abundance. This adds further weight to the concept of PIC being more important for ballasting than BSi [*Klaas and Archer*, 2002], and the concept that coccolithophore associated exported material has higher transfer efficiencies, due to greater sinking speeds, than diatom associated exported material [*Francois et al.*, 2002].

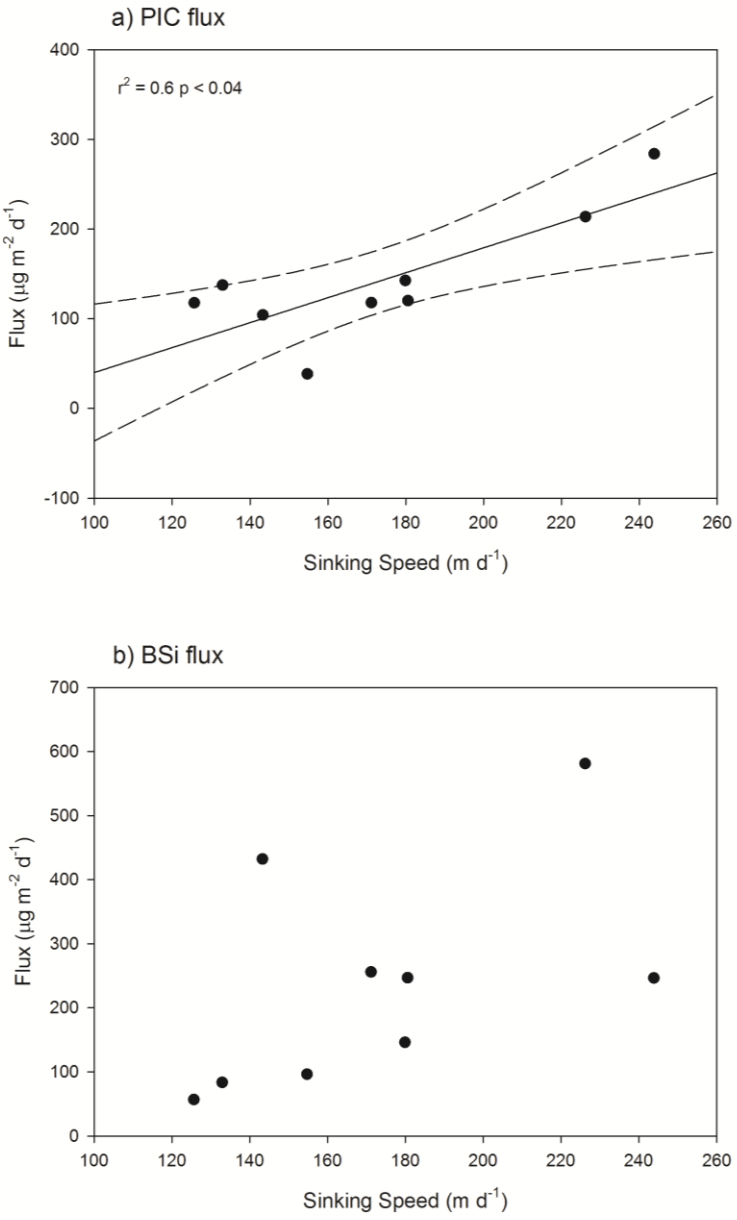

Figure 4.6 Relationship between individually measured particle sinking speeds and (a) cell bound coccolithophore PIC flux and (b) cell bound diatom BSi flux from cell counts of MSA collected using the MSC.

It was proposed at the outset of this chapter that the transfer of diatom POC to the deep ocean was facilitated by coccolithophore PIC based on the observations of PAP site deep 3000 m) sediment traps by *Salter et al.* [2010] and sea floor sediments by *Ziveri et al.* [2000]. If this is the case the signal in the sediments indicates that diatom

BSi has been preferentially remineralised leaving PIC as the major biomineral phase. In the surface community the average BSi concentration is more abundant (83 % of the total biomineral concentration) than the average PIC concentration (17 % of the total biomineral concentration; Table 4.4). Clearly there must be a shift with increasing depth between an abundance of diatom BSi and coccolithophore PIC. Examining the relative abundance biominerals in the MSA (which are thought to reach the deep ocean sediments, Chapter 3) it is clear that coccolithophore PIC constitutes ~ 50 % and diatom BSi ~ 50 % of the total biomineral flux.

Significant alteration of the sinking material must also occur throughout the water column to affect this change in the diatom BSi: coccolithophore PIC ratio. *Honjo and Manganini* [1993] observed that in the deep ocean Si is less resistant to remineralisation that calcite. Furthermore, Si remineralisation has been postulated to be greater in aggregates [*Brzezinski et al.*, 1997]. Thus although equal amounts of BSi and PIC are exported to the deep at 50 m, some of the BSi biomineral may be removed through remineralisation and dissolution processes in the mesopelagic, thus supplying a greater percentage mass of PIC to the sediments.

The multivariate analysis of the samples collected between the 50 and 600 m indicates only diatom species play a role in grouping and discriminating between POC sample clusters (Figure 4.5a). However, according to the biomineral clusters (Figure 4.5b) both diatoms and coccolithophore biominerals are important in discriminating between clusters. In particular *Syracosphera pulchra* and *Calcudiscus leptoporus* contribute to the differences between clusters. This suggests that coccolithophore PIC may be more important with respect to the export flux than coccolithophore POC contribution. In comparison diatom POC may be more important to the export flux than diatom BSi contribution. Examining the ratio of diatom POC : coccolithophore PIC in the MSA and DF samples (Table 4.5) it is clear that the MSA ratio is significantly lower (1.5) than the DF ratios (range of 1200 – 7781). This indicates that in MSA particles coccolithophore PIC is relatively more abundant than in the DF samples. Combining this observation with the documented relationship between increased sinking speeds and PIC content suggests that diatom POC is transferred to the deep ocean in MSA, by coccolithophore PIC.

4.6 Conclusions

The data presented in this chapter indicates diatoms are associated with the slow flux, penetrating at least 600 m into the oceans interior. The speed at which the material

sinks enables a seasonal succession of diatoms to be traced with depth, thus the fluxes at depth may not relate to the current surface production. Secondly the data indicates that the PIC flux is associated with MSA. Coccolithophore PIC flux is positively correlated with the MSA sinking speed, indicative of a ballasting effect [*Klaas and Archer*, 2002]. Finally shifts in the diatom BSi to coccolithophore PIC flux are likely to take place in the mesopelagic resulting in the sedimentation patterns observed by *Salter et al.* [2010] and *Zieveri et al.* [2000] where diatom POC but coccolithophore PIC are abundant in the sediments/deep ocean fluxes. As diatom BSi is preferentially dissolved it is proposed that coccolithophore PIC becomes increasingly important for transferring the diatom POC to depth.

Future work should look to further elucidate the relationship between the seasonal succession of phytoplankton species and export fluxes at depth. The data presented in this chapter is merely qualitative and a quantitative evaluation of the concepts discussed is still required. Furthermore these results are based on a limited number of observations and only on the cell bound fluxes of POC and biominerals. Therefore further analysis of the bulk fluxes including the detrital phases are needed to further elucidate the relationships presented in this chapter.

Chapter 5: Fast and slow POC fluxes in the Arctic

5.1 Abstract

The biological carbon pump in the European Arctic is driven by a complex balance between physics and biology of the environment. Physical characteristics such as the presence of light and sea ice, regulate the onset of the productive season and the biological coupling between phytoplankton and zooplankton communities, which in turn influence carbon export. Seasonal shifts in sea ice extent cause changes in primary production between solely water column phytoplankton in open water regions to a combination of water column, ice core and algal floc phytoplankton communities in ice covered regions. Carbon export, measured with the MSC can be classified into a fast and slow sinking flux. However these measurements have only previously been undertaken at the PAP site using this technology (Chapter 3), where it was observed that the slow sinking flux contributed 60 % to total export and the fast sinking flux contributed 40 % to total export at 50 m. The MSC was deployed at 4 ice covered and 3 open water stations in the Arctic at 50 and 100 m to measure the particulate organic carbon (POC) export from the surface ocean. No differences were observed between 50 and 100 m fluxes or between fluxes in the two environments. The average fast and slow fluxes in the European Arctic region are estimated at 159 (± 212) mg C m^{-2} d^{-1} and 76 (± 86) mg C m^{-2} d^{-1} respectively. Of the fast flux marine snow aggregates contributed 8 (± 8) mg C m^{-2} d^{-1} and FP 151 (± 211) mg C m^{-2} d^{-1}. Overall it was concluded that (1) the fast and slow flux can be detected in the Arctic environment using the MSC; (2) no attenuation of the flux was observed between 50 and 100 m at the time of deployment; (3) no differences were observed between ice covered and ice free environments leading to a fast and slow sinking flux contributing 68 % and 32 % of total export respectively; (4) zooplankton faecal pellets export more carbon than MSA and; (5) productivity from the ice phytoplankton communities are important in sustaining export fluxes.

5.2 Introduction

The Arctic Ocean is one of the most extreme marine environments on earth with strong seasonal variations in light and temperature [*Gradinger*, 1995] and it is of global significance for deep water formation, thermohaline circulation of the ocean and therefore global climate. The strong seasonality in light and sea ice cover across the region has implications for the functioning of the biological carbon pump. Currently the Arctic is warming at least twice as fast as the global average [*Trenberth et al.*, 2007]. Reductions in Arctic sea ice extent [*Stroeve et al.*, 2008] will likely be profound, potentially resulting in increases in water column primary productivity (PP) in ice free areas [*Arrigo et al.*, 2008; *Arrigo and van Dijken*, 2011; *Wassmann and Reigstad*, 2011]. Such changes are likely to have impacts on ecosystem dynamics and potentially cause increased carbon export [*Bates and Mathis*, 2009; *Lalande et al.*, 2009].

Primary productivity (PP) shows a strong degree of seasonality in the Arctic Ocean with no photosynthesis occurring in the dark winter months. The productive season is restricted to the summer months when light is sufficient to sustain phytoplankton growth. Surface irradiance is significantly reduced by > 95 % immediately below the sea ice [*Sakshaug*, 2004]. Furthermore sea ice related vertical stratification results in reduced mixing, limiting nutrient availability and decreasing PP [*Carmack and Wassmann*, 2006; *Wassmann*, 2011]. A recent modelling study by *Popova et al.* [2010] has indicated that it is these physical parameters (light availability and mixing) which explains much of the variability in Arctic Ocean primary production.

In ice covered environments primary production is fuelled by both the algae photosynthesising in the water column and ice algae growing within and on the underside of sea ice, and in algal flocs floating under the sea ice. The sympagic (meaning an environment where water exists mostly as a solid ice) algal communities, dominated by diatoms is thought to contribute up to 57 % of the total system PP in ice covered areas [*Gosselin et al.*, 1997; *Tamelander et al.*, 2009]. Coccolithophore species are less common in the Arctic possibly due to sub optimal growth temperatures [*Holligan et al.*, 1993; *Raitsos et al.*, 2006], although some species of coccolithophore (in particular *Emiliana huxleyi*) are thought to be advancing into some Arctic domains [*Smyth et al.*, 2004; *Hegseth and Sundfjord*, 2008].

The onset of the spring bloom results in a seasonal zooplankton succession [*Wassmann et al.*, 2004]. Two main zooplankton communities are found within the Arctic. Autochthonous populations consisting predominantly of Copepods (e.g. *Calanus glacialis* and *Canalus hyperboreus*) and allochthonous communities (e.g.

O*ithona atlantica*, *Calanus* fi*nmarchicus* and *Aglantha digitale*), which are advected into the Arctic Ocean [*Kosobokova and Hirche*, 2000; *Olli et al.*, 2007]. Zooplankton grazing strongly reduces the export of individually sinking phytoplankton cells, resulting in significant fluxes of faecal pellets (FP) [*Olli et al.*, 2002]. It is possible for zooplankton grazing to exceed water column phytoplankton primary production. However, food shortages can be alleviated by grazing on ice algae communities, detrital aggregates, FP (coprophagy) or via allochthonous transport of expatriate zooplankton species [*Olli et al.*, 2007].

Carbon export across the Arctic increases during the summer melting of the sea ice and is linked to the onset of seasonal production [*Lalande et al.*, 2009; *Lalande et al.*, 2011]. In the Arctic fluxes are highly regulated by the zooplankton community [*Andreassen et al.*, 1996; *Wassmann and Reigstad*, 2011]. Decoupling between the phytoplankton and zooplankton blooms, driven by the physical forcing of light and sea ice, can result in episodic flux events of un-grazed phytoplankton cells [*Wassmann et al.*, 1990; *Wassmann et al.*, 1996] which are typically dominated by diatoms. Carbon flux profile measurements from the Barents Sea indicate that flux attenuation is greatest in the top 100 m [*Andreassen and Wassmann*, 1998].

In other regions of the ocean the flux of organic carbon shows a bimodal distribution of a fast (> 300 m d^{-1}) and slow (< 11 m d^{-1}) sinking flux [*Alonso-González et al.*, 2010]. In the North Atlantic the fast sinking flux comprised ~ 40 % of the total flux out of the mixed layer, and was predicted to supply the deep ocean sediments with POC. Comparatively, the slow flux comprised ~ 60 % of the total flux and was likely entirely remineralised in the mesopelagic (Chapters 3 and 4). However no known measurements of the fast and slow flux have been made in the Arctic.

With the primary physical and biological characteristics described above, the Arctic can be broadly classified into three environments; multiyear ice, seasonal ice and open ocean [*Carmack and Wassmann*, 2006]. Multiyear ice regions have annual ice cover and are characterised by low productivity and phytoplankton biomass with shallow mixed later depths (MLD) and euphotic zones. Carbon export in these regions is typically very low with thorium-234 export measurements as low as 2.4 mg C m^{-2} d^{-1} [*Cai et al.*, 2010]. Seasonal ice zones (SIZ, i.e. areas of the ocean which can be covered by sea ice, depending on its maximal winter extent but may also have ice free waters for some months during the summer, classified as β ocean in figure 5.1) show transient periods of increased productivity and suspended biomass, with variable euphotic zone depths and shallower MLD than the multiyear ice [*Carmack and Wassmann*, 2006], due to the fresh water surface layer produced from the ice melt

[*Niebauer*, 1991]. Export in these regions of the Arctic are relatively higher than in multiyear sea ice areas and composed of relatively fresh detritus. The open water regions of the Arctic related to the SIZ (Open Ocean β in figure 5.1) show stratification driven by salinity, but have greater MLD resulting in mixing of the phytoplankton community below the euphotic zone [*Carmack and Wassmann*, 2006]. Open water MLD will vary seasonally and be dependent upon the degree of solar heating the surface waters receive [*Sarimento*, 2006]. Export is typically much higher than both multiyear ice and seasonal ice zones (Table 5.1) and is much more degraded in nature due to processes such as zooplankton grazing. Areas of the Arctic Ocean which are annually ice free show little fresh melt-water stratification and have the deepest MLD, mixing phytoplankton well below the euphotic zone (termed Open Ocean α in figure 5.1) [*Carmack and Wassmann*, 2006].

Area	Flux (mg C m^{-2} d^{-1})	Depth (m)	Year	Method	Reference
			Open water		
Barents Sea	185 ± 30	top 90	2003 – 2005*	Sediment trap	[*Reigstad et al.*, 2008]
Barents Sea	720	top 100	May-05	Sediment trap	[*Reigstad et al.*, 2008]
Barents Sea	500 (750) 1000	top 100	May-98	Sediment trap	[*Olli et al.*, 2002]
Fram Strait	24 (27) 30	top 100	Jul-91	Drifting sediment trap	[*Andreassen et al.*, 1996]
Fram Strait	35	top 300	Aug-00	Sediment trap	[*Bauerfeind et al.*, 2009]
Fram Strait	7	top 300	Jul-01	Sediment trap	[*Bauerfeind et al.*, 2009]
Fram Strait	5	top 300	Jul-04	Sediment trap	[*Bauerfeind et al.*, 2009]
Greenland Sea	5	top 200	Aug-93	Sediment trap	[*Noji et al.*, 1999]
Greenland Sea	10	top 200	Aug-93	Sediment trap	[*Noji et al.*, 1999]
Average	213				
SD	306				
			Ice covered		
Fram Strait	15	340	April – July 03	Sediment trap	[*Lalande et al.*, 2011]
Fram Strait	25	top 300	Jul-03	Sediment trap	[*Bauerfeind et al.*, 2009]
Barents Sea	18 (55) 78	top 100	Jul-91	Sediment trap	[*Andreassen et al.*, 1996]
Barents Sea	165 ± 83	top 90	2003 – 2005*	Sediment trap	[*Reigstad et al.*, 2008]
Barents Sea	200 (350) 450	50	Jul-03	Sediment trap	[*Reigstad et al.*, 2008]
Barents Sea	200 (275) 350	100	Jul-03	Sediment trap	[*Reigstad et al.*, 2008]
Barents Sea	140 (170) 200	top 100	Jul-98	Sediment trap	[*Olli et al.*, 2002]
Average	150				
SD	119				

Table 5.1 POC flux measurements made in areas surrounding the open water and sea ice sampling sites presented in this study. Where ranges have been quoted an approximate midpoint has been selected, indicated in brackets, for the mean and standard deviations.
*** This is an average for either open water or ice covered areas based on multiple studies and compiled by *Reigstad et al.* [2008]**

This chapter presents carbon export data, measured using the Marine Snow Catcher (MSC) at 50 and 100 m, in the European Arctic (summer 2010), sampling both ice covered (IC) SIZ (β), and open water (OW, α) environments.

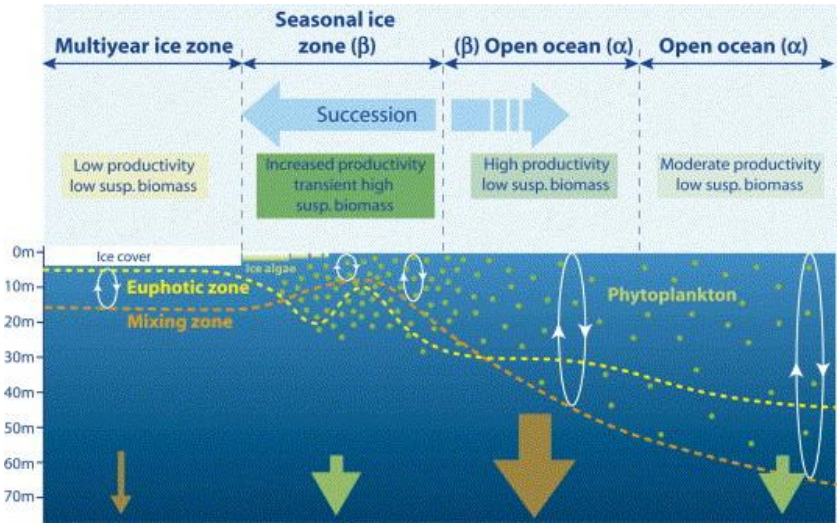

Figure 5.1 Schematic representation of the multiyear ice zone, seasonal ice zone and open water regions of the Arctic. β represents the areas of the Arctic which can be ice covered during years of maximal ice extent, whilst α refers to permanently ice free regions of the Arctic Ocean. The vertical arrows highlight the relative magnitudes of carbon export from these regions and the colour represents the freshness (green) or degradation (brown) of the exported material. This figure has been taken from *Carmack and Wassmann* [2006].

5.3 Methods

5.3.1 Study Area and Sampling

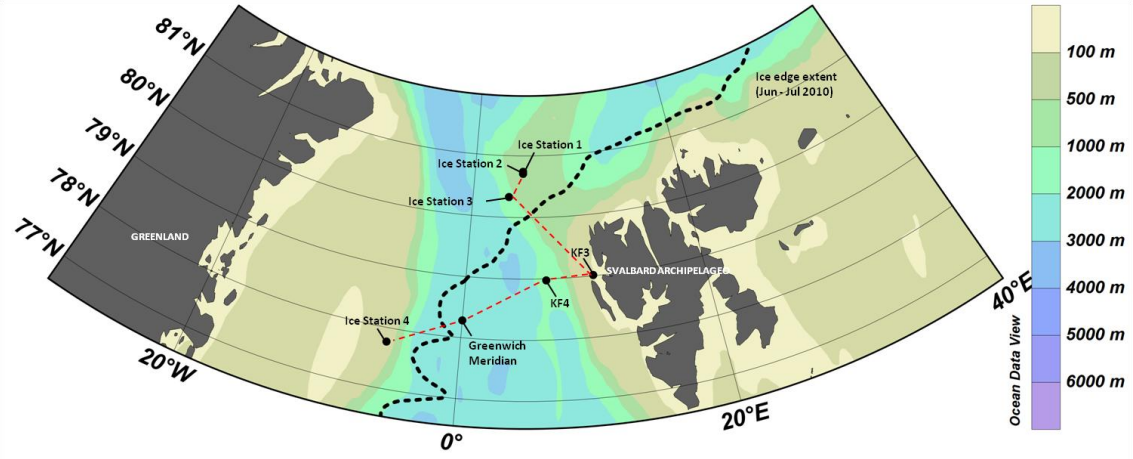

Figure 5.2 Location of sampling stations in ice covered environment and open water environment. The approximate extent of the sea ice coverage is indicated by the dashed line. The cruise track is indicated by the red dashed line.

The study area was situated in the European Arctic between Svalbard and Greenland (77°N to 81°N and 5°W to 10°E; Figure 5.2, Table 5.2) in both IC and OW environments of the Arctic. Sampling took place during the summer (June – July) 2010 ICE CHASER 2 cruise on board the RRS *James Clark Ross*. For the SI (sea ice) sampling the ship drifted with an ice floe in a semi lagrangian fashion starting on the Yermack Plateau on 22nd June 2010 and finishing in the Spitsbergen Fracture Zone, 100km south south-west on 2nd July 2010. The main current affecting this area is the West Spitsbergen current (WSC) bringing warmer, more saline Atlantic waters northwards. A second ice covered area was sampled closer to Greenland (Ice Station 4) and was affected by the East Greenland Current (EGC). The OW samples ranged in location between Svalbard (influenced by the WSC) and the Greenland shelf (influenced by the EGC) [*Rudels et al.*, 2002]. Vertical CTD profiles were used to collect water samples for nutrients, PP, phytoplankton community composition and calculation of mixed layer depth (MLD). The Marine Snow Catcher (MSC) was also deployed at two depths across all sampling locations in conjunction with the CTD casts to measure POC flux. In total 4 IC and 3 OW stations were sampled between 50 and 100 m, which was below the mixed layer depth at all stations.

Station	Date	Lat	Long	Depth (m)
Ice Covered				
Ice Station 1	23/06/10	80 44.7	04 35.5	50
Ice Station 2	24/06/10	80 42.4	04 20.7	50
Ice Station 2	24/06/10	80 42.4	04 20.7	100
Ice Station 3	25/06/10	80 35.4	04 18.8	100
Ice Station 4	08/07/10	77 46.0	05 35.9	100
Open Water				
KF3	05/07/10	79 00.9	10 41.3	50
KF4	06/07/10	79 00.9	10 41.3	50
KF4	06/07/10	78 58.5	06 42.4	100
GM	10/07/10	78 17.0	0 00.0	50
GM	10/07/10	78 17.0	0 00.0	100

Table 5.2 Locations of stations sampled in the sea ice and open water environments.

5.3.2 Carbon Fluxes

Samples for POC flux measurements were taken using the MSC. Full details on the MSC deployment and sampling methodology are discussed in the methods section of chapter 3. After deployment the MSC was left to settle for between 2.5 and 3 hours. Water samples were taken from the top 93 L and bottom 7 L to measure the slow

sinking POC flux. Slow sinking fluxes were calculated following the equation 3.1 in chapter 3.

All particles collected were collected and classed as either Marine Snow Aggregates (MSA) or FP (Figure 5.3). Each particle's sinking speed was measured and then each particle was digitally imaged. Individual MSA carbon contents were estimated following the equation for 'all types' of aggregates presented by *Alldredge* [1998] and were then converted into fluxes following equation 3.3 in chapter 3. The total carbon flux at each station was calculated from the sum of all the MSA particles collected. Depth averaged carbon fluxes were then calculated in both the sea ice and open water environments.

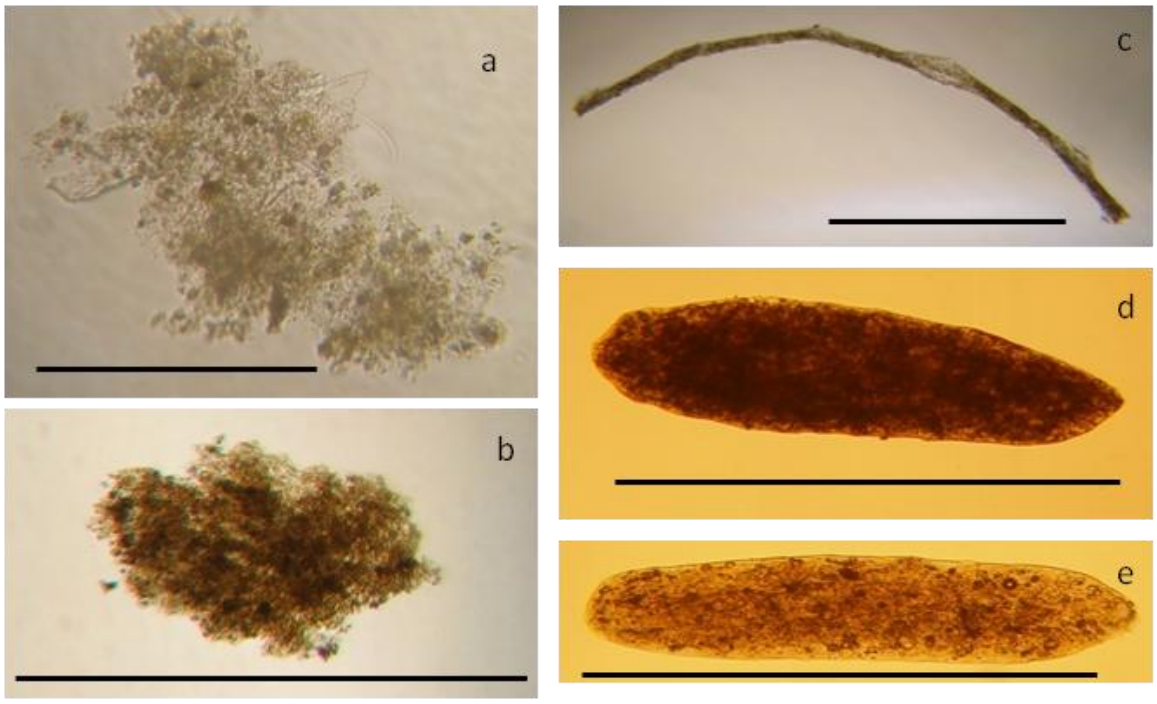

Figure 5.3 Types of particles collected. (a and b) Marine snow aggregate (c) euphausiid faecal pellet, (d and e) copepod FP. The scale bar in each image is 1 mm.

Individual FP carbon contents were calculated for all FP collected, utilising the conversion factors of *Wexels Riser et al.* [2007] for euphausiids (94 µg C mm^{-3}) and copepods (45 µg C mm^{-3}). No errors were reported for these values. As for MSA particles the total carbon flux at each station was calculated, following equation 3.3, chapter 3, from all of the FP particles collected. Depth averaged carbon fluxes were then calculated in both the SI and OW environments (Appendix D.1; Table D.2 and D.3).

5.3.3 Primary Productivity

Primary productivity of ice cores and water column samples was measured by Eithne Tynan (NOC, Southampton). Daily rates of PP from water column samples were measured by radioisotope incorporation using the micro diffusion techniques of *Paasche and Brubak* [1994] as modified by *Balch et al.* [2000]. Water samples were collected from 5 depths corresponding to 55, 33, 14, 5 and 1 % of the incident light level at the surface in the open water conditions in both OW and SI (i.e. in the leads between ice floes in the SI) and from 2 depths corresponding to 5 and 1 % light level directly under the SI. Each water sample was spiked with ^{14}C-labelled sodium bicarbonate and incubated in on-deck incubators at the appropriate light level.

During the incubation samples were kept at sea surface temperature with a continuous flow of surface sea water from the ship's underway supply. Incubations were terminated via filtration of samples through 25 mm 0.2 µm polycarbonate filters. Filters were then fumed with hydrochloric acid for 24 hours prior to the activity of each sample being measured using a liquid scintillation counter. PP was measured twice in the SI environment and 3 times in the OW environment. Values were integrated across the light levels sampled. In the sea ice environment PP was measured in both the leads and directly under ice flows. Observations of the spatial extent of the sea ice cover each day were noted and used to calculate a weighted average and weighted standard deviation for the SI environment.

Weighted averages were calculated by summing the individual PP values multiplied by their respective weights, dividing by the sum of all the parameter weights. This is described mathematically by equation 5.1 [*Cochran*, 1977; *Galassi et al.*, 2009].

$$M_w = \frac{\sum_i^N (W_i \cdot M_i)}{\sum_i^N (W_i)} \qquad \text{(Eq. 5.1)}$$

Where M_w is the weighted integrated productivity across the sampled light levels, i is the individual station sample, N is the total number of stations sampled, W_i is the weighting of the integrated productivity value at station i and M_i is the integrated PP value across the sample light levels at station i.

The weighted standard deviation is calculated by summing the individual sample weights, divided by the sum of all the weights squared, minus the sum of the individual weights squared. This value is then multiplied by the sum over all of the individual weights multiplied by the difference between the integrated PP value and the

weighted PP value squared. This value is then square rooted to give the weighted standard deviation [*Galassi et al.*, 2009]. Mathematically this is described by equation 5.2.

$$Weighted\ SD = \sqrt{\left(\frac{\sum_i^N (W_i)}{(\sum_i^N (W_i)^2 - \sum_i^N W_i^{\,2}} \right) \cdot \sum_i^N W_i \cdot (M_i - M_w)^2} \qquad \text{(Eq. 5.2)}$$

Nine ice cores (0.98 – 0.89 m thick) were collected, by Ronnie Glud (SAMS) from the SI environment and analysed for PP, by Eithne Tynan (NOC, Southampton) following the method as described above. The cores were cut into 10 cm pieces and a section from the top, middle and base of each core was melted in a cool room (4°C overnight), spiked with ^{14}C-labelled sodium bicarbonate and incubated in on-deck incubators for 24 hours at 80, 55, 33, 14, 4.5, 1% incident light levels.

The PP of the algal flocs floating below the sea ice was measured by Ronnie Glud (Scottish Association of Marine Science, SAMS). The integrated distribution of the algal floc biomass on the underside of the ice was estimated using a pulse-amplitude-modulated (PAM) fluorometer (calibrated to ship board chlorophyll-a measurements). Individual algal flocs were collected by divers underneath the sea ice and returned to the ship where O_2 fluxes were measured via incubations at down welling incident light levels [*Glud et al.*, 2002]. The combination of the PAM fluorescence and O_2 fluxes allowed PP estimates to be made for large areas of the sea ice, thus compensating for any spatial heterogeneity in the distribution of the algal flocs.

5.3.4 Macronutrients, Salinity, Temperature and Mixed Layer Depth

Nutrient measurements were carried out by Tim Brand and Sharon McNeil (SAMS). Water samples were collected from at least 3 depths between 5 and 50 m for nitrate, silicate and phosphate concentrations. Samples were analysed in triplicate using a Lachat QuikChem 8500 flow injection autoanalyser following the manufacturers methods (Lachat method nos. 31-107-04-1-A, 31-114-27-1-A and 31-115-01-1-I). A salt correction was applied by analysing low nutrient sea water samples (OSIL, salinity 35) at the start and end of each run. Methodological precision was > 99 % for concentrations > 1 µM, 95 % for concentrations between 0.1 and 1 µM and < 90 % for concentrations below 0.1 µM. Instrumental accuracy was > 95 % determined by measuring independent standard referencing materials at the beginning and end of each sample run.

Measurements of water column conductivity, temperature and density were measured using a CTD (SBE911). Data processing followed the protocols set out in Dumont and Sherwin [2008]. The mixed layer depth (MLD) of each station was determined as the shallowest depth corresponding to a temperature difference of 0.5°C from the surface waters [*Steinhoff et al.*, 2010].

	Cell POC [pg C]	Ref
Water column and MSA diatom species conversion factors		
Pseudonitzschia spp.	427	[*Kovala and Larrance*, 1966]
Navicula spp.	477	[*Kovala and Larrance*, 1966]
Chaetocerous spp.	70	[*Kovala and Larrance*, 1966]
Coscinodiscus spp.	501	[*Kovala and Larrance*, 1966]
Thalassiosira spp.	353	[*Kovala and Larrance*, 1966]
Pleurosigma spp.	4054	[*Kovala and Larrance*, 1966]
Fragilariaopsis spp.	882	[*Kovala and Larrance*, 1966]
Cylindrotheca spp.	166	[*Kovala and Larrance*, 1966]
Rhizosolenia spp.	4956	[*Kovala and Larrance*, 1966]
Thalassionema spp.	20.5	[*Kovala and Larrance*, 1966]
Algal floc and sea ice algae diatom species conversion factors		
Navicula spp.	693	[*Menden-Deuer et al.*, 2001; *Montagnes and Franklin*, 2001]
Tropidones group	82	[*Menden-Deuer et al.*, 2001; *Montagnes and Franklin*, 2001]
Achnanthes spp.	208	[*Menden-Deuer et al.*, 2001; *Montagnes and Franklin*, 2001]
Entomoneis spp.	2131	[*Menden-Deuer et al.*, 2001; *Montagnes and Franklin*, 2001]
Nitzschia spp.	44	[*Menden-Deuer et al.*, 2001; *Montagnes and Franklin*, 2001]
Pleurosiga spp.	1069	[*Menden-Deuer et al.*, 2001; *Montagnes and Franklin*, 2001]
Thalassiosira spp.	296	[*Menden-Deuer et al.*, 2001; *Montagnes and Franklin*, 2001]
Cylindrotheca spp.	23	[*Menden-Deuer et al.*, 2001; *Montagnes and Franklin*, 2001]

Table 5.3 Conversion factors for cell POC, PIC and BSi. Coccolith calcite estimates were calculated by multiplying individual coccolith calcite with the estimated numbers of coccoliths per coccosphere. Diatom POC was calculated by applying the conversion factors of [*Kovala and Larrance*, 1966] as applied in [*Poulton et al.*, 2007]. Whilst biogenic silica was calculated assuming a silica: carbon ratio of 0.13 following Brzezinski [1985] and taking the size specific POC content of each diatom species. A minimum of 10 different diatom cell dimensions for each species of diatom were measured microscopically during the counting process. Algal floc and sea ice algae conversion factors were calculated by Ray Leakey and Sian Lordsmith (Scottish Association for Marine Science) based on cell volumes and lengths.

5.3.5 Phytoplankton community

Since diatoms are more prevalent across both the water column and sympagic phytoplankton communities than coccolithophores [*Hegseth and Sundfjord*, 2008] only diatom species were counted. 1L water samples were taken from 5, 25 and 50 m and gently homogenised into one sample in a large darkened bottle. A 100 mL sub sample was then measured, preserved with 2 mL of Lugols iodide solution in a brown glass bottle and stored in a cool dark environment until analysis. Individual marine snow aggregates (MSA) from the SI and OW were preserved on filters, mounted onto glass slides and diatom communities were counted following the methods presented in chapter 4. The carbon contribution of each species within the MSA was then calculated by multiplying the cell counts by the conversion factors (Table 5.3, Equation 5.3). The

relative abundance of each species was then calculated in each sample type (i.e. water column and MSA) in both environments.

$$Carbon\ biomass = CF \times D_C \quad \text{(Eq. 5.3)}$$

Where CF is the conversion factor listed in table 5.3 and D_C counted is the cell density (Equation 4.1, chapter 4). Algal floc and ice core samples were also taken by Ray Leakey and Sian Lordsmith (SAMS), for taxonomic analysis of the diatom species present. POC biomass was calculated for each species following volumetric conversion factors presented by [*Menden-Deuer et al.*, 2001; *Montagnes and Franklin*, 2001] and converted into a total carbon biomass following equation 5.3. Scanning electron microscopy (SEM) was undertaken on some of the FP exported in the SI environment to determine which diatom species were exported within them. However, this analysis was only qualitative as the intact nature of the peritrophic membrane on many of the samples prevented full enumeration of species.

5.4 Results

5.4.1 Particle size and sinking speeds

Two types of MSA were collected, aggregates and FP (Figure 5.3). The average sinking speed of the MSA in the SI environment was 61 (± 71) m day^{-1} (n = 17) and in the OW environment was 102 (± 253) m day^{-1} (n = 16). By comparison the sinking speed of FP was 138 (± 96) m day^{-1} (n = 6) in the SI and 208 (± 121) m day^{-1} (n = 12) in the OW (Appendix D.1).

5.4.2 POC export fluxes

Fluxes were measured at both 50 and 100 m across both environments (Table 5.4, Appendix D2 and D3). Statistical analysis of the fluxes (SI n = 5 and OW n = 5) showed no significant difference between the fluxes at 50 m and 100 m within either environment. Consequently fluxes were averaged across the top 100 m of the water column. Statistical analysis shows no significant differences in the total flux, fast or slow flux between the SI and OW environments. Furthermore, neither the FP nor the MSA fluxes are significantly different from one another between the two environments.

Date	Depth (m)	Total Flux (mg C m^{-2} d^{-1})	Slow Flux (mg C m^{-2} d^{-1})	Fast Flux (mg C m^{-2} d^{-1})	MSA Flux (mg C m^{-2} d^{-1})	FP Flux (mg C m^{-2} d^{-1})
SI	50	170 (± 183)	144 (± 182)	26 (± 18)	6 (± 4)	20 (± 17)
SI	100	135 (± 94)	46 (±64)	89 (± 69)	6 (± 10)	83 (± 69)
SI	Top 100	153 (± 206)	95 (± 193)	57 (± 71)	6 (± 11)	51 (± 71)
OW	50	441 (± 321)	72 (±79)	369 (± 311)	10 (± 9)	359 (± 311)
OW	100	184 (± 85)	60 (± 24)	125 (± 81)	9 (± 12)	116 (± 80)
OW	Top 100	313 (± 332)	66 (± 82)	247 (± 321)	9 (± 15)	237 (± 321)

Table 5.4 Fast, slow and total fluxes measured at 50 and 100 m in both the sea ice and open water seasonal ice zone. The fast flux is further broken down into the constituent MSA and FP fluxes. Averages and errors for each environment were calculated from the individual station means (Appendix D2).

	Integrated water column production						
	24/06 (mgC m^{-2} day^{-1})	Weight	29/06 (mgC m^{-2} day^{-1})	Weight	04/07 (mgC m^{-2} day^{-1})	06/07 (mgC m^{-2} day^{-1})	10/07 (mgC m^{-2} day^{-1})
SI Sea Ice Lead	147 (± 0.5)	0.1	130 (± 1)	0.2	-	-	-
SI Sea Ice Below Ice	33 (± 0.4)	0.9	13 (± 0.2)	0.8	-	-	-
SI Sea Ice Weighted Mean	45		36		-	-	-
SI Sea Ice Weighted SD	34		47		-	-	-
OW Open Water	-		-		74 (± 1)	454 (± 4)	909 (± 3)

	SI (mgC m^{-2} day^{-1})	OW (mgC m^{-2} day^{-1})	Ice Core (mgC m^{-2} day^{-1})	Algal Floc (mgC m^{-2} day^{-1})
Average integrated primary production	40 (± 58)	681 (± 6)	9 (± 5)	233 (± 1)

Table 5.5 Integrated PP values for the water column, calculated from PP profiles as documented in appendix D.4. The errors for the integrated production in the sea ice leads, below ice samples and open water are standard deviations based on replicate samples. The weighted integrated production values were based on the observations of the extent of sea ice cover on the days when sampling for PP took place. The weighted mean and weighted standard deviation are calculated following equations 5.1 and 5.2. The average integrated production values for sea ice and open water were calculated from the average of the weighted means and the propagation of the weighted standard deviations. The average integrated ice core and algal floc values were calculated from replicate measurements and the propagation of the individual errors (Appendix D.5 and D.6). Sampling was undertaken in the same area or as close as possible to the areas where the MSC was deployed. Water column PP data courtesy of Eithne Tynan (NOC, Southampton), Algal floc data courtesy of Ronnie Glud (SAMS).

5.4.3 Primary productivity

In the SI environment the integrated PP (Table 5.6) in the leads was 147 (± 0.5) and 130 (± 1) mg C m^{-2} day^{-1} on 24/6 and 29/06 respectively. Directly below the sea ice in the SI environment the PP was 33 (± 0.4) and 13 (± 0.2) mg C m^{-2} day^{-1} on 24/6 and 29/06 respectively. The calculated weighted mean and standard deviation was 45 (± 34) mg C m^{-2} day^{-1} and 36 (± 47) mg C m^{-2} day^{-1} on the 24/06 and 29/06 respectively. The average sea ice environment integrated PP value, calculated from the weighted means and standard deviations was 40 (± 58) mg C m^{-2} day^{-1} (n = 2). The average ice core PP was 9.5 (± 5) mg C m^{-2} d^{-1} (n = 9), whilst the estimated productivity of the algal flocs floating beneath the sea ice was 233.4 (± 0.6) mg C m^{-2} d^{-1} (n = 2). In the OW environment the average water column PP was 681 (± 6) mg C m^{-2} day^{-1} (n = 3; see Appendix D4 – D6 for full data).

Station	Average Nitrate [µmol m^{-3}]	Average Phosphate [µmol m^{-3}]	Average Silicate [µmol m^{-3}]	Temp @ 5 m (°C)	Salinity @ 5 m	MLD (m)
Sea ice samples						
Ice Station 1	2386 (± 179)	178 (± 73)	969 (± 179)	-0.8	32.9	15.85
Ice Station 2	2306 (± 84)	165 (± 47)	1011 (± 76)	-1.2	32.9	9.9
Ice Station 3	1935 (± 40)	172 (± 86)	913 (± 128)	-1.3	32.6	13.86
Ice Station 4	2007 (± 64)	429 (± 50)	3051 (± 110)	-1.0	31.02	29.71
Average	2159	236	1486	-1	32	17
SD	191	112	904	0.2	1	9
Open water samples						
KF3	1438 (± 65)	202 (± 80)	293 (± 64)	5	33.74	7.92
KF4	4692 (± 60)	303 (± 64)	2386 (± 172)	6.7	35.02	11.88
Greenwich Meridian	4472 (± 105)	286 (± 92)	2147 (± 149)	-1	32.81	19.8
Average	3534	264	1609	4	34	13
SD	1485	44	935	3.9	1.1	6

Table 5.6 Ancillary parameters measured at each station in the sea ice and open water environments. Nutrients, temperature and salinity were measured at a minimum of three depths between 5 and 50 m depth. Average nutrient values refer to the average concentration between 0 and 50 m. MLD is the mixed layer depth and was defined following the definition of Steinhoff et al. [2010]. The error values associated with the individual station nutrient samples are standard deviations based on the sample replicates analysed. The average standard deviations are calculated from the variability of the individual samples. Data courtesy of Tim Brand and Sharon McNeill (SAMS).

5.4.4 Physiochemical setting

Average (5 – 50 m) nitrate, phosphate and silicate concentrations were 2159 (± 191) and 3534 (± 1485), 236 (± 112) and 264 (± 44), and 1486 (± 904) and 1609 (± 935) µ mol m^{-2} in SI and OW environments, respectively (Table 5.6; for full data and depths

over which nutrients were measured refer to appendix D7). Under the SI the water temperature at 5 m was on average -1 (± 0.2) °C whilst in the OW the average temperature was 4 (± 4)°C. Average salinity at 5 m was 32 (± 1) under the SI and 34 (± 1) in the OW environment. Mixed layer depths were variable at all sites averaging at 17 (± 9) m in the SI environment and 13 (± 6) m in the OW environment. For each individual physicochemical parameter there is no statistically significant difference between the SI and OW environment average value.

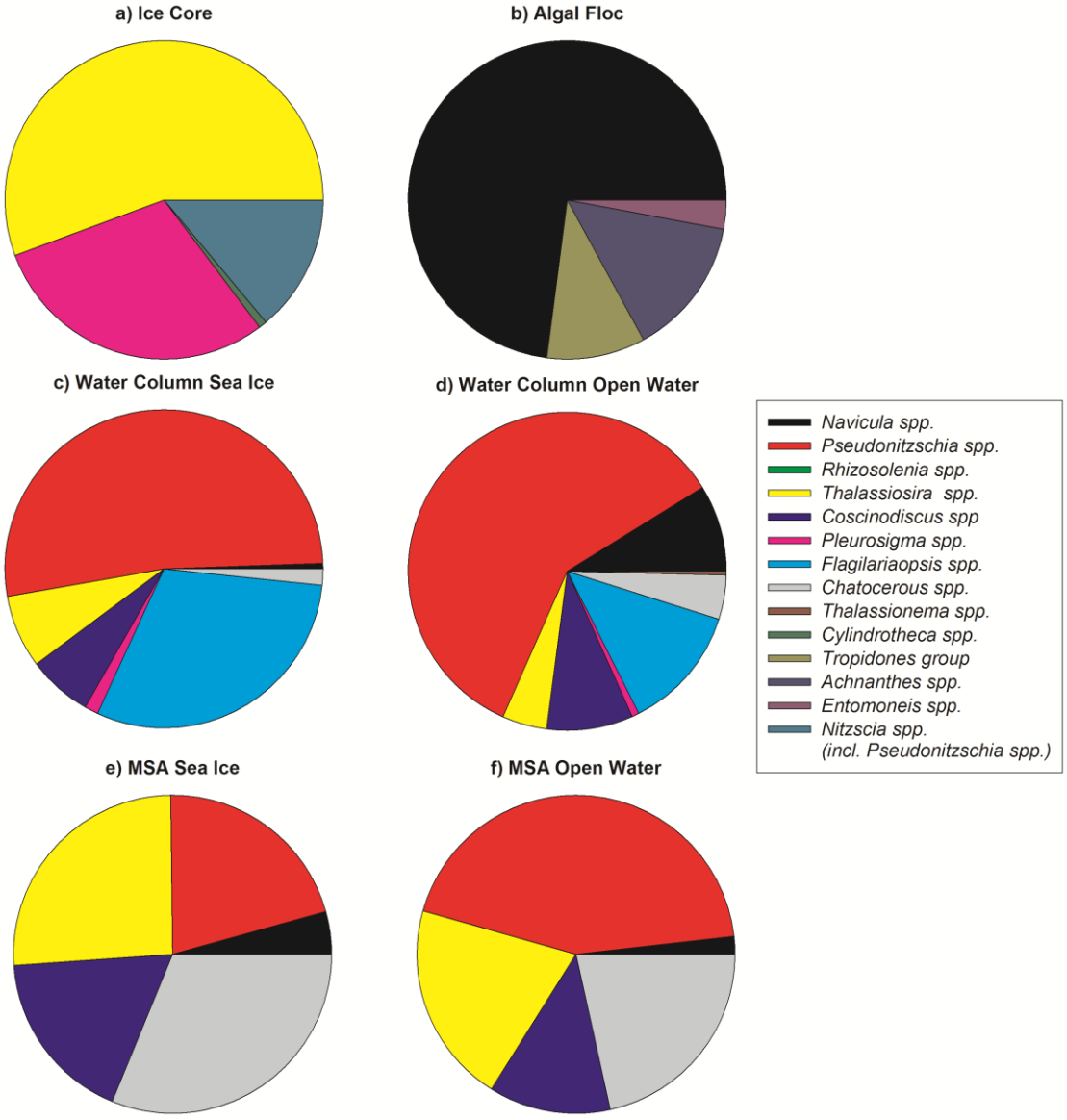

Figure 5.4 Relative percentage carbon biomass of the different diatom species presence in a) Ice core b) Algal Floc c) Water column sea ice d) water column open water e) MSA sea ice and f) MSA open water samples. For full data tables and absolute values and errors refer to appendix D8. Ice Core and Algal floc data courtesy of Ray Leakey and Sian Lordsmith (SAMS).

5.4.5 Phytoplankton standing stocks and exported biomass

Four diatom species were identified in the ice core community with > 75 % carbon biomass being supplied by *Thalassiosira spp.* and *Pleurosigma spp.* (Figure 5.4, Appendix D8). Four species of diatom were present in the algal floc floating beneath the sea ice with *Navicula spp.* contributing ~ 75 % of the total carbon biomass. Nine species of diatom were identified in the surface integrated water samples. Of these species *Pseudonitzscia spp.* contributed ~ 66 % of the total carbon biomass. Five species of diatom were identified in the MSA with *Thalassiosira spp.* and *Pseudonitzscia spp.* contributing ~ 60 % of the total carbon biomass. Species noted to be present in the FP samples included *Navicula spp.* and *Thalassiosira spp.,* similar to the algal floc community (Figure 5.5).

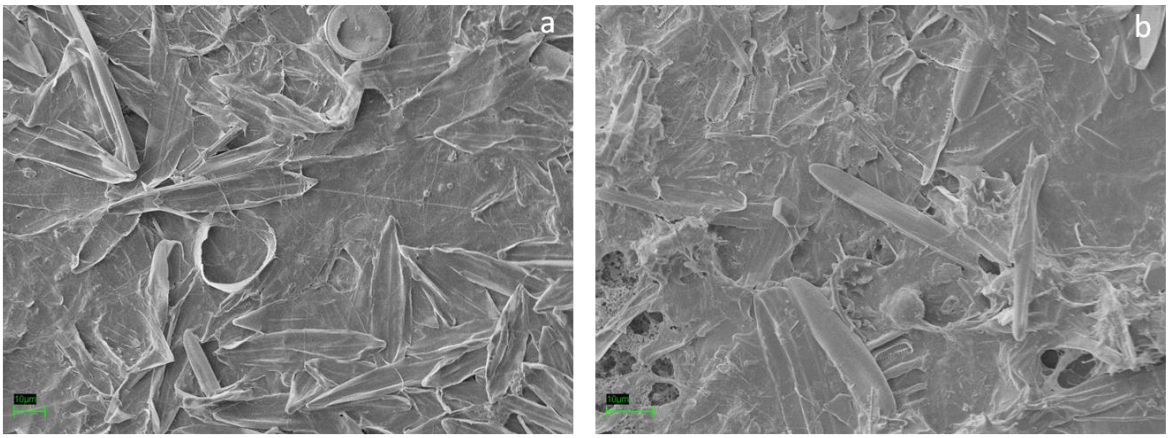

Figure 5.5 (a) Scanning electron microscope image of algal mat floating below sea ice. (b) SEM image of zooplankton faecal pellet.

5.5 Discussion

5.5.1 Characteristics of the sea ice and open water environments

Ice Stations 1 – 4 were still ice covered at the time of sampling and clearly had a sympagic algae community living in both the sea ice itself and the algal flocs floating below the sea ice. The PP measurements from the open water stations (KF3, KF4 and Greenwich Meridian (GM)) originated from water column phytoplankton only.

Examination of the average physiochemical parameters (Table 5.4) for each environment highlights considerable variability. Physical classification of the water masses according to their temperature and salinity was undertaken by Estelle Dumont (SAMS), following *Cottier et al.* [2005]. Ice stations 1 – 3 water masses were classified

as Atlantic water with a slightly fresher surface water signal. In contrast ice station 4 showed a much stronger Arctic water influence in both the surface waters and at depth. This may account for the lower salinities, increased MLD and higher average phosphate and silicate concentrations at this station, increasing the overall variability in the environmental averages. In the open water environment KF3 and KF4 water masses were characterised as surface waters typified by slightly fresher salinities and higher temperatures, with a transition from Arctic to Atlantic waters with depth. Greenwich Meridian showed a slightly different trend with polar surface waters, transitioning to re-circulated Atlantic waters at depth.

This raises some questions as to the validity of the initial classification of stations into SI and OW Arctic environments. It may be more appropriate to classify the stations according to water mass rather than ice cover. However, the issue with water mass classification is that 3 different groupings are apparent with only a few stations sampled per water mass (Arctic water, n = 1 (Ice Station 4), Atlantic waters, n= 5 (Ice Stations 1 – 3, KF3 and KF4) and Recycled Atlantic waters, n = 1 (Greenwich Meridian)). Such small station numbers makes comparisons difficult. Therefore although not homogenous in terms of water mass, the initial classification of the SI and OW, based upon ice cover provides distinct environments (with respect to PP) against which to compare the export measurements.

5.5.2 Nature of the flux

No previous studies have examined the relative contributions of individual MSA and FP to carbon export in the Arctic. The results presented in this chapter indicate that on average FP fluxes are much greater than MSA fluxes contributing ~ 90 % of the total fast sinking flux in both SI (51 (± 71) mg C m^{-2} d^{-1}) and OW (237 (± 320) mg C m^{-2} d^{-1}) environments. These values are comparable with literature estimates of faecal pellet export fluxes in the Barents Sea at seasonally equivalent times (150 mg C m^{-2} d^{-1} – 160 mg C m^{-2} d^{-1} under SI and 170 mg C m^{-2} d^{-1} – 225 mg C m^{-2} d^{-1} in OW [*Olli et al.*, 2002; *Wexels Riser et al.*, 2002]). Thus at the time of sampling MSA were of secondary importance in terms of the magnitude of POC exported below 100 m.

Thalassiosira spp. and *Pseudonitzschia spp.* contribute ~ 50 % of the total exported diatom biomass in both SI and OW environments. *Pseudonitzschia spp.* was the dominant species contributing to the water column biomass in both environments, whilst *Thalassiosira spp.* was most prevalent in the ice core community. This indicates that the production of biomass in both the ice core and the water column are important for MSA export. Examination of the algal mats floating below the sea ice

revealed a diatom population dominated by *Navicula spp.* (~ 70 % biomass; Figure 5.5). Qualitative examination of the SI FPs using SEM revealed fragments and some whole diatoms cells, with the most prominent species being *Navicula spp.* and *Thalassiosira spp.* (Figure 5.5). *Navicula spp.* and *Thalassiosira spp.* constituted on average < 10 % of the total diatom population in the water column community (integrated between 5 and 50 m) but 70 % of the algal floc community and ~ 60 % of the sea ice community. This indicates that the zooplankton community is likely to graze on the algal flocs and sea ice to sustain their metabolic demands.

5.5.3 Primary productivity and export fluxes in the Arctic

Sea ice PP is driven by both water column phytoplankton and the sympagic algal community. It is likely that in the SI environment the sympagic community are essential in sustaining export fluxes. In order to assess if this is the case the magnitude of the export fluxes must be compared to the rate of production. However, since the fast sinking export flux was dominated by FPs, the zooplankton ingestion rate must also be accounted for in order to determine all losses from the biomass produced (i.e. the sum of the rate of zooplankton carbon ingestion, MSA flux and slow sinking flux).

Equation 5.3 can be used to estimate ingestion as a function of the rate of egestion (E, or FP flux) and the assimilation efficiency (AE) [*Harris et al.*, 2000].

$$I = E / (1 - AE) \qquad \text{(Eq. 5.3)}$$

No direct measurement of AE were available, thus values were taken from the literature. Digital images of the FPs enabled classification of the zooplankton present, identifying both Copepods and Euphasiids (Figure 5.2) as contributors to export fluxes. Arctic copepod assimilation efficiencies quoted in literature range between 40 and 87 % [*Conover*, 1966]. Comparatively literature euphasiid assimilation efficiencies range between 64 and 83 % [*Dilling et al.*, 1998]. Following *Wexels-Riser et al.* [2008] an AE of 60 % was assumed to calculate the zooplankton ingestion rates. The range of maximum and minimum possible ingestion rates based on the AE values were also calculated for reference (Table 5.8). It was also assumed that no FPs were being retained at any depth or that in the carbon conversion estimation there was no major loss of carbon due to breakdown of the peritrophic membrane, in both cases this would alter the flux of FP POC.

Ingestion rates were calculated to be 593 (369 – 1825) mg C m^{-2} d^{-1} in the open water environment and 128 (86 – 395) mg C m^{-2} d^{-1} in the sea ice environment (Table 5.8).

The calculated ranges are quite large especially in the open water environment, due to the much greater faecal pellet flux. Without more detailed taxonomic zooplankton community analysis it is impossible to be able to reduce the variability in these calculations. However identification of both euphasiid and copepod FP indicated a mono-specific zooplankton community did not exist, thus the absolute upper and lower ingestion estimates based on either an 87 % or 40 % AE is not a likely scenario. Therefore the midpoint estimate, using an AE of 60 % is the more likely scenario and is the value which will be focused upon for the rest of this discussion.

	FP Flux (mg C m^{-2} d^{-1})	Ingestion (AE 60%) (mg C m^{-2} d^{-1})	Ingestion (AE 40 %) (mg C m^{-2} d^{-1})	Ingestion (AE 87 %) (mg C m^{-2} d^{-1})
Ice top 100m	51	128	86	395
Open top 100m	237	593	396	1825

Table 5.7 Calculated ingestion rates following equation 5.3, utilising the average FP fluxes in the top 100 m in both sea ice and open water environments and a range of assimilation efficiencies.

Figure 5.6 synthesises the different components of the primary production, export fluxes and ingestion rates in both the SI and OW environments. In the SI environment the total POC loss from the production is 229 mg C m^{-2} d^{-1} (the sum of the slow flux, MSA flux and ingestion rate). This is significantly higher than both the water column and ice core productivity alone and combined. However it is within the same range as the algal floc productivity suggesting that it is this component which is of the greatest importance for sustaining export fluxes under sea ice. In contrast in the OW the total POC losses from the POC produced is 668 mg C m^{2} d^{-1}. This is within the same range as the water column production. Clearly other organisms such as dinoflagellates will be grazing on the production therefore it seems likely that there is a mismatch between the rate of production and the losses of carbon via grazing and export processes in the OW.

Mismatches between zooplankton ingestion and water column PP have previously been documented by *Olli et al.* [2007]. They suggested that advection of zooplankton species into the environment that has grazed elsewhere may explain the mismatch. Examining the diatom biomass composition (Figure 5.5) it is clear that ~ 25 % of the biomass exported in MSA in both SI and OW originates from *Thalassiosira spp.,* a species most common to the ice core community biomass. In the OW there is no sea ice, therefore lateral advection processes may be occurring bringing the sea ice algae biomass into the open water environment. The average current direction was SSE (~ 46 m d^{-1}) in the SI environment, i.e. towards the open water regions. It therefore seems

plausible that the melting of the base of the sea ice, releases *Thalassiosira spp.* which either aggregate and sink out as MSA and are advected into open water regions or are grazed by zooplankton which themselves or their defecated FP are advected to open water regions.

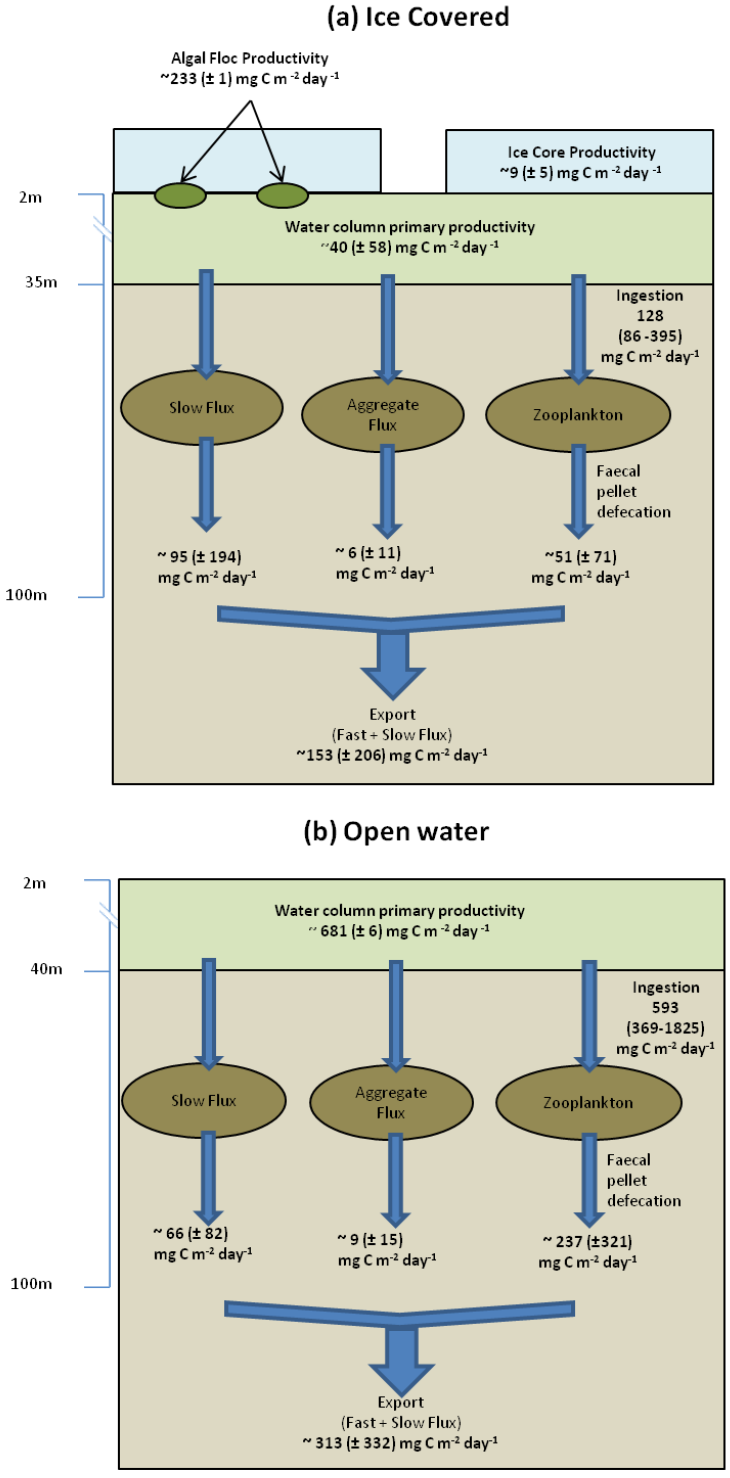

Figure 5.6 Schematics of sea ice (a) and open water (b) environments with measured PP and export fluxes as well as calculated zooplankton ingestion rates.

5.5.4 Comparability of flux estimates in sea ice and open ocean environments.

All flux measurements were made well below the mixed layer depth (Table 5.3) at each station. Thus it is highly likely that the truly sinking material was sampled rather than that caught in the mixed layer. It is clear that the flux values are highly variable and show no statistical differences between depths or environments at the time of sampling. This raises the question as to the accuracy of the calculated average fluxes, given the assumptions made for the calculation of the fast fluxes, specifically the MSA and FP carbon conversion factors and the low number of sample replicates in each environment. In order to answer this question comparison with other flux estimates is needed. No concurrent flux estimates were made in the upper ocean during the cruise. Therefore comparison with previous literature estimates is necessary from other areas of the European Arctic. Table 5.1 shows seasonally comparable estimates of POC export flux in both ice covered and ice free environments of the Bering Sea, Fram Strait, Greenland Sea and Central Arctic Ocean.

In general it is clear that fluxes are highly variable both between and within different regions of the Arctic. Literature OW fluxes range 3 orders of magnitude between different regions of the European Arctic (5 mg C m^{-2} day^{-1} in the Greenland Sea to 1000 mg C m^{-2} day^{-1} in the Bearing sea) and range an order of magnitude within regions (500 – 1000 mg C m^{-2} day^{-1} in the Barents Sea). These values are broadly comparable with the flux estimates made using the MSC for the OW environment (268 (± 332) mg C m^{-2} day^{-1}).

The literature values for the SI POC fluxes show one order of magnitude difference between regions of the European Arctic (15 mg C m^{-2} day^{-1} in the Fram Strait and 450 mg C m^{-2} day^{-1} in the Barents Sea) and generally less than an order of magnitude variability within regions (200 – 450 mg C m^{-2} day^{-1} in the Barents Sea). These values are also broadly comparable with the MSC flux measurements for the SI environment (158 (± 206) mg C m^{-2} day^{-1}) presented in this chapter.

This variability in the literature for both the SI and OW environments suggests that although the data presented in this chapter is variable, it is unlikely to be a result of the fundamental assumptions regarding the fast sinking flux but more due to the heterogeneous nature of the environment. The lack of statistical differences indicates that despite being two very different environments in terms of productivity, fluxes are the broadly similar. Averaging the flux across the two environments yields a total flux estimate of 235 (± 203) mg C m^{-2} d^{-1} which divides into a fast flux of 159 (±212) mg C m^{-2} d^{-1} and a slow flux of 76 (± 86) mg C m^{-2} d^{-1} (averages and standard deviations calculated from station averages in appendix D2). This gives an Arctic regional average

of 32 % slow sinking and 68 % fast sinking. This is different to the distribution of fast and slow flux observed at the PAP site (Chapter 3) and raises the question as to what drives the magnitudes of the fast and slow flux. Future work should focus on both refining the flux measurements made in this chapter, reducing the variability in the data set through increased sampling whilst addressing the issue of what drives the variability in the flux magnitudes.

5.6 Conclusions

This study set out to examine the flux of carbon in the Arctic Ocean using the MSC, which had previously only been deployed at the PAP site. The conclusions drawn from the data presented in this chapter it is clear that the slow and fast fluxes can be measured in the Arctic using the MSC. The two environments examined (OW and SI) had highly different sources of PP but overall very similar export fluxes. The results suggest that PP from the sea ice and algal floc communities may be important for sustaining export fluxes in both sea ice and open water regions, however more work needs to be undertaken to better quantify this.

Overall it was observed that in the European Arctic the average fast and slow fluxes contributed 68 % and 32 % of the total flux respectively. This is different from the PAP site fast and slow flux distribution (40 % and 60 % respectively) and further work should be undertaken to understand what drives the differences between oceanic regions. Furthermore no attenuation of the flux was observed at the time of sampling between 50 and 100m. This result is contradictory to previous studies which indicated that between 50 and 100 m is the region of the water column which undergoes rapid attenuation [*Andreassen and Wassmann*, 1998]. Further work should be carried out with the MSC to further investigate the attenuation of the flux in the European Arctic. Both MSA and FP were observed contributing to the fast sinking flux. However FP showed higher average fluxes than MSA indicative of the strong zooplankton influence in Arctic export and a lesser importance of MSA in the Arctic compared to other regions of the ocean such as the PAP site.

Chapter 6: Discussion

Understanding how fast and slow sinking particles contribute to carbon export in the ocean is important since the speed at which particles sink dictates, in part, how much carbon reaches the deep ocean and how much is remineralised and released back into the atmosphere. The slower a particle sinks the more carbon will be remineralised [*Armstrong et al.*, 2009]. The larger the magnitude of the slow sinking flux, the more particles will be sinking slowly, therefore the greater the rate of remineralisation potentially resulting in more CO_2 returning to the atmosphere [*Kwon et al.*, 2009].

The aims of this thesis were to:

1) Investigate the sensitivity of individual particle sinking speeds to changes in particle excess density and diameter.
2) Develop and test a methodology to measure bulk export fluxes using the MSC.
3) Investigate the magnitudes of POC fluxes in various marine settings using the marine snow catcher.
4) Investigate the depth to which the fast and slow flux penetrates into the interior of the ocean.

The data presented in this thesis took advantage of two research cruises to examine the properties and magnitudes of the flux. This chapter presents a summary of the data presented in this thesis, discussed in the context of the 4 aims outlined above, and in a comparative context between the two areas (PAP site and Arctic) investigated in the thesis, and with other studies presented in the literature which have measured the relative abundance of the fast and slow fluxes. The wider context of the findings of this thesis will be discussed and potential directions for future research suggested.

Summary

6.1.1 Investigations of the sensitivity of individual particle sinking speeds to changes in particle excess density and diameter.

The data presented in Chapter 2 focused on the roles of particle size and density in determining sinking speed. Marine snow aggregates collected in both the north east Atlantic and the Arctic were included in the data set. Various equations are available in the literature to predict particle properties such as size, density, drag coefficient and sinking speed. However, only one equation (2.2) presented by Dietrich [1982] enabled the prediction of particle sinking speeds from size and density parameters, without using the particle sinking speed in the calculation.

Application of the Dietrich [1982] equation to the observed particle size and density data indicates for APC variations in particle density are likely to determine particle sinking speeds throughout the water column. However, for MSA which constitute the majority of carbon export out of the surface ocean, changes in particle size drive greater variability in particle sinking speeds throughout the water column. It is thus proposed that higher density particles such as APC are more susceptible to particle ballasting.

As particles sink through the water column remineralisation of organic matter results in decreasing POC:biomineral ratio and utilisation of the Dietrich [1982] equation (2.2, Chapter 2) predicted increases in particle density of ~0.09 g cm^{-3} between 0 and 500 m. Such a change in density would result in MSA particles becoming similar in density to APC particles and their sinking speeds being density driven. Thus it is proposed that size is likely to determine sinking speeds in the surface ocean but density is likely to become more influential deeper than 500 m after much of the POC has been remineralised. This is a new way of conceptualizing the mechanisms influencing carbon export.

6.1.2 Methodological development of MSC technology to measure bulk fluxes

Prior to the work presented in this thesis no methodology had been developed using the MSC to collect both individual large sinking particles and quantify the bulk fluxes from the same sample. Chapter 3 [*Riley et al.*, 2012] presents the development of the methodology and derivation of calculations to measure the bulk fluxes using the MSC. Differences in the concentration of particles between the top and the base sections of the MSC are the basis of these calculations. In chapter 3 the development of this methodology has been validated against independent contemporaneous flux

measurements. Thus the MSC is a tool which has now been developed to collect both individual sinking particles and measure bulk flux properties. The advantage of the MSC is that unlike technologies such as PELAGRA, it can divide the fluxes into both a fast and slow sinking component which can provide different and unique insights into the nature of the particle export into the mesopelagic ocean.

The work undertaken to develop the MSC technology is by no means exhaustive and many areas can be improved upon in light of the results presented in this thesis. The settling period of around 2 hours was chosen because it related to the approximate sinking speed of the slowest sinking pool of particles [*Alonso-González et al.*, 2010]. Thus after 2 hours the majority of the flux would have reached the base chamber of the MSC. In order to better justify the settling time, extended settling periods should be undertaken to observe how the difference between the concentrations in the top and base of the MSC change over time. With increasing time after the two hour mark it would be expected any increases in concentration in the base section would be relatively small.

Measurement of the slow sinking POC flux is undertaken via differences in concentration between the top and base sections of the MSC (the latter, including a combination of both the suspended and slow sinking material). This means undertaking direct analysis of solely the slow sinking flux is impossible and uncertainty is introduced as to the absolute magnitude of the slow flux (as discussed in chapter 3). Other technologies such as the Indented Rotating Sphere Carousel (IRSC) sediment trap, physically collects the slow sinking material allowing analyses to be undertaken to better characterize the flux. This is therefore, one major drawback of the MSC technology.

Collection of the fast sinking particles is determined by how well an individual can see the particles. Furthermore in scenarios where large numbers of particles may be sinking, isolation of individual particles may prove difficult. Therefore further development of the technology is required. Use of polyacrylamide gels [*Lundsgaard*, 1995; *Ebersbach and Trull*, 2008] in one half of the base chamber may be useful to isolate individual particles for enumeration, measurement for flux calculations, whilst the other half of the chamber could be left as it is to collect individual particles and measure their sinking speeds (as documented in Chapter 3).

Use of literature relationships between particle size and POC content to determine the fast sinking carbon flux limits the robustness of the flux data (as discussed in Chapter 5). However, since the bulk flux calculations made at the PAP site (Chapter 3) have been compared and calibrated against contemporaneous flux measurements it seems

likely that the equations used for MSA are accurate. However, it would be more robust if the POC concentrations of particles at each deployment could be determined. This is easier said than done since the particles collected *in situ* in open ocean areas are relatively small (~ 500 µm), their abundance variable and individual particle POC content low. This makes multiple analyses for particle POC and other parameters such as sinking speed and size, difficult from just one snapshot deployment. Deployment of the MSC in areas of the water column where particle concentrations are high would enable more analyses to be carried out due to a greater number of replicate particles. Therefore concurrent deployment of the MSC with other technologies such as CTDs and transmissometers may be helpful in determining precise depths and water properties, for example nepheloid layers where particles can accumulate, as well as targeting areas of the water column where particle export is greatest, thus at least reducing the problem of low particle numbers.

6.1.3 Measuring the fast and slow fluxes using the MSC

Fast and slow fluxes were measured in two environments, the north east Atlantic where the MSC method was developed, and the Arctic. In the north east Atlantic (Chapter 3) the slow sinking flux was 92 (± 11) mg C m^{-2} d^{-1} (~60 % of the total flux at 50 m) and sank at 9 (± 9) m d^{-1}. The fast flux was measured to be 54 (± 25) mg C m^{-2} d^{-1} (~40 % of the total flux at 50 m) and sank at 206 m d^{-1} (average of MSA and APC sinking speeds documented in chapter 3). The fast flux was composed of two particle types MSA and APC, with the former contributing to the majority of the fast POC flux. The presence of APC particles and previous observations at the PAP site of increased POC fluxes corresponding to periods of increased radiolarian fluxes [*Lampitt et al.*, 2009] led to the conclusion that biomineralising organisms such as radiolaria or foraminifera are likely to act as nucleation points for aggregate formation.

In the Arctic (Chapter 5) flux measurements were made in the seasonal ice covered and open water regions at two depths, 50 and 100 m using the same methodology as applied in chapter 3. Two oceanographically different environments were sampled, ice covered and open water. However no statistically significant differences were observed between the fluxes at 50 and 100 m or between the sea ice and open water environments. Therefore the average the total flux across both depths and environments was calculated to be 235 (± 203) mg C m^{-2} d^{-1} which divides into a fast flux of 159 (±212) mg C m^{-2} d^{-1} (68 %) and a slow flux of 76 (± 86) mg C m^{-2} d^{-1} (32 %). Of the fast flux marine snow aggregates contributed 8 (± 8) mg C m^{-2} d^{-1} and FP 151 (± 211) mg C m^{-2} d^{-1}. The sinking speed of the fast flux in the open water environment was 127 m d^{-1} (calculated as an average of the FP and MSA sinking speeds in both environments in the Arctic as documented in Chapter 5). The deployment of the MSC in

the Arctic and the measurement of both a fast and slow flux shows that the presence of the slow flux can be detected in multiple locations and is not restricted to the PAP site. The distribution of the fast and slow fluxes are very different between the PAP site and the Arctic, is likely driven by the presence of zooplankton FP in the Arctic.

6.1.4 Penetration of the fast and slow flux into the interior of the ocean

Chapters 3, 4 and 5 all discuss data detailing observations of the fast and slow flux sinking into the interior of the ocean. From the data collected at the PAP site (Chapter 3) it is predicted that the fast flux, is likely to supply the abyss with POC but the slow flux is likely to be entirely remineralised in the mesopelagic region (~ 500 m) of the ocean. These predictions are based on the sinking speed of the fast and slow sinking pools and the *Martin et al.* [1987] flux attenuation parameterisation. The slow sinking pool sinks at 9 (± 9) m d^{-1} and would take ~ 500 days to reach the abyss. In comparison the fast flux has a sinking speed of 181 m d^{-1} and would reach the abyss in ~ 40 days. This lag time of 40 days is similar to the observed time difference between peak seasonal productivity and the peak fluxes in the deep sediment trap record [*Lampitt et al.*, 2010].

The attenuation of the fluxes in Chapter 3 from measured fluxes at 50 m were undertaken following the Martin et al. [1987] parameterisation, which was developed using bulk sediment trap fluxes. The slower a particle sinks the more carbon will be remineralised and vice versa [*Armstrong et al.*, 2009]. Therefore viewing the *Martin et al.* [1987] parameterisation as an average attenuation of the total sinking material, it may be that it overestimates/underestimates the degree of attenuation of the fast and slow fluxes respectively.

Taxonomic identification of diatom species in chapter 4, as a tracer of the flux with depth and comparison with the CPR record of the surface seasonal succession of diatoms in the surface ocean at and around the PAP site revealed that some component of the slow flux reaches ~ 630 m. However, ~ 80 % of the species that occurred in the surface community at the start of the spring bloom are not represented in the flux at depth, ~ 2 months on from the time of sampling. This may be a result of remineralisation and dissolution of biominerals in the slow sinking material, reducing the number of species preserved. If this is the case it seems plausible that remineralisation of the slow flux is greater than predicted by *Martin et al.* [1987] due to its slow sinking speed [*Armstrong et al.*, 2009]. Therefore viewing the *Martin et al.* [1987] parameterisation of flux attenuation may underestimate the attenuation of the slow sinking flux at depth. However, more work needs to be undertaken to quantitatively understand the attenuation of the fast and slow fluxes.

In chapter 5 where the MSC was deployed at multiple depths the attenuation of the fast and slow fluxes were also investigated. The results of the flux measurements at 50 and 100 m showed no attenuation with depth. This is different to previous studies in the Arctic region which have documented significant flux attenuation in the top 100 m of the water column [*Andreassen and Wassmann*, 1998]. Some of this consistency in the flux magnitude between 50 and 100 m may be explained by the variability in the data (discussed in more detail in Chapter 5). Nevertheless, the fast flux on average contributed 68 % of the total flux and the lack of attenuation may be because the fast flux (the dominant component) was sinking quicker than the rate of remineralisation.

Further conclusions drawn in chapter 3 suggest that no flux of slow sinking calcite occurs at the PAP site but there is a flux of slow sinking opal. Correlative analysis of the slow sinking flux of opal indicated no statistical relationship with the flux of slow sinking POC suggesting that the slow sinking flux is possibly unballasted and diatomaceous in origin. The taxonomic analysis of PAP site samples in chapter 4 indicates that some component of the slow sinking flux is diatom related. Furthermore, the lack of calcite flux observed at the PAP site seems improbable since calcite oozes are documented on the sea floor in this region [*Broerse et al.*, 2000; *Ziveri et al.*, 2000]. Taxonomic examination of the fast sinking MSA from the PAP site highlights the fact that the MSA had relatively higher coccolithophore POC and coccosphere PIC than bulk fluxes sampled by PELAGRA traps. Thus it is concluded that the fast sinking flux transports the majority of the PIC to the sediments in the north east Atlantic. Further statistical analysis indicates a linear relationship between coccosphere calcite and MSA sinking speed ($r^2 = 0.6$, $p < 0.04$) indicative of a ballasting relationship, as proposed by *Armstrong et al.* [2002], *Francois et al.* [2002] and *Klaas and Archer* [2002].

6.2 Comparison of the fast and slow sinking fluxes

The distribution of the flux between the fast and slow sinking fractions were different between the PAP site (fast: slow 40:60 %) and the Arctic (fast: slow 68:32 %). It may be that these differences are due to differences in nutrient concentrations between the two environments as hypothesised in Chapter 4. This follows the conclusion that at least some component of the slow sinking flux is related to diatoms, which are known to alter their buoyancy as a result of nutrient concentrations [*Nelson and Brzezinski*, 1990].

In order to determine which, if any, environmental variables determine the relative abundance of the fast and the slow flux comparison with more measurements, other than those presented in this thesis, is necessary. Other studies utilising the IRSC sediment trap have been undertaken in North Atlantic, close to the Canary Islands [*Alonso-González et al.*, 2010], in the north west Mediterranean (MEDFLUX) [*Lee et al.*, 2009] and in the Pacific (VERTIGO) [*Trull et al.*, 2008] at subtropical oligotrophic ALOHA site and subarctic site K2. Table 6.1 presents the synthesised data from this thesis, the MEDFLUX and VERTIGO studies. The table also indicates the relevant data sources which are used to analyse the relationship between the distribution of fast and slow fluxes at the time of sampling and the environmental parameters.

The measurement of the fast and slow fluxes using the IRSC sediment trap integrates the magnitude of the fast and slow fluxes over the settling velocities measured. Across all the studies using the IRSC sediment trap the sinking speed of the slow flux is relatively constant, ranging between 0.7 and 11 m d^{-1} and similar to the sinking speed of the slow sinking flux measured by the MSC (~ 9 m d^{-1}). However the sinking speeds of the fast sinking flux are much more variable (181 – 326 m d^{-1}; Table 6.1), thus not as comparable to the sinking speed of the fast fluxes using the MSC (206 m d^{-1} and 127 m d^{-1} at PAP site and Arctic, respectively). Therefore comparison of the distribution of the fast fluxes with the environmental variables would not reveal as meaningful a trend (if any exist) in the data. This highlights the need for a more formalised definition of the sinking speed of the fast and slow sinking pools between technologies.

Comparing the relative magnitude of the slow fluxes (Figure 6.1) it is clear that for all stations except the Arctic and Med Period 2 the slow flux is ~ 60 % of the total flux. In the Arctic and Med Period 2 samples the slow flux is < ~30 % and the fast flux is > 65 % of the total flux. The comparison presented in this chapter between IRSC data and the MSC data and the noted similarity in the magnitude of the slow flux provides further confidence in the ability of the MSC technology to measure the slow sinking particles. The data from the studies presented in table 6.1 are at a range of depths between 50 and 300 m. The fact that the slow sinking flux contributes 60 % of the total export throughout most of these depths suggests either that the fast and slow fluxes are remineralised at the same rate or there is a source of slow sinking particles that is not restricted to the euphotic zone, for example slow sinking particles may be sourced from the decomposition of fast sinking particles. A final alternate explanation is that the slow flux undergoes greater remineralisation than the fast flux due to a longer residence time in the upper water column, and therefore, if 60 % of the total flux is slow sinking at 300 m, it must be significantly larger at the surface.

Study	Depth sampled (m)	Speed fast	Speed slow	Total POC flux (mg C m^{-1} d^{-1})	% Slow POC flux [a]	% Fast POC flux [a]	Temp @ 5m (deg C) [d]	MLD (m) [e]	Nitrate @ 5m (uM)	Phosphate @ 5m (uM)	Silicate @ 5m (uM)	Current Speed @ flux depth (cm s^{-1})
PAP [b]	50	181	9	146	60	40	15	52	0.4	0.07	0.94	17
Arctic	Top 100	127	9	159	32	68	1.5	15	0.139	0.879	0.468	7.5
Med. Period 1 [c]	260	326	0.7 – 11	5.8	62	25	19	50	0.1	0.1	0.1	7
Med. Period 2 [c]	260	326	0.7 – 11	5.1	10	53	15	65	2.5	0.17	2.5	10
Med. Period 3 [c]	260	326	0.7 – 11	1.63	62	25	19	50	0.1	0.1	0.1	–
ALOHA [d]	272	> 137	< 10	283	45	11	26	49	0.001	0.001	0.001	8
K2 [d]	280	> 137	< 10	1121	58	23	10	25	12	1.3	13	3

Table 6.1 Compilation of data documenting the relative abundance of fast and slow sinking particles and the comparable ambient environmental conditions. The sinking speeds for the quantification of the mass flux of fast and slow sinking particles has also been included for comparative purposes.

a) The % fast and slow sinking at PAP and Arctic stations is calculated from the total flux measured in the MSC, thus the relative abundance sums to 100 %. In the Med Periods 1-3, ALOHA and K2 data the sum of the % fast and % slow sinking flux does not sum to 100 % because the relative abundances were calculated using IRSC sediment trap data where the mass flux was integrated across the sinking speeds measured. The definition of the fast and slow sinking speeds therefore governs the relative abundance of fast and slow sinking particles.

b) The temperatures, nutrients, MLD and current speed were calculated as an average over the sampling period in the PAP site and over all of the individual deployments in the Arctic region. Mixed Layer Depth (MLD) calculated for PAP and Arctic studies following Steinhoff et al. [*Steinhoff et al.*, 2010] and a 0.5°C temperature difference from the surface.

c) All data obtained for *Alonso-González et al.* [2010] except for the nutrient concentrations at 5 m which were obtained from *Marty et al.* [2002]. Period 1 spanned June 2005 – December 2005, Period 2 spanned December 2005 to June 2006 and Period 3 spanned June 2006 to December 2006. Resultantly the nutrient concentrations and temperature had to be integrated over 6 months of the year due to the sampling period in the MEDFLUX study. Temperature data was obtained for for the DYFAMED study site accessed via the EuroSITES data archive [*EuroSITES*, 2012]. No current data was available for Med Period 3.

d) Data obtained from *Trull et al.* [2008] unless stated. ALOHA was sampled in June 2004, K2 was sampled twice in July 2005. Two deployments of the IRSC sediment trap occurred at K2 thus the data presented here is an average of those two deployments. Temperature, chlorophyll and nutrient data were obtained from [*Buesseler et al.*, 2008; *Steinberg et al.*, 2008a].

Furthermore, the fact that the slow flux contributes ~ 60 % of the total export flux at multiple, geographically distinct locations suggests, that across much of the globe the majority of carbon export is driven by the slow sinking pool, interspersed with episodic flux events, as proposed in chapter 3. This is different to the traditional viewpoint that it is the rapidly sinking particles, associated with the spring bloom, which exports the majority of the annual carbon flux from the surface ocean into the mesopelagic [*Deuser and Ross*, 1980; *Billett et al.*, 1983; *Bender et al.*, 1992].

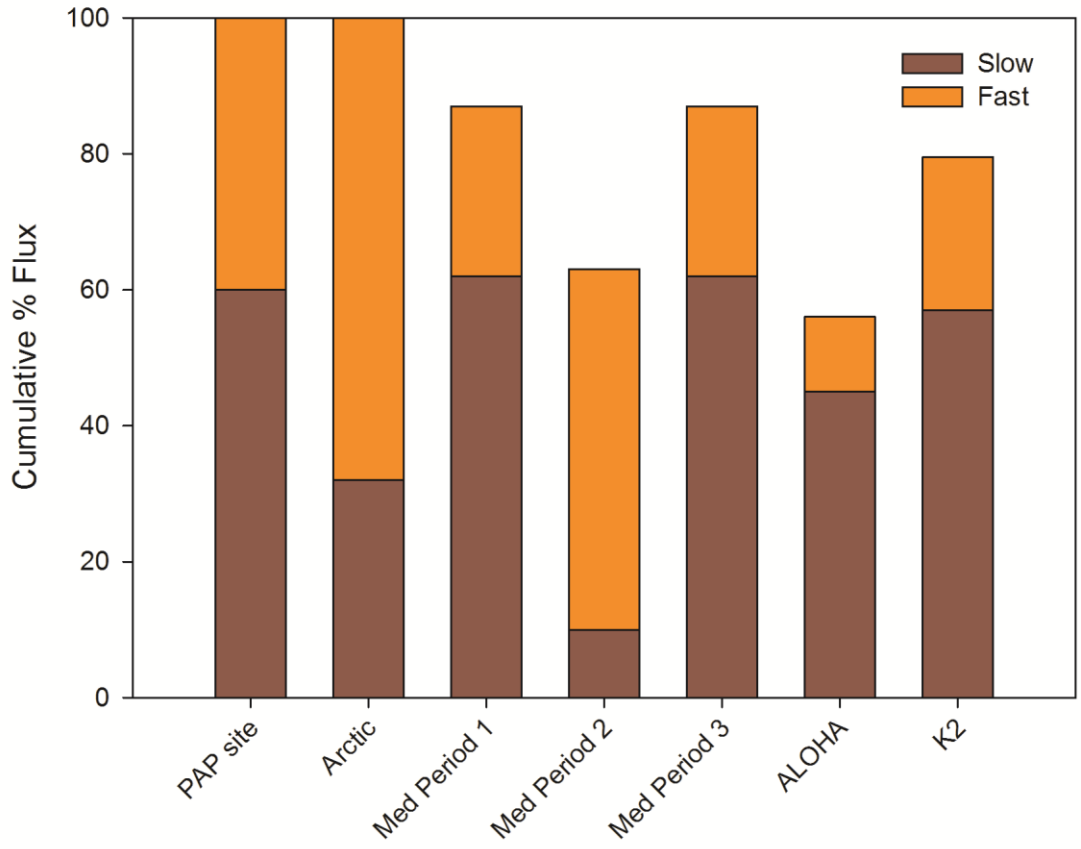

Figure 6.1 Relative contributions of the fast and slow sinking fluxes measured using the marine snow catcher (MSC) and the Indented Rotating Sphere Carousel (IRSC).

Spearman's Rank correlation coefficients (Rs) of the environmental variables and the % fast and % slow fluxes (separately) was undertaken to determine which (if any) environmental parameters could best explain the abundance of fast and slow sinking particles (Table 6.2). No correlations were observed between the slow or fast flux and any of the environmental parameters at the 95 % confidence interval ($p < 0.05$). The Rs value between the % fast flux and temperature at 5 m are close to the 90 % confidence

interval (p = 0.12) suggestive of a potential relationship between the % fast flux and the temperature of the environment.

Warmer, more oligotrophic environments have a microbial community dominance and fewer larger zooplankton species [*Heywood et al.*, 2006]. This may result in fewer fast sinking faecal pellets and aggregates being produced and more efficient remineralisation processes breaking down larger particles which form. In comparison colder water environments which support a more classic diatom-zooplankton food web [*Lenz et al.*, 1993] are more likely to result in the production of rapidly sinking aggregates and faecal pellets and a greater proportion of fast sinking particles, as observed in the Arctic Ocean. Alternatively seasonal changes in temperature may change the distribution of particles being exported with late winter blooms, associated with relatively cooler temperatures resulting in greater fast sinking particle export [*Alonso-González et al.*, 2010]. Consequently, there is therefore a need for more data to be collected to better determine any true relationships and the driving forces behind them and increase the number of data points for correlative analyses such as that undertaken in this chapter.

Parameter	% Slow Flux Rs (p value)	% Fast Flux Rs (p value)
Temperature	0.4 (0.29)	-0.6 (0.12)
MLD	0.09 (0.78)	0.2 (0.6)
Nitrate	-0.3 (0.38)	0.3 (0.38)
Phosphate	-0.3 (0.38)	0.3 (0.38)
Silicate	-0.3 (0.38)	0.3 (0.38)
Current Speed	-0.4 (0.29)	0.4 (0.29)

Table 6.2 Spearman's Rank correlation coefficients and p values to indicate significance

6.3 Wider implications and future directions for research

The conclusions drawn in this thesis are that size determines the sinking speed of particles in the upper ocean whilst density is the more important factor in the deep ocean. Furthermore when the flux is segregated into a fast and slow sinking component it is found that in general 60 % of the flux from the surface ocean is slow sinking with the relative abundance remaining constant until at least 300 m. There is further evidence that the slow sinking flux sinks to at least 600 m and is unballasted whilst the fast sinking flux is likely to supply the deep sediments with POC and is likely ballasted by calcite in the north Atlantic. The different sinking speeds of the fast and

slow flux are likely to have implications for the degree of remineralisation each component undergoes. Thus whilst the parameterisation presented by *Martin et al.* [1987] may be an average rate of attenuation, the overall attenuation of the slow flux may be greater and the fast flux less than this average.

If the majority of the export flux is slow sinking and is mostly remineralised in the top 600 m, this remineralised carbon is more likely to be mixed back into the surface and return to the atmosphere. Furthermore if in the upper ocean particle size is the dominant control of sinking speeds and fluxes of lower density particles are less likely to have density driven sinking speeds, potential future changes in phytoplankton community structure resulting in smaller particle sizes [*Bopp et al.*, 2005] and biomineralisation [*Riebesell and Tortell*, 2011] potentially reducing PIC concentrations, may have implications for the mechanisms (size or density) controlling carbon export. If such changes increase the magnitude of the slow sinking flux this may result in more remineralsiation in the mid water column and thus more CO_2 ultimately returning to the atmosphere as predicted by *Kown et al.* [2009].

In order to better understand how future changes to aspects of the biological carbon pump such as the community structure and biomineralisation will impact on the distribution of fast and slow sinking particles and POC transfer into the deep ocean research should focus upon the variability in the density of individual marine snow aggregates and how both particle size and density varies throughout the water column. This will enable a better understanding of what processes drive particle sinking speeds, thus ultimately how particle remineralisation and POC sequestration will be affected. Furthermore, work should be undertaken to determine the nature of the slow sinking flux and its origins. This would also aid in a better understanding of the extent to which the slow flux is remineralised as it sinks through the water column. Ultimately more measurements of the fast and the slow fluxes are needed in a much wider array of environments and across environmental gradients to better understand what environmental parameters influence the relative magnitudes of the fast and slow sinking fluxes in the ocean.

Appendix A: The influence of particle size and density on carbon export

A.1 PAP site MSA sinking speeds and equivalent spherical diameters

Cruise	Type	Date	Depth (m)	Area (mm2)	ESD (µm)	U (m d^{-1})
Arctic	MSA	24/06/2010	100	0.21	517	12
Arctic	MSA	24/06/2010	100	0.30	618	12
Arctic	MSA	24/06/2010	100	0.34	658	12
Arctic	MSA	24/06/2010	100	0.93	1088	12
Arctic	MSA	30/06/2010	300	0.24	553	23
Arctic	MSA	06/07/2010	100	0.91	1076	25
Arctic	MSA	30/06/2010	400	0.10	357	26
Arctic	MSA	29/06/2010	200	0.18	479	31
Arctic	MSA	06/07/2010	50	0.13	407	39
Arctic	MSA	06/07/2010	50	0.46	765	41
Arctic	MSA	10/07/2010	50	0.12	391	43
Arctic	MSA	26/06/2010	400	0.05	252	48
Arctic	MSA	10/07/2010	100	0.22	529	49
Arctic	MSA	02/07/2010	200	0.10	357	50
Arctic	MSA	15/07/2010	100	0.90	1070	52
Arctic	MSA	15/07/2010	100	0.23	541	54
Arctic	MSA	29/06/2010	200	0.17	465	57
Arctic	MSA	24/06/2010	100	0.38	696	61
Arctic	MSA	24/06/2010	100	0.32	638	61
Arctic	MSA	30/06/2010	300	0.09	339	62
Arctic	MSA	30/06/2010	300	0.17	465	62
Arctic	MSA	08/07/2010	100	0.14	422	62
Arctic	MSA	30/06/2010	400	0.62	888	66
Arctic	MSA	06/07/2010	100	1.06	1162	68
Arctic	MSA	09/07/2010	100	0.34	658	69
Arctic	MSA	24/06/2010	100	0.68	930	70
Arctic	MSA	06/07/2010	50	0.50	798	75
Arctic	MSA	24/06/2010	100	0.64	903	80
Arctic	MSA	10/07/2010	100	0.09	339	84
Arctic	MSA	10/07/2010	100	0.17	465	88
Arctic	MSA	09/07/2010	100	0.13	407	88

Table continued from previous page

Cruise	Type	Date	Depth (m)	Area (mm2)	ESD (µm)	U (m d^{-1})
Arctic	MSA	24/06/2010	100	1.24	1257	91
Arctic	MSA	30/06/2010	400	0.36	677	107
Arctic	MSA	30/06/2010	300	0.22	529	108
Arctic	MSA	02/07/2010	200	0.12	391	113
Arctic	MSA	06/07/2010	50	0.14	422	129
Arctic	MSA	09/07/2010	100	0.23	541	132
Arctic	MSA	24/06/2010	100	0.33	648	154
Arctic	MSA	06/07/2010	100	0.82	1022	154
Arctic	MSA	24/06/2010	100	0.55	837	180
Arctic	MSA	15/07/2010	50	0.24	553	198
Arctic	MSA	06/07/2010	100	0.25	564	255
Arctic	MSA	02/07/2010	200	0.43	740	289
Arctic	MSA	15/07/2010	50	0.09	339	300
Average				0.36	631	86
SD				0.30	255	69

Table A.1 Arctic Marine snow aggregate area, equivalent spherical diameter (calculated from the area) and sinking speeds

Cruise	Type	Date	Depth (m)	Area (mm2)	ESD (µm)	U (m d^{-1})
PAP	MSA	08/08/2009	50	0.33	648	49
PAP	MSA	30/07/2009	50	0.92	1082	51
PAP	MSA	03/08/2009	50	0.52	814	65
PAP	MSA	01/08/2009	50	0.30	618	69
PAP	MSA	08/08/2009	50	0.30	618	74
PAP	MSA	08/08/2009	50	0.28	597	76
PAP	MSA	01/08/2009	50	0.54	829	80
PAP	MSA	01/08/2009	50	0.42	731	86
PAP	MSA	30/07/2009	50	0.65	910	89
PAP	MSA	01/08/2009	50	0.27	586	89
PAP	MSA	01/08/2009	50	0.12	391	93
PAP	MSA	31/07/2009	50	0.15	437	95
PAP	MSA	08/08/2009	50	0.29	608	104
PAP	MSA	08/08/2009	50	0.50	798	104
PAP	MSA	08/08/2009	50	0.47	774	110
PAP	MSA	03/08/2009	50	0.46	765	111
PAP	MSA	30/07/2009	50	0.16	451	113
PAP	MSA	01/08/2009	50	0.08	319	114
PAP	MSA	08/08/2009	50	0.37	686	114
PAP	MSA	01/08/2009	50	0.30	618	124
PAP	MSA	03/08/2009	50	0.27	586	126
PAP	MSA	08/08/2009	50	0.32	638	126
PAP	MSA	30/07/2009	50	0.27	586	130
PAP	MSA	03/08/2009	50	0.27	586	132

Table continued from previous page

Cruise	Type	Date	Depth (m)	Area (mm2)	ESD (µm)	U (m d^{-1})
PAP	MSA	03/08/2009	50	0.85	1040	133
PAP	MSA	31/07/2009	50	0.48	782	133
PAP	MSA	30/07/2009	50	0.16	451	136
PAP	MSA	08/08/2009	50	0.37	686	136
PAP	MSA	01/08/2009	50	0.33	648	139
PAP	MSA	03/08/2009	50	0.48	782	143
PAP	MSA	31/07/2009	50	0.31	628	149
PAP	MSA	30/07/2009	50	0.69	937	150
PAP	MSA	30/07/2009	50	0.75	977	150
PAP	MSA	03/08/2009	50	0.16	451	155
PAP	MSA	01/08/2009	50	0.03	195	160
PAP	MSA	30/07/2009	50	0.62	888	160
PAP	MSA	03/08/2009	50	0.57	852	161
PAP	MSA	08/08/2009	50	0.22	529	168
PAP	MSA	03/08/2009	50	0.35	668	171
PAP	MSA	01/08/2009	50	0.48	782	174
PAP	MSA	01/08/2009	50	0.22	529	178
PAP	MSA	03/08/2009	50	0.66	917	180
PAP	MSA	03/08/2009	50	0.21	517	181
PAP	MSA	03/08/2009	50	0.48	782	186
PAP	MSA	30/07/2009	50	1.19	1231	190
PAP	MSA	30/07/2009	50	1.07	1167	191
PAP	MSA	01/08/2009	50	0.53	821	194
PAP	MSA	31/07/2009	50	0.45	757	203
PAP	MSA	08/08/2009	50	0.91	1076	204
PAP	MSA	31/07/2009	50	0.64	903	211
PAP	MSA	08/08/2009	50	0.40	714	222
PAP	MSA	03/08/2009	50	0.48	782	226
PAP	MSA	08/08/2009	50	0.76	984	238
PAP	MSA	03/08/2009	50	0.71	951	244
PAP	MSA	08/08/2009	50	0.58	859	244
PAP	MSA	08/08/2009	50	0.25	564	261
PAP	MSA	08/08/2009	50	1.14	1205	261
PAP	MSA	01/08/2009	50	1.22	1246	280
PAP	MSA	30/07/2009	50	0.10	357	317
PAP	MSA	31/07/2009	50	0.19	492	324
PAP	MSA	01/08/2009	50	1.19	1231	338
PAP	MSA	01/08/2009	50	0.24	553	416
Average				0.47	736	162
SD				0.29	236	74

Table A.2 PAP site Marine snow aggregate area, equivalent spherical diameter (calculated from the area) and sinking speeds.

Cruise	Type	Date	Depth (m)	Area (mm2)	ESD (µm)	U (m d^{-1})
PAP	APC	31/07/2009	50	0.18	479	414
PAP	APC	21/07/2005	50	0.26	575	178
PAP	APC	21/07/2005	50	0.55	837	66
PAP	APC	16/07/2005	50	0.75	977	261
PAP	APC	21/07/2005	50	0.86	1046	475
PAP	APC	21/07/2005	50	0.95	1100	285
Average				0.59	836	280
SD				0.32	257	150

Table A.3 PAP site Aggregate protist complex area, equivalent spherical diameter (calculated from the area) and sinking speeds.

Appendix B: The relative contribution of fast and slow sinking particles to ocean carbon export

B.1 Location of MSC deployments

Station Number	Latitude (Degrees)	Longitude (Degrees)
16491	49.06	16.55
16496	48.98	16.42
16527	48.89	17.17
16537	48.90	16.92
16589	48.80	16.46
16593	48.82	16.51
16605	48.70	16.56
16620	48.97	16.52
16660	48.78	17.00

Table B.1 Location of stations for MSC deployments. Only the last 5 stations were sampled for POC in the top and base sections of the MSC. However MSA and APC particles were collected from all 9 stations.

B.2 Concentrations of POC, calcite and opal in the top and base sections of the MSC immediately after settling

Station Number	POC conc. in MSC top section (µg L^{-1})	POC conc. in MSC bottom section (µg L^{-1})
16589	109	179
16593	119	205
16605	78	141
16620	89	156
16660	92	168
Average	97	170
SD	17	24

Table B.2 Concentrations of POC measured in the top and base sections of the MSC after the two hour settling period.

Station Number	Calcite conc. in MSC top section (µg L^{-1})	Calcite conc. in MSC bottom section (µg L^{-1})
16589	0.2	5
16593	9	10
16605	2	6
16620	5	4
16660	4	11
Average	4	8
SD	3	3

Table B.3 Concentrations of calcite measured in the top and base sections of the MSC after the two hour settling period.

Station Number	Opal conc. in MSC top section (µg L^{-1})	Opal conc. in MSC bottom section (µg L^{-1})
16589	5	6
16593	3	10
16605	No data	No data
16620	4	9
16660	2	7
Average	3	8
SD	1	2

Table B.4 Concentrations of opal measured in the top and base sections of the MSC after the two hour settling period.

B.3 Calculation of the mass and concentrations of slow sinking material

Station Number	POC conc. Top (µg L^{-1})	POC conc. Base (µg L^{-1})	Difference (µg L^{-1})[a]	Mass of slow sinking POC (µg)[b]	Conc. of slow sinking POC (µg L^{-1})[c]
16589	109	179	70	488	5
16593	119	205	86	602	6
16605	78	141	63	444	5
16620	89	156	67	470	5
16660	92	168	76	535	5
Average	97	170	73	508	5
SD	17	24	9	62	1

Table B.5 POC concentration measured in top and base sections of MSC and calculation of mass and slow sinking POC. Values are rounded to the nearest whole number.

a. This is the difference in concentration between the top and base sections of the MSC

b. The difference in concentration multiplied by the volume of the base chamber (7 L) gives the total mass of slow sinking POC.

c. The total concentration of slow sinking POC is calculated by dividing the mass to the fraction of the total volume of the MSC (100 L; Equation 1 in manuscript).

Station Number	Opal conc. Top (µg L^{-1})	Opal conc. Base (µg L^{-1})	Difference (µg L^{-1})[a]	Mass of slow sinking Opal (µg)[b]	Conc. of slow sinking Opal (µg L^{-1})[c]
16589	5	6	2	13	0.1
16593	3	10	7	51	0.5
16605	No Data	No Data	No Data	No Data	No Data
16620	4	9	6	41	0.4
16660	2	7	5	32	0.3
Average	3	8	5	34	0.3
SD	1	2	2	16	0.2

Table B.6 Opal concentration measured in top and base sections of MSC and calculation of mass and slow sinking opal.

a. This is the difference in concentration between the top and base sections of the MSC

b. The difference in concentration multiplied by the volume of the base chamber (7 L) gives the total mass of slow sinking POC.

c. The total concentration of slow sinking POC is calculated by dividing the mass to the fraction of the total volume of the MSC (100 L; Equation 1 in manuscript).

B.4 Assessment of the validity of the calculations

If the slow sinking particles are uniformly distributed with a sinking speed of 9 m day^{-1} some particles originally above the midpoint of the MSC may be unaccounted for in the slow sinking pool. If after settling, an underestimation of say 50 %, of the slow sinking pool is assumed, then the mass of material in the top and base sections of the MSC can be described as:

$$Mass\ in\ Top = Suspended_{Top} + 50\%\ Slow\ sinking_{Top} \quad (1)$$

$$Mass\ in\ Base = Suspended_{Base} + Slow\ sinking_{Base} + 50\%\ Slow\ sinking_{Top} \quad (2)$$

Defining the mass of the suspended pool in the MSC at the beginning of the settling period as x and the mass of slow sinking material in the MSC at the beginning of the settling period as y and knowing that the total volume of the MSC is 100 L with a top section of 93 L and a base section of 7 L, enables the derivation of equations 3 and 4.

$$Mass\ in\ Top = \left(x \cdot \left[\frac{93}{100}\right]\right) + \left(y \cdot \left[\frac{93}{100}\right] \cdot 0.5\right) \quad (3)$$

$$= 0.93x + 0.465y$$

$$Mass\ in\ Base = \left(x \cdot \left[\frac{7}{100}\right]\right) + \left(y \cdot \left[\frac{7}{100}\right]\right) + \left(y \cdot \left[\frac{93}{100}\right] \cdot 0.5\right) \quad (4)$$

$$= 0.07x + 0.07y + 0.465y$$

Thus the suspended and slow sinking material is calculated as a function of the volumes of the top and base chambers relative to the total volume. The POC concentration in the top and base of the MSC averaged over the 5 stations, were 97 µg L^{-1} and 170 µg L^{-1} respectively and can be converted into masses:

$$Mass\ in\ MSC\ top = concentration \times volume$$

$$= 97 \times 93 \quad (5)$$

$$= 9021\ \mu g\ L^{-1}$$

$$Mass\ in\ MSC\ base = 170 \times 7$$

$$= 1190\ \mu g\ L^{-1} \quad (6)$$

Thus equations 3 and 4 can be re-written as;

$$9021 = 0.93x + 0.465y \quad (7)$$

$$1190 = 0.07x + 0.07y + 0.465y \quad (8)$$

And solved simultaneously to give;

$$x = suspended\ mass = 9188\ \mu g \quad (9)$$

$$y = slow\ sinking\ mass = 1022\ \mu g \quad (10)$$

Table B7 shows the sizes and fluxes associated with the suspended, slow and fast sinking pools of material as presented in the manuscript. It is assumed that the totality of the slow sinking pool is in the base chamber following settling and in the supplementary material where it is assumed that only 50 % of the slow sinking pool is in the base. Slow sinking fluxes under both scenarios are calculated assuming a sinking speed of 9 m day^{-1}.

	Assuming all slow sinking is in the MSC base. (Manuscript equations 1 – 3)				Assuming only 50 % of slow sinking is in the MSC base. (Supplementary Material equations 7 – 8)			
	Mass (µg)	Conc. (µg L^{-1})	% Conc.	Flux (mg m– day^{-1})	Mass (µg)	Conc. (µg L^{-1})	% Conc.	Flux (mg m^{-2} day^{-1})
Suspended	9021	97	96	–	9188	92	89	–
Slow Sinking	391	5	5	92	1022	10	10	191
Fast Sinking	17	0.2	0.2	54	17	0.2	0.2	54

Table B.7 Comparison of equations presented in the manuscript and in the supplementary material used to calculate suspended, slow and fast sinking masses, concentrations and fluxes. Fluxes are calculated assuming a sinking speed of 9 m day^{-1}

The calculations of particle mass assuming a 50 % underestimation of the slow sinking pool (as set out above) are different to those in Chapter 3, however the concentrations are highly similar, with approximately the same distribution of particle concentrations between the suspended, slow sinking and fast sinking pools (90 – 95%, 5 – 10% and < 1% respectively). Examination of the slow sinking flux (the calculation for which used the mass of the particle) calculated using the new masses detailed here, are approximately twice as large (191 *mg C* m^{-2} day^{-1}) as those estimated in the manuscript (91 *mg C* m^{-2} day^{-1}). Resultantly, the total flux in the new calculations 40 % larger (245 *mg C* m^{-2} day^{-1}) than the estimation presented in the manuscript (assuming no underestimation of the slow sinking pool), from the MSC (146 *mg C* m^{-2} day^{-1}), and ~ 60 % larger than PELAGRA (84 *mg C* m^{-2} day^{-1}) and ^{234}Th (99 *mg C* m^{-2} day^{-1}). Thus the calculations presented in the manuscript are likely to be more representative of the absolute size of the suspended and slow sinking pools. Therefore, the original calculations set out in the manuscript are a robust estimate of POC concentrations, verified by independent flux estimates from both PELAGRA and ^{234}Th samples.

Appendix C: Coccolithophore and diatom export in the north east Atlantic

C.1 MSA raw cell counts

Species	1	2	3	4	5	6	7	8	9
E huxleyi / G. Mullerae	13	27	17	35	30	11	22	11	21
S. pulchra	51	32	33	27	39	7	30	15	30
C. Leptoporus	0	6	8	10	10	30	12	1	31
C. Pelagicus	5	1	2	0	2	2	0	0	0
Bacteriastrum spp.	0	0	0	0	0	0	0	0	0
Thalassiosira spp.	2	0	2	0	1	0	0	4	1
Rhizosolenia spp.	0	0	0	0	0	0	0	0	0
Cylindrotheca spp.	4	0	0	0	0	0	0	0	0
Navicula spp.	30	17	23	9	32	13	5	14	6
Pseudonitzschia spp.	0	15	5	15	25	3	36	4	11

Table C.1 Raw cell counts from each of the 9 MSA particles collected at station 16620 using the MSC.

C.2 MSA particle properties

Species	1	2	3	4	5	6	7	8	9
Particle Area (mm^2)	0.85	0.35	0.66	0.21	0.48	0.27	0.48	0.16	0.71
Particle radius (mm)	0.52	0.33	0.46	0.26	0.39	0.29	0.39	0.23	0.48
Particle volume (mm^3)	0.59	0.16	0.40	0.07	0.25	0.11	0.25	0.05	0.45
SS ($m\ day^{-1}$)	133	171	180	181	226	126	143	155	244

Table C.2 Individual particle properties. Sinking speeds were measured on board the ship and Particle Area was measured from digital images as described in chapter 3. Particle volume and radius are calculated from the area measurements.

C.3 MSA cell fluxes

Species	1	2	3	4	5	6	7	8	9
E huxleyi / G. Mullerae	38411	102714	67962	140451	150800	30717	70053	37825	113797
S. pulchra	150688	121735	131927	108348	196040	19547	95527	51580	162567
C. Leptoporus	0	22825	31982	40129	50267	83773	38211	3439	167986
C. Pelagicus	14773	3804	7996	0	10053	5585	0	0	0
Bacteriastrum spp.	0	0	0	0	0	0	0	0	0
Thalassiosira spp.	5909	0	7996	0	5027	0	0	13755	5419
Rhizosolenia spp.	0	0	0	0	0	0	0	0	0
Cylindrotheca spp.	11819	0	0	0	0	0	0	0	0
Navicula spp.	88640	64672	91949	36116	160853	36302	15921	48141	32513
Pseudonitzschia spp.	0	57063	19989	60193	125667	8377	114632	13755	59608

Table C.3 Cell fluxes calculated from raw counts (Appendix C.1, Table C.1) and MSA sinking speeds (Appendix C.2, Table C.2) following equation 4.1 in chapter 4. Flux units are cells $m^{-2}\ d^{-1}$.

C.4 MSA POC and biomineral Fluxes

Species	1	2	3	4	5	6	7	8	9
E huxleyi / G. Mullerae	0.28	0.74	0.49	1.01	1.09	0.22	0.50	0.27	0.82
S. pulchra	7.78	6.28	6.81	5.59	10.12	1.01	4.93	2.66	8.39
C. Leptoporus	0.00	1.23	1.73	2.17	2.71	4.52	2.06	0.19	9.07
C. Pelagicus	0.69	0.18	0.37	0.00	0.47	0.26	0.00	0.00	0.00
Bacteriastrum spp.	0.00	0.00	0.00	0.00	0.00	0.00	0.00	0.00	0.00
Thalassiosira spp.	4.40	0.00	5.95	0.00	3.74	0.00	0.00	10.23	4.03
Rhizosolenia spp.	0.00	0.00	0.00	0.00	0.00	0.00	0.00	0.00	0.00
Cylindrotheca spp.	13.76	0.00	0.00	0.00	0.00	0.00	0.00	0.00	0.00
Navicula spp.	58.50	42.68	60.69	23.84	106.16	23.96	10.51	31.77	21.46
Pseudonitzschia spp.	0.00	193.10	67.64	203.69	425.26	28.35	387.91	46.55	201.71

Table C.4 Species specific cell bound POC flux calculated from cell flux (Appendix C.3, Table C.3) and species specific conversion factors (Chapter 4, Table 4.2). Flux units are µg C m^{-2} d^{-1}.

Species	1	2	3	4	5	6	7	8	9
E huxleyi / G. Mullerae	3.36	8.99	5.95	12.30	13.20	2.69	6.13	3.31	9.96
S. pulchra	91.92	74.26	80.48	66.09	119.58	11.92	58.27	31.46	99.17
C. Leptoporus	0.00	23.97	33.58	42.14	52.78	87.96	40.12	3.61	176.38
C. Pelagicus	42.10	10.84	22.79	0.00	28.65	15.92	0.00	0.00	0.00
Bacteriastrum spp.	0.00	0.00	0.00	0.00	0.00	0.00	0.00	0.00	0.00
Thalassiosira spp.	2.87	0.00	3.89	0.00	2.44	0.00	0.00	6.68	2.63
Rhizosolenia spp.	0.00	0.00	0.00	0.00	0.00	0.00	0.00	0.00	0.00
Cylindrotheca spp.	8.93	0.00	0.00	0.00	0.00	0.00	0.00	0.00	0.00
Navicula spp.	38.29	27.94	39.72	15.60	69.49	15.68	6.88	20.80	14.05
Pseudonitzschia spp.	0.00	125.65	44.02	132.55	276.72	18.45	252.42	30.29	131.26

Table C.5 Species specific cell bound biomineral flux calculated from cell flux (Appendix C.3, Table C.3) and species specific conversion factors (Chapter 4, Table 4.2). Flux units are µg PIC m^{-2} d^{-1} for coccolithophores and µg BSi m^{-2} d^{-1} for diatoms.

C.5 Total MSA fluxes

Species	Average POC Flux	Average Biomineral Flux	Total POC Flux	Total Biomineral Flux
E huxleyi / G. Mullerae	0.60 (± 0.3)	7.32 (± 4)	18.07 (± 10)	219.67 (± 119)
S. pulchra	5.95 (± 3)	70.35 (± 33)	178.53 (± 85)	2110.52 (± 1002)
C. Leptoporus	2.63 (± 3)	51.17 (± 54)	78.95 (± 83)	1535.14 (± 1614)
C. Pelagicus	0.22 (± 0.3)	13.37 (±15)	6.58 (± 8)	401.01 (± 459)
Bacteriastrum spp.	0.00	0.00	0.00	0.00
Thalassiosira spp.	3.15 (± 4)	2.06 (± 2)	94.50 (± 106)	61.73 (± 69)
Rhizosolenia spp.	0.00	0.00	0.00	0.00
Cylindrotheca spp.	1.53 (± 5)	0.99 (± 3)	45.86 (± 138)	29.78 (± 89)
Navicula spp.	42.17 (± 29)	27.61 (± 19)	1265.24 (± 882)	828.15 (± 577)
Pseudonitzschia spp.	172.69 (± 154)	112.37 (± 100)	5180.72 (± 4623)	3371.14 (± 3008)
Total Coccolithophore			282 (± 119)	4266 (± 1959)
Total Diatom			6586 (± 4709)	4291 (± 3065)

Table C.6 Total fluxes calculated for the total number of MSA collected during deployment 16620. Average POC and biomineral are calculated from tables C.4 and C.5 from the 9 individual particles counted. The error in brackets is the standard deviation calculated from the 9 MSA samples. The total fluxes are calculated from the average POC and biomineral fluxes multiplied by the total number of MSA collected (n = 30) during the MSC deployment. Errors were propagated through by multiplying the SD of the average fluxes by the number of particles (constant of 30). The total coccolithophore and diatom POC and Biomineral fluxes were calculated from the sum of the species fluxes and standard deviations.

C.6 PELAGRA sampling time, cone area and filtered mass

Depth	Sample Time (days)	Single Cone Area (m^2)	Filter only (mg)	Filter + Sample (mg)	Mass filtered (mg)	Mass per pot (mg)
175 m	2	0.115	19.7	20.2	0.5	20.76
175 m	2	0.115	19.5	19.7	0.2	20.76
280 m	2	0.115	19.8	20.2	0.4	21.32
280 m	2	0.115	19.7	20.7	1	21.32
300 m	2	0.115	19.6	20.1	0.5	15.39
300 m	2	0.115	21.1	21.6	0.5	15.39
450 m	5.5	0.115	19.7	19.8	0.1	11.4
450 m	5.5	0.115	19.6	19.7	0.1	11.4
630 m	2	0.115	19.7	20.1	0.4	23.88
630 m	2	0.115	19.5	19.9	0.4	23.88

Table C.7 Sampling times for each PELAGRA deployment, area of collecting cone and mass of filter and filtrate for each of the DF samples. Masses were measured using a Sartorius ME-5 microbalance (± 1µg precision)

C.7 PELAGRA raw cell counts

Species	175 m	175 m	280 m	280 m	300 m	300 m	450 m	450 m	630 m	630 m
E huxleyi / G. Mullerae	0	6	1	3	2	8	3	0	2	3
S. pulchra	12	23	3	6	1	5	0	1	5	13
C. Leptoporus	7	2	10	18	9	16	1	3	6	4
C. Pelagicus	0	0	0	0	0	1	0	0	0	0
Pseudonitzschia spp.	300	185	154	221	162	167	28	31	91	92
Rhizosolenia spp.	12	17	4	1	3	5	1	1	0	1
Cylindrotheca spp.	0	4	16	16	10	8	11	10	26	21
Thalassiosira spp.	52	38	59	68	41	33	11	14	39	45
Navicula spp.	25	31	14	14	14	24	3	3	1	5
Bacteriastrum spp.	4	0	1	2	1	0	0	0	1	8

Table C.8 Raw cell counts from each of the PELAGRA sampled collected. Two replicated were measured for each sample.

C.8 Fields of view counted

Species	175 m	175 m	280 m	280 m	300 m	300 m	450 m	450 m	630 m	630 m
E huxleyi / G. Mullerae	225	225	217	221	220	221	222	223	222	206
S. pulchra	225	225	217	221	220	221	222	223	222	206
C. Leptoporus	225	225	217	221	220	221	222	223	222	206
C. Pelagicus	225	225	217	221	220	221	222	223	222	206
Pseudonitzschia spp.	277	275	50	50	50	50	50	50	50	50
Rhizosolenia spp.	277	275	50	50	50	50	50	50	50	50
Cylindrotheca spp.	277	275	50	50	50	50	50	50	50	50
Thalassiosira spp.	277	275	50	50	50	50	50	50	50	50
Navicula spp.	277	275	50	50	50	50	50	50	50	50
Bacteriastrum spp.	277	275	50	50	50	50	50	50	50	50

Table C.9 Number of fields of view counted for coccolithophore and diatom cells under SEM and light microscope respectively.

C.9 Analysed area of filter

Species	175 m	175 m	280 m	280 m	300 m	300 m	450 m	450 m	630 m	630 m
E huxleyi / G. Mullerae	204	204	197	200	199	200	201	202	201	187
S. pulchra	204	204	197	200	199	200	201	202	201	187
C. Leptoporus	204	204	197	200	199	200	201	202	201	187
C. Pelagicus	204	204	197	200	199	200	201	202	201	187
Pseudonitzschia spp.	62	62	11	11	11	11	11	11	11	11
Rhizosolenia spp.	251	62	11	11	11	11	11	11	11	11
Cylindrotheca spp.	251	62	11	11	11	11	11	11	11	11
Thalassiosira spp.	251	62	11	11	11	11	11	11	11	11
Navicula spp.	251	62	11	11	11	11	11	11	11	11
Bacteriastrum spp.	251	62	11	11	11	11	11	11	11	11

Table C.10 The actual area of the filter counted based on the magnification (x 5000 for coccolithophores and x 40 for diatoms) and the number of fields of view counted under the SEM and light microscope.

C.10 Cells per mg filtered material

Species	175 m	175 m	280 m	280 m	300 m	300 m	450 m	450 m	630 m	630 m
E huxleyi / G. Mullerae	0	26	2	3	4	14	26	0	4	12
S. pulchra	21	99	7	5	2	9	0	9	11	30
C. Leptoporus	12	9	22	16	16	28	9	26	13	9
C. Pelagicus	0	0	0	0	0	2	0	0	0	0
Pseudonitzschia spp.	1705	2628	6016	3453	5062	5219	4375	4844	3555	3594
Rhizosolenia spp.	68	241	156	16	94	156	156	156	0	39
Cylindrotheca spp.	0	57	625	250	313	250	1719	1563	1016	820
Thalassiosira spp.	295	540	2305	1063	1281	1031	1719	2188	1523	1758
Navicula spp.	142	440	547	219	438	750	469	469	39	195
Bacteriastrum spp.	23	0	39	31	31	0	0	0	39	312

Table C.11 The number of cells per mg of PELAGRA material filtered. Calculated following *Bollman et al.* [2002] based on the filtered area (175 mm^2), analysed area (Table C.10), number of cells counted (Table C.8) and the mass filtered (C.7).

C.11 Cells per PELAGRA collection pot

Species	175 m	175 m	280 m	280 m	300 m	300 m	450 m	450 m	630 m	630 m
E huxleyi / G. Mullerae	0	534	47	56	54	215	297	0	104	280
S. pulchra	428	2049	142	112	27	134	0	99	260	727
C. Leptoporus	249	178	474	335	243	430	99	296	312	224
C. Pelagicus	0	0	0	0	0	27	0	0	0	0
Pseudonitzschia spp.	35386	54554	128253	73621	77912	80317	49875	55219	84886	85819
Rhizosolenia spp.	1415	5013	3331	333	1443	2405	1781	1781	0	933
Cylindrotheca spp.	0	1180	13325	5330	4809	3848	19594	17813	24253	19589
Thalassiosira spp.	6134	11206	49136	22653	19718	15871	19594	24938	36380	41977
Navicula spp.	2949	9141	11659	4664	6733	11543	5344	5344	933	4664
Bacteriastrum spp.	472	0	833	666	481	0	0	0	933	7462

Table C.12 The number of cells in a PELAGRA collection pot calculated from the number of cells per mg filtered and the total mass of each collection pot (Appendix C.1, table C.7).

C.12 PELAGRA Cell flux

Species	175 m	175 m	280 m	280 m	300 m	300 m	450 m	450 m	630 m	630 m
E huxleyi / G. Mullerae	0E+00	2E+03	2E+02	2E+02	2E+02	9E+02	5E+02	0E+00	5E+02	1E+03
S. pulchra	2E+03	9E+03	6E+02	5E+02	1E+02	6E+02	0E+00	2E+02	1E+03	3E+03
C. Leptoporus	1E+03	8E+02	2E+03	1E+03	1E+03	2E+03	2E+02	5E+02	1E+03	1E+03
C. Pelagicus	0E+00	0E+00	0E+00	0E+00	0E+00	1E+02	0E+00	0E+00	0E+00	0E+00
Pseudonitzschia spp.	2E+05	2E+05	6E+05	3E+05	3E+05	3E+05	8E+04	9E+04	4E+05	4E+05
Rhizosolenia spp.	6E+03	2E+04	1E+04	1E+03	6E+03	1E+04	3E+03	3E+03	0E+00	4E+03
Cylindrotheca spp.	0E+00	5E+03	6E+04	2E+04	2E+04	2E+04	3E+04	3E+04	1E+05	9E+04
Thalassiosira spp.	3E+04	5E+04	2E+05	1E+05	9E+04	7E+04	3E+04	4E+04	2E+05	2E+05
Navicula spp.	1E+04	4E+04	5E+04	2E+04	3E+04	5E+04	8E+03	8E+03	4E+03	2E+04
Bacteriastrum spp.	2E+03	0E+00	4E+03	3E+03	2E+03	0E+00	0E+00	0E+00	4E+03	3E+04

Table C.13 Cell fluxes calculated from cells per collection pot (Appendix C.1, Table C.12 following equation 4.2 in chapter 4. Flux units are cells m^{-2} d^{-1}.

C.13 PELAGRA POC and Biomineral Fluxes

Species	175 m	175 m	280 m	280 m	300 m	300 m	450 m	450 m	630 m	630 m
E huxleyi / G. Mullerae	0.0	0.0	0.0	0.0	0.0	0.0	0.0	0.0	0.0	0.0
S. pulchra	0.1	0.0	0.1	0.1	0.1	0.1	0.0	0.0	0.1	0.1
C. Leptoporus	0.1	0.0	0.1	0.1	0.1	0.1	0.0	0.0	0.1	0.1
C. Pelagicus	0.0	0.0	0.0	0.0	0.0	0.0	0.0	0.0	0.0	0.0
Pseudonitzschia spp.	520.6	802.7	1887.0	1083.2	1146.3	1181.7	266.8	295.4	1248.9	1262.7
Rhizosolenia spp.	30.5	108.0	71.8	7.2	31.1	51.8	14.0	14.0	0.0	20.1
Cylindrotheca spp.	0.0	6.0	67.4	27.0	24.3	19.5	36.1	32.8	122.7	99.1
Thalassiosira spp.	19.8	36.2	158.9	73.3	63.8	51.3	23.0	29.3	117.7	135.8
Navicula spp.	8.5	26.2	33.5	13.4	19.3	33.1	5.6	5.6	2.7	13.4
Bacteriastrum spp.	0.5	0.0	0.9	0.7	0.5	0.0	0.0	0.0	1.0	7.8

Table C.14 Species specific cell bound POC flux calculated from cell flux (Appendix C.12, Table C.13) and species specific conversion factors (Chapter 4, Table 4.2). Flux units are µg C m^{-2} d^{-1}.

Species	175 m	175 m	280 m	280 m	300 m	300 m	450 m	450 m	630 m	630 m
E huxleyi / G. Mullerae	0.00	0.20	0.02	0.02	0.02	0.08	0.04	0.00	0.04	0.11
S. pulchra	0.16	0.78	0.05	0.04	0.01	0.05	0.00	0.01	0.10	0.28
C. Leptoporus	0.09	0.07	0.18	0.13	0.09	0.16	0.01	0.04	0.12	0.09
C. Pelagicus	0.00	0.00	0.00	0.00	0.00	0.01	0.00	0.00	0.00	0.00
Pseudonitzschia spp.	13.47	20.77	48.82	28.02	29.66	30.57	6.90	7.64	32.31	32.67
Rhizosolenia spp.	0.54	1.91	1.27	0.13	0.55	0.92	0.25	0.25	0.00	0.36
Cylindrotheca spp.	0.00	0.45	5.07	2.03	1.83	1.46	2.71	2.47	9.23	7.46
Thalassiosira spp.	2.33	4.27	18.70	8.62	7.51	6.04	2.71	3.45	13.85	15.98
Navicula spp.	1.12	3.48	4.44	1.78	2.56	4.39	0.74	0.74	0.36	1.78
Bacteriastrum spp.	0.18	0.00	0.32	0.25	0.18	0.00	0.00	0.00	0.36	2.84

Table C.15 Species specific cell bound Biomineral flux calculated from cell flux (Appendix C.12, Table C.13) and species specific conversion factors (Chapter 4, Table 4.2). Flux units are µg PIC m^{-2} d^{-1} for coccolithophores and µg BSi m^{-2} d^{-1} for diatoms.

C.14 PELAGRA Total fluxes

Species	175 m	280 m	300 m	450 m	630 m
E huxleyi / G. Mullerae	0.01 (± 0.01)	0.00	0.00	0.00	0.01 (± 0)
S. pulchra	0.07 (± 0.04)	0.09 (± 0.02)	0.08 (± 0.03)	0.02 (± 0.01)	0.06 (± 0.01)
C. Leptoporus	0.05 (± 0.01)	0.10 (± 0.02)	0.08 (± 0.03)	0.02 (± 0.01)	0.06 (± 0.01)
C. Pelagicus	0.00	0.00	0.00	0.00	0.00
Pseudonitzschia spp.	662 (± 199)	1485 (± 568)	1164 (± 25)	281 (± 20)	1256 (± 10)
Rhizosolenia spp.	69 (± 55)	40 (± 46)	41 (± 15)	14 (± 0)	10 (± 14)
Cylindrotheca spp.	3 (± 4)	47 (± 28)	22 (± 3)	34 (± 2)	111 (± 17)
Thalassiosira spp.	28 (± 12)	116 (± 61)	58 (± 9)	26 (± 4)	127 (± 13)
Navicula spp.	17 (± 13)	23 (± 14)	26 (± 10)	6 (± 0)	8 (± 8)
Bacteriastrum spp.	0.25 (± 0.35)	0.78 (± 0.12)	0.25 (± 0.35)	0.00	4.38 (± 5)
Total Coccolithophore	0.13 (± 0.25)	0.19 (± 0.21)	0.16 (± 0.26)	0.03 (± 0.16)	0.13 (± 0.18)
Total Diatom	780 (± 0.17)	1712 (± 0.27)	1311 (± 8)	361 (± 5)	1516 (± 8)

Table C.16 Average and standard deviations of POC fluxes for each depth calculated from the two replicate measurements (table C.14). Errors for the total coccolithophore and diatom fluxes at each depth are calculated from the propagated error for each individual species flux. Flux units are µg C m^{-2} d^{-1}.

Species	175 m	280 m	300 m	450 m	630 m
E huxleyi / G. Mullerae	0.10 (± 0.14)	0.02 (± 0)	0.05 (± 0.04)	0.02 (± 0.03)	0.07 (± 0.05)
S. pulchra	0.47 (± 0.44)	0.05 (± 0.01)	0.03 (± 0.03)	0.01 (± 0.01)	0.19 (± 0.13)
C. Leptoporus	0.08 (± 0.02)	0.15 (± 0.04)	0.13 (± 0.05)	0.03 (± 0.02)	0.10 (± 0.02)
C. Pelagicus	0.00	0.00	0.01 (± 0.01)	0.00	0.00
Pseudonitzschia spp.	17 (± 5)	38 (± 15)	30 (± 0.7)	7 (± 0.52)	32.5 (± 0.25)
Rhizosolenia spp.	1.22 (± 1)	0.70 (± 1)	0.7 (± 0.3)	0.25 (± 0)	0.18 (± 0.25)
Cylindrotheca spp.	0.22 (± 0.3)	4 (± 2)	1.7 (± 0.3)	3 (± 0.17)	8.34 (± 1.3)
Thalassiosira spp.	3.30 (± 1.4)	14 (± 7)	7 (± 1)	3 (± 0.5)	15 (± 1.5)
Navicula spp.	2.30 (± 1.7)	3 (± 2)	3 (± 1.3)	0.74 (± 0)	1.07 (± 1)
Bacteriastrum spp.	0.09 (± 0.13)	0.29 (± 0.04)	0.1 (± 0.13)	0.00	2 (± 2)
Total Coccolithophore	0.65 (± 0.4)	0.22 (± 0.04)	0.22 (± 0.07)	0.1 (± 0.04)	0.36 (± 0.13)
Total Diatom	24 (± 6)	60 (± 17)	43 (± 2)	14 (± 0.8)	59 (± 2.8)

Table C.17 Average and standard deviations of Biomineral fluxes for each depth calculated from the two replicate measurements (table C.15). Errors for the total coccolithophore and diatom fluxes at each depth are calculated from the propagated error for each individual species flux. Flux units are µg PIC m^{-2} d^{-1} for coccolithophores and µg BSi m^{-2} d^{-1} for diatoms.

C.15 CPR data

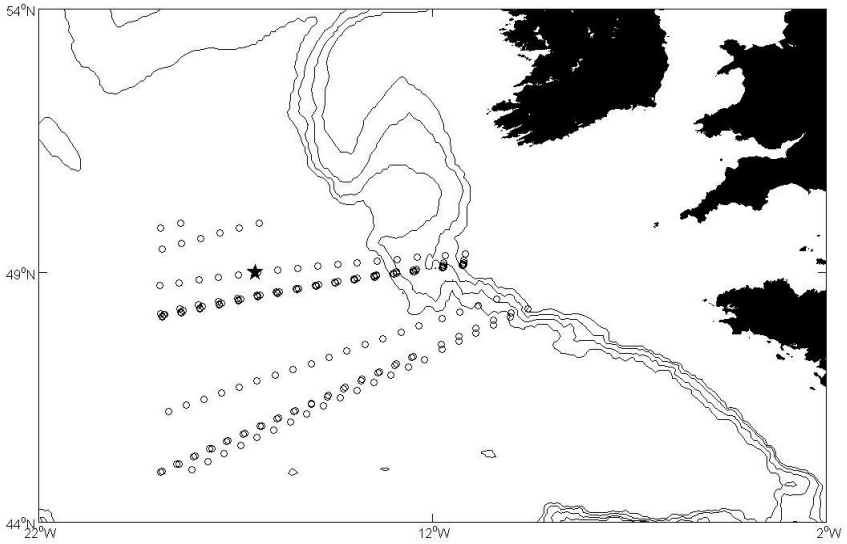

Fig. C.1 Locations of CPR sampling tracks across the E5 regions for February – August 2009. The star denotes the PAP site mooring. Contours are 3000, 2000, 1000 and 500m depth.

	Abundance m^{-3}				
Species	Apr	May	Jun	Jul	Aug
Paralia sulcata	0	0	0	714	0
Thalassiosira spp.	714	18500	500	714	1667
Dactyliosolen mediterraneus	0	2167	500	0	263
Rhizosolenia spp.	0	3000	0	0	526
Chaetoceros spp.	6429	12000	2833	714	526
Thalassiothrix longissima	0	16167	0	0	263
Thalassionema nitzschioides	3810	38667	500	0	263
Pseudo nitzschia spp.	2143	15333	1500	1429	1316
Bacteriastrum spp.	0	7500	0	0	0
Fragilaria spp.	0	500	0	0	0
Cylindrotheca closterium	0	0	0	714	263
Nitzchia spp.	0	0	500	0	0
Total	13095	113833	6333	4286	5088

Table C.18 Continuous plankton recorder data showing the absolute abundance of diatom species per cubic meter sampled averaged across the E5 region.

	% abundance					
Species	Mar	Apr	May	Jun	Jul	Aug
Paralia sulcata	20	0	0	0	17	0
Thalassiosira spp.	20	5	16	8	17	33
Dactyliosolen mediterraneus	20	0	2	8	0	5
Rhizosolenia spp.	0	0	3	0	0	10
Chaetoceros spp.	0	49	11	45	17	10
Thalassiothrix longissima	20	0	14	0	0	5
Thalassionema nitzschioides	20	29	34	8	0	5
Pseudo nitzschia spp.	0	16	13	24	33	26
Bacteriastrum spp.	0	0	7	0	0	0
Fragilaria spp.	0	0	0	0	0	0
Cylindrotheca closterium	0	0	0	0	17	5
Nitzchia spp.	0	0	0	8	0	0
Total	100	100	100	100	100	100

Table C.19 Continuous plankton recorder data showing the % relative abundance of diatom species sampled averaged across the E5 region.

C.16 Mixed Layer Community Data

		MLC (14/07/2009)		
	Cells mL-1	POC [pg mL^{-1}]	PIC [pg mL^{-1}]	BSi [pg mL^{-1}]
E .huxleyi and G. Muellerae	33	236	2875	-
Syrasosphera pulchra	337	17389	205570	-
Calcidiscus leptoporus	6	324	6240	-
Coccolithus pelagicus	192	8986	547200	-
Bacteriastrum sp	0	0	-	0
Coscinodiscus sp	0	0	-	0
Rhizosolenia sp	0	0	-	0
Cylindrotheca sp.	69	80782	-	52466
Navicula sp	8	5247	-	3434
Pseudonitzschia sp.	0	0	-	0

Table C.20 Mixed layer community cell counts sampled on 14/07/2009 and biomass conversions by multiplying by the conversion factors in chapter 4 (Table 4.2).

	MLC (03/08/2009)			
	Cells mL-1	POC [pg mL^{-1}]	PIC [pg mL^{-1}]	BSi [pg mL^{-1}]
E .huxleyi and G. Muellerae	254	1829	22238	-
Syrasosphera pulchra	879	45356	536190	-
Calcidiscus leptoporus	19	1026	19760	-
Coccolithus pelagicus	100	4680	285000	-
Bacteriastrum sp	0.2	48	-	31
Coscinodiscus sp	0	0	-	0
Rhizosolenia sp	0	0	-	0
Cylindrotheca sp.	190	221160	-	143640
Navicula sp	16	10560	-	6912
Pseudonitzschia sp.	14	45684	-	29727

Table C.21 Mixed layer community cell counts sampled on 03/08/2009 and biomass conversions by multiplying by the conversion factors in chapter 4 (Table 4.2).

Appendix D: Fast and slow POC fluxes in the Arctic

D.1 FP and MSA sinking speeds, size and flux calculations

Date	Depth (m)	Av.Sinking Speed (m d^{-1})	Time (d)	Max Length (mm)	Min Length (mm)	Vol. (mm^3)	C content (µg)	MSA Flux ($mgCm^{-2}d^{-1}$)
				Sea Ice				
Ice Station 1	50	240	0.003	0.343	0.18	0.0	0.2 (± 0.01)	1.0 (± 0.6)
Ice Station 1	50	154	0.005	0.259	0.207	0.0	0.2 (± 0.01)	0.6 (± 0.04)
Ice Station 1	50	93.9	0.008	0.763	0.462	0.7	0.8 (± 0.18)	1.6 (± 0.35)
Ice Station 2	50	108	0.007	0.365	0.298	0.1	0.4 (± 0.04)	0.8 (± 0.1)
Ice Station 2	100	18	0.042	0.337	0.144	0.0	0.2 (± 0.001)	0.1 (± 0.001)
Ice Station 3	100	12	0.063	0.55	0.48	0.5	0.7 (± 0.15)	0.2 (± 0.04)
Ice Station 3	100	61	0.012	0.79	0.61	1.2	1.1 (± 0.28)	1.4 (± 0.35)
Ice Station 3	100	180	0.004	1.21	0.58	1.7	1.3 (± 0.36)	4.9 (± 1.33)
Ice Station 3	100	12	0.063	0.86	0.44	0.7	0.8 (± 0.18)	0.2 (± 0.04)
Ice Station 3	100	61	0.012	0.72	0.56	0.9	1.0 (± 0.23)	1.2 (± 0.29)
Ice Station 3	100	12	0.063	1.39	0.86	4.3	2.1 (± 0.7)	0.5 (± 0.17)
Ice Station 3	100	12	0.063	1.59	1.1	8.1	3.0 (± 1.08)	0.7 (± 0.27)
Ice Station 3	100	154	0.005	0.81	0.52	0.9	1.0 (± 0.22)	3.0 (± 0.72)
Ice Station 3	100	12	0.063	0.9	0.48	0.9	0.9 (± 0.22)	0.2 (± 0.05)
Ice Station 3	100	91	0.008	1.6	0.99	6.6	2.7 (± 0.94)	5.0 (± 1.76)
Ice Station 4	100	62	0.012	0.52	0.37	0.3	0.5 (± 0.09)	0.7 (± 0.12)

Table D.1 Aggregate sinking speed and size measurements for sea ice environment. Sinking time was calculated from the sinking speed, assuming a distance sank of 0.75 m. Maximum and minimum lengths were taken from the 2D area of the digital images. Volumes were calculated assuming the third dimension was the same as the shortest length. Carbon content was estimated from Alldredge [1998]. Flux was calculated following equation 3.3 in Chapter 3). The C content ranges (in brackets) are calculated from the potential range of values based on the standard errors quoted by Alldredge [1998]. The flux error (in brackets) is the propagation of the C content error into the flux calculation.

Date	Depth (m)	Av.Sinking Speed (m d^{-1})	Time (d)	Max Length (mm)	Min Length (mm)	Vol. (mm^3)	C content (µg)	MSA Flux (mg$Cm^{-2}d^{-1}$)
Open Water								
KF3	50	1080	0.001	0.5	0.3	0.2	0.5 (± 0.07)	10 (± 1.57)
KF4	50	75	0.010	1.06	0.63	1.8	1.3 (± 0.37)	2.1 (± 0.57)
KF4	50	39	0.019	0.56	0.31	0.2	0.5 (± 0.07)	0.4 (± 0.06)
KF4	50	41	0.018	0.95	0.62	1.5	1.2 (± 0.33)	1.1 (± 0.28)
KF4	50	173	0.004	1.93	1.17	11.1	3.5 (± 1.34)	12.4 (± 4.8)
KF4	50	129	0.006	0.52	0.38	0.3	0.5 (± 0.09)	1.5 (± 0.25)
KF4	50	144	0.005	0.321	0.27	0.1	0.3(± 0.03)	0.9 (± 0.09)
KF4	100	154	0.005	1.05	1	4.4	2.2 (± 0.71)	6.9 (± 2.3)
KF4	100	25	0.031	1.41	0.82	4.0	2.0 (± 0.66)	1.0 (± 0.33)
KF4	100	68	0.011	1.47	0.92	5.2	2.4 (± 0.8)	3.3 (± 1.1)
KF4	100	166	0.005	0.432	0.266	0.1	0.3 (± 0.04)	1.2 (± 0.14)
KF4	100	255	0.003	0.67	0.49	0.7	0.8 (± 0.18)	4.3 (± 0.93)
GM	50	43	0.017	0.45	0.35	0.2	0.5 (± 0.07)	0.4 (± 0.06)
GM	100	49	0.015	0.71	0.43	0.5	0.7 (± 0.15)	0.7 (± 0.15)
GM	100	84	0.009	0.39	0.32	0.2	0.4 (± 0.05)	0.7 (± 0.09)
GM	100	88	0.009	0.47	0.46	0.4	0.6 (± 0.12)	1.1 (± 0.22)

Table D.2 Aggregate sinking speed and size measurements for open water environment. Sinking time was calculated from the sinking speed, assuming a distance sank of 0.75 m. Maximum and minimum lengths were taken from the 2D area of the digital images. Volumes were calculated assuming the third dimension was the same as the shortest length. Carbon content was estimated from Alldredge [1998]. Flux was calculated following equation 3.3 in Chapter 3). The C content ranges (in brackets) are calculated from the potential range of values based on the standard errors quoted by Alldredge [1998]. The flux error (in brackets) is the propagation of the C content error into the flux calculation.

Date	Depth (m)	Type	Sinking Speed (m d^{-1})	Sinking time (d)	Length (mm)	Average Width (mm)	Volume (mm3)	Carbon content (µg)	FP Flux (mg C m^{-2} d^{-1})
Sea Ice									
Ice Station 1	50	Copepod	240	0.0031	0.45	0.09	0.0	2	7.5
Ice Station 2	50	Euphasid	18	0.0417	1.7	0.15	0.1	7	2.5
Ice Station 2	50	Euphasid	233	0.0032	1.83	0.13	0.1	6	29.1
Ice Station 3	100	Copepod	196	0.0038	1.56	0.23	0.3	32	131.6
Ice Station 4	100	FP	86	0.0087	-	-	-	-	20.9
Ice Station 4	100	FP	57	0.0132	-	-	-	-	13.7
Open Water									
KF3	100	Copepod	360	0.0021	1.46	0.28	0.5	43	323.5
KF3	50	Euphasid	36	0.0208	2.31	0.35	1.2	52	38.6
KF3	50	Copepod	216	0.0035	0.49	0.31	0.2	18	81.4
KF3	50	Euphasid	-	-	1.44	0.30	0.6	25	86.4
KF3	50	Euphasid	64	0.0117	1.28	0.10	0.1	3	3.4
KF4	50	Euphasid	108	0.0069	0.49	0.04	0.0	0.1	0.3
KF4	100	Euphasid	108	0.0069	3.01	0.15	0.3	13	29.5
KF4	100	Euphasid	216	0.0035	4.76	0.16	0.5	24	105.8
KF4	100	Euphasid	196	0.0038	1.48	0.13	0.1	5	18.4
KF4	100	Euphasid	114	0.0066	2.43	0.13	0.2	8	18.9
GM	100	Copepod	180	0.0042	0.87	0.22	0.2	16	58.9
GM	50	Euphasid	432	0.0017	1.92	0.41	1.4	61	543.2

Table D.3 Faecal pellet sinking speed and size measurements. Sinking time was calculated from the sinking speed, assuming a distance sank of 0.75 m. Maximum and minimum lengths were taken from the 2D area of the digital images. 4 measurements of the width were made and averaged to give a final number. Volumes were calculated assuming the third dimension was the same as the shortest length. Carbon content was estimated assuming 94 µg C mm^{-3} for copepod faecal pellets and 45 µg C mm^{-3} for euphausiid faecal pellets [*Wexels Riser et al.* 2007]. No error were quoted with the FP carbon contents. Where no faecal pellet dimensions were available the average faecal pellet carbon content in the sea ice environment (11 ± 14) was used to estimate the total flux.

D.2 Depth averaged MSA and FP POC fluxes

	Depth	Total Flux (mg C m^{-2} d^{-1})	Slow Flux (mg C m^{-2} d^{-1})	Total Fast Flux (mg C m^{-2} d^{-1})	Total MSA Flux (mg C m^{-2} d^{-1})	Total FP flux (mg C m^{-2} d^{-1})	Depth Average MSA Flux (mg C m^{-2} d^{-1})	Depth Average FP Flux (mg C m^{-2} d^{-1})
Sea Ice								
Ice Station 1	50	284 (± 0.4)	274	11 (± 0.4)	3 (± 0.4)	7		
Ice Station 2	50	56 (± 0.4)	15	40 (± 0.4)	9 (± 0.4)	32	6 (± 3.96)	20 (± 17)
Ice Station 2	100	4 (± 0.002)	4	0.1 (± 0.002)	0.1 (± 0.002)	0		
Ice Station 3	100	268 (± 2)	119	149 (± 2)	17 (± 2)	132		
Ice Station 4	100	50 (± 0.1)	15	35 (± 0.1)	1 (± 0.1)	35	6.0 (± 9.83)	83 (± 69)
Open Water								
KF3	50	581 (± 1.6)	37	544	10 (± 1.6)	533		
KF4	50	181 (± 5.1)	162	19	18 (± 5.1)	0		
GM	50	560 (± 0.06)	17	544	0.4 (± 0.06)	543	9.7 (± 8.95)	359 (± 311)
KF4	100	266 (± 2.7)	76	190	17 (± 2.7)	173		
GM	100	103 (± 0.23)	43	60	1 (± 0.23)	59	9.1 (± 11.65)	116 (± 80)

Table D.4 MSA and FP POC fluxes in the sea ice and open water environments. The total flux is the sum of the fast and slow fluxes. The error is the propagated error from the calculations of the MSA flux. The errors in brackets for the total aggregate flux are those propagated from the carbon contents in table 1. The errors shown for the depth average fluxes (both MSA and FP) are the standard deviations calculated from the average of the total flux values.

D.3 Slow sinking flux

Date	Depth (m)	POC Conc. Top (µg L^{-1})	POC Conc. Base (µg L^{-1})	Difference (µg L^{-1})[a]	Mass Difference (µg)[b]	Settling Time (days)[d]	Slow Sinking Flux (mg C m^{-2} day^{-1})[e]
				Sea Ice			
Ice Station 1	50	217.31	479.89	262.58	1838	0.104	274
Ice Station 2	50	76.28	97.02	20.74	145	0.146	15
Ice Station 2	100	55.48	60.26	4.78	33	0.146	4
Ice Station 3	100	48.63	186.23	137.60	963	0.125	119
Ice Station 4	100	14.75	31.53	16.78	117	0.125	15
				Open Water			
KF3	50	49.78	99.47	49.68	348	0.1458	37
KF4	50	155.47	342.49	187.02	1309	0.125	162
GM	50	43.99	66.49	22.50	157	0.1458	17
KF4	100	100.28	188.17	87.89	615	0.125	76
GM	100	36.46	94.07	57.61	403	0.1458	43

Table D.5 Calculation of the slow sinking fluxes at each station. The POC conc. Top and Base refer to the concentration of POC in the top and base of the MSC respectively.

a. Difference is the concentration in the base of the MSC minus the concentration in the top of the MSC.

b. The mass difference is calculated by multiplying the concentration difference by the volume of the base chamber (7 L).

c. The slow sinking concentration is calculated by multiplying the mass difference by the total volume of the MSC (100 L).

d. The settling time varied as during this cruise the MSC was left to settle between 2 and 3.5 hours depending on the deployment due to other activities occurring on the ship.

e. The slow sinking flux was then calculated by dividing the mass difference by the MSC area (0.06 m^2) and the settling time. This number was then scaled to the volume of the top section of the MSC.

D.4 Water Column Primary Productivity

Date	Location	Sample Depth	Light Level	Primary Productivity (mg C m^{-3})	SD
24/06/2010	Sea Ice Lead	5	55	9.32	0.00
	Sea Ice Lead	10	33	5.80	0.36
	Sea Ice Lead	16	14	5.12	0.28
	Sea Ice Lead	30	5	2.30	0.16
	Sea Ice Lead	45	1	0.57	0.03
24/06/2010	Below Ice	5	5	5.41	0.40
	Below Ice	10	1	1.28	0.05
29/06/2010	Sea Ice Lead	5	80	2.20	0.22
	Sea Ice Lead	11	55	4.54	0.18
	Sea Ice Lead	13	33	4.49	0.76
	Sea Ice Lead	20	14	2.41	0.18
	Sea Ice Lead	30	5	5.09	0.46
29/06/2010	Below Ice	5	5	2.18	0.16
	Below Ice	10	1	0.34	0.04
04/07/2010	KF3	4	55	4.61	0.73
	KF3	7	33	4.80	0.15
	KF3	15	14	3.73	0.75
	KF3	26	5	0.83	0.16
	KF3	45	1	0.15	0.04
05/07/2010	KF4	2	80	24.05	2.83
	KF4	5	55	15.80	0.74
	KF4	8	33	24.00	2.93
	KF4	13	14	35.22	1.08
	KF4	19	5	16.17	0.36
	KF4	25	1	2.16	0.44
10/07/2010	GM	2	80	11.37	0.29
	GM	3	55	11.06	0.60
	GM	9	33	94.32	3.12
	GM	18	14	32.31	0.89
	GM	27	5	1.21	0.10
	GM	50	1	0.33	0.03

Table D.6 Water column primary productivity based on radionuclide ^{14}C method. Values for each light level at each station (including individual ice leads and below ice samples) were integrated to give a total value of primary productivity per m^{-2}. Values provided by Eithne Tynan (NOC, Southampton).

D.5 Ice core primary productivity

Sample	Date	Lat	Long	Primary Productivity (mg m^{-2} d^{-1})
1	24/06/10	80°33.810	004°13.580	15.36
2	26/06/10	80° 27.69	003°44.08	9.72
3	28/06/10	80° 17.46	003° 11.4	3.84
4	30/06/10	80° 13.08	002° 20.04	8.28
Average				9.3
SD				5

Table D.7 Ice core primary productivity values based on ^{14}C method. Data supplied by Ronnie Glud (SAMS).

D.6 Algal floc primary productivity

Sample	Date	Lat	Long	Primary Productivity (mg m^{-2} d^{-1})
1	28/06/10	80° 17.46	003° 11.4	232.8
2	30/06/10	80° 13.08	002° 20.04	234
Average				233.4
SD				0.6

Table D.8 Algal floc primary productivity estimate based on O_2 flux measurements. Data provided by Ronnie Glud (SAMS).

D.7 Nutrient Data

Date	Depth (m)	Phosphate μ mol m^{-3}	Error μ mol m^{-3}	Silicate μ mol m^{-3}	Error μ mol m^{-3}	NO3,NO2 μ mol m^{-3}	Error μ mol m^{-3}
23/06/2010	5	59	11	169	53	77	3
	18	85	39	725	68	308	5
	25	91	31	874	13	416	0
	30	193	8	1184	91	2565	8
	46	270	36	1258	99	5007	10
	50	369	38	1603	80	5943	6
	Average conc. (μ mol m^{-2})	178	73	969	179	2386	179
24/06/2010	5	45	12	285	28	123	17
	25	80	35	717	67	163	58
	50	371	29	2032	22	6633	58
	Average conc. (μ mol m^{-2})	165	47	1011	76	2306	84
26/06/2010	5	233	72	1508	45	209	6
	10	62	10	15	79	131	8
	25	132	14	547	53	2027	26
	40	136	38	642	36	1747	12
	50	299	20	1850	63	5564	26
	Average conc. (μ mol m^{-2})	172	86	913	128	1935	40
08/07/2010	2	301	12	1364	11	152	35
	5	480	37	1255	77	166	9
	9	486	18	2595	27	608	23
	14	438	6	3483	31	1421	13
	16	488	13	4231	23	2505	31
	29	384	10	4148	31	3653	19
	50	428	19	4278	54	5544	26
	Average conc. (μ mol m^{-2})	429	50	3051	110	2007	64

Table D.9 Sea Ice nutrient depths, concentrations and average concentration between 0 and 50 m.

Date	Depth (m)	Phosphate μ mol m^{-3}	Error μ mol m^{-3}	Silicate μ mol m^{-3}	Error μ mol m^{-3}	NO3,NO2 μ mol m^{-3}	Error μ mol m^{-3}
05/07/2010	5	49	8	454	36	75	13
	10	149	18	75	37	165	30
	25	184	25	263	31	1313	52
	32	171	35	261	6	1580	16
	50	454	65	410	21	4057	11
	Average conc. (μ mol m^{-2})	202	80	293	64	1438	65
06/07/2010	2	14	10	526	36	67	22
	5	26	13	525	33	4	7
	8	114	52	962	24	284	11
	10	99	10	1999	33	2632	20
	13	226	8	2819	73	5754	10
	19	682	9	3238	60	7030	20
	21	452	8	3261	16	7193	19
	25	440	17	3313	96	7430	21
	30	472	10	3419	54	7991	34
	50	503	23	3798	66	8532	9
	Average conc. (μ mol m^{-2})	303	64	2386	172	4692	60
10/07/2010	2	272	30	1846	32	2573	36
	5	154	38	1674	17	2295	35
	10	188	30	2136	43	3499	24
	18	401	35	2277	99	5737	51
	27	368	60	2492	66	6933	45
	50	331	21	2454	69	5796	57
	Average conc. (μ mol m^{-2})	286	92	2147	149	4472	105

Table D.10 Open Water nutrient depths, concentrations and average concentration between 0 and 50 m.

D.8 Phytoplankton biomass

Cells m^{-3}	IS1	IS2	IS3	IS4	KF3	KF4	GM
Navicula spp.	1262406	73056	0	226335	35350	164376	105200
Pseudonitzscia spp.	11081117	115752995	3058990	1508900	3393564	64289181	70134
Rhizosolenia spp.	140267	0	0	0	0	0	0
Thalassiosira spp.	701337	0	0	8148058	70699	1862925	0
Coscinodiscus spp.	385735	365279	575810	1923847	176748	547919	70134
Pleurosigma spp.	35067	0	35988	0	0	0	0
Fragilariaopsis spp.	0	34774602	1007667	5658373	0	2958763	35067
Chatocerous spp.	0	0	0	9242010	70699	36342992	140267
Thalesonemia spp.	0	0	0	0	0	1808133	105200
Total Diatoms	13605928	150965933	4678456	26707522	3747060	107974290	526002

Table D.11 Diatom species concentration per cubic meter of water in both the sea ice and open water environments

µg POC m^{-3}	IS1	IS2	IS3	IS4	Av	KF3	KF4	GM	Average
Navicula spp.	602	35	0	108	186 (± 281)	17	78	50	48 (± 31)
Pseudonitzscia spp.	4732	49427	1306	644	14027 (± 23667)	1449	27451	30	9643 (± 15438)
Rhizosolenia spp.	695	0	0	0	174 (± 348)	0	0	0	0
Thalassiosira spp.	248	0	0	2876	781 (± 1402)	25	658	0	228 (± 373)
Coscinodiscus spp.	193	183	288	964	407 (± 374)	89	275	35	133 (± 126)
Pleurosigma spp.	142	0	146	0	72 (± 83)	0	0	0	0
Fragilariaopsis spp.	0	30671	889	4991	9138 (± 14519)	0	2610	31	880 (± 1498)
Chatocerous spp.	0	0	0	647	162 (± 323)	5	2544	10	853 (± 1465)
Thalesonemia spp.	0	0	0	0	0	0	37	2	13 (± 21)
Total Diatoms	6612	80316	2629	10230	24947 (± 37043)	1584	33653	158	11798 (± 18940)

Table D.12 Concentration of diatom cell bound carbon per cubic meter of water in both the sea ice and open water environments. Biomass calculated by multiplying the concentration of cells (cell density) by the POC conversion factor (Table 5.3 Chapter 5)

Cells MSA^{-1}	Depth (m)	Pseudonitzscia spp.	Navicula spp.	Chatocerous spp.	Coscinodiscus spp.	Pleurosigma spp.	Thalassiosira spp.	Fragilariaopsis sp.	Cylindrotheca spp.
IS 1	50	0	0	0	0	0	0	0	0
IS 1	50	0	0	0	0	0	0	0	0
IS 1	50	4	0	0	0	0	0	0	0
IS 2	100	4	1	0	9	0	0	0	0
IS 3	100	3	0	9	2	0	15	0	0
IS 3	100	0	0	21	2	0	1	0	0
IS 3	100	0	1	23	0	0	0	0	0
IS 3	100	0	1	19	1	0	3	0	0
IS 3	100	2	0	5	2	0	12	0	0
IS 3	100	1	1	29	0	0	0	0	0
IS 3	100	1	0	46	3	0	1	0	0
IS 3	100	0	0	12	4	0	2	0	0
IS 3	100	0	0	9	0	0	3	0	0
IS 3	100	1	0	26	1	0	0	0	0
IS 4	100	5	0	0	0	0	0	0	0
IS 4	100	0	0	0	0	0	0	0	0
IS 4	100	0	0	0	0	0	108	0	0
Av		1.2	0.2	11.7	1.4	0.0	8.5	0.0	0.0
SD		1.7	0.4	13.6	2.3	0.0	26.0	0.0	0.0
KF3	50	3	0	0	0	0	0	0	0
KF3	50	3	0	0	0	0	0	0	0
KF3	100	3	0	0	0	0	0	0	0
KF4	100	0	0	0	0	0	0	0	0
GM	100	3	0	1	0	0	0	0	0
GM	100	9	0	3	4	0	0	0	0
Av		2.0	0.1	9.2	1.0	0.0	9.4	0.0	0.0
SD		2.3	0.3	13.2	1.5	0.0	26.3	0.0	0.0

Table D.13 The number of cells counted in each marine snow aggregate collected

µg POC MSA^{-1}	Depth (m)	Pseudonitzscia spp.	Navicula spp.	Chatocerous spp.	Coscinodiscus spp.	Pleurosigma spp.	Thalassiosira spp.	Fragilariaopsis sp.	Cylindrotheca spp.
IS 1	50	0	0	0	0	0	0	0	0
IS 1	50	0	0	0	0	0	0	0	0
IS 1	50	1708	0	0	0	0	0	0	0
IS 2	100	1708	477	0	4509	0	0	0	0
IS 3	100	1281	0	630	1002	0	5295	0	0
IS 3	100	0	0	1470	1002	0	353	0	0
IS 3	100	0	477	1610	0	0	0	0	0
IS 3	100	0	477	1330	501	0	1059	0	0
IS 3	100	854	0	350	1002	0	4236	0	0
IS 3	100	427	477	2030	0	0	0	0	0
IS 3	100	427	0	3220	1503	0	353	0	0
IS 3	100	0	0	840	2004	0	706	0	0
IS 3	100	0	0	630	0	0	1059	0	0
IS 3	100	427	0	1820	501	0	0	0	0
IS 4	100	2135	0	0	0	0	0	0	0
IS 4	100	0	0	0	0	0	0	0	0
IS 4	100	0	0	0	0	0	38124	0	0
Av		527	112	819	707	0	3011	0	0
SD		732	209	953	1162	0	9180	0	0
KF3	50	1281	0	0	0	0	0	0	0
KF3	50	1281	0	0	0	0	0	0	0
KF3	100	1281	0	0	0	0	0	0	0
KF4	100	0	0	0	0	0	0	0	0
GM	100	1281	0	70	0	0	0	0	0
GM	100	3843	0	210	2004	0	0	0	0
Av		853	47	644	523	0	3333	0	0
SD		988	124	922	740	0	9279	0	0

Table D.14 Concentration of cell bound diatom POC in each MSA. Biomass calculated by multiplying the concentration of cells (cell density) by the POC conversion factor (Table 5.3 Chapter 5)

	Individual transects (x20 magnification)			Average in 25 µL	SD	POC cell^{-1} [pg]	Biomass [µg m^{-3}]
	in 25µl	in 25µl	in 25µ				
Algal floc							
Navicula spp.	14678	17491	20859	17676	3095	2080	342 (± 3095)
Tropidones group	3770	5992	4503	4755	1132	82	16 (± 4755)
Achnanthes spp.	1276	2222	4432	2643	1619	208	22 (± 1619)
Entomoneis spp.	95	177	473	248	199	2131	5 (± 2131)
Total							385 (± 1209)
Ice Core							
Nitzschia spp (inc. P-n)	1785	1903	2742	2143	522	44	4 (± 522)
Pleurosiga spp.	118	118	319	185	116	1069	8 (± 116)
Thalassiosira spp.	1265	520	1985	1257	733	296	15 (± 733)
Cylindrotheca spp.	355	165	201	240	101	23	0.2 (± 101)
Total							27 (± 312)

Table D.15 Carbon biomass for diatoms species counted in the algal floc floating below the sea ice and the ice core sample. Three independent transects were counted and multiplied up to give the number of cells in a 25 µL sample. An average of these three transects was then taken and multiplied by the call POC conversions calculated at SAMS and then averaged to give a total biomass.

References

Abramoff, M. D., Magelhaes, P. J., and Ram, S. J. (2004), *Image Processing with ImageJ*, *Biophotonics International, 11*(7), 36-42.

Alldredge, A. (1998), *The carbon, nitrogen and mass content of marine snow as a function of aggregate size*, *Deep-Sea Research Part I-Oceanographic Research Papers, 45*(4-5), 529-541, 10.1016/S0967-0637(97)00048-4: 10.1016/S0967-0637(97)00048-4.

Alldredge, A. L., and Youngbluth, M. J. (1985), *The significance of macroscopic aggregates (marine snow) as sites for heterotrophic bacterial production in the mesopelagic zone of the subtropical Atlantic*, *Deep Sea Research Part A. Oceanographic Research Papers*, *32*(12), 1445-1456, 10.1016/0198-0149(85)90096-2.

Alldredge, A. L., and Gotschalk, C. (1988), *The in situ settling behaviour of marine snow*, *Limnol. Oceanogr., 33*(3), 10.4319/lo.1988.33.3.0339: 10.4319/lo.1988.33.3.0339.

Alldredge, A. L., and Silver, M. W. (1988), *Characteristics, Dynamics and Significance of Marine Snow*, *Progress In Oceanography, 20*(1), 41 - 82, 10.1016/0079-6611(88)90053-5: 10.1016/0079-6611(88)90053-5.

Alldredge, A. L., and Gotschalk, C. (1990), *The relative contribution of marine snow of different origins to biological processes in coastal waters*, *Continental Shelf Research, 10*(1), 41-58, 10.1016/0278-4343(90)90034-J: 10.1016/0278-4343(90)90034-J.

Alldredge, A. L., and Jackson, G. A. (1995), *Preface: Aggregation in marine system*, *Deep Sea Research Part II: Topical Studies in Oceanography*, *42*(1), 1-7

Alonso-González, I. J., Arístegui, J., Lee, C., Sanchez-Vidal, A., Calafat, A., Fabrés, J., Sangrá, P., Masqué, P., Hernández-Guerra, A., and Benítez-Barrios, V. (2010), *Role of slowly settling particles in the ocean carbon cycle*, *Geophys. Res. Lett., 37*(13), L13608, 10.1029/2010gl043827: 10.1029/2010gl043827.

Andreassen, I., Nothig, E. M., and Wassmann, P. (1996), *Vertical particle flux on the shelf off northern Spitsbergen, Norway*, *Marine Ecology-Progress Series*, *137*(1-3), 215-228

Andreassen, I. J., and Wassmann, P. (1998), *Vertical flux of phytoplankton and particulate biogenic matter in the marginal ice zone of the Barents Sea in May 1993*, *Marine Ecology Progress Series*, *170*, 1-14, 10.3354/meps170001.

Antia, A. N., Koeve, W., Fischer, G., Blanz, T., Schulz-Bull, D., SchÃlten, J., Neuer, S., Kremling, K., Kuss, J., Peinert, R., Hebblin, D., Bathmann, U., Conte, M., Fehner, U., and Zeitzschel, B. (2001), *Basin-Wide Particulate Carbon Flux in the Atlantic Ocean: Regional Export Patterns and Potential for Atmospheric CO_2 Sequestration*, *Global Biogeochemical Cycles, 15*, 10.1029/2000gb001376: 10.1029/2000gb001376.

Armstrong, A., Lee, C., Hedges, J. I., Honjo, S., and Wakeham, S. G. (2002), *A new, mechanistic model for organic carbon fluxes in the ocean based on the quantitative association of POC with ballast minerals*, *Deep Sea Research Part II: Topical Studies in Oceanography, 49*(1-3), 219-236, 10.1016/S0967-0645(01)00101-1: 10.1016/S0967-0645(01)00101-1.

Armstrong, R. A., Peterson, M. L., Lee, C., and Wakeham, S. G. (2009), *Settling velocity spectra and the ballast ratio hypothesis*, *Deep Sea Research Part II: Topical Studies in Oceanography*, *56*(18), 1470-1478

Arrigo, K. R. (2005), *Marine microorganisms and global nutrient cycles*, *Nature*, *437*(7057), 349-355

Arrigo, K. R., van Dijken, G., and Pabi, S. (2008), *Impact of a shrinking Arctic ice cover on marine primary production*, *Geophys. Res. Lett.*, *35*(19), L19603, 10.1029/2008gl035028.

Arrigo, K. R., and van Dijken, G. L. (2011), *Secular trends in Arctic Ocean net primary production*, *Journal of Geophysical Research-Oceans*, *116*, Artn C09011
DOI 10.1029/2011jc007151.

Asper, V. L. (1987), *Measuring the flux and sinking speed of marine snow aggregates*, *Deep Sea Research Part A. Oceanographic Research Papers*, *34*(1), 1-17, 10.1016/0198-0149(87)90117-8.

Ayukai, T., and Nishizawa, S. (1986), *Defecation rate as a possible measure of ingestion rate of calanus-pacificus-pacificus copepoda calanoida*
Bulletin of Plankton Society of Japan, *33*(1), 3-10, 10.1029/2004jc002757.

Azetsu-Scott, K., and Passow, U. (2004), *Ascending Marine Particles: Significance of Transparent Exopolymer Particles (TEP) in the Upper Ocean*, *Limnol. Oceanogr.*, *49*(3), 741-748

Balch, W. M., Drapeau, D. T., and Fritz, J. J. (2000), *Monsoonal forcing of calcification in the Arabian Sea*, *Deep Sea Research Part II: Topical Studies in Oceanography*, *47*(7-8), 1301-1337, 10.1016/s0967-0645(99)00145-9.

Bates, N. R., and Mathis, J. T. (2009), *The Arctic Ocean marine carbon cycle: evaluation of air-sea CO_2 exchanges, ocean acidification impacts and potential feedbacks*, *Biogeosciences*, *6*, 2433-2459

Batten, S. D., Clark, R., Flinkman, J., Hays, G., John, E., John, A. W. G., Jonas, T., Lindley, J. A., Stevens, D. P., and Walne, A. (2003), *CPR sampling: the technical background, materials and methods, consistency and comparability*, *Progress In Oceanography*, *58*(2-4), 193-215, 10.1016/j.pocean.2003.08.004.

Bauerfeind, E., Nöthig, E.-M., Beszczynska, A., Fahl, K., Kaleschke, L., Kreker, K., Klages, M., Soltwedel, T., Lorenzen, C., and Wegner, J. (2009), *Particle sedimentation patterns in the eastern Fram Strait during 2000-2005: Results from the Arctic long-term observatory HAUSGARTEN*, *Deep Sea Research Part I: Oceanographic Research Papers*, *56*(9), 1471-1487

Bender, M., Ducklow, H., Kiddon, J., Marra, J., and Martin, J. (1992), *The carbon balance during the 1989 spring bloom in the North Atlantic Ocean, 47°N, 20°W*, *Deep Sea Research Part A. Oceanographic Research Papers*, *39*(10), 1707-1725, 10.1016/0198-0149(92)90025-o.

Berdalet, E., and Estrada, M. (1997), *Phytoplankton in a turbulent world*

Berner, W., Stauffer, B., and Oeschger, H. (1978), *Past atmospheric composition and climate, gas parameters measured on ice cores*, *Nature*, *276*(5683), 53-55

Bienfang, P. K. (1981), *Sinking rate dynamics of Cricosphaera carterae Braarud. II. Senescence response to various limiting substrates in non-steady state populations*, *Journal of Experimental Marine Biology and Ecology*, *49*(2-3), 235-244, 10.1016/0022-0981(81)90073-3.

Bienfang, P. K., Harrison, P. J., and Quarmby, L. M. (1982), *Sinking rate response to depletion of nitrate, phosphate and silicate in four marine diatoms*, *Marine Biology*, *67*(3), 295-302, 10.1007/bf00397670.

Billett, D. S. M., Lampitt, R. S., Rice, A. L., and Mantoura, R. F. C. (1983), *Seasonal sedimentation of phytoplankton to the deep-sea benthos*, *Nature*, *302*(5908), 520-522

Bishop, J. K. B., Edmond, J. M., Ketten, D. R., Bacon, M. P., and Silker, W. B. (1977), *The chemistry, biology, and vertical flux of particulate matter from the upper 400 m of the equatorial Atlantic Ocean*, *Deep Sea Research*, *24*(6), 511-548, 10.1016/0146-6291(77)90526-4.

Bishop, J. K. B., Collier, R. W., Kettens, D. R., and Edmond, J. M. (1980), *The chemistry, biology, and vertical flux of particulate matter from the upper 1500 m of the Panama Basin*, *Deep Sea Research Part A. Oceanographic Research Papers, 27*(8), 625-640, 10.1016/0198-0149(80)90077-1: 10.1016/0198-0149(80)90077-1.

Boeckel, B., and Baumann, K.-H. (2008), *Vertical and lateral variations in coccolithophore community structure across the subtropical frontal zone in the South Atlantic Ocean*, *Mar. Micropaleontol.*, *67*(3-4), 255-273, 10.1016/j.marmicro.2008.01.014.

Bollmann, J., Cortés, M. Y., Haidar, A. T., Brabec, B., Close, A., Hofmann, R., Palma, S., Tupas, L., and Thierstein, H. R. (2002), *Techniques for quantitative analyses of calcareous marine phytoplankton*, *Mar. Micropaleontol.*, *44*(3-4), 163-185, 10.1016/s0377-8398(01)00040-8.

Bopp, L., Aumont, O., Cadule, P., Alvain, S., and Gehlen, M. (2005), *Response of diatoms distribution to global warming and potential implications: A global model study*, *Geophys. Res. Lett.*, *32*(19), L19606, 10.1029/2005gl023653.

Boyd, P. W., and Stevens, C. L. (2002), *Modelling particle transformations and the downward organic carbon flux in the NE Atlantic Ocean*, *Progress In Oceanography, 52*(1), 1-29, 10.1016/S0079-6611(02)00020-4: 10.1016/S0079-6611(02)00020-4.

Boyd, P. W., Jickells, T., Law, C. S., Blain, S., Boyle, E. A., Buesseler, K. O., Coale, K. H., Cullen, J. J., de Baar, H. J. W., Follows, M., Harvey, M., Lancelot, C., Levasseur, M., Owens, N. P. J., Pollard, R., Rivkin, R. B., Sarmiento, J., Schoemann, V., Smetacek, V., Takeda, S., Tsuda, A., Turner, S., and Watson, A. J. (2007), *Mesoscale Iron Enrichment Experiments 1993-2005: Synthesis and Future Directions*, *Science*, *315*(5812), 612-617, 10.1126/science.1131669.

Boyd, P. W., and Trull, T. W. (2007), *Understanding the export of biogenic particles in oceanic waters: Is there consensus?*, *Progress In Oceanography, 72*(4), 276-312, 10.1016/j.pocean.2006.10.007: 10.1016/j.pocean.2006.10.007.

Broecker, W. S. (1982), *Ocean chemistry during glacial time*, *Geochimica Et Cosmochimica Acta*, *46*(10), 1689-1705

Broerse, A. T. C., Ziveri, P., van Hinte, J. E., and Honjo, S. (2000), *Coccolithophore export production, species composition, and coccolith-CaCO3 fluxes in the NE Atlantic (34°,21°W and 48°N,21°W)*, *Deep Sea Research Part II: Topical Studies in Oceanography*, *47*(9-11), 1877-1905, 10.1016/s0967-0645(00)00010-2.

Brown, C., and Yoder, J. A. (1994), *Coccolithophorid blooms in the global ocean*, *Geophysical Research Letters*, *99*(C4), 7467-7482

Brown, E., Colling, A., Parkes, D., Phillips, P., Rothery, D., and Wright, J. (2001), *Ocean Circuation*, The Open University, Oxford.

Brzezinski, M., Alldredge, A. L., and O'Bryan, L. (1997), *Silica cycling within marine snow*, *Limnol. Oceanogr.*, *42*(8)

Brzezinski, M. A. (1985), *The Si:C ratio of marine diatoms: Interspecific variability and the effect of some environmental variables*, *Journal of Phycology*, *21*, 347-357

Buesseler, K. O., Bacon, M. P., Kirk Cochran, J., and Livingston, H. D. (1993), *Carbon and nitrogen export during the JGOFS North Atlantic Bloom experiment estimated from ^{234}Th: ^{238}U disequilibria*, *Deep Sea Research Part A. Oceanographic Research Papers, 39*(7-8), 1115-1137, 10.1016/0198-0149(92)90060-7: 10.1016/0198-0149(92)90060-7.

Buesseler, K. O. (1998), *The decoupling of production and particulate export in the surface ocean*, *Global Biogeochemical Cycles*, *12*(2), 297-310

Buesseler, K. O., Steinberg, D. K., Michaels, A. F., Johnson, R. J., Andrews, J. E., Valdes, J. R., and Price, J. F. (2000), *A comparison of the quantity and composition of material caught in a neutrally buoyant versus surface-tethered sediment trap*, *Deep Sea Research Part I: Oceanographic Research Papers, 47*(2), 277-294, 10.1016/s0967-0637(99)00056-4: 10.1016/s0967-0637(99)00056-4.

Buesseler, K. O., Antia, A. N., Chen, M., Fowler, S. W., Gardner, W. D., Gustafsson, O., Harada, K., Michaels, A. F., Van der Loeff, M. R., Sarin, M., Steinberg, D., and Trull, T.

(2007a), *An assessment of the use of sediment traps for estimating upper ocean particle fluxes*, *Journal of Marine Research*, *65*, 345-416

Buesseler, K. O., Lamborg, C. H., Boyd, P. W., Lam, P. J., Trull, T. W., Bidigare, R. R., Bishop, J. K. B., Casciotti, K. L., Dehairs, F., Elskens, M., Honda, M., Karl, D. M., Siegel, D. A., Silver, M. W., Steinberg, D. K., Valdes, J., Van Mooy, B., and Wilson, S. (2007b), *Revisiting Carbon Flux Through the Ocean's Twilight Zone*, *Science, 316*(5824), 567-570, 10.1126/science.1137959: 10.1126/science.1137959.

Buesseler, K. O., Trull, T. W., Steinber, D. K., Silver, M. W., Siegel, D. A., Saitoh, S. I., Lamborg, C. H., Lam, P. J., Karl, D. M., Jiao, N. Z., Honda, M. C., Elskens, M., Dehairs, F., Brown, S. L., Boyd, P. W., Bishop, J. K. B., and Bidigare, R. R. (2008), *VERTIGO (VERtical Transport in the Global Ocean): A study of particle sources and flux attenuation in the North Pacific*, *Deep-Sea Research Part II-Topical Studies in Oceanography*, *55*(14-15), 1522-1539, DOI 10.1016/j.dsr2.2008.04.024.

Buesseler, K. O., and Boyd, P. W. (2009), *Shedding light on processes that control particle export and flux attenuation in the twilight zone of the open ocean*, *Limnol. Oceanogr.*, *54*(4), 1210-1230

Burd, A. B., and Jackson, G. A. (2009), *Particle Aggregation*, *Annual Review of Marine Science*, *1*, 65-90, 10.1146/annurev.marine.010908.163904.

Butler, M., and Dam, H. G. (1994), *Production-Rates and Characteristics of Fecal Pellets of the Copepod Acartia-Tonsa under Simulated Phytoplankton Bloom Conditions - Implications for Vertical Fluxes*, *Marine Ecology-Progress Series*, *114*(1-2), 81-91

Cai, P., Rutgers van der Loeff, M., Stimac, I., Nöthig, E. M., Lepore, K., and Moran, S. B. (2010), *Low export flux of particulate organic carbon in the central Arctic Ocean as revealed by 234Th:238U disequilibrium*, *J. Geophys. Res.*, *115*(C10), C10037, 10.1029/2009jc005595.

Carmack, E., and Wassmann, P. (2006), *Food webs and physical–biological coupling on pan-Arctic shelves: Unifying concepts and comprehensive perspectives*, *Progress In Oceanography*, *71*(2-4), 446-477, 10.1016/j.pocean.2006.10.004.

Carmelo, T. R. (1997), *Identifying Marine Phytoplankton*, ix-x pp., Academic Press, San Diego.

Charalampopoulou, A., Poulton, A. J., Tyrrell, T., and Lucas, M. I. (2011), *Irradiance and pH affect coccolithophore community composition on a transect between the North Sea and the Arctic Ocean*, *Marine Ecology Progress Series*, *431*, 25-43, 10.3354/meps09140.

Cho, B. C., and Azam, F. (1988), *Major role of bacteria in biogeochemical fluxes in the ocean's interior*, *Nature*, *332*(6163), 441-443

Christian, J. R., Lewis, M. R., and Karl, D. M. (1997), *Vertical fluxes of carbon, nitrogen, and phosphorus in the North Pacific Subtropical Gyre near Hawaii*, *J. Geophys. Res.*, *102*(C7), 15667-15677, 10.1029/97jc00369.

Clarke, A., Quetin, L. B., and Ross, R. M. (1988), *Laboratory and field estimates of the rate of faecal pellet production by Antarctic krill, Euphausia superba*, *Marine Biology*, *98*(4), 557-563, 10.1007/bf00391547.

Clarke, K. R., and Gorley, R. N. (2006), *PRIMER v6: User Manual/Tutorial.*, PRIMER-E, Plymouth.

Cochran, W. G. (1977), *Sampling techniques*, Third ed., New York.

Conover, R. J. (1966), *Factors Affecting the Assimilation of Organic Matter by Zooplankton and the Question of Superfluous Feeding*, *Limnol. Oceanogr.*, *11*(3), 346-354, 10.1029/2004jc002757.

Cottier, F., Tverberg, V., Inall, M., Svendsen, H., Nilsen, F., and Griffiths, C. (2005), *Water mass modification in an Arctic fjord through cross-shelf exchange: The seasonal hydrography of Kongsfjorden, Svalbard*, *Journal of Geophysical Research-Oceans*, *110*(C12), Artn C12005
Doi 10.1029/2004jc002757.

Dam, H. G., Zhang, X., Butler, M., and Roman, M. R. (1995), *Mesozooplankton grazing and metabolism at the equator in the central Pacific: Implications for carbon and nitrogen fluxes*, *Deep Sea Research Part II: Topical Studies in Oceanography, 42*(2-3), 735-756, 10.1016/0967-0645(95)00036-P: 10.1016/0967-0645(95)00036-P.

De La Rocha, C. L., and Passow, U. (2007), *Factors influencing the sinking of POC and the efficiency of the biological carbon pump*, *Deep-Sea Research Part II-Topical Studies in Oceanography, 54*(5-7), 639-658, 10.1016/j.dsr2.2007.01.004: 10.1016/j.dsr2.2007.01.004.

Denny, M. (1993), *Air and Water. The Physics and Biology of Life's Media*, Princeton University Press.

Deuser, W. G., and Ross, E. H. (1980), *Seasonal change in the flux of organic carbon to the deep Sargasso Sea*, *Nature*, *283*(5745), 364-365

Dietrich, W. E. (1982), *Settling velocity of natural particles*, *Water Resources Research*, *18*(6), 1615 - 1626

Dilling, L., Wilson, J., Steinberg, D., and Alldredge, A. (1998), *Feeding by the euphausiid Euphausia pacifica and the copepod Calanus pacificus on marine snow*, *Marine Ecology Progress Series*, *170*, 189-201, 10.3354/meps170189.

Doney, S. C., Ruckelshaus, M., Emmett Duffy, J., Barry, J. P., Chan, F., English, C. A., Galindo, H. M., Grebmeier, J. M., Hollowed, A. B., Knowlton, N., Polovina, J., Rabalais, N. N., and Sydeman, W. J. (2011), *Climate change impacts on marine ecosystems*, *Annual Review of Marine Science*, *4*, 11 - 37, 10.1146/annurev-marine-041911-111611.

Duce, R. A., Liss, P. S., Merrill, J. T., Atlas, E. L., Buat-Menard, P., Hicks, B. B., Miller, J. M., Prospero, J. M., Arimoto, R., Church, T. M., Ellis, W., Galloway, J. N., Hansen, L., Jickells, T. D., Knap, A. H., Reinhardt, K. H., Schneider, B., Soudine, A., Tokos, J. J., Tsunogai, S., Wollast, R., and Zhou, M. (1991), *The atmospheric input of trace species to the world ocean*, *Global Biogeochem. Cycles*, *5*(3), 193-259, 10.1029/91gb01778.

Ducklow, H., Kirchman, D. L., and Rowe, G. T. (1982), *Production and vertical flux of attached bacteria in the hudson river plume of the new york bight as studied with floating sediment traps.*, *Applied and Environmental Microbiology 43*, 769-776

Ducklow, H., Steinberg, D., and Buesseler, K. O. (2001), *Upper Ocean Carbon Export and the Biological Pump*, *Oceanography*, *14*(4), 50 - 58

Dugdale, R. C., and Goering, J. J. (1967), *Uptake of New and Regenerated Forms of Nitrogen in Primary Productivity*, *Limnol. Oceanogr.*, *12*(2), 196-206

Dumont, E., and Sherwin, T. (2008), SAMS CTD data processing protocol, Issue 1, Scottish Association for Marine Science, Oban, Argyll.

Ebersbach, E., and Trull, T. (2008), *Sinking particle properties from polyacrylamide gels during the KErguelen Ocean and Plateau compared Study (KEOPS): Zooplankton control of carbon export in an area of persistent natural iron inputs in the Southern Ocean*, *Limnol. Oceanogr.*, *51*(1), 212-224

Egge, J. K., and Aksnes, D. L. (1992), *Silicate as Regulating Nutrient in Phytoplankton Competition*, *Marine Ecology-Progress Series*, *83*(2-3), 281-289

Eppley, R. W., Rogers, J. N., and McCarthy, J. J. (1969), *Half saturation constant for uptake of nitrate and ammonium by marine phytoplankton*, *Limnol. Oceanogr.*, *14*, 912-920

Eppley, R. W., and Peterson, B. J. (1979), *Particulate organic matter flux and planktonic new production in the deep ocean*, *Nature, 282*(5740), 677-680, 10.1038/282677a0: 10.1038/282677a0.

EuroSITES DYFAMED 2005 / 2005 Temperature data http://www.eurosites.info/dyfamed/2005/index.php 07th March

Falkowski, P. G., Barber, R. T., and Smetacek, V. (1998), *Biogeochemical Controls and Feedbacks on Ocean Primary Production*, *Science*, *281*(5374), 200-206, 10.1126/science.281.5374.200.

Falkowski, P. G., Laws, E. A., R.T., B., and Maurray, J. W. (2003), *Phytoplankton and their role in primary, new and export production*, in *Ocean Biogeochemistry*, edited by M. J. R. Fasham, Springer, New York.

Fasham, M. J. R., Ducklow, H., and McKelvie, S. M. (1990), *A nitrogen-based model of plankton dynamics in the ocean mixed layer*, *Journal of Marine Research*, *48*, 591-639

Frada, M., Young, J., Cachao, M., Lino, S., Martins, A., NArciso, A., Probert, I., and de Vargas, C. (2010), *A guide to extant coccolithophores (Calcihaptophycidae, Haptophyta) using light microscopy*, *Journal of Nannoplankton Research*, *32*(2), 58-122

Francois, R., Honjo, S., Krishfield, R., and Manganini, S. (2002), *Factors controlling the flux of organic carbon to the bathypelagic zone of the ocean*, *Global Biogeochem. Cycles, 16*, 10.1029/2001GB001722: 10.1029/2001GB001722.

Friedli, H., Lotscher, H., Oeschger, H., Siegenthaler, U., and Stauffer, B. (1986), *Ice core record of the 13C/12C ratio of atmospheric CO2 in the past two centuries*, *Nature*, *324*(6094), 237-238

Galassi, M., Davies, J., Theiler, J., Gough, B., Jungman, G., Alken, P., Booth, M., and Rossi, F. (2009), *GNU Scientific Library Reference Manual (v1.12)*, Third Edition ed., GNU Scientific Library.

Gardes, A., Iversen, M. H., Grossart, H.-P., Passow, U., and Ullrich, M. S. (2011), *Diatom-associated bacteria are required for aggregation of Thalassiosira weissflogii*, *ISME J*, *5*(3), 436-445 http://www.nature.com/ismej/journal/v5/n3/suppinfo/ismej2010145s1.html.

Glud, R. N., Rysgaard, S., and Kühl, M. (2002), *A laboratory study on O2 dynamics and photosynthesis in ice algal communities: quantification by microsensors, O2 exchange rates, 14C incubations and a PAM fluorometer*, *Aquatic Microbial Ecology*, *27*(3), 301-311, 10.3354/ame027301.

Goldthwait, S., Yen, J., Brown, J., and Alldredge, A. (2004), *Quantification of marine snow fragmentation by swimming euphausiids*, *Limnol. Oceanogr.*, *49*(4), 940-952

Gordon, D. C. (1970), *A microscopic study of organic particles in the North Atlantic ocean*, *Deep Sea Research and Oceanographic Abstracts*, *17*(1), 175-185, 10.1016/0011-7471(70)90096-3.

Gosselin, M., Levasseur, M., Wheeler, P. A., Horner, R. A., and Booth, B. C. (1997), *New measurements of phytoplankton and ice algal production in the Arctic Ocean*, *Deep Sea Research Part II: Topical Studies in Oceanography*, *44*(8), 1623-1644, 10.1016/s0967-0645(97)00054-4.

Gradinger, R. (1995), *Climate Change and Biological Oceanography of the Arctic Ocean*, *Philosophical Transactions of the Royal Society of London. Series A: Physical and Engineering Sciences*, *352*(1699), 277-286, 10.1098/rsta.1995.0070.

Gregory, J. (1997), *The density of particle aggregates*, *Water Science and Technology*, *36*(4), 1-13, 10.1016/s0273-1223(97)00452-6.

Guieu, C., Roy-Barman, M., Leblond, N., Jeandel, C., Souhaut, M., Le Cann, B., Dufour, A., and Bournot, C. (2005), *Vertical particle flux in the northeast Atlantic Ocean (POMME experiment)*, *J. Geophys. Res., 110*(C7), C07S18, 10.1029/2004jc002672: 10.1029/2004jc002672.

Hamm, C. E. (2002), *Interactive aggregation and sedimentation of diatoms and clay sized lithogenic material*, *Limnol. Oceanogr.*, *47*(6), 1790-1795

Harris, R. P., Wiebe, P. H., Lenz, J., Skjoldal, H. R., and Huntley, M. (Eds.) (2000), *Zooplankton Methodology Manual*, Academic Press, London.

Hayward, T. L. (1991), *Primary Production in the North Pacific Central Gyre - a Controversy with Important Implications*, *Trends in Ecology & Evolution*, *6*(9), 281-284

Hegseth, E. N., and Sundfjord, A. (2008), *Intrusion and blooming of Atlantic phytoplankton species in the high Arctic*, *Journal of Marine Systems*, *74*(1–2), 108–119, DOI 10.1016/j.jmarsys.2007.11.011.

Henson, S., R., S., and Madsen, E. (2012), *Global patterns in efficiency of particle organic carbon export and transfer to the deep ocean*, *Global Biogeochemical Cycles*, *26*(1), 10.1029/2011GB004099.

Henson, S. A., Dunne, J. P., and Sarmiento, J. L. (2009), *Decadal variability in North Atlantic phytoplankton blooms*, *J. Geophys. Res.*, *114*(C4), C04013, 10.1029/2008jc005139.

Henson, S. A., Sanders, R., Madsen, E., Morris, P. J., Le Moigne, F., and Quartly, G. D. (2011), *A reduced estimate of the strength of the ocean's biological carbon pump*, *Geophys. Res. Lett.*, *38*(4), L04606, 10.1029/2011gl046735.

Heywood, J. L., Zubkov, M. V., Tarran, G. A., Fuchs, B. M., and Holligan, P. M. (2006), *Prokaryoplankton standing stocks in oligotrophic gyre and equatorial provinces of the Atlantic Ocean: Evaluation of inter-annual variability*, *Deep Sea Research Part II: Topical Studies in Oceanography*, *53*(14–16), 1530–1547, 10.1016/j.dsr2.2006.05.005.

Holligan, P. M., Groom, S. B., and Harbour, D. S. (1993), *What controls the distribution of the coccolithophore, Emiliania huxleyi, in the North Sea?*, *Fisheries Oceanography*, *2*(3–4), 175–183, 10.1111/j.1365–2419.1993.tb00133.x.

Honjo, S., and Manganini, S. J. (1993), *Annual biogenic particle fluxes to the interior of the North Atlantic Ocean; studied at 34°N 21°W and 48°N 21°W*, *Deep Sea Research Part II: Topical Studies in Oceanography*, *40*(1–2), 587–607, 10.1016/0967–0645(93)90034–k.

Howard, M. T., Winguth, A. M. E., Klaas, C., and Maier-Reimer, E. (2006), *Sensitivity of ocean carbon tracer distributions to particulate organic flux parameterizations*, *Global Biogeochem. Cycles*, *20*(3), GB3011, 10.1029/2005gb002499.

Huskin, I., Anadón, R., Álvarez-Marqués, F., and Harris, R. P. (2000), *Ingestion, faecal pellet and egg production rates of Calanus helgolandicus feeding coccolithophorid versus non-coccolithophorid diets*, *Journal of Experimental Marine Biology and Ecology*, *248*(2), 239–254, 10.1016/s0022–0981(00)00167–2.

IPCC (2007), Climate Change 2007: The Physical Science Basis.

Iversen, M. H., and Poulsen, L. K. (2007), *Coprorhexy, coprophagy, and coprochaly in the copepods Calanus helgolandicus, Pseudocalanus elongatus, and Oithona similis*, *Marine Ecology Progress Series*, *350*, 79–89, 10.3354/meps07095.

Jackson, G. A., and Burd, A. B. (1998), *Aggregation in the marine environment*, *Environmental Science & Technology*, *32*(19), 2805–2814

Jenkins, W. J. (1982), *Oxygen utilization rates in North Atlantic subtropical gyre and primary production in oligotrophic systems*, *Nature*, *300*(5889), 246–248

Jenkins, W. J., and Goldman, J. C. (1985), *Seasonal Oxygen Cycling and Primary Production in the Sargasso Sea*, *Journal of Marine Research*, *43*(2), 465-491

Jiang, Q., and Logan, B. E. (1991), *Fractal dimensions of aggregates determined from steady-state size distributions*, *Environmental Science & Technology*, *25*(12), 2031-2038, 10.1021/es00024a007.

Johnson, C. P., Li, X., and Logan, B. E. (1996), *Settling Velocities of Fractal Aggregates*, *Environmental Science & Technology*, *30*(6), 1911-1918, 10.1021/es950604g.

Kajihara, M. (1971), *Settling velocity and porosity of large suspended particle*, *Journal of Oceanography*, *27*(4), 158-162, 10.1007/bf02109135.

Tables of Physical and Chemical Constants (16th edition 1995), 2.7.9 Physical properties of sea water, Version 1.0 (2005), www.kayelaby.npl.co.uk.

Kiorboe, T. (2000), *Colonization of Marine Snow Aggregates by Invertebrate Zooplankton: Abundance, Scaling, and Possible Role*, *Limnol. Oceanogr., 45*(2), 479-484, 10.4319/lo.2000.45.2.0479: 10.4319/lo.2000.45.2.0479.

Kiorboe, T. (2001), *Formation and fate of marine snow: small-scale processes with large-scale implications*, *Sci. Mar.*, *65*, 57-71

Kiørboe, T., Andersen, K. P., and Dam, H. G. (1990), *Coagulation efficiency and aggregate formation in marine phytoplankton*, *Marine Biology*, *107*(2), 235-245, 10.1007/bf01319822.

Klaas, C., and Archer, D. (2002), *Association of sinking organic matter with various types of mineral ballast in the deep sea: Implications for the rain ratio*, *Biogeochemical Cycles, 16*(4), 1116 - 1130, 10.1029/2001GB001765: 10.1029/2001GB001765.

Klausmeier, C. A., Litchman, E., Daufresne, T., and Levin, S. A. (2004), *Optimal nitrogen-to-phosphorus stoichiometry of phytoplankton*, *Nature*, *429*(6988), 171-174, http://www.nature.com/nature/journal/v429/n6988/suppinfo/nature02454_S1.html.

Koeve, W. (2002), *Upper ocean carbon fluxes in the Atlantic Ocean: The importance of the POC : PIC ratio*, *Global Biogeochemical Cycles*, *16*(4), 1056 10.1029/2001gb001836.

Kosobokova, K., and Hirche, H. J. (2000), *Zooplankton distribution across the Lomonosov Ridge, Arctic Ocean: species inventory, biomass and vertical structure*, *Deep-Sea Research Part I-Oceanographic Research Papers*, *47*(11), 2029-2060

Kovala, P. E., and Larrance, J. D. (1966), Computation of phytoplankton cell numbers, cell volume, cell surface and plasma volume perlitre from microscopical counts, Office of Naval Research, Seattle, Washington, USA.

Kriest, I., and Evans, G. T. (1999), *Representing phytoplankton aggregates in biogeochemical models*, *Deep Sea Research Part I: Oceanographic Research Papers, 46*(11), 1841-1859, 10.1016/s0967-0637(99)00032-1: 10.1016/s0967-0637(99)00032-1.

Kuwata, A., and Takahashi, M. (1999), *Survival and recovery of resting spores and resting cells of the marine planktonic diatom Chaetoceros pseudocurvisetus under fluctuating nitrate conditions*, *Marine Biology*, *134*(3), 471-478

Kwon, E. Y., Primeau, F., and Sarmiento, J. L. (2009), *The impact of remineralization depth on the air-sea carbon balance*, *Nature Geosci, 2*(9), 630-635, 10.1038/ngeo612: 10.1038/ngeo612.

Lalande, C., Belanger, S., and Fortier, L. (2009), *Impact of a decreasing sea ice cover on the vertical export of particulate organic carbon in the northern Laptev Sea, Siberian Arctic Ocean*, *Geophysical Research Letters*, *36*

Lalande, C., Bauerfeind, E., and Nöthig, E. M. (2011), *Downward particulate organic carbon export at high temporal resolution in the eastern Fram Strait: influence of Atlantic Water on flux composition*, *Marine Ecology Progress Series*, *440*, 127-136, 10.3354/meps09385.

Lampitt, R. S. (1985), *Evidence for the seasonal deposition of detritus to the deep-sea floor and its subsequent resuspension*, *Deep Sea Research Part A. Oceanographic Research Papers*, *32*(8), 885-897, 10.1016/0198-0149(85)90034-2.

Lampitt, R. S. (1992), *The contribution of deep-sea macroplankton to organic remineralization: results from sediment trap and zooplankton studies over the Madeira Abyssal Plain*, *Deep Sea Research Part A. Oceanographic Research Papers*, *39*(2), 221-233, 10.1016/0198-0149(92)90106-4.

Lampitt, R. S., Wishner, K. F., Turley, C. M., and Angel, M. V. (1993), *Marine snow studies in the Northeast Atlantic Ocean: distribution, composition and role as a food source for migrating plankton*, *Marine Biology, 116*(4), 689-702, 10.1007/BF00355486: 10.1007/BF00355486.

Lampitt, R. S., Boorman, B., Brown, L., Lucas, M., Salter, I., Sanders, R., Saw, K., Seeyave, S., Thomalla, S. J., and Turnewitsch, R. (2008), *Particle export from the euphotic zone: Estimates using a novel drifting sediment trap, ^{234}Th and new production*, *Deep Sea Research Part I: Oceanographic Research Papers, 55*(11), 1484-1502, 10.1016/j.dsr.2008.07.002: 10.1016/j.dsr.2008.07.002.

Lampitt, R. S., Salter, I., and Johns, D. (2009), *Radiolaria: Major exporters of organic carbon to the deep ocean*, *Global Biogeochem. Cycles, 23*, 10.1029/2008gb003221: 10.1029/2008gb003221.

Lampitt, R. S., Salter, I., de Cuevas, B. A., Hartman, S., Larkin, K. E., and Pebody, C. A. (2010), *Long-term variability of downward particle flux in the deep northeast Atlantic: Causes and trends*, *Deep Sea Research Part II: Topical Studies in Oceanography, 57*(15), 1346-1361, 10.1016/j.dsr2.2010.01.01: 10.1016/j.dsr2.2010.01.01.

Lawrence, M. M. (1994), *Surface area control of organic carbon accumulation in continental shelf sediments*, *Geochimica Et Cosmochimica Acta*, *58*(4), 1271-1284, 10.1016/0016-7037(94)90381-6.

Laws, E. A., Falkowski, P. G., Smith, W. O., Jr., Ducklow, H., and McCarthy, J. J. (2000), *Temperature effects on export production in the open ocean*, *Global Biogeochem. Cycles*, *14*(4), 1231-1246, DOI: 10.1029/1999gb001229.

Leblanc, K., Hare, C. E., Feng, Y., Berg, G. M., DiTullio, G. R., Neeley, A., Benner, I., Sprengel, C., Beck, A., Sanudo-Wilhelmy, S. A., Passow, U., Klinck, K., Rowe, J. M., Wilhelm, S. W., Brown, C. W., and Hutchins, D. A. (2009), *Distribution of calcifying and silicifying phytoplankton in relation to environmental and biogeochemical parameters during the late stages of the 2005*, *Biogeosciences*, *6*(10), 2155 - 2179, DOI: 10.5194/bg-6-2155-2009.

Lee, C., Peterson, M. L., Wakeham, S. G., Armstrong, R. A., Cochran, J. K., Miquel, J. C., Fowler, S. W., Hirschberg, D., Beck, A., and Xue, J. (2009), *Particulate organic matter and ballast fluxes measured using time-series and settling velocity sediment traps in the northwestern Mediterranean Sea*, *Deep Sea Research Part II: Topical Studies in Oceanography,* *56*(18), 1420-1436, 10.1016/j.dsr2.2008.11.029: 10.1016/j.dsr2.2008.11.029.

Lenz, J., Morales, A., and Gunkel, J. (1993), *Mesozooplankton Standing Stock during the North-Atlantic Spring Bloom Study in 1989 and Its Potential Grazing Pressure on Phytoplankton - a Comparison between Low, Medium and High-Latitudes*, *Deep-Sea Research Part Ii-Topical Studies in Oceanography*, *40*(1-2), 559-572

Li, X.-Y., and Logan, B. E. (2001), *Permeability of Fractal Aggregates*, *Water Res*, *35*(14), 3373-3380, 10.1016/s0043-1354(01)00061-6.

Li, X. Y., and Logan, B. E. (1997), *Collision frequencies of fractal aggregates with small particles by differential sedimentation*, *Environmental Science & Technology*, *31*(4), 1229-1236

Lignell, R., Heiskanen, A. S., Kuosa, H., Gundersen, K., Kuuppoleinikki, P., Pajuniemi, R., and Uitto, A. (1993), *Fate of a Phytoplankton Spring Bloom - Sedimentation and Carbon Flow in the Planktonic Food Web in the Northern Baltic*, *Marine Ecology-Progress Series*, *94*(3), 239-252

Logan, B. E., and Hunt, J. R. (1987), *Advantages to Microbes of Growth in Permeable Aggregates in Marine Systems*, *Limnol. Oceanogr.*, *32*(5), 1034-1048

Logan, B. E., and Wilkinson, D. B. (1990), *Fractal geometry of marine snow and other biological aggregates*, *Limnol. Oceanogr.*, *35*(1), 130-136, citeulike-article-id:906708.

Lowenstam, H. A., and Weiner, S. (1989), *On biomineralization*, ix, 324 p. pp., Oxford University Press, New York.

Lundsgaard, C. (1995), *Use of a high viscosity medium in studies of aggregates*, in *Sediment trap studies in the Nordic countries 3. Proceeding of the Symposium on Seasonal Dynamics of Planktonic Ecosystems and Sedimentation in Coastal Nordic Waters.*, edited by S. Floderus, Heiksakanen, A.-S., Oleson, M. and Wassmann, P., pp. 141-152, Helsing, Denmark.

Mann, K. H., and Lazier, J. R. N. (1996), *Dynamics of Marine Ecosystems, biological-physical interactions in the oceans*, 2nd ed., Blackwell Science.

Martin, J. H., Knauer, G. A., Karl, D. M., and Broenkow, W. W. (1987), *VERTEX: carbon cycling in the northeast Pacific*, *Deep Sea Research Part A. Oceanographic Research Papers,* *34*(2), 267-285, 10.1016/0198-0149(87)90086-0: 10.1016/0198-0149(87)90086-0.

Martin, P., Allen, J. T., Cooper, M. J., Johns, D. G., Lampitt, R. S., Sanders, R., and Teagle, D. A. H. (2010), *Sedimentation of acantharian cysts in the Iceland Basin: Strontium as a ballast for deep ocean particle flux, and implications for acantharian reproductive strategies*, *Limnol. Oceanogr.*, *55*(2), 604 - 614, 10.4319/lo.2010.55.2.0604: 10.4319/lo.2010.55.2.0604.

Marty, J.-C., Chiavérini, J., Pizay, M.-D., and Avril, B. (2002), *Seasonal and interannual dynamics of nutrients and phytoplankton pigments in the western Mediterranean Sea at the DYFAMED time-series station (1991-1999)*, *Deep Sea Research Part II: Topical Studies in Oceanography*, *49*(11), 1965-1985, 10.1016/s0967-0645(02)00022-x.

McCave, I. N. (1975), *Vertical flux of particles in the ocean*, *Deep Sea Research and Oceanographic Abstracts*, *22*(7), 491-502

Meakin, P. (1987), *Fractal aggregates*, *Advances in Colloid and Interface Science*, *28*(0), 249-331, 10.1016/0001-8686(87)80016-7.

Menden-Deuer, S., Lessard, E. J., and Satterberg, J. (2001), *Effect of preservation on dinoflagellate and diatom cell volume and consequences for carbon biomass predictions*, *Marine Ecology Progress Series*, *222*, 41-50, 10.3354/meps222041.

Michaels, A. F., and Silver, M. W. (1988), *Primary production, sinking fluxes and the microbial food web*, *Deep Sea Research Part A. Oceanographic Research Papers*, *35*(4), 473-490

Millero, F. J., and Huang, F. (2010), *The density of seawater as a function of salinity (5 to 70 g kg(-1)) and temperature (273.15 to 363.15 K) (vol 5, pg 91, 2009)*, *Ocean Sci*, *6*(1), 379-379

Montagnes, D. J. S., and Franklin, D. J. (2001), *Effect of temperature on diatom volume, growth rate, and carbon and nitrogen content: Reconsidering some paradigms*, *Limnol. Oceanogr.*, *46*(8), 2008-2018

Moore, C. M., Mills, M. M., Langlois, R., Milne, A., Achterberg, E. P., La Roche, J., and Geider, R. J. (2008), *Relative influence of nitrogen and phosphorous availability on phytoplankton physiology and productivity in the oligotrophic sub-tropical North Atlantic Limnol. Oceanogr.*, *53*(1), 291-305

Mullin, M. M. (1965), *Size Fractionation of Particulate Organic Carbon in the Surface Waters of the Western Indian Ocean*, *Limnol. Oceanogr.*, *10*(3), 459-462

Neftel, A., Moor, E., Oeschger, H., and Stauffer, B. (1985), *Evidence from polar ice cores for the increase in atmospheric CO2 in the past two centuries*, *Nature*, *315*(6014), 45-47

Nelson, D. M., and Brzezinski, M. A. (1990), *Kinetics of Silicic-Acid Uptake by Natural Diatom Assemblages in 2 Gulf-Stream Warm-Core Rings*, *Marine Ecology-Progress Series*, *62*(3), 283-292

Niebauer, H. J. (1991), *Bio-physical oceanographic interactions at the edge of the Arctic ice pack*, *Journal of Marine Systems*, *2*(1-2), 209-232, 10.1016/0924-7963(91)90025-p.

Noji, T. T., Rey, F., Miller, L. A., Yngve Børsheim, K., and Urban-Rich, J. (1999), *Fate of biogenic carbon in the upper 200 m of the central Greenland Sea*, *Deep Sea Research Part II: Topical Studies in Oceanography*, *46*(6-7), 1497-1509

Nowald, N., Fischer, G., Ratmeyer, V., Iversen, M., Reuter, C., and Wefer, G. (2009), *In-situ sinking speed measurements of marine snow aggregates acquired with a settling chamber mounted to the Cherokee ROV*, *Oceans 2009-Europe (Oceans)*, 6 pp., 10.1109/oceanse.2009.5278186: 10.1109/oceanse.2009.5278186.

Olli, K., Wexels Riser, C., Wassmann, P., Ratkova, T., Arashkevich, E., and Pasternak, A. (2002), *Seasonal variation in vertical flux of biogenic matter in the marginal ice zone and the central Barents Sea*, *Journal of Marine Systems*, *38*(1-2), 189-204, 10.1016/s0924-7963(02)00177-x.

Olli, K., Wassmann, P., Reigstad, M., Ratkova, T. N., Arashkevich, E., Pasternak, A., Matrai, P. A., Knulst, J., Tranvik, L., Klais, R., and Jacobsen, A. (2007), *The fate of production in the central Arctic Ocean - top-down regulation by zooplankton expatriates?*, *Progress In Oceanography*, *72*(1), 84-113, 10.1016/j.pocean.2006.08.002.

Paasche, E., and Brubak, S. (1994), *Enhanced calcification in the coccolithophorid Emiliania huxleyi (Haptophyceae) under phosphorus limitation*, *Phycologia*, *33*(5), 324-330, 10.2216/i0031-8884-33-5-324.1.

Painter, S. C. (2012), Schematic representation of the interconnectivity of the individual components constituting the biological carbon pump, edited.

Parekh, P., Dutkiewicz, S., Follows, M. J., and Ito, T. (2006), *Atmospheric carbon dioxide in a less dusty world*, *Geophys. Res. Lett.*, *33*(3), L03610, 10.1029/2005gl025098.

Passow, U. (1991), *Species-specific sedimentation and sinking velocities of diatoms*, *Marine Biology*, *108*(3), 449-455, 10.1007/bf01313655.

Passow, U., and Peinert, R. (1993), *The role of plankton in particle flux: two case studies from the northeast Atlantic*, *Deep Sea Research Part II: Topical Studies in Oceanography*, *40*(1-2), 573-585, 10.1016/0967-0645(93)90033-j.

Passow, U., Alldredge, A. L., and Logan, B. E. (1994), *The role of particulate carbohydrate exudates in the flocculation of diatom blooms*, *Deep Sea Research Part I: Oceanographic Research Papers*, *41*(2), 335-357, 10.1016/0967-0637(94)90007-8.

Passow, U., and Alldredge, A. L. (1995), *A Dye-Binding Assay for the Spectrophotometric Measurement of Transparent Exopolymer Particles (TEP)*, *Limnol. Oceanogr.*, *40*(7), 1326-1335

Passow, U., Shipe, R. F., Murray, A., Pak, D. K., Brzezinski, M. A., and Alldredge, A. L. (2001), *The origin of transparent exopolymer particles (TEP) and their role in the sedimentation of particulate matter*, *Continental Shelf Research, 21*(4), 327-346, 10.1016/S0278-4343(00)00101-1: 10.1016/S0278-4343(00)00101-1.

Passow, U. (2002), *Transparent exopolymer particles (TEP) in aquatic environments*, *Progress In Oceanography*, *55*(3-4), 287-333

Passow, U. (2004), *Switching perspectives: Do mineral fluxes determine particulate organic carbon fluxes or vice versa?*, *Geochem. Geophys. Geosyst., 5*(4), Q04002, 10.1029/2003gc000670: 10.1029/2003gc000670.

Passow, U., and De La Rocha, C. L. (2006), *Accumulation of mineral ballast on organic aggregates*, *Global Biogeochem. Cycles, 20*(1), GB1013, 10.1029/2005gb002579: 10.1029/2005gb002579.

Peters, G. P., Marland, G., Le Quere, C., Boden, T., Canadell, J. G., and Raupach, M. R. (2012), *Rapid growth in CO2 emissions after the 2008-2009 global financial crisis*, *Nature Clim. Change*, *2*(1), 2-4, http://www.nature.com/nclimate/journal/v2/n1/abs/nclimate1332.html#supplementary-information.

Peterson, M., Hernes, P. J., Thoreson, D. S., Hedges, J. I., Lee, C., and Wakeham, S. G. (1993), *Field Evaluation of a Valved Sediment Trap*, *Limnol. Oceanogr.*, *38*(8), 1741-1761

Peterson, M., Wakeham, S. G., Lee, C., Askea, M. A., and Miquel, J. C. (2005), *Novel techniques for collection of sinking particles in the ocean and determining their settling rates*, *Limnology and Oceanography: Methods, 3*, 520-532.

Pilskaln, C. H., and Honjo, S. (1987), *The Fecal Pellet fraction of biogeochemical particle fluxes to the deep sea*, *Global Biogeochem. Cycles*, *1*(1), 31-48, 10.1029/GB001i001p00031.

Ploug, H., Grossart, H.-P., Azam, F., and Jørgensen, B. B. (1999), *Photosynthesis, respiration, and carbon turnover in sinking marine snow from surface waters of Southern California Bight: implications for the carbon cycle in the ocean*, *Marine Ecology Progress Series*, *179*, 1-11, 10.3354/meps179001.

Pommier, J., Gosselin, M., and Michel, C. (2009), *Size-fractionated phytoplankton production and biomass during the decline of the northwest Atlantic spring bloom*, *Journal of Plankton Research*, *31*(4), 429-446, 10.1093/plankt/fbn127.

Popova, E. E., Yool, A., Coward, A. C., Aksenov, Y. K., Alderson, S. G., de Cuevas, B. A., and Anderson, T. R. (2010), *Control of primary production in the Arctic by nutrients and light: insights from a high resolution ocean general circulation model*, *Biogeosciences*, *7*(11), 3569-3591, DOI 10.5194/bg-7-3569-2010.

Poulton, A. J., Sanders, R., Holligan, P. M., Stinchcombe, M. C., Adey, T. R., Brown, L., and Chamberlain, K. (2006), *Phytoplankton mineralization in the tropical and subtropical Atlantic Ocean*, *Global Biogeochem. Cycles, 20*(4), GB4002, 10.1029/2006gb002712: 10.1029/2006gb002712.

Poulton, A. J., Mark Moore, C., Seeyave, S., Lucas, M. I., Fielding, S., and Ward, P. (2007), *Phytoplankton community composition around the Crozet Plateau, with emphasis on diatoms and Phaeocystis*, *Deep Sea Research Part II: Topical Studies in Oceanography*, *54*(18-20), 2085-2105, 10.1016/j.dsr2.2007.06.005.

Poulton, A. J., Charalampopoulou, A., Young, J. R., Tarran, G. A., Lucas, M. I., and Quartly, G. D. (2010), *Coccolithophore dynamics in non-bloom conditions during late*

summer in the central Iceland Basin (July-August 2007), *Limnol. Oceanogr.*, *55*(4), 1601-1613, 10.4319/lo.2010.55.4.1601.

Raitsos, D. E., Lavender, S. J., Pradhan, Y., Tyrrell, T., Reid, P. C., and Edwards, M. (2006), *Coccolithophore bloom size variation in response to the regional environment of the subarctic North Atlantic*, *Limnol. Oceanogr.*, *51*(5), 2122-2130

Redfield, A. C. (1934), *On the proportions of organic derivatives in sea water and their relation to the composition of plankton*, in *James Johnstone Memorial Volume*, edited by J. R. Daniel, pp. 176-192, Liverpool University Press.

Reigstad, M., Wexels Riser, C., Wassmann, P., and Ratkova, T. (2008), *Vertical export of particulate organic carbon: Attenuation, composition and loss rates in the northern Barents Sea*, *Deep Sea Research Part II: Topical Studies in Oceanography*, *55*(20-21), 2308-2319

Richardson, A. J., Walne, A. W., John, A. W. G., Jonas, T. D., Lindley, J. A., Sims, D. W., Stevens, D., and Witt, M. (2006), *Using continuous plankton recorder data*, *Progress In Oceanography*, *68*(1), 27-74, 10.1016/j.pocean.2005.09.011.

Riebesell, U., and Tortell, P. D. (2011), *Effects of ocean acidification on pelagic organisms and ecosystems*, in *Ocean acidification*, edited by G. J.P. and L., H., pp. 99 - 121, Oxford University Press, Oxford.

Riley, J. S., Sanders, R., Marsay, C., Le Moigne, F., Achterberg, E. P., and Poulton, A. (2012), *The relative contribution of fast and slow sinking particles to ocean carbon export*, *Global Biogeochemical Cycles*, 10.1029/2011GB004085.

Robinson, C., Steinberg, D. K., Anderson, T. R., Arístegui, J., Carlson, C. A., Frost, J. R., Ghiglione, J.-F., Hernández-León, S., Jackson, G. A., Koppelmann, R., Quéguiner, B., Ragueneau, O., Rassoulzadegan, F., Robison, B. H., Tamburini, C., Tanaka, T., Wishner, K. F., and Zhang, J. (2010), *Mesopelagic zone ecology and biogeochemistry - a synthesis*, *Deep Sea Research Part II: Topical Studies in Oceanography, 57*(16), 1504-1518, 10.1016/j.dsr2.2010.02.018: 10.1016/j.dsr2.2010.02.018.

Roman, M., Smith, S., Wishner, K., Zhang, X., and Gowing, M. (2000), *Mesozooplankton production and grazing in the Arabian Sea*, *Deep Sea Research Part II: Topical Studies in Oceanography, 47*(7-8), 1423-1450, 10.1016/S0967-0645(99)00149-6: 10.1016/S0967-0645(99)00149-6.

Rudels, B., Fahrbach, E., Meincke, J., Budeus, G., and Eriksson, P. (2002), *The East Greenland Current and its contribution to the Denmark Strait overflow*, *Ices Journal of Marine Science*, *59*(6), 1133-1154, DOI 10.1006/jmsc.2002.1284.

Sabine, C. L., Feely, R. A., and Gruber, N. (2004), *The Oceanic Sink for Anthropogenic CO2*, *Science*, *305*(5682), 367-371, 10.1126/science.1097403.

Sakshaug, E. (2004), *Primary and Secondary production in the Arctic Seas*, in *The Organic Carbon Cycle in the Arctic Ocean*, edited by R. Stein and Macdonald, R., pp. 57 - 81, Springer.

Salter, I., Kemp, A. E. S., Lampitt, R. S., and Gledhill, M. (2010), *The association between biogenic and inorganic minerals and the amino acid composition of settling particles*, *Limnol. Oceanogr.*, *55*(5), 2207-2218, 10.4319/lo.2010.55.5.2207.

Sanders, R., Brown, L., Henson, S., and Lucas, M. (2005), *New production in the Irminger Basin during 2002*, *Journal of Marine Systems*, *55*(3-4), 291-310, 10.1016/j.jmarsys.2004.09.002.

Sanders, R., Morris, P., Poulton, A. J., Stinchcombe, M. C., Charalampopoulou, A., Lucas, M. I., and Thomalla, S. J. (2010), *Does a ballast effect occur in the surface ocean?*, *Geophys. Res. Lett.*, *37*(8), L08602, 10.1029/2010gl042574: 10.1029/2010gl042574.

Sarimento, J. L. G., N. (2006), *Ocean Biogeochemical Dynamics*, 1 ed., 503 pp., Princeton University Press.

Sarin, M. M., Kim, G., and Church, T. M. (1999), *210Po and 210Pb in the South-equatorial Atlantic:: distribution and disequilibrium in the Upper 500 m*, *Deep Sea Research Part II: Topical Studies in Oceanography*, *46*(5), 907-917, 10.1016/s0967-0645(99)00008-9.

Sarmiento, J. L., Gruber, N., and Sundermann, J. (2006), *Ocean biogeochemical dynamics*, Princeton University Press, Princeton.

Scholten, J. C., Fietzke, J., Vogler, S., Rutgers van der Loeff, M. M., Mangini, A., Koeve, W., Waniek, J., Stoffers, P., Antia, A., and Kuss, J. (2001), *Trapping efficiencies of sediment traps from the deep Eastern North Atlantic:: the 230Th calibration*, *Deep Sea Research Part II: Topical Studies in Oceanography*, *48*(10), 2383-2408, 10.1016/s0967-0645(00)00176-4.

Schroder-Ritzrau, A., Andruliet, H., Jensen, S., Samtleben, C., Schafer, P., Matthiessen, J., Hass, H. C., Kohly, A., and Thiede, J. (2001), *Distribution, Export and Alteration of Fossilizable Plankotn in the Nordic Seas*, in *The Northern North Atlantic: A Changing Environment*, edited by P. Shafer, Schluter, M. and Thiede, J., pp. 81-104, Springer, Berlin.

Sheldon, R. W., Prakash, A., and Stucliffe, W. H., Jr. (1972), *The size distribution of particles in the ocean*, *Limnol. Oceanogr.*, *17*(3), 327 - 340

Sieracki, M. E., Verity, P. G., and Stoecker, D. K. (1993), *Plankton community response to sequential silicate and nitrate depletion during the 1989 North Atlantic spring bloom*, *Deep Sea Research Part II: Topical Studies in Oceanography, 40*(1-2), 213-225, 10.1016/0967-0645(93)90014-E: 10.1016/0967-0645(93)90014-E.

Sigman, D. M., and Boyle, E. A. (2000), *Glacial/interglacial variations in atmospheric carbon dioxide*, *Nature, 407*(6806), 859-869, 10.1038/35038000: 10.1038/35038000.

Silver, M. W., Shanks, A. L., and Trent, J. D. (1978), *Marine Snow: Microplankton Habitat and Source of Small-Scale Patchiness in Pelagic Populations*, *Science*, *201*(4353), 371-373, 10.1126/science.201.4353.371.

Smayda, T. J. (1971), *Normal and accelerated sinking of phytoplankton in the sea*, *Marine Geology*, *11*(2), 105-122

Smith, D. C., Simon, M., Alldredge, A. L., and Azam, F. (1992), *Intense hydrolytic enzyme activity on marine aggregates and implications for rapid particle dissolution*, *Nature, 359*(6391), 139-142, 10.1038/359139a0: 10.1038/359139a0.

Smyth, T. J., Tyrrell, T., and Tarrant, B. (2004), *Time series of coccolithophore activity in the Barents Sea, from twenty years of satellite imagery*, *Geophysical Research Letters*, *31*(11), Artn L11302
Doi 10.1029/2004gl019735.

Steinberg, D. K., Cope, J. S., Wilson, S. E., and Kobari, T. (2008a), *A comparison of mesopelagic mesozooplankton community structure in the subtropical and subarctic North Pacific Ocean*, *Deep-Sea Research Part Ii-Topical Studies in Oceanography*, *55*(14-15), 1615-1635, DOI 10.1016/j.dsr2.2008.04.025.

Steinberg, D. K., Van Mooy, B. A. S., Buesseler, K., Boyd, P., Kobari, T., and Karl, D. M. (2008b), *Bacterial vs. zooplankton control of sinking particle flux in the ocean's twilight zone*, *Limnol. Oceanogr., 53*(4), 1327 - 1338, 10.4319/lo.2008.53.4.1327: 10.4319/lo.2008.53.4.1327.

Steinhoff, T., Friedrich, T., Hartman, S. E., Oschlies, A., Wallace, D. W. R., and Kortzinger, A. (2010), *Estimating mixed layer nitrate in the North Atlantic Ocean*, *Biogeosciences, 7*(3), 795-807, 10.5194/bg-7-795-2010: 10.5194/bg-7-795-2010.

Stemmann, L., Gorsky, G., Marty, J.-C., Picheral, M., and Miquel, J.-C. (2002), *Four year study of large particle vertical distribution (0 - 1000 m) in the MW Mediterranean in relation to hydrology, phytoplankton, and vertical flux*, *Deep Sea Research II*, *49*, 2143 - 2162, 10.1016/S0967-0645(02)00032-2.

Stewart, G. M., Fowler, S. W., Teyssié, J.-L., Cotret, O., Cochran, J. K., and Fisher, N. S. (2005), *Contrasting transfer of polonium-210 and lead-210 across three trophic levels in marine plankton*, *Marine Ecology Progress Series*, *290*, 27-33, 10.3354/meps290027.

Stroeve, J., Serreze, M., Drobot, S., Gearheard, S., Holland, M., Maslanik, J., Meier, W., and Scambos, T. (2008), Arctic Sea Ice extent plummets in 2007, in *EOS Transactions*, edited.

Takahashi, K., and Be, A. W. H. (1984), *Planktonic foraminifera: factors controlling sinking speeds*, *Deep Sea Research Part A. Oceanographic Research Papers*, *31*(12), 1477-1500

Tamelander, T., Reigstad, M., Hop, H., and Ratkova, T. (2009), *Ice algal assemblages and vertical export of organic matter from sea ice in the Barents Sea and Nansen Basin (Arctic Ocean)*, *Polar Biology*, *32*(9), 1261-1273, 10.1007/s00300-009-0622-5.

Tans, P., and Keeling, R. NOAA/ESRL www.esrl.noaa.gov/gmd/ccgg/trends/ and www.scrippsco2.ucsd.edu/

Thomalla, S. J., Poulton, A. J., Sanders, R., Turnewitsch, R., Holligan, P. M., and Lucas, M. I. (2008), *Variable export fluxes and efficiencies for calcite, opal, and organic*

carbon in the Atlantic Ocean: A ballast effect in action?, *Global Biogeochemical Cycles, 22*(1), 10, Gb1010 10.1029/2007gb002982: Gb1010 10.1029/2007gb002982.

Trenberth, K. E., Jones, P. D., Ambenje, P., Bojariu, R., Easterling, D., Klein Tank, A., Parker, D., Rahimzadeh, F., Renwick, J. A., Rusticucci, M., Soden, B., and Zhai, P. (2007), *Observations: Surface and Atmospheric Climate Change.*, in *Climate Change 2007: The Physical Science Basis. Contribution of Working Group I to the Fourth Assessment Report of the Intergovernmental Panel on Climate Change*, edited by S. Solomon, Qin, D., Manning, M., Chen, Z., Marquis, M., Averyt, K. B., Tignor, M. and Miller, H. L., Cambridge University Press, Cambridge, UK.

Trull, T. W., Bray, S. G., Buesseler, K. O., Lamborg, C. H., Manganini, S., Moy, C., and Valdes, J. (2008), *In situ measurement of mesopelagic particle sinking rates and the control of carbon transfer to the ocean interior during the Vertical Flux in the Global Ocean (VERTIGO) voyages in the North Pacific*, *Deep Sea Research Part II: Topical Studies in Oceanography, 55*(14-15), 1684-1695, 10.1016/j.dsr2.2008.04.021: 10.1016/j.dsr2.2008.04.021.

Turner, J. T. (2002), *Zooplankton fecal pellets, marine snow and sinking phytoplankton blooms*, *Aquatic Microbial Ecology, 27*(1), 57-102, 10.3354/ame027057: 10.3354/ame027057.

Tyrrell, T. (1999), *The relative influences of nitrogen and phosphorus on oceanic primary production*, *Nature*, *400*(6744), 525-531

Uye, S.-i., and Kaname, K. (1994), *Relations between fecal pellet volume and body size for major zooplankters of the Inland Sea of Japan*, *Journal of Oceanography*, *50*(1), 43-49, 10.1007/bf02233855.

Van der Loeff, M. R., Sarin, M. M., Baskaran, M., Benitez-Nelson, C., Buesseler, K. O., Charette, M., Dai, M., Gustafsson, Ö., Masque, P., Morris, P. J., Orlandini, K., Rodriguez y Baena, A., Savoye, N., Schmidt, S., Turnewitsch, R., Vöge, I., and Waples, J. T. (2006), *A review of present techniques and methodological advances in analyzing ^{234}Th in aquatic systems*, *Marine Chemistry*, *100*(3-4), 190-212

Verdeny, E., Masqué, P., Maiti, K., Garcia-Orellana, J., Bruach, J. M., Mahaffey, C., and Benitez-Nelson, C. R. (2008), *Particle export within cyclonic Hawaiian lee eddies derived from 210Pb-210Po disequilibrium*, *Deep Sea Research Part II: Topical Studies in Oceanography*, *55*(10-13), 1461-1472, 10.1016/j.dsr2.2008.02.009.

Verdeny, E., Masqué, P., Garcia-Orellana, J., Hanfland, C., Kirk Cochran, J., and Stewart, G. M. (2009), *POC export from ocean surface waters by means of 234Th/238U and 210Po/210Pb disequilibria: A review of the use of two radiotracer pairs*, *Deep Sea Research Part II: Topical Studies in Oceanography*, *56*(18), 1502-1518, 10.1016/j.dsr2.2008.12.018.

Vicsek, T. (1989), *Fractal Growth Phenomena*, 2nd ed., World Scientific, Singapore.

Vogel, S. (1994), *Life in Moving Fluids, the physical biology of flow.*, 2nd ed., Princeton Univeristy Press, Princeton.

Volk, T., and Hoffert, M. I. (1985), *Ocean carbon pumps - Analysis of relative strengths and efficiencies in ocean-driven atmospheric CO_2 changes*, in *The Carbon Cycle and*

Atmospheric CO2 : Natural Variations Archean to Present, edited by E. T. Sandquist and Broecker, W. S., AGU, Washington D.C. .

Waite, A. M., Olson, R. J., Dam, H. G., and Passow, U. (1995), *Sugar-containing compounds on the cell surfaces of marine diatoms measured using concanavalin a and flow cytometry*
Journal of Phycology, *31*(6), 925-933, 10.1111/j.0022-3646.1995.00925.x.

Wakeham, S. G., Lee, C., Peterson, M. L., Liu, Z., Szlosek, J., Putnam, I. F., and Xue, J. (2009), *Organic biomarkers in the twilight zone--Time series and settling velocity sediment traps during MedFlux*, *Deep Sea Research Part II: Topical Studies in Oceanography*, *56*(18), 1437-1453, 10.1016/j.dsr2.2008.11.030: 10.1016/j.dsr2.2008.11.030.

Wassmann, P., Vernet, M., Mitchell, B. G., and Rey, F. (1990), *Mass sedimentation of phaeocystis-pouchetii in the barents sea*
Marine Ecology-Progress Series, *66*(1-2), 183-195, 10.3354/meps066183.

Wassmann, P., Andreassen, I., Reigstad, M., and Slagstad, D. (1996), *Pelagic-benthic coupling in the Nordic Seas: The role of episodic events*, *Marine Ecology Pubblicazioni Della Stazione Zoologica Di Napoli I*, *17*(1-3), 447-471

Wassmann, P. (1998), *Retention versus export food chains: processes controlling sinking loss from marine pelagic systems*, *Hydrobiologia*, *363*, 29-57

Wassmann, P., Bauerfeind, E., Fortier, E., Fukuchi, B., Hargrave, B., Moran, B., Noji, T., Nothig, E.-M., Olli, K., Peinert, R., Sasaki, H., and Shevchenko, V. P. (2004), *Particulate Organic Carbon Flux to the Arctic Ocean Sea Floor*, in *The Organic Carbon Cycle in the Arctic Ocean*, edited by R. Stein and Macdonald, R. W., pp. 101-138, Springer, Berlin.

Wassmann, P. (2011), *Arctic marine ecosystems in an era of rapid climate change*, *Progress In Oceanography*, *90*(1-4), 1-17, DOI 10.1016/j.pocean.2011.02.002.

Wassmann, P., and Reigstad, M. (2011), *Future Arctic Ocean Seasonal Ice Zones and Implications for Pelagic-Benthic Coupling*, *Oceanography*, *24*(3), 220-231

Wexels Riser, C., Wassmann, P., Olli, K., Pasternak, A., and Arashkevich, E. (2002), *Seasonal variation in production, retention and export of zooplankton faecal pellets in the marginal ice zone and central Barents Sea*, *Journal of Marine Systems*, *38*(1-2), 175-188, 10.1016/s0924-7963(02)00176-8.

Wexels Riser, C., Reigstad, M., Wassmann, P., Arashkevich, E., and Falk-Petersen, S. (2007), *Export or retention? Copepod abundance, faecal pellet production and vertical flux in the marginal ice zone through snap shots from the northern Barents Sea*, *Polar Biology*, *30*(6), 719-730, 10.1007/s00300-006-0229-z.

Wexels Riser, C., Wassmann, P., Reigstad, M., and Seuthe, L. (2008), *Vertical flux regulation by zooplankton in the northern Barents Sea during Arctic spring*, *Deep Sea Research Part II: Topical Studies in Oceanography*, *55*(20-21), 2320-2329

Wilson, S. E., Steinberg, D. K., and Buesseler, K. O. (2008), *Changes in fecal pellet characteristics with depth as indicators of zooplankton repackaging of particles in the mesopelagic zone of the subtropical and subarctic North Pacific Ocean*, *Deep Sea*

Research Part II: Topical Studies in Oceanography, 55(14-15), 1636-1647, 10.1016/j.dsr2.2008.04.019: 10.1016/j.dsr2.2008.04.019.

Xue, J., and Armstrong, R. A. (2009), *An improved "benchmark" method for estimating particle settling velocities from time-series sediment trap fluxes*, *Deep Sea Research Part II: Topical Studies in Oceanography*, *56*(18), 1479-1486, 10.1016/j.dsr2.2008.11.033.

Young, J. (Ed.) (1994), *Functions of coccoliths*, 63-82 pp., Cambridge Univeristy Press.

Young, J., Geisen, M., Cros, L., Kleijne, A., Sprengel, C., Probert, I., and Østergaard, J. B. (2003), *A guide to extant coccolithophore taxonomy*, *Journal of Nannoplankton Research*, *1*, 1 - 132

Young, J. R., and Ziveri, P. (2000), *Calculation of coccolith volume and it use in calibration of carbonate flux estimates*, *Deep Sea Research Part II: Topical Studies in Oceanography*, *47*(9-11), 1679-1700, 10.1016/s0967-0645(00)00003-5.

Zehr, J. P., and Kudela, R. M. (2009), *Photosynthesis in the Open Ocean*, *Science*, *326*(5955), 945-946, 10.1126/science.1181277.

Ziveri, P., Broerse, A. T. C., van Hinte, J. E., Westbroek, P., and Honjo, S. (2000), *The fate of coccoliths at 48°N 21°W, Northeastern Atlantic*, *Deep Sea Research Part II: Topical Studies in Oceanography*, *47*(9-11), 1853-1875, 10.1016/s0967-0645(00)00009-6.